Investigation of methods for the generation of selective small-molecule kinase inhibitors.

by

Kristoffer Brandvold

A dissertation submitted in partial fulfillment
of the requirements for the degree of
Doctor of Philosophy
(Medicinal Chemistry)
in The University of Michigan
2014

Doctoral Committee:

Assistant Professor Matthew B. Soellner, Chair
Professor George A. Garcia
Professor John Montgomery
Professor Henry I. Mosberg

Acknowledgements

I would first like to express sincere thanks to my mentor Professor Matthew B. Soellner for his guidance and support throughout my graduate studies at the University of Michigan. Matt has made a lasting mark on how I approach problem solving in chemical biology. I appreciate the amount of freedom he has granted me in my graduate research; it has been a challenging and personally rewarding experience. I have received exceptional training as a graduate student

I also would like to thank those who have made direct contributions to the research projects that I have worked on at while at Michigan. Christel Fox provided many of the isolated kinase proteins that were used for biochemical assays throughout the dissertation. Chris was also often a much needed and appreciated stabilizing force in the developing laboratory of an assistant professor. Mike Steffey was responsible for acquisition of most of the cell-based data for my compounds, and his contributions have led to results that I potentially consider to be more exciting than my own. Frank Kwarcinski invested significant effort to solve the co-crystal structures for the compounds described Chapters 2 &3. Eric Lachacz was kind enough to acquire the cancer cell data for Chapter 4.

I also owe many thanks to those in the Soellner-lab; the lab has been a great working environment. I look forward to following the continued excellence of my Soellner-lab peers. I would like to explicitly thank the postdoctoral research associates that I worked alongside as a junior graduate student. Dr. Peter Barker provided many useful discussions with respect to synthetic organic chemistry. Dr. Sonali Kurup provided many helpful conversations regarding medicinal chemistry concepts. Dr. Steven Bremmer provided many discussions, debates, and brain-storming sessions regarding diverse topics that varied from materials chemistry to cell biology.

I would like to acknowledge all of the friends I have had the good fortune of meeting in Ann Arbor. I would like to especially acknowledge Ron Jenkins, Doug Hansen, Kyle Heslip and Bryan Yestrepski. Being a productive scientist requires the occasional distraction. I will have many fond memories of my time in Ann Arbor.

I am also grateful for the support of my family. I would especially like to thank my mother Kelly, who encouraged me to pursue graduate studies.

Table of contents

Acknowledgements ii

List of Tables vii

List of Figures ix

List of Schemes xii

Abstract xiii

Chapter 1

Chemical inhibition of protein kinases 1

1.1 Protein kinases and their role in cell signaling 2

1.2 Approaches to modulation of kinase activity 2

1.3 General features of small-molecule kinase inhibitors 3

1.4 DFG-out inhibitors 5

1.5 c-helix out inhibitors 8

1.6 Bisubstrate-competitive inhibitors 11

1.7 References 14

Chapter 2

Rational design of DFG-out inhibitors 18

2.1 Introduction 18

2.2 Results and discussion..... 19

2.3 Conclusions..... 24

2.4 Experimental section 25

2.5 References..... 65

Chapter 3

Rational design of c-helix out inhibitors..... 66

3.1 Introduction 66

3.2 Results and discussion..... 67

3.3 Conclusions..... 70

3.4 Experimental section 71

3.5 References..... 103

Chapter 4

A rational and modular approach to bisubstrate inhibition of protein kinases..... 104

4.1 Introduction 104

4.2 Results and discussion..... 105

4.3 Conclusions..... 111

4.4 Experimental section 112

4.5 References..... 140

Chapter 5

Development of a highly selective c-Src kinase inhibitor 141

5.1 Introduction 141

5.2 Results and discussion 142

5.3 Conclusions 149

5.4 Experimental section 150

5.5 References 207

List of Tables

Table 1.1 Categorization of FDA-approved small-molecule kinase inhibitors by binding conformation 8

Table 1.2 Analysis of potency improvement for conjugates versus parent compounds ... 13

Table 1.3 Summary of selectivity analysis of several bisubstrate protein kinase inhibitors 14

Table 2.1 Treatment of breast cancer cell lines using compound **2.3** and dasatinib 22

Table 2.2 Selected KiNativ profiling data for compound **2.3** and dasatinib 23

Table 3.1 Treatment of breast cancer cells using **3.4** and dasatinib 70

Table 4.1 Optimization of linker length for a c-Src bisubstrate inhibitor 106

Table 4.2 Biochemical characterization of the individual fragments of a bisubstrate inhibitor designed for c-Src 106

Table 4.3 Inhibitor K_d determination using probe **4.7** 108

Table 4.4 Biochemical characterization of a bisubstrate inhibitor designed to bind PDGFRB 109

Table 5.1 Summary of K_i values obtained for compounds **5.1–5.6** 144

Table 5.2 K_d values obtained by KINOMEscan for Src family kinases with compound **5.4** 146

Table 5.3 Biochemical and characterization of PP2 and compound **5.4** 147

List of Figures

Figure 1.1 Strategies for the modulation of kinase activity 3

Figure 1.2 General structural features of the kinase domain and potential ligand binding sites. 4

Figure 1.3 Spectrum of kinase inhibitor selectivity. 4

Figure 1.4 Detailed interactions of a DFG-in inhibitor with the ATP-pocket. 5

Figure 1.5 The first example of a kinase observed in the DFG-out conformation 6

Figure 1.6 Examples of kinases other than Abl that adopt DFG-out in the presence of a small-molecule inhibitor 6

Figure 1.7 General features of DFG-out inhibitors as represented by sorafenib bound to BRAF kinase. 7

Figure 1.8 A general method for converting DFG-in to DFG-out inhibitors, as initially proposed by Gray et al. 7

Figure 1.9 DFG-out inhibitors impact protein-protein differently than DFG-in inhibitors 8

Figure 1.10 Selectivity profile of a lapatinib, a selected c-helix out kinase inhibitor. 9

Figure 1.11 c-Src adopts c-helix out upon engagement of the regulatory SH2 and SH3 domains. 10

Figure 1.12 Small molecule binding of the c-helix out conformation results in organization of the SH2 and SH3 domains. 10

Figure 1.13 General features of a c-helix out inhibitor. 11

Figure 1.14 General classes of bisubstrate kinase inhibitors..... 12

Figure 2.1 Chemical structure of dasatinib 18

Figure 2.2 Design of a dasatinib derivative that will bind the DFG-out conformation..... 19

Figure 2.3 Selectivity profile for compound **2.1** using a single-point binding assay 20

Figure 2.4 Biochemical kinase inhibition data for dasatinib and two DFG-out derivatives. 20

Figure 2.5 X-ray co-crystal structure of compound **2.2** bound to c-Src kinase. 21

Figure 2.6 Kinome profiling of dasatinib, **2.2**, and **2.3** using a single point binding assay. 21

Figure 2.7 Assessment of dual inhibitor treatment of a breast cancer cell line using dasatinib and a p38β inhibitor (BIRB-796) 23

Figure 3.1 General strategy for conversion of a DFG-in to c-helix out inhibitor 66

Figure 3.2 General chemical features of DFG-out and c-helix out kinase inhibitors 67

Figure 3.3 Structures and biochemical inhibition assays for compounds **3.1-3.3** 68

Figure 3.4 Activity-based kinase inhibition assays for compound **3.4**..... 68

Figure 3.5 Overlay of co-crystal structures of compound **3.1** bound respectively to Src and Abl..... 69

Figure 3.6 Kinome selectivity profile for compound **3.4** using a single point binding assay. 69

Figure 4.1 Structure of compound **4.1** and selectivity profile of compound **4.1** using a single-point binding assay. 105

Figure 4.2 General structure for bisubstrate inhibitors..... 105

Figure 4.3 Measurement of the affinity of a fluorescently labeled bisubstrate probe **4.7** for c-Src 107

Figure 4.4 Selectivity profile for compound **4.3** at 115 nM against a panel of 200 kinases 108

Figure 4.5 Structure and biochemical characterization of a truncated c-Src bisubstrate inhibitor **4.7** 109

Figure 4.6 ATP-competitive vs. bisubstrate-competitive inhibition of a clinically observed resistance mutation 110

Figure 4.S-1 Prediction of distance between N1-Phenylpyrazolopyrimidine (**4.1**) and a representative substrate peptide bound to a kinase based upon a molecular model 112

Figure 5.1 A. Structure of PP2. B. Kinome dendrogram of PP2 selectivity profiling at 10 µM 142

Figure 5.2 Alignment of structures with dasatinib bound to c-Src 143

Figure 5.3 A. Structure of compound **4**. B. Kinome dendrogram of compound **4** selectivity profiling at 10 µM 145

Figure 5.4 4T1 cell proliferation in 3D culture 148

Figure 5.S-1 Model image of compound **5.2** bound to c-Src (starting structure from PDB code 3DQW) 150

List of Schemes

Scheme 2.S-1 Representative synthesis of compounds **2.1-2.3** 26

Scheme 3.S-1 Representative synthetic routes for final compounds **3.1 –3.4**..... 71

Scheme 4.S-1 General synthetic scheme for bisubstrate competitive kinase inhibitors using solid phase peptide synthesis..... 114

Scheme 5.1 Synthesis and biochemical characterization of benzyl triazole compound **5.2**..... 143

Scheme 5.S-1 Synthesis of PP2~alkyne (**5-1**)..... 152

Abstract

Protein kinases have evolved as key players in the signaling processes that allow the mammalian cell to respond to environmental stimuli. Determination of the function of each the individual members of this large class of enzymes is aided by development of selective inhibitors. Most kinase inhibitors function through binding the highly conserved ATP-pocket and are often poorly selective as a result. This dissertation assesses two general strategies to improve kinase inhibitor selectivity. One strategy regards ATP-competitive inhibitors which target distinct kinase folds, and an orthogonal strategy regards targeting inhibitor binding sites outside of the highly conserved ATP-pocket.

First, the drug dasatinib is rationally altered to provide two sets of inhibitors which respectively bind distinct “inactive” kinase folds (DFG-out and c-helix out). Large scale selectivity profiling reveals that most of dasatinib’s kinase targets can adopt the DFG-out conformation, while the c-helix out conformation appears less conserved. These results imply that targeting inactive conformations does not necessarily entail higher kinase inhibitor selectivity.

Second, inhibitors that target regions outside of the ATP-pocket are developed using a bivalent approach. A fragment intended to target a region outside of the ATP-pocket is covalently tethered to an ATP-competitive inhibitor. Application of this strategy demonstrates the amount of selectivity that can be gained from targeting alternate pockets. In one example, we show that the site at which kinases bind their protein target can be modularly targeted for highly selective inhibition. In another example, the development of a highly selective c-Src inhibitor is achieved through targeting the phosphate binding-loop region. In an application of our c-Src selective inhibitor, it is

shown that selective inhibition is more effective than multi-kinase inhibition in the treatment of several cancer cell lines.

Altogether this dissertation provides insight regarding the design of selective kinase inhibitors. One study reveals that ATP-competitive inhibitors that bind “inactive” kinase folds appear to be much less selective than previously suggested. A second study demonstrates that targeting sites outside of the ATP-pocket can provide very highly selective kinase inhibitors.

CHAPTER 1

Chemical inhibition of protein kinases

The focus of the graduate research described herein has been the development of chemical tools for the investigation of structural features of protein kinases which may be exploited for selective inhibition.

There are two separate-but-interrelated themes throughout the dissertation:

1) How does binding an "inactive" fold influence kinase inhibitor selectivity?

Chapters 2 and 3 describe the rational syntheses of ATP-competitive inhibitors which bind distinct inactive kinase forms (DFG-out and c-helix out). These compounds are based upon an inhibitor which is known to bind the active DFG-in form. This research allowed for an analysis of the selectivity differences between kinase inhibitors which respectively bind the DFG-in, DFG-out and c-helix out folds. It is revealed that all three conformations appear largely conserved across the kinome. One particular derivative displays exceptional activity in the treatment of several cancer cell lines.

2) How much selectivity may be gained by exploiting structural features outside of the canonical ATP-pocket?

Chapters 4 and 5 are devoted to kinase inhibitors that interact with structural features outside of the ATP-pocket. Both chapters employ a common strategy using an ATP-competitive "anchor" to tether another chemical fragment which is intended to interact with a site outside of the ATP-pocket. Chapter 4 highlights the level of selectivity that may be obtained through inhibitor interactions with the substrate-binding site. In an related approach, Chapter 5 discusses the development of the most highly selective cell-permeable inhibitor of c-Src kinase which is proposed to exploit an interaction with the phosphate-binding loop.

1.1 Protein kinases and their role in cell-signaling

Eukaryotic life requires that all of the individual components of the cell intercommunicate in a manner that promotes healthy growth and division. Cell-signaling is a complex process which is regulated, in part, by protein phosphorylation.[1,2] Protein phosphorylation cascades result from the activity of protein kinases, which are a family of enzymes with over 500 unique members encoded within the human genome.[3] The process of reversible protein-phosphorylation catalyzed by protein kinases accounts for one of the most important post-translational modifications involved in eukaryotic cell signaling.[4,5] While protein kinases account for only two percent of the human genome, it has been estimated that at least half of human proteins contain at least one site which undergoes a physiologically relevant phosphorylation[6]. Phosphorylation of protein targets has a variety of effects including, but not limited to, activation, translocalization and degradation.[7,8] Many proteins contain several phosphorylation sites which allow for fine tuning of function.

Protein phosphorylation events must be tightly regulated to ensure appropriate cellular response to the given environmental cues. Deregulation of protein kinase activity can significantly affect the morphology of a cell and eventually the surrounding tissue, which leads to a variety of diseases including cancer.[9-11] Protein kinase inhibitors (PKIs) represent the largest class of new cancer drugs[12,13] with six biologic examples and twenty small-molecule drugs currently approved by the FDA.

1.2 Approaches to modulation of kinase activity

Methods for the selective modulation of protein kinase activity are critical for understanding the individual roles for these enzymes *in cellulo*, and also how deregulation leads to disease. While genetic knockout/knockdown experiments provide highly selective removal of the desired target there are several drawbacks to this approach,[14] but these shortcomings can be addressed using chemical inhibition (Figure

1.1). Chemical inhibition is attractive due to reversible and dose-dependent action with good spatiotemporal control. Furthermore, when selective small-molecule inhibition is used in combination with genetic techniques, meaningful insights that would be missed by employing either method independently can be obtained.[15,16]

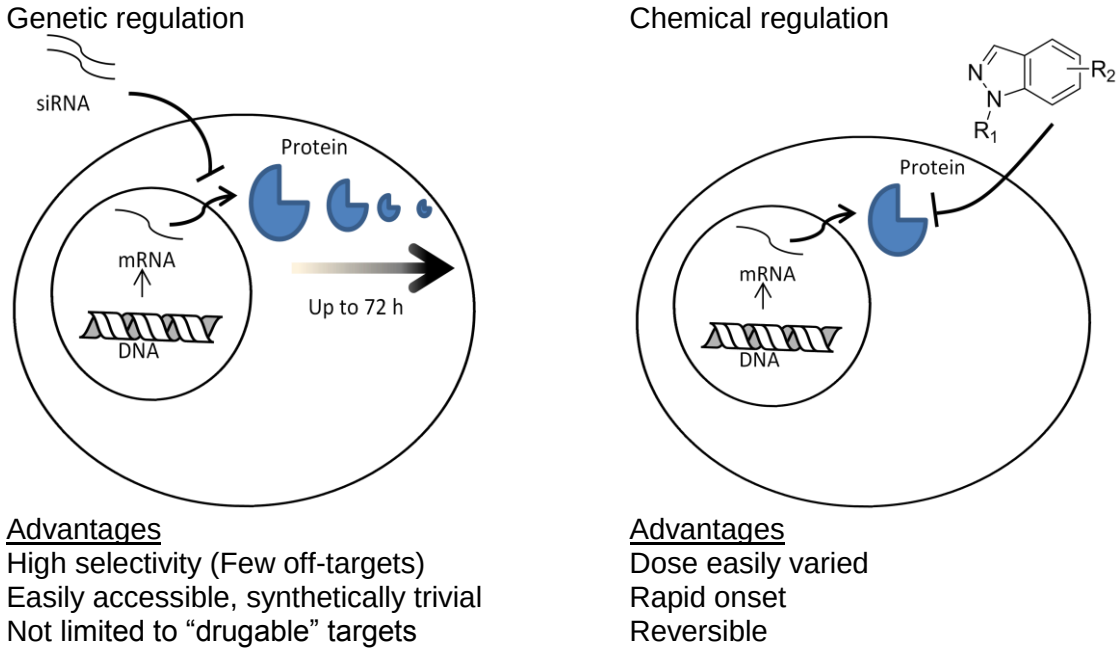

Figure 1.1. Strategies for the modulation of kinase activity. Figure adapted from reference 14.

Unlike RNAi, development of selective small-molecule inhibitors is a challenging process. According to criteria set by Knapp et al[17] there are only 25 inhibitors which can be defined as 'high-quality' kinase probes. Given that there are over 500 human kinases there is clearly an unmet research need. Most selective kinase inhibitors have been discovered serendipitously through high-throughput screening. Rational inhibitor design could greatly contribute to reducing this deficit. Development of selective kinase inhibitors also contributes to the foundation of drug discovery.[18-20]

1.3 General features of small-molecule kinase inhibitors

Protein kinases can generally be categorized as phosphotransfersases. They contain respective binding sites for both adenosine triphosphate (ATP) and protein substrate. Upon binding both ATP and substrate, a kinase-assisted transfer of a phosphate unit from ATP to protein substrate occurs. Thus, in the design of small-molecule kinase

inhibitors there are two major sites that can be targeted (Figure 1.2). An overwhelming majority of small-molecule protein kinase inhibitors function through binding the ATP pocket.

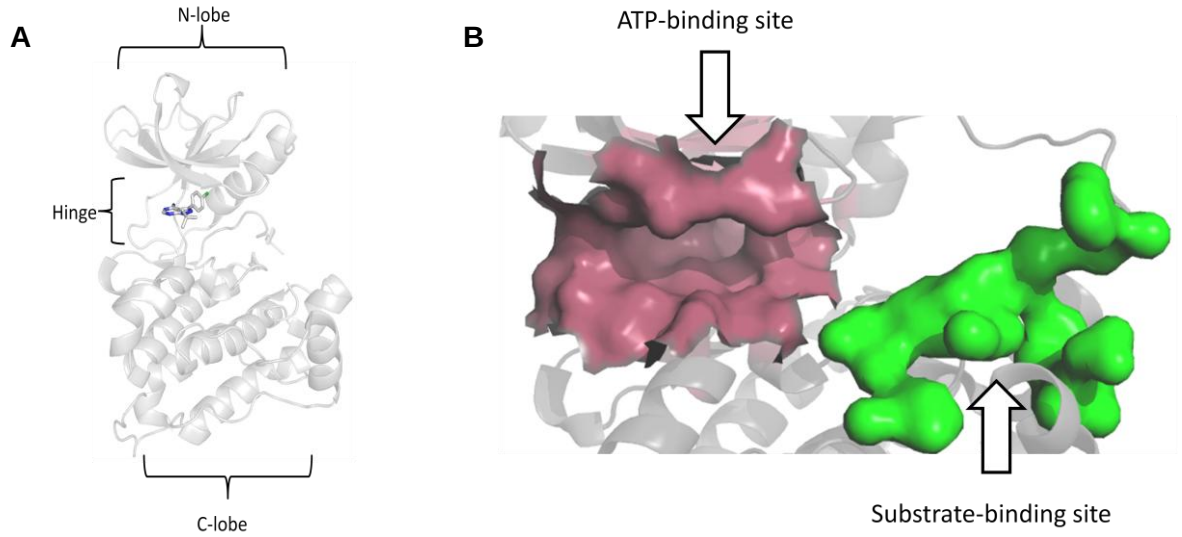

Figure 1.2. General structural features of A) the kinase domain and B) potential ligand binding sites within the kinase domain highlighted using space filling. Images were rendered using Pymol. PDBID: 2ZV9 (A) and 2G1T (B).

The ATP-pocket is a hydrophobic cleft[21] which has evolved to accommodate the heterocycle adenine, and thus small-molecule inhibitors have a natural inclination for occupation of this site. In contrast, the substrate-binding site has evolved to serve as an interface for protein-protein interaction. Small-molecule inhibitor binding of the substrate-binding site is generally unfavorable due to its flat and solvent-exposed nature.

The selectivity of ATP-competitive kinase inhibitors has been observed to vary greatly (Figure 1.3).[22-24] Most kinase inhibitor selectivity profiles fall somewhere in between the two extremes. While kinse inhibitor selectivity is not necessarily paramount for drug development,

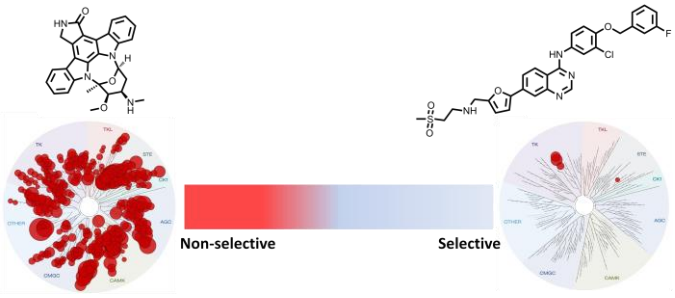

Figure 1.3. Spectrum of kinase inhibitor selectivity. Staurosporine (left) is a representative non-selective inhibitor, whereas lapatinib (right) is a representative selective inhibitor.

their use as probes necessitates high fidelity for the target of interest.[17] Achieving high selectivity in this region is difficult due to the low sequence variability of this region.[25]

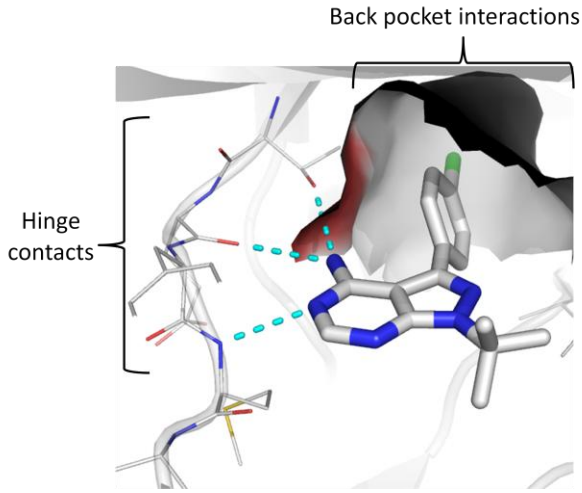

Figure 1.4. Detailed interactions of a DFG-in inhibitor with the ATP-pocket. Shown is PP2 bound to c-Src (PDB: 2ZV9). Hydrogen bonds to residues within the hinge region are highlighted in cyan.

ATP-competitive kinase inhibitors ubiquitously display interactions with the hinge region, which are to similar to those of adenine (Figure 1.4). Unlike adenine, many inhibitors exploit interactions with a hydrophobic pocket in the back of the ATP-binding site. Inhibitor binding of this back pocket can influence the positioning of structural features such as the activation loop and c-helix of the kinase. It has been proposed that interaction with this back pocket may improve inhibitor selectivity.

1.4 DFG-out inhibitors

Protein kinases dynamically interchange between active and inactive structural conformations.[26] The first observed instance of a kinase in its inactive form was the co-crystal structure of Abl kinase bound to the small-molecule inhibitor imatinib[27,28] (Figure 1.5). In this structure, the benzamide moiety of imatinib occupies a pocket that usually accommodates the phenylalanine residue of the DFG motif at the base of the activation loop. Binding this pocket results in a 'DFG-flip', and this perturbs the orientation of the aspartic acid (DFG) residue necessary for catalysis. Furthermore, displacement of the DFG phenylalanine (DFG) dismantles a series of hydrophobic residues referred to as the 'regulatory spine.[21,29]

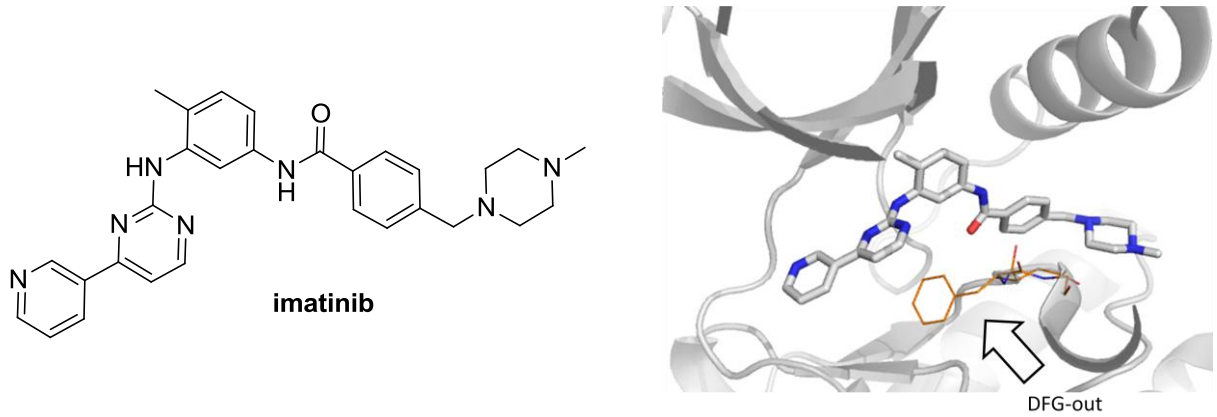

Figure 1.5. The first example of a kinase observed in the DFG-out conformation. A) Chemical structure of imatinib; and B) co-crystal structure of imatinib bound to Abl kinase. The DFG motif is highlighted in orange. Portions of the kinase have been removed for clarity. PDB: 1IEP.

Imatinib was the first FDA approved kinase inhibitor and has generated considerable attention due to its success in the treatment of chronic myelogenous leukemia driven by the BCR-Abl oncogene.[30-32] The clinical success of imatinib was largely credited to high selectivity for the ATP-binding site of the BCR-Abl kinase oncoprotein.[24] The selectivity was assumed to be the result of binding a structural pose (DFG-out) that only BCR-Abl could assume. However, subsequent to these seminal findings it has been determined that at least 16% of all protein kinases can assume this fold[33,34] (Figure 1.6). Despite these confounding observations, targeting the DFG-out conformation remains highly cited as a valid mechanism for improving kinase inhibitor selectivity.[35-40]

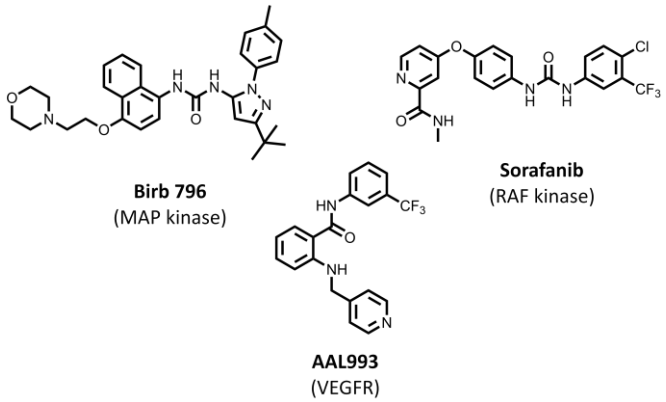

Figure 1.6. Examples of kinases other than Abl that adopt DFG-out in the presence of a small-molecule inhibitor.

The general features of DFG-out inhibitors are represented by the structure of sorafenib bound to BRAF kinase (Figure 1.7). As with most kinase inhibitors, DFG-out inhibitors usually have hydrogen bond interactions with the "hinge" region analogous to those of adenine. Additionally, as nomenclature would imply, the defining feature of DFG-out inhibitors is the flipping of the DFG motif at the base of the activation loop. The DFG flip is usually induced by

inhibitor occupation of the pocket that usually accommodates the displaced DFG phenylalanine. The flip of the activation loop disallows protein substrate binding, and this is why DFG-out is frequently referred to as an inactive form. Additionally, DFG-out inhibitors routinely make hydrogen-bond interactions with the backbone of the activation loop and a glutamate sidechain of the c-helix at the back of the ATP-pocket.

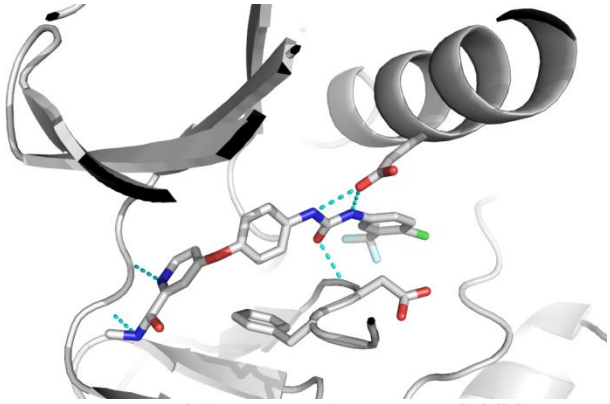

Figure 1.7. General features of DFG-out inhibitors as represented by sorafenib bound to BRAF kinase. Hydrogen bonding interactions are represented as cyan dashes. The image was constructed using PDBID: 1UWH. Part of the kinase has been removed for clarity.

DFG-out inhibitors have received so much attention that a general method for the conversion of a DFG-in to a DFG out inhibitor has been developed, [41,42] and this method is graphically summarized in Figure 1.8. Briefly, assisted by x-ray co-crystal structures the authors rationally append a m-trifluoromethyl-benzamide moiety to a known DFG-in inhibitor. This serves to both occupy the back hydrophobic pocket of the ATP-binding site, and also provide a hydrogen bond donor interaction with the glutamate side chain of the c-helix. The authors report four successful examples of application of this method. There is a limited examination of the selectivity of the respective pairs, and in general there is little difference in the profiles. The panels employed were relatively small which makes definitive conclusions difficult.

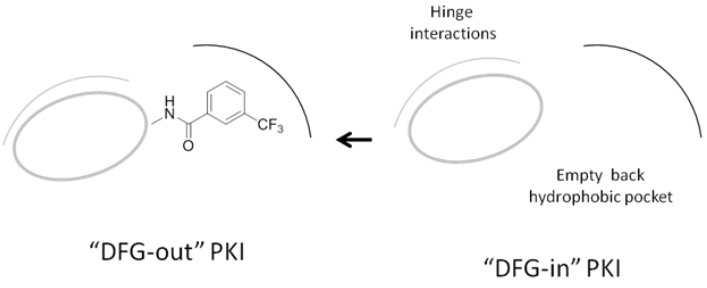

Figure 1.8. A general method for converting DFG-in to DFG-out inhibitors, as initially proposed by Gray et al.

Unexpectedly, DFG-out inhibitors have been observed to display different properties *in cellulo* relative to their DFG-in counterparts that are not due to selectivity differences (Figure 1.9). For example, Raf kinase has been observed to undergo dimerization upon

treatment with a DFG-in inhibitor,[43] and DFG-out inhibitors have been shown to have a strikingly different influences on heterodimerization of BRAF kinase mutants.[44] Another example is IRE1α's kinase-controlled RNase.[45] DFG-out inhibitors of the IRE1α kinase domain have been shown to allosterically modulate the activity of fused RNase domain.

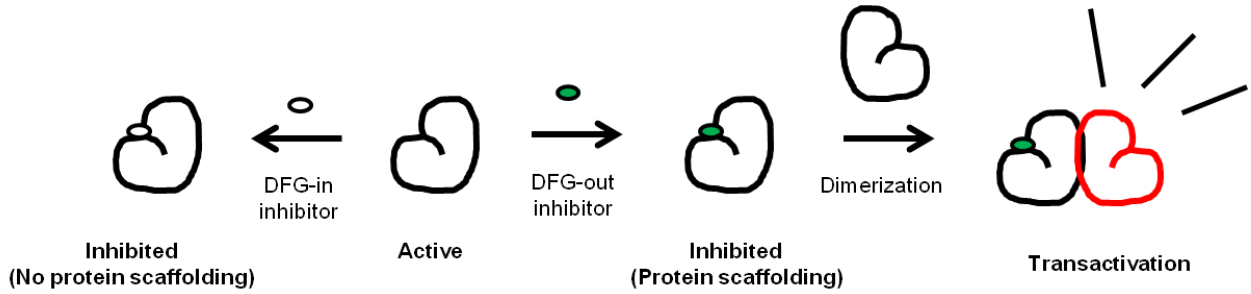

Figure 1.9. DFG-out inhibitors impact protein-protein differently than DFG-in inhibitors.

Despite significant investment in the development of DFG-out inhibitors there has not been a thorough analysis of how their general properties might diverge from their DFG-in counterparts. A side-by-side comparison has been made difficult because there has not been an appropriate set of inhibitors. Using a set from the aforementioned manuscript is not ideal because the DFG-out inhibitors are generally much more potent than their DFG-in parent. Chapter 2 describes a set of inhibitors which is aptly suited for such analyses.

1.5 c-helix out inhibitors

DFG-in	DFG-out	c-helix out	unknown
afatinib bosutinib crizotinib dasatinib erlotinib gefinitinib pazopanib sunitinib	axitinib imatinib nilotinib sorafanib ponatinib	lapatinib	ruxolitinib SU6656 tofacitinib vemurafenib ibrutinib everolimus

Table 1.1. Categorization of FDA approved small-molecule kinase inhibitors by binding conformation.

The ability of protein kinases to adopt both active and inactive conformations has allowed for a variety of methods for medicinal chemists to design small-molecule inhibitors of a desired target. Small-molecule engagement of a specific structural conformation results in trapping of the protein in a local thermodynamic minimum that is associated with a given shape. There is increasing evidence that stabilization of a specific structural conformation using a small-molecule kinase inhibitor can influence biological activities that are not directly related to catalysis, such as participation in protein-protein

interactions (PPIs).[43,45,46] Therefore, a kinase inhibitor may have an effects beyond just turning the enzyme "off". Design of inhibitors which can engage alternative conformations could serve as valuable tools to interrogate these ancillary PPIs.

The current bias for kinase inhibitor development is represented by the categorization presented in Table 1.1. The majority of inhibitors bind the "active" DFG-in fold. Half as many inhibitors have been found the inactive DFG-out state. Only one FDA approved kinase inhibitor has been observed to bind the alternative c-helix out inactive conformation.[47] Studies from our laboratory suggest that targeting the inactive DFG-out conformation of protein kinases is not a valid approach for improving selectivity (see chapter 2). Conversely, inhibitors which engage the c-helix out conformation have been observed to be highly selective for their given targets and this is represented by the selectivity profile of lapatinib (Figure 1.10).[36]

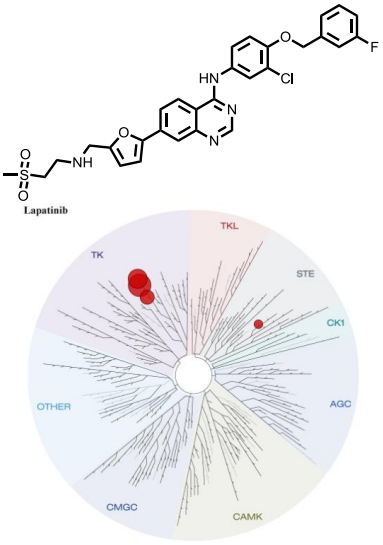

Figure 1.10. Selectivity profile of a lapatinib, a selected c-helix out kinase inhibitor. Data have been modified from Nat. Chem. Biol.[36].

The c-helix out conformation is represented by the structure of c-Src kinase in its autoinhibited state in the presence of its regulatory domains[48] (Figure 1.11). The authors suggest that clamping effect of the SH2 and SH3 domains upon the kinase domain results in a torsional forces which twist the c-helix outward from its catalytically conducive position. This autoinhibitory mechanism is believed to be shared by most other nonreceptor protein tyrosine kinases.[49]

It has since been proposed that c-helix out is the biologically relevant inactive pose for most protein kinases, in contrast with DFG-out which is thought to be induced solely through small-molecule engagement. Small-molecule binding of the c-helix out pose is therefore particularly attractive because of the potential of influencing the regulatory domains with have cellular activities unrelated to catalysis.

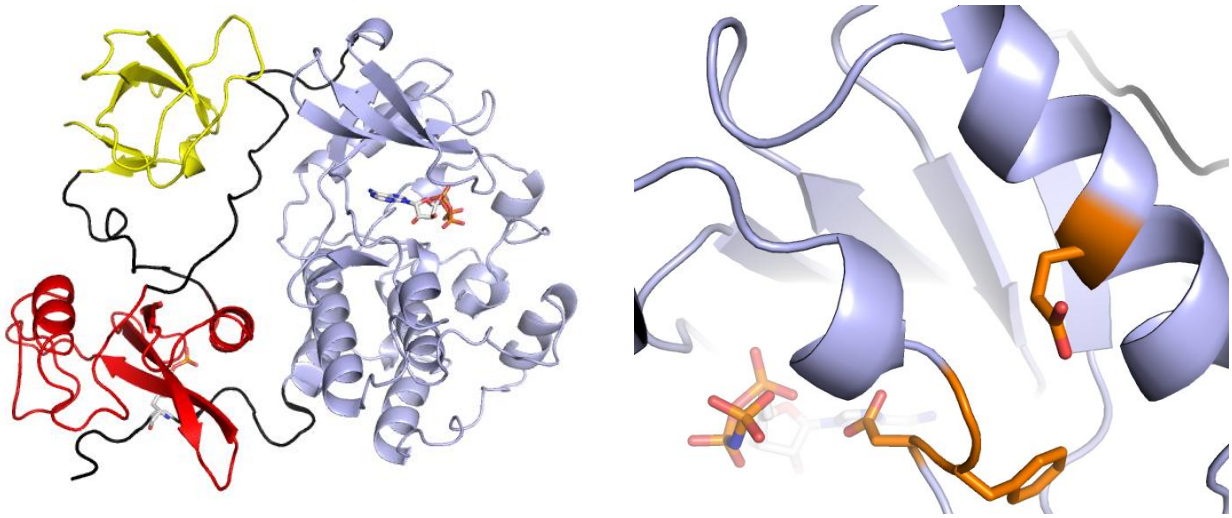

Figure 1.11. c-Src adopts c-helix out upon engagement of the regulatory SH2 and SH3 domains. A) c-Src's kinase domain (blue) in its autoinhibited state in the presence of its regulatory SH2 (red) and SH3 yellow domains. AMPNP is bound in the ATP-binding site. B) A close-up image of the rotated c-helix showing the conserved Glu in a position not compatible with catalysis. DFG motif is observed in the DFG-in conformation and is additionally highlighted in orange. Images constructed using PDBID: 2SRC.

Small-molecule stabilization of the c-helix out conformation of the kinase domain has been shown to have a profound effect on the organization of the regulatory domains of c-Src[46] (Figure 1.12). In one example a set of small-molecule inhibitors which preferentially bind to the c-helix out conformation of the kinase domain are shown to induce engagement of the SH2 and SH3 domains. Kinase inhibitors which influence the regulatory domains offer a unique mechanism of inhibition because the SH2 and SH3 domains participate in many protein-protein interactions.

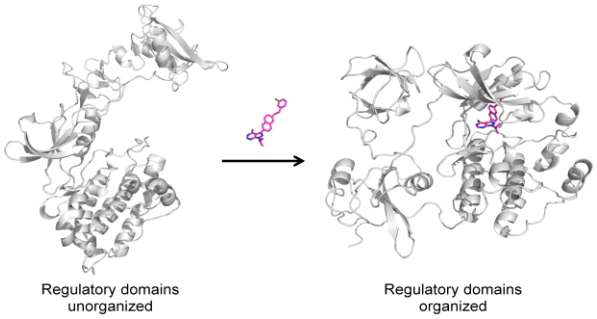

Figure 1.12. Small-molecule binding of the c-helix out conformation results in organization of the SH2 and SH3 domains.

In related studies, it has been found that while both DFG-in and c-helix out inhibitors efficiently diminish the catalytic activity of the kinase domain, they diverge in their ability to regulate dimerization of receptor tyrosine kinases.[50,51]

A typical binding mode for a c-helix out inhibitor is represented by Figure 1.13. Similar to most kinase inhibitors, c-helix out inhibitors generally have hydrogen bond interactions with the hinge region of the ATP-pocket. Similar to DFG-out inhibitors, c-helix out inhibitors also have a hydrophobic substituent which engages the back hydrophobic pocket. c-helix out inhibitors differ from DFG-out inhibitors because they lack a hydrogen bond interaction with the glutamate side chain of the c-helix.

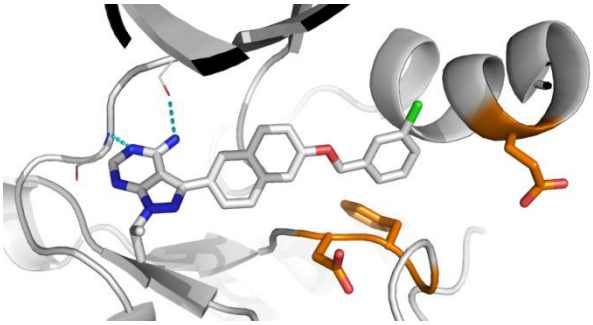

Figure 1.13. General features of a c-helix out inhibitor.

There is no general strategy currently available for converting a DFG-in to c-helix out inhibitor as there is for DFG-out inhibitors. This is a topic of discussion in Chapter 3. Development of this strategy has allowed for a cross-comparison of the DFG-in, DFG-out, and c-helix out conformations in terms of general biochemical properties.

1.6 Bisubstrate-competitive inhibitors

Small-molecule strategies for inhibition of kinase activity mainly rely upon ATP-competitive inhibition of the catalytic domain[52]. Development of selective small-molecule kinase inhibitors remains a significant challenge due to the highly conserved nature of the ATP pocket.[25,53,54] One particularly promising alternative strategy is the targeting of the less conserved substrate-binding site[55-57] (for a review of this topic see reference 58). Substrate-competitive inhibitors offer high selectivity,[59,60] but generally suffer from poor potency due to the lack of a conventional small-molecule ligand pocket. Conversely, bisubstrate kinase inhibition attempts to compensate for the low potency of substrate-competitive inhibitors through covalent linkage to an ATP-competitive inhibitor. Theoretically, the merging of two inhibitors which have mutually exclusive binding sites should result in an inhibitor with improved potency relative to the parent compounds. Bisubstrate kinase inhibition has been of interest for some time[61] yet there

are sparse examples in which potency is dramatically improved upon merging the respective fragments.

The bivalent inhibition strategy has a history that is closely tied to the transition-state inhibition theory. Unlike other enzymes such as proteases or phosphatases there is no covalent intermediate in the phosphotransferase reaction catalyzed by protein kinases. This makes targeting the phosphotransfer transition-state a considerable challenge. Rather than irreversibly trapping a catalytic cysteine, as is the case with phosphatase transition state mimetics, two inhibitor ligands must be tethered with a geometry that is representative of the phosphotransfer event.

Inhibitors that interact with the substrate-binding site offer several potential promising outcomes that cannot be achieved solely with conventional ATP-competitive inhibitors. First, ligand binding of the substrate-binding site has been established to be coupled to dimerization and autophosphorylation as has been observed with PKR.[62,63] Second, interference with protein-protein interactions associated with this site may have other interesting advantages that have yet to reveal themselves.

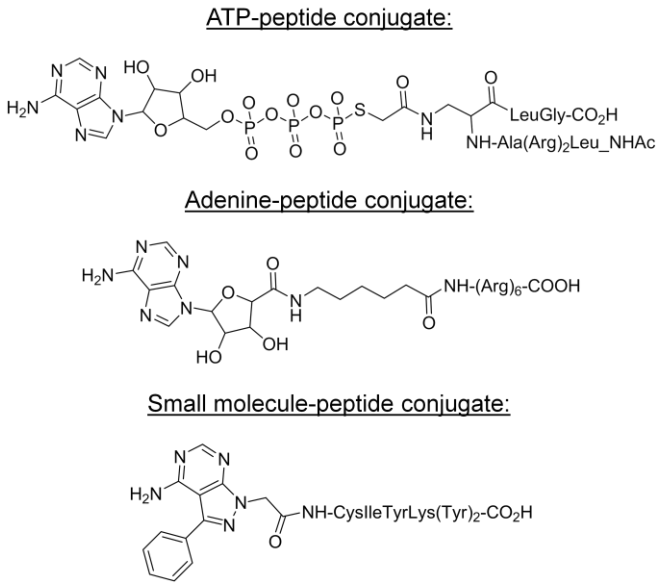

Figure 1.14. General classes of bisubstrate kinase inhibitors.

By definition, bisubstrate kinase inhibitors simultaneously interact with both the ATP and substrate-binding sites. Bisubstrate PKI inhibitors can be divided into three general classes 1) ATP-peptide conjugates 2) Adenine-peptide conjugates and 3) ATP-competitive inhibitor-peptide conjugates (Figure 1.14). The latter are the primary focus of Chapter 5 and thus will solely be discussed here.

The biochemical potency of bisubstrate kinase inhibitors has been reported to range from low nanomolar to high micromolar. The ATP-competitive fragment is usually the largest contributor to affinity.

A synergistic increase in potency upon covalent linkage of the respective inhibitors is expected due to a lower entropic penalty for inhibitor binding,[64] although this is not always observed in practice. Conjugation of the two fragments does not always appreciably increase potency with respect to the two individual components (Table 1.2). The lack of synergistic improvement in potency is frequently attributed to suboptimal linker length.[65]

Reference	Fold improvement of conjugate vs parent[a]
Enkvist et al[66]	698
Ho et al[67]	0.51
Meyer et al[68]	93
Loog et al[69]	1,180
Enkvist et al[70]	137,000
Hines et al[65]	0.23
Nam et al[71]	33
Loog et al[72]	1,020

Table 1.2. Analysis of potency improvement for conjugates versus parent compounds.
a) Varying metrics were used between authors to determine affinity so 'fold improvement' is used in order to normalize the value. ATP-competitive parents are in general more potent so this was selected to be the representative 'parent'.

Table 1.2 summarizes data extracted from a list of references from a recent review focused on bisubstrate inhibition of protein kinases.[58] All citations which included data for both the final and parent ATP-competitive fragment are listed. As expected, most examples show an increase in potency relative to the ATP-competitive parent. Two examples surprisingly show instances in which the parent compound is actually made worse.

The most promising advantage of bisubstrate protein kinase inhibitors over their ATP-competitive counterparts is improved selectivity. However bisubstrate inhibitor selectivity is often only minimally investigated. In a recent review on bisubstrate inhibition[58] there were only four examples[66,70,73,74] in which a bisubstrate inhibitor was profiled against a panel of greater than thirty kinases (Table 1.3), and all other references included panels of less than six. A panel of thirty kinases represents only six percent of the human kinome. Furthermore the compounds that were profiled against large panels displayed relatively poor selectivity, and all fail to meet the definition of a "quality kinase probe"[17].

The four examples of bisubstrate inhibitors that were subjected to large kinase panels (Table 1.3) were all inhibitors specifically designed for PKA. In three of the citations, a highly positively charged peptide was linked to an ATP-competitive inhibitor, and this may explain the low selectivity. The general tendencies of basophilic kinases were exploited rather than the individual preferences of their target. The one reference

(Shomin et al[74]) that deviated from this model, and tailored the peptidic inhibitor specifically to the target, achieved the highest selectivity. There has been little examination of the selectivity of bisubstrate inhibitors designed for non-basophilic kinases such as tyrosine kinases.

Reference	Total kinases in panel	Kinases with affinity for inhibitor[a]	S(35) selectivity score[b]
Enkvist et al[66]	52	18	0.34
Lavogina et al[73]	50	29	0.58
Shomin et al[74]	90	10	0.11
Enkvist et al[70]	34	19	0.56

Table 1.3. Summary of selectivity analysis of several bisubstrate protein kinase inhibitors.
a) Affinity is defined as observing < 35 % activity or remaining kinase unbound (including target) upon inhibitor treatment in the respective assays used by the authors.
b) S(35) is the ratio of kinases with affinity(as defined above)/total kinases in panel

In summary, the high selectivity boasted by bisubstrate kinase inhibition has not been fully validated. Chapter 4 describes a modular method for the synthesis of bisubstrate inhibitors for tyrosine kinases. Also in this chapter, an optimized bisubstrate inhibitor for c-Src kinase is submitted to selectivity profiling to demonstrate an unprecedented improvement in selectivity relative to its ATP-competitive parent.

1.7 References

(1) Hunter, T. *Cell* **1995**, *80*, 225-236.
(2) Marshall, C. J. *Cell* **1995**, *80*, 179-185.
(3) Manning, G.; Whyte, D. B.; Martinez, R.; Hunter, T.; Sudarsanam, S. *Science* **2002**, *298*, 1912-1934.
(4) Manning, G.; Whyte, D. B.; Martinez, R.; Hunter, T.; Sudarsanam, S. *Science* **2002**, *298*, 1912.
(5) Marshall, C. J. *Cell* **1995**, *80*, 179.
(6) Reinders, J.; Sickmann, A. *PROTEOMICS* **2005**, *5*, 4052-4061.
(7) Graves, J. D.; Krebs, E. G. *Pharmacology & Therapeutics* **1999**, *82*, 111-121.
(8) Hunter, T. *Cell* **2000**, *100*, 113-127.
(9) Roberts, P. J.; Der, C. J. *Oncogene* **2007**, *26*, 3291-3310.
(10) Bartek, J.; Lukas, J. *Cancer Cell* **2003**, *3*, 421-429.
(11) Gschwind, A.; Fischer, O. M.; Ullrich, A. *Nature Reviews Cancer* **2004**, *4*, 361-370.
(12) Knight, Z. A.; Lin, H.; Shokat, K. M. *Nat Rev Cancer* **2010**, *10*, 130-137.
(13) Cohen, P. *Nat Rev Drug Discov* **2002**, *1*, 309-315.
(14) Weiss, W. A.; Taylor, S. S.; Shokat, K. M. *Nat Chem Biol* **2007**, *3*, 739-744.

(15) Ditchfield, C.; Johnson, V. L.; Tighe, A.; Ellston, R.; Haworth, C.; Johnson, T.; Mortlock, A.; Keen, N.; Taylor, S. S. *The Journal of Cell Biology* **2003**, *161*, 267-280.
(16) Keen, N.; Taylor, S. *Nat Rev Cancer* **2004**, *4*, 927-936.
(17) Knapp, S.; Arruda, P.; Blagg, J.; Burley, S.; Drewry, D. H.; Edwards, A.; Fabbro, D.; Gillespie, P.; Gray, N. S.; Kuster, B.; Lackey, K. E.; Mazzafera, P.; Tomkinson, N. C. O.; Willson, T. M.; Workman, P.; Zuercher, W. J. *Nat Chem Biol* **2013**, *9*, 3-6.
(18) Krause, D. S.; Van Etten, R. A. *New England Journal of Medicine* **2005**, *353*, 172-187.
(19) Zhang, J.; Yang, P. L.; Gray, N. S. *Nat Rev Cancer* **2009**, *9*, 28-39.
(20) Knight, Z. A.; Shokat, K. M. *Chemistry & Biology* **2005**, *12*, 621-637.
(21) Kornev, A. P.; Taylor, S. S.; Ten Eyck, L. F. *Proceedings of the National Academy of Sciences* **2008**, *105*, 14377-14382.
(22) Bain, J.; Plater, L.; Elliott, M.; Shpiro, N.; Hastie, C. J.; McLauchlan, H.; Klevernic, I.; Arthur, J. S. C.; Alessi, D. R.; Cohen, P. *Biochemical Journal* **2007**, *408*, 297-315.
(23) Bain, J.; McLauchlan, H.; Elliott, M.; Cohen, P. *Biochemical Journal* **2003**, *371*, 199-204.
(24) Fabian, M. A.; Biggs, W. H.; Treiber, D. K.; Atteridge, C. E.; Azimioara, M. D.; Benedetti, M. G.; Carter, T. A.; Ciceri, P.; Edeen, P. T.; Floyd, M.; Ford, J. M.; Galvin, M.; Gerlach, J. L.; Grotzfeld, R. M.; Herrgard, S.; Insko, D. E.; Insko, M. A.; Lai, A. G.; Lelias, J.-M.; Mehta, S. A.; Milanov, Z. V.; Velasco, A. M.; Wodicka, L. M.; Patel, H. K.; Zarrinkar, P. P.; Lockhart, D. J. *Nat Biotech* **2005**, *23*, 329-336.
(25) Huang, D. Z.; Zhou, T.; Lafleur, K.; Nevado, C.; Caflisch, A. *Bioinformatics* **2010**, *26*, 198-204.
(26) Taylor, S. S.; Kornev, A. P. *Trends in Biochemical Sciences* **2011**, *36*, 65-77.
(27) Nagar, B.; Bornmann, W. G.; Pellicena, P.; Schindler, T.; Veach, D. R.; Miller, W. T.; Clarkson, B.; Kuriyan, J. *Cancer Research* **2002**, *62*, 4236-4243.
(28) Schindler, T.; Bornmann, W.; Pellicena, P.; Miller, W. T.; Clarkson, B.; Kuriyan, J. *Science* **2000**, *289*, 1938-1942.
(29) Kornev, A. P.; Haste, N. M.; Taylor, S. S.; Ten Eyck, L. F. *Proceedings of the National Academy of Sciences* **2006**, *103*, 17783-17788.
(30) O'Brien, S. G.; Guilhot, F.; Larson, R. A.; Gathmann, I.; Baccarani, M.; Cervantes, F.; Cornelissen, J. J.; Fischer, T.; Hochhaus, A.; Hughes, T.; Lechner, K.; Nielsen, J. L.; Rousselot, P.; Reiffers, J.; Saglio, G.; Shepherd, J.; Simonsson, B.; Gratwohl, A.; Goldman, J. M.; Kantarjian, H.; Taylor, K.; Verhoef, G.; Bolton, A. E.; Capdeville, R.; Druker, B. J.; Durrant, S.; Schwarer, A.; Joske, D.; Seymour, J.; Grigg, A.; Ma, D.; Arthur, C.; Bradstock, K.; Joshua, D.; Louwagie, A.; Martiat, P.; Straetmans, N.; Bosly, A.; Shustik, C.; Lipton, J.; Forrest, D.; Walker, I.; Roy, D. C.; Rubinger, M.; Bence-Bruckler, I.; Kovacs, M.; Turner, A. R.; Birgens, H.; Bjerrum, O.; Facon, T.; Harousseau, J. L.; Tulliez, M.; Guerci, A.; Blaise, D.; Maloisel, F.; Michallet, M.; Hossfeld, D.; Mertelsmann, R.; Andreesen, R.; Nerl, C.; Freund, M.; Gattermann, N.; Hoeffken, K.; Ehninger, G.; Deininger, M.; Ottmann, O.; Peschel, C.; Fruehauf, S.; Neubauer, A.; Le Coutre, P.; Aulitzky, W.; Fanin, R.; Rosti, G.; Mandelli, F.; Morra, E.; Carella, A.; Lazzarino, M.; Petrini, M.; Ferrini, P. R.; Nobile, F.; Liso, V.; Ferrara, F.; Rizzoli, V.; Fioritoni, G.; Martinelli, G.; Ossenkoppele, G.; Browett, P.; Gedde-Dahl, T.; Tangen, J. M.; Dahl, I.; Odriozola, J.; Boluda, J. C. H.; Steegmann, J. L.; Canizo, C.; Sureda, A.; Diaz, J.; Granena, A.; Fernandez, M. N.; Stenke, L.; Paul, C. *New England Journal of Medicine* **2003**, *348*, 994-1004.
(31) Druker, B. J.; Guilhot, F.; O'Brien, S. G.; Gathmann, I.; Kantarjian, H.; Gattermann, N.; Deininger, M. W. N.; Silver, R. T.; Goldman, J. M.; Stone, R. M.; Cervantes, F.; Hochhaus, A.; Powell, B. L.; Gabrilove, J. L.; Rousselot, P.; Reiffers, J.; Cornelissen, J. J.; Hughes, T.; Agis, H.; Fischer, T.; Verhoef, G.; Shepherd, J.; Saglio, G.; Gratwohl, A.; Nielsen, J. L.; Radich, J. P.;

Simonsson, B.; Taylor, K.; Baccarani, M.; So, C.; Letvak, L.; Larson, R. A.; Investigators, I. *New England Journal of Medicine* **2006**, *355*, 2408-2417.
(32) Kantarjian, H.; Sawyers, C.; Hochhaus, A.; Guilhot, F.; Schiffer, C.; Gambacorti-Passerini, C.; Niederwieser, D.; Resta, D.; Capdeville, R.; Zoellner, U.; Talpaz, M.; Druker, B.; Int, S. T. I. C. M. L. S. G. *New England Journal of Medicine* **2002**, *346*, 645-652.
(33) Leproult, E.; Barluenga, S.; Moras, D.; Wurtz, J.-M.; Winssinger, N. *Journal of Medicinal Chemistry* **2011**, *54*, 1347-1355.
(34) van Linden, O. P. J.; Kooistra, A. J.; Leurs, R.; de Esch, I. J. P.; de Graaf, C. *Journal of Medicinal Chemistry* **2013**, *57*, 249-277.
(35) Bhattacharya, S. K.; Aspnes, G. E.; Bagley, S. W.; Boehm, M.; Brosius, A. D.; Buckbinder, L.; Chang, J. S.; Dibrino, J.; Eng, H.; Frederick, K. S.; Griffith, D. A.; Griffor, M. C.; GuimarÃ£es, C. R. W.; Guzman-Perez, A.; Han, S.; Kalgutkar, A. S.; Klug-McLeod, J.; Garcia-Irizarry, C.; Li, J.; Lippa, B.; Price, D. A.; Southers, J. A.; Walker, D. P.; Wei, L.; Xiao, J.; Zawistoski, M. P.; Zhao, X. *Bioorganic & Medicinal Chemistry Letters* **2012**, *22*, 7523-7529.
(36) Davis, M. I.; Hunt, J. P.; Herrgard, S.; Ciceri, P.; Wodicka, L. M.; Pallares, G.; Hocker, M.; Treiber, D. K.; Zarrinkar, P. P. *Nat Biotech* **2011**, *29*, 1046-1051.
(37) Iwata, H.; Oki, H.; Okada, K.; Takagi, T.; Tawada, M.; Miyazaki, Y.; Imamura, S.; Hori, A.; Lawson, J. D.; Hixon, M. S.; Kimura, H.; Miki, H. *ACS Medicinal Chemistry Letters* **2012**, *3*, 342-346.
(38) Su, B.-H.; Huang, Y.-S.; Chang, C.-Y.; Tu, Y.-S.; Tseng, Y. *Molecules* **2013**, *18*, 13487-13509.
(39) Lovering, F.; McDonald, J.; Whitlock, G. A.; Glossop, P. A.; Phillips, C.; Bent, A.; Sabnis, Y.; Ryan, M.; Fitz, L.; Lee, J.; Chang, J. S.; Han, S.; Kurumbail, R.; Thorarensen, A. *Chemical Biology & Drug Design* **2012**, *80*, 657-664.
(40) Blanc, J.; Geney, R.; Menet, C. *Anti-Cancer Agents in Medicinal Chemistry* **2013**, *13*, 731-747.
(41) Okram, B.; Nagle, A.; AdriÃ¡n, F. J.; Lee, C.; Ren, P.; Wang, X.; Sim, T.; Xie, Y.; Wang, X.; Xia, G.; Spraggon, G.; Warmuth, M.; Liu, Y.; Gray, N. S. *Chemistry & Biology* **2006**, *13*, 779-786.
(42) Liu, Y.; Gray, N. S. *Nat Chem Biol* **2006**, *2*, 358-364.
(43) Poulikakos, P. I.; Zhang, C.; Bollag, G.; Shokat, K. M.; Rosen, N. *Nature* **2010**, *464*, 427-U126.
(44) Lavoie, H.; Thevakumaran, N.; Gavory, G. l.; Li, J. J.; Padeganeh, A.; Guiral, S. b.; Duchaine, J.; Mao, D. Y. L.; Bouvier, M.; Sicheri, F.; Therrien, M. *Nat Chem Biol* **2013**, *9*, 428-436.
(45) Wang, L.; Perera, B. G. K.; Hari, S. B.; Bhhatarai, B.; Backes, B. J.; Seeliger, M. A.; SchÃ¼rer, S. C.; Oakes, S. A.; Papa, F. R.; Maly, D. J. *Nat Chem Biol* **2012**, *8*, 982-989.
(46) Krishnamurty, R.; Brigham, J. L.; Leonard, S. E.; Ranjitkar, P.; Larson, E. T.; Dale, E. J.; Merritt, E. A.; Maly, D. J. *Nat Chem Biol* **2013**, *9*, 43-50.
(47) Wood, E. R.; Truesdale, A. T.; McDonald, O. B.; Yuan, D.; Hassell, A.; Dickerson, S. H.; Ellis, B.; Pennisi, C.; Horne, E.; Lackey, K.; Alligood, K. J.; Rusnak, D. W.; Gilmer, T. M.; Shewchuk, L. *Cancer Research* **2004**, *64*, 6652-6659.
(48) Xu, W.; Doshi, A.; Lei, M.; Eck, M. J.; Harrison, S. C. *Molecular Cell* **1999**, *3*, 629-638.
(49) Hubbard, S. R.; Mohammadi, M.; Schlessinger, J. *Journal of Biological Chemistry* **1998**, *273*, 11987-11990.
(50) Lu, C.; Mi, L.-Z.; SchÃ¼rpf, T.; Walz, T.; Springer, T. A. *Journal of Biological Chemistry* **2012**, *287*, 38244-38253.
(51) Macdonald-Obermann, J. L.; Adak, S.; Landgraf, R.; Piwnica-Worms, D.; Pike, L. J. *Journal of Biological Chemistry* **2013**, *288*, 30773-30784.

(52) Zuccotto, F.; Ardini, E.; Casale, E.; Angiolini, M. *Journal of Medicinal Chemistry* **2009**, *53*, 2681-2694.
(53) Zhang, J. M.; Yang, P. L.; Gray, N. S. *Nat. Rev. Cancer* **2009**, *9*, 28.
(54) Knight, Z. A.; Shokat, K. M. *Chem. Biol.* **2005**, *12*, 621.
(55) Pinna, L.; Cohen, P. W.; Lawrence, D. S. In *Inhibitors of Protein Kinases and Protein Phosphates*; Springer Berlin Heidelberg: 2005; Vol. 167, p 11-44.
(56) Kayser, K. J.; Glenn, M. P.; Sebti, S. M.; Cheng, J. Q.; Hamilton, A. D. *Bioorganic & Medicinal Chemistry Letters* **2007**, *17*, 2068-2073.
(57) Kayser-Bricker, K. J.; Glenn, M. P.; Lee, S. H.; Sebti, S. M.; Cheng, J. Q.; Hamilton, A. D. *Bioorganic & Medicinal Chemistry* **2009**, *17*, 1764-1771.
(58) Lavogina, D.; Enkvist, E.; Uri, A. *ChemMedChem* **2010**, *5*, 23-34.
(59) Blum, G.; Gazit, A.; Levitzki, A. *Biochemistry* **2000**, *39*, 15705-15712.
(60) Castanedo, G.; Clark, K.; Wang, S.; Tsui, V.; Wong, M.; Nicholas, J.; Wickramasinghe, D.; Marsters Jr, J. C.; Sutherlin, D. *Bioorganic & Medicinal Chemistry Letters* **2006**, *16*, 1716-1720.
(61) Lienhard, G. E.; Secemski, I. I. *Journal of Biological Chemistry* **1973**, *248*, 1121-1123.
(62) Dey, M.; Cao, C.; Dar, A. C.; Tamura, T.; Ozato, K.; Sicheri, F.; Dever, T. E. *Cell* **2005**, *122*, 901-913.
(63) Dar, A. C.; Dever, T. E.; Sicheri, F. *Cell* **2005**, *122*, 887-900.
(64) Jencks, W. P. *Proceedings of the National Academy of Sciences* **1981**, *78*, 4046-4050.
(65) Hines, A. C.; Parang, K.; Kohanski, R. A.; Hubbard, S. R.; Cole, P. A. *Bioorganic Chemistry* **2005**, *33*, 285-297.
(66) Enkvist, E.; Lavogina, D.; Raidaru, G.; Vaasa, A.; Viil, I.; Lust, M.; Viht, K.; Uri, A. *Journal of Medicinal Chemistry* **2006**, *49*, 7150-7159.
(67) Ho, M.; Wilson, B. A.; Katampe, I. *Bioorganic & Medicinal Chemistry Letters* **1996**, *6*, 899-902.
(68) Meyer, S. C.; Shomin, C. D.; Gaj, T.; Ghosh, I. *Journal of the American Chemical Society* **2007**, *129*, 13812-13813.
(69) Loog, M.; Uri, A.; Raidaru, G.; JÃ¤rv, J.; Ek, P. *Bioorganic & Medicinal Chemistry Letters* **1999**, *9*, 1447-1452.
(70) Enkvist, E.; Raidaru, G.; Vaasa, A.; Pehk, T. n.; Lavogina, D.; Uri, A. *Bioorganic & Medicinal Chemistry Letters* **2007**, *17*, 5336-5339.
(71) Nam, N.-H.; Lee, S.; Ye, G.; Sun, G.; Parang, K. *Bioorganic & Medicinal Chemistry* **2004**, *12*, 5753-5766.
(72) Loog, M.; Uri, A.; JÃ¤rv, J.; Ek, P. *FEBS Letters* **2000**, *480*, 244-248.
(73) Lavogina, D.; Lust, M.; Viil, I.; KÃ¶nig, N.; Raidaru, G.; Rogozina, J.; Enkvist, E.; Uri, A.; Bossemeyer, D. *Journal of Medicinal Chemistry* **2008**, *52*, 308-321.
(74) Shomin, C. D.; Meyer, S. C.; Ghosh, I. *Bioorganic & Medicinal Chemistry* **2009**, *17*, 6196-6202.

CHAPTER 2

Rational design of DFG-out inhibitors

This chapter begins to address the question of "*How does binding an "inactive" fold influence kinase inhibitor selectivity?"* Specifically, this chapter regards the targeting of the DFG-out inactive kinase conformation. (For an introduction to DFG-out inhibitors see Chapter 1.4.) Derivatives of a DFG-in inhibitor (dasatinib) are created to target the DFG-out fold. Creation of these analogs allows for a head-to-head comparison of inhibitor selectivity with dasatinib. Using a large kinase panel, we determine if targeting the DFG-out conformation is a valid strategy for improving inhibitor selectivity. To date, this work represents the most extensive analysis of the impact of binding the inactive DFG-out fold on inhibitor selectivity. Additionally, one DFG-out derivative is discovered to have exceptionally high activity in the treatment of aggressive breast cancer cell lines.

2.1 Introduction

The DFG-out conformation has long been stated to be non-conserved across protein kinases. Therefore it has been assumed that targeting the DFG-out fold should entail high inhibitor selectivity. Despite this assumption, an increasing number of kinases have been observed to adopt the DFG-out conformation. These observations led to the development of the hypothesis that most, if not all, kinases are capable of adopting the DFG-out conformation. Toward this end the promiscuous kinase inhibitor dasatinib (Figure 2.1) was rationally augmented to provide analogs designed to target the DFG-out fold.

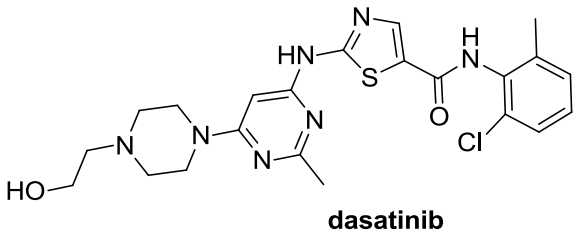

dasatinib

Figure 2.1. Chemical structure of dasatinib.

2.2 Results and Discussion

In order to assess how binding the DFG-out conformation influences kinase inhibitor selectivity, a complementary pair of inhibitors needed to be developed. A strategy which has previously been applied toward transforming a DFG-in inhibitor into a DFG-out inhibitor was employed.[2,3] The drug dasatinib,[4,5] a pan-kinase DFG-in inhibitor, was selected as a starting point. Briefly, the structure of dastanib bound to Abl[6] was overlayed with several other structures of Abl complexed with DFG-out inhibitors (such as imatinib[7], Figure 2.2A). This overlay revealed a distinct molecular overlap between dasatinib and the DFG-out inhibitors via a common phenyl ring. The juxtaposition suggested that incorporation of a benzamide moiety into dasatinib would result in an inhibitor which would bind the DFG-out fold.

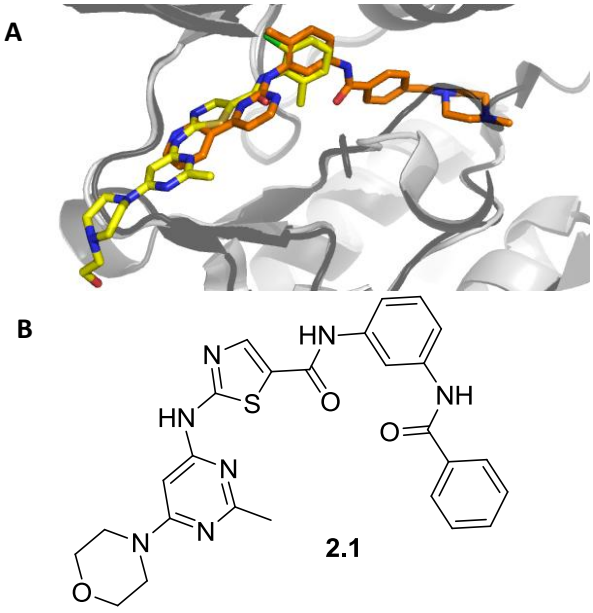

Figure 2.2. Design of a dasatinib derivative that will bind the DFG-out conformation. A) Overlay of dasatinib (yellow) and imatinib (orange) respectively bound to c-Abl (PDBIDS: 2GQG &1IEP); and B) Chemical structure for model compound **2.1** along with inhibition constants for c-Src and homologous kinase Abl derived from an activity based assay[1]..

A model compound that incorporated this benzamide feature was synthesized (Figure 2.2B). In order to make comparisons with dasatinib it was necessary for the DFG-out analog to be comparable in binding affinity. We selected two kinases that are already known to adopt the DFG-out fold and conducted an activity-based phosphorylation assay to assess inhibitor potency. It was found that compound **2.1** strongly inhibited both Abl and Src kinase, which are also potently bound by the parent dasatinib scaffold.[8]

The activity of compound **2.1** was subsequently determined against a panel of the top twenty-five kinase targets of dasatinib[8]. All kinases selected for profiling exhibited high affinity for DFG-out compound **2.1** (Figure 2.3). As a control, five kinases which poorly

bind dasatinib were also included in the panel; compound **2.1** did not display appreciable affinity for these kinases (data not shown). Altogether, these data begin to imply that most kinases that are targets of dasatinib can adopt the DFG-out fold.

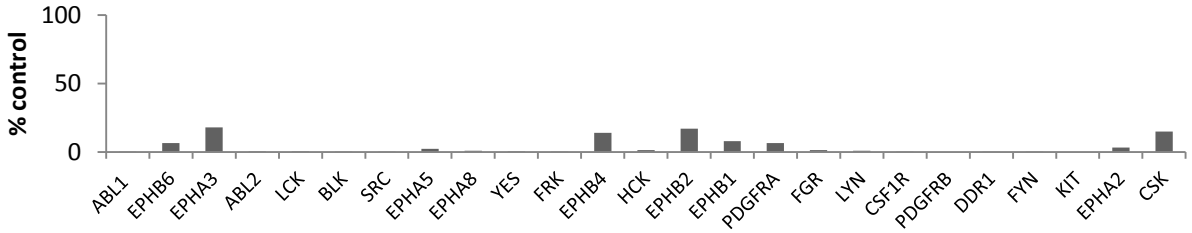

Figure 2.3. Selectivity profile for compound **2.1** using a single-point binding assay. Compound 2.1 was screened at a final concentration of 1 μM. Kinases were selected based upon affinity for dasatinib with the kinases displaying the highest potency listed on the left. For tabulated data see experimental section.

Targeted kinase inhibitor therapy has revealed that cancer cells are prone to acquisition of mutations which confer resistance to small-molecule inhibitors[9-12]. Compound **2.1** and dasatinib were assayed against a representative "gatekeeper mutation" in c-Src kinase, a mutation that has been observed in many forms of cancer. While dasatinib retains micromolar affinity (Figure 2.4), compound **2.1** disappointingly displayed negligible binding to the mutant kinase (data not shown).

Compound **2.1** was minimally altered to incorporate features commonly found in other DFG-out inhibitors. Specifically, a m-trifluoromethyl substituent was incorporated into in the benzamide moiety (compound **2.2**), and a methyl group was incorporated in the central phenyl ring (compound **2.3**). These features can be found in a similar position in inhibitors such as nilotinib and imatinib.

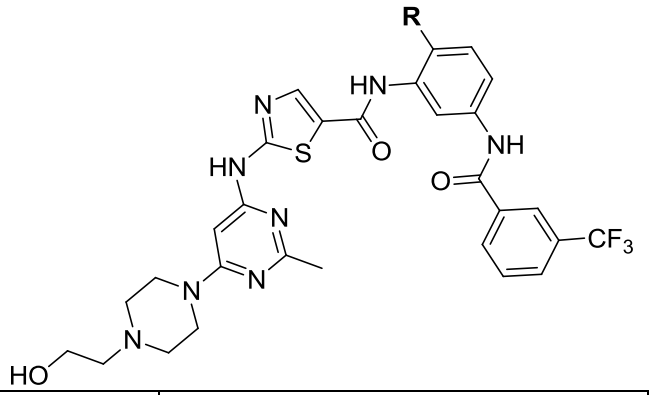

	K_i (nM)				
Compound	**R =**	**Src wt**	**Abl wt**	**Src T341I**	**Src T341M**
dasatinib	n/a	< 0.6	< 3.4	1,586	3,300
2.2	H	< 0.6	< 3.4	56	403
2.3	Me	< 0.6	< 3.4	2.2	3.1

Figure 2.4. Biochemical kinase inhibition data for dasatinib and two DFG-out derivatives. from an activity-based continuous kinase inhibition assay.

Both of these chemical changes positively contributed to inhibition of the gatekeeper mutant (Figure 2.4). Compound **2.3**

is one of the most potent inhibitors of this important resistance mutation to date. Currently, ponatinib[13] (which has recently been clinically withdrawn) is the only viable option for treating the gatekeeper mutation, so the discovery of **2.3** can be regarded as a finding of potential therapeutic significance.

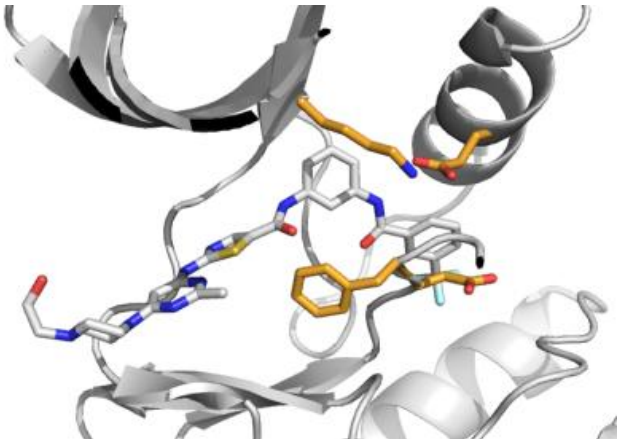

Figure 2.5. X-ray co-crystal structure of compound **2.2** bound to c-Src kinase (2.61 Å resolution). The DFG motif in addition to the c-helix Glu and catalytic Lys are highlighted in orange. Data kindly provided by Frank Kwarcinski (Soellner Lab).

After obtaining the encouraging initial results for the DFG-out analogs, it was desired to confirm that they were indeed binding the proposed structural conformation. Compound **2.2** provided an adequate resolution (2.61 Å) structure bound to c-Src (Figure 2.5). Compound **2.2** was observed to bind c-Src with a clearly flipped DFG motif. The m-trifluormethyl benzamide moiety of **2.2** correlates with density in the DFG-out pocket, and the DFG motif is adequately resolved in the predicted inactive conformation.

After binding the DFG-out fold was structurally confirmed, compounds **2.2** and **2.3** were profiled[14] against a large panel of 131 kinases alongside dasatinib. In agreement with the preliminary profiling of **2.1**, the DFG-out inhibitors were not more selective than dasatinib (Figure 2.6). To the contrary, compound **2.3** was found to be as poorly selective as dasatinib (S(35) = 0.20). Altogether, these data indicate that binding the DFG-out fold does not significantly improve kinase inhibitor selectivity.

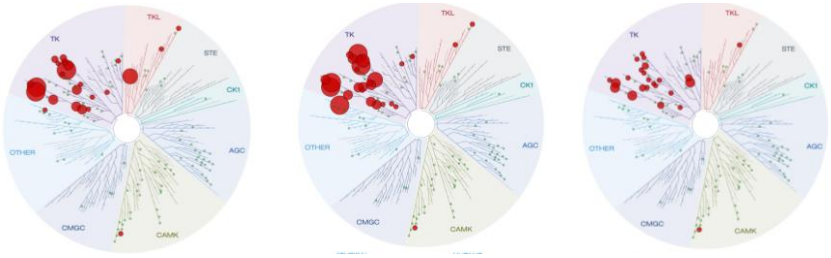

dasatinib **2.2** **2.3**

Figure 2.6. Kinome profiling of dasatinib, **2.2**, and **2.3** using a single point binding assay. All compounds were screened at a final concentration of 500 nM. A tabulated list of binding data is included in the experimental section.

Given the high biochemical similarity of compound **2.3** and dasatinib, it was surprising to observe differences in the treatment of several cell lines (Table 2.1). Compound **2.3** was more effective than dasatinib in treating two aggressive breast cancer cell lines (MDA-MB-453 and MDA-MB-23) in 2-dimensional cell culture models. Further investigation of compound **2.3** in three-dimensional culture conditions revealed an amplified performance of compound **2.3** relative to dasatinib (twenty-fold advantage). Cell culture under 3-D conditions is considered to be more representative of *in vivo* conditions. As a crude toxicity model human mammary epithelial (HME) cells were also treated. The Therapeutic Index (T.I.) was significantly improved for **2.3** relative to dasatinib (T.I. = 200, and 132 respectively). In this case T.I. is defined as HME GI_{50}/MDA-MB-231 (3D) GI_{50}.

	GI_{50} (μM)			
compound	**MDA-MB-453 (2D)**	**MDA-MB-231 (2D)**	**MDA-MB-231 (3D)**	**HME (2D)**
dasatinib	6.17	0.15	0.043	5.7
2.3	0.04	0.08	0.002	0.4

Table 2.1. Treatment of breast cancer cell lines using compound **2.3** and dasatinib. Data kindly provided by Michael Steffey (Soellner Lab).

The divergence in *in cellulo* activity for dasatinib and compound **2.3** was somewhat puzzling. It is possible that factors within the cell may influence inhibitor binding that would not be detected using the isolated recombinant kinase assays employed for profiling. Additionally, it is also possible that compound **2.3** may have ATPase targets that dasatinib does not. In order to address both of these issues the *in cellulo* selectivity for ATP-binding proteins was determined using KiNativ profiling[15] (Table 2.2). Briefly, the KiNativ assay employs a biotinylated acyl phosphate of ATP the irreversibly reacts specifically with conserved lysines within the ATP-binding site of protein kinases. Upon treatment with a small molecule, any reduction in labeling of a given kinase relative to control can be attributed to inhibitor binding. The KiNativ probe is also known to label other ATPases in a similar fashion, which makes it particularly well suited for answering the current selectivity questions.

Kinase	dasatinib	Compound 2.3
EphA2	>96	68.7
EphB2	>96	>96
LYN	>95	>95
EphB4	>93	88.9
ACK	>92	79.9
ABL,ARG	>85	>85
SRC	>84	>84
QSK	>70	-13.1
CSK	98.6	96.5
FYN,SRC,YES	96.7	95.3
CSK	96.5	94
ZAK	93.7	93.9
MAP2K5	88	40.5
STLK5	78.7	-7.5
KHS1	75.8	38.9
TEC	73	64
Wee1	69.2	21.9
ILK	67.9	25.7
p38a	67.9	95.2
TESK1	65.6	12.7
STLK5	59.5	-6.7
MAP3K4	54.8	28.8
MAP3K1	47.6	36.4
KHS2	36.4	11.6
GCK	32.8	41.8
EGFR	18.8	46.1
ROCK1,ROCK2	15.3	35.1
p38b	2.4	76.6

Table 2.2. Selected KiNativ profiling data for compound **2.3** and dasatinib. Both inhibitors were screened at a final concentration of 0.5 µM. The twenty-five kinases shown are ranked in terms of dasatinib affinity.

The KiNativ data show that selectivity profiles for dasatinib and compound **2.3** largely overlap, which is in good agreement with biochemical profiling experiments. One difference does stand out though; compound **2.3** is a potent inhibitor of p38β kinase whereas dasatinib is not. It was considered that p38β inhibition might explain the improved performance of compound **2.3** relative to dasatinib. This was briefly investigated in an experiment using a combination of dasatinib with BIRB-796 (BIRB-796 is a well established inhibitor of p38β[16]) in the treatment MDA-MB-231 cancer cells (Figure 2.7). The growth inhibition from the inhibitor combination was greater than what would mathematically be expected from additive inhibition. Thus we suggest that improved cellular performance of compound **2.3** relative to dasatinib is, in part, due to p38β inhibition.

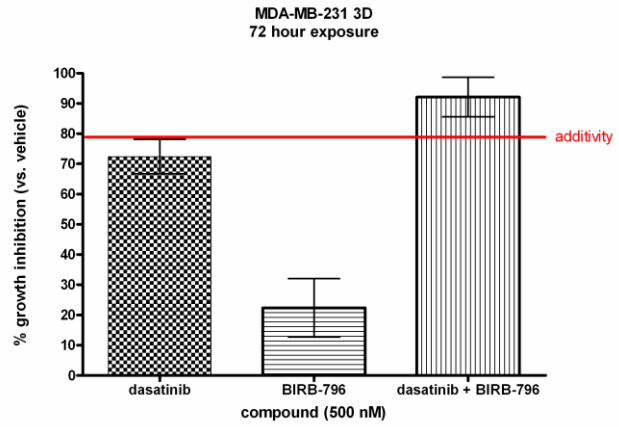

Figure 2.7. Assessment of dual inhibitor treatment of a breast cancer cell line using dasatinib and a p38β inhibitor (BIRB-796). Data kindly provided by Mike Steffey.

2.3 Conclusions

In this chapter we have compared the selectivity profiles of dasatinib and two derivatives which were designed to bind the DFG-out conformation of protein kinases. It was found that were few differences between the profile of dasatinib, compound **2.2**, and compound **2.3**. Overall these data are consistent with the hypothesis that targeting the DFG-out conformation is not a valid approach to improving kinase inhibitor selectivity.

One of the novel DFG-out derivatives (compound **2.3**) displayed a surprising increase in the effectiveness of treating cancer cells. *In cellulo* profiling revealed a minor selectivity difference between **2.3** and dastinib. Specifically **2.3** strongly inhibited p38β whereas dasatinib does not. In combination experiments it was shown that adding a p38β inhibitor to dasatinib treatment significantly improves performance in slowing breast cancer cell growth.

2.4 Experimental Section

GENERAL SYNTHETIC METHODS. Unless otherwise noted, all reagents were obtained via commercial sources and used without further purification. Tetrahydrofuran (THF) and dichloromethane (CH_2Cl_2) were dried over alumina under a nitrogen atmosphere. All ^{1}H and ^{13}C NMR spectra were measured with a Varian MR400, Varian VNMRS 500 or Inova 500 spectrometer. Mass Spectrometry (HRMS) was carried out by the University of Michigan Mass Spectrometry Facility (J. Windak, director).

SYNTHESIS OF COMPOUNDS 2.S-1- 2.3

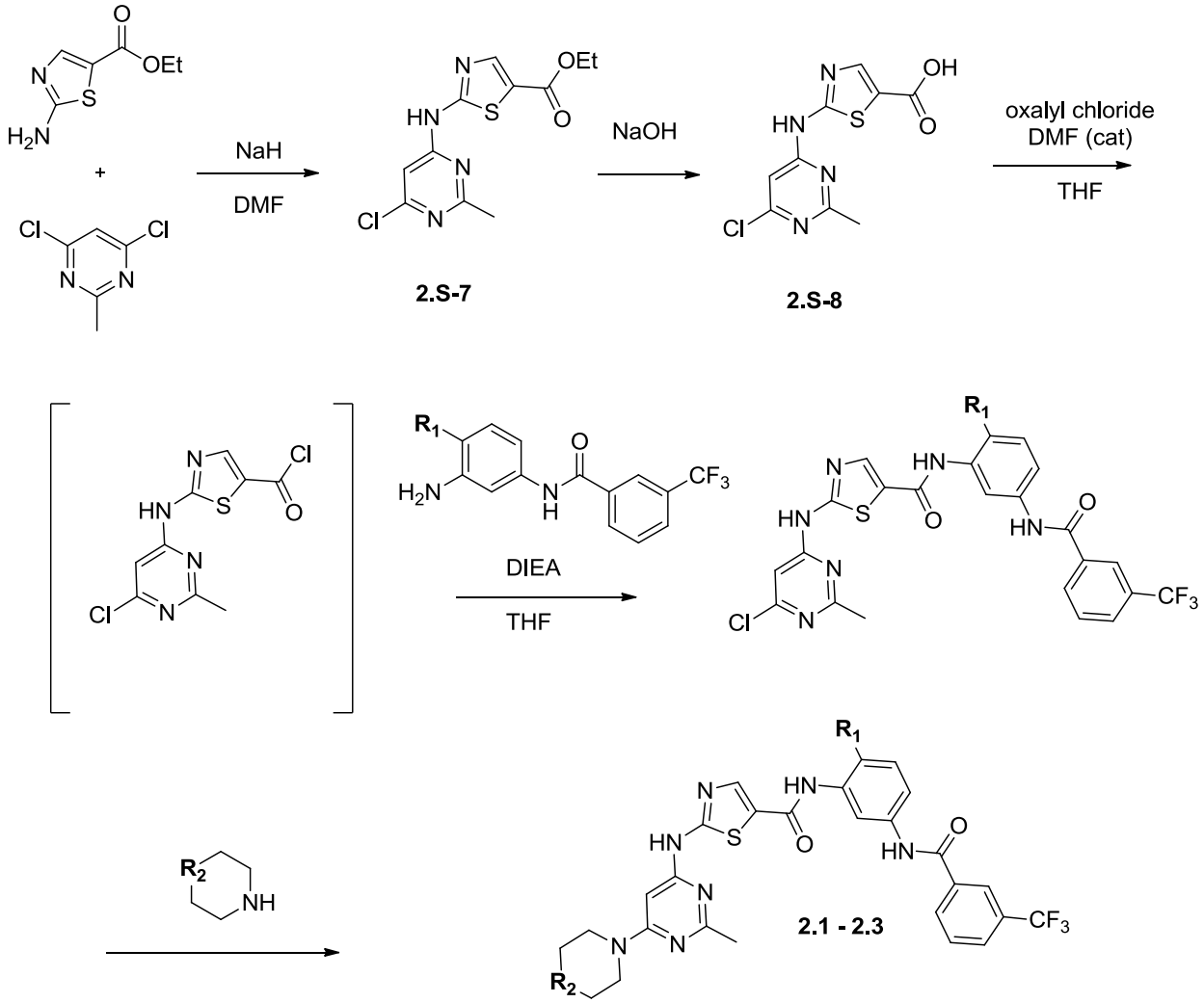

Scheme 2.S-1. Synthesis of compounds **2.1 - 2.3.**

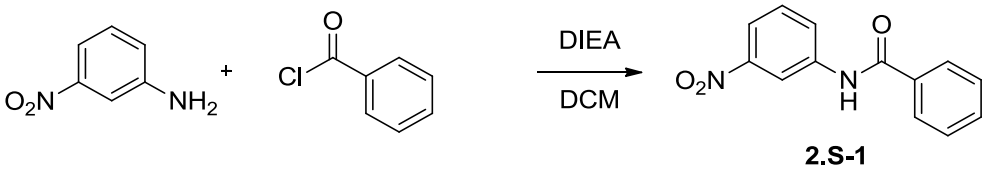

Synthesis of 2.S-1: Compound **2.S-1** was synthesized using a literature protocol. Product yields and spectral properties agreed with those reported.

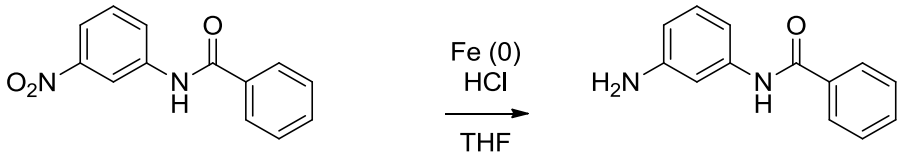

2.S-1 **2.S-2**

Synthesis of 2.S-2: Compound **2.S-2** was synthesized using a literature protocol. Product yields and spectral properties agreed with those reported. **Spectral data.** ^{1}H NMR (500 MHz, Chloroform-*d*) δ 7.86 (d, *J* = 7.6 Hz, 2H), 7.77 (s, 1H), 7.56 (t, *J* = 7.4 Hz, 1H), 7.54 – 7.45 (m, 2H), 7.33 (d, *J* = 2.0 Hz, 1H), 7.14 (t, *J* = 7.9 Hz, 1H), 6.80 (dd, *J* = 8.0, 1.9 Hz, 1H), 6.49 (dd, *J* = 8.0, 2.1 Hz, 1H), 3.75 (s, 2H). ^{13}C NMR (100 MHz, cdcl3) δ 165.65, 147.30, 138.92, 135.12, 131.74, 129.75, 128.74, 126.94, 111.28, 109.96, 106.77; HRMS-ESI (*m/z*): $[M + H]^+$ calcd for $C_{13}H_{12}N_2O$, 213.1022; found 213.1035.

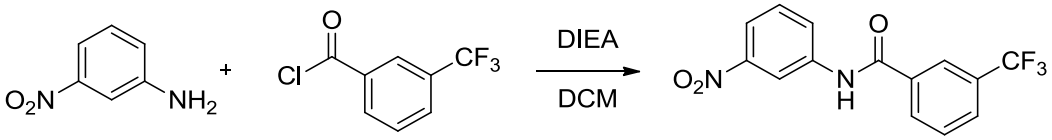

2.S-3

Synthesis of 2.S-3: 3-nitroaniline (7.5 g, 54.3 mmol) was added to an oven-dried flask. Dichloromethane (271 mL) was added. The reaction mixture was then cooled to 0^{o}C using an ice bath. 3-trifluoromethylbenzoyl chloride (12.4 g, 59.7 mmol) was then added, followed by diisopropylethylamine (8.42 g, 65.2 mmol). The reaction mixture was then allowed to warm to room temperature and stir overnight. Dichloromethane (270 mL) was then added. The reaction mixture was then washed with 1 N HCl (270 mL), the aqueous layer was then back-extracted three times with dichloromethane (100 mL). The organic layers were then collected and dried over sodium sulfate. The solvent was then removed under reduced pressure. The crude reaction mixture was then purified via silica gel chromatography using a Biotage Isolera One to yield 16 g of compound **2.S-3** as a light yellow solid (95 % yield). **Spectral data.** ^{1}H NMR (400 MHz, DMSO-d_6): δ 10.92 (s, 1 H), 8.77-8.74 (m, 1 H), 8.32-8.26 (m, 2 H), 8.21-8.17 (m, 1 H), 7.98-7.92 (m, 2 H), 7.80-7.74 (m, 1 H), 7.66-7.61 (m, 1 H); ^{19}F NMR (376 MHz, dmso) δ -61.15; HRMS-ESI (*m/z*): $[M + H]^+$ calcd for $C_{14}H_9F_3N_2O_3$, 311.0638; found 311.0638.

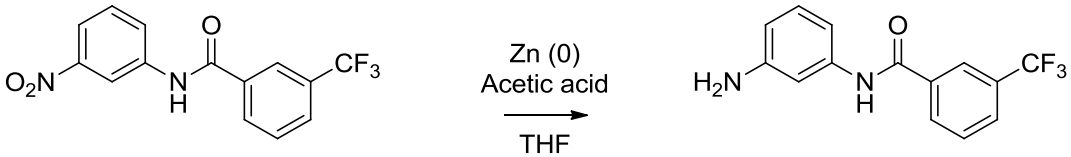

2.S-3 **2.S-4**

Synthesis of 2.S-4: Compound **2.S-3** (2.3 g, 7.2 mmol) was added to an oven dried flask. Zinc dust (2.3 g, 34.8 mmol) was then added. The reaction vessel was evacuated using a vacuum pump and subsequently filled with N_2; this was repeated for a total of three cycles. Tetrahydrofuran (24 mL) was added, followed by acetic acid (4 mL). The reaction mixture was then allowed to stir at room temperature for 48 hours. The crude reaction mixture was then filtered through celite. Solvent was removed under reduced pressure. The reaction mixture was then dissolved in ethyl actetate (100 mL) and washed with 1 N NaOH (100 mL), followed by a brine wash (100 mL). The organic layer was then dried over sodium sulfate. The solvent was removed under reduced pressure to provide a viscous yellow oil. The oil was triturated with an ether/hexanes mixture to provide compound **2.S-4** as a light yellow solid (90 % yield). **Spectral data.** ^{1}H NMR (400 MHz, DMSO-d_6): δ 10.15 (s, 1 H), 8.23-8.17 (m, 2 H), 7.93-7.89 (m, 1 H), 7.76-7.70 (m, 1 H), 7.06-7.03 (m, 1 H), 6.97-6.91 (m, 1 H), 6.85-6.80 (m, 1 H), 6.32-6.27 (m, 1 H), 5.09 (s, 2 H); HRMS-ESI (*m/z*): $[M + H]^+$ calcd for $C_{14}H_{11}F_3N_2O$, 281.0896; found 281.0905.

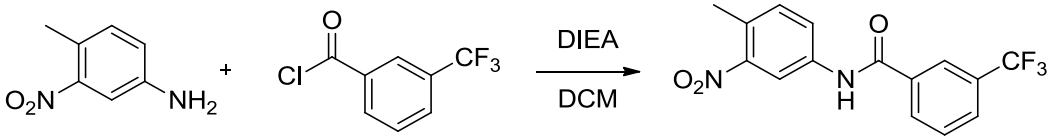

2.S-5

Synthesis of 2.S-5: 4-methyl-3-nitroaniline (2.0 g, 13.1 mmol) was added to an oven-dried flask. Tetrahydrofuran (66 mL) was added. The reaction mixture was then cooled to 0^{o}C using an ice bath. 3-trifluoromethylbenzoyl chloride (2.742 g, 13.1 mmol) was then added, followed by diisopropylethylamine (2.039 g, 15.77 mmol). The reaction mixture was then allowed to warm to room temperature and stir overnight. Tetrahydrofuran was then removed via rotary vaporization. The crude mixture was then suspended in water, filtered, and then rinsed with water twice. After drying 4.1 g of **2.S-5** as a light yellow solid was obtained (96 % yield). **Spectral data.** ^{1}H NMR (400 MHz, DMSO-d_6) δ 10.77 (s, 1H), 8.50 (d, *J* = 2.3 Hz, 1H), 8.31 – 8.22 (m, 2H), 7.97 (t, *J* = 9.4 Hz, 2H), 7.77 (t, *J* = 7.8 Hz, 1H), 7.47 (d, *J* = 8.4 Hz, 1H), 1.23 (s, 3 H) ; ^{19}F NMR (376 MHz, dmso) δ -61.14.; HRMS-ESI (*m/z*): $[M + H]^+$ calcd for $C_{15}H_{11}F_3N_2O_3$, 325.0795; found 325.0794.

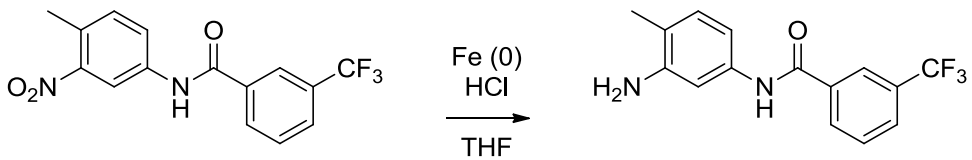

2.S-5 **2.S-6**

Synthesis of 2.S-6: Compound **2.S-5** (2.0 g, 6.2 mmol) and iron (1.72 g, 30.8 mmol) were added to an oven-dried flask. Ethanol (25 mL) and water (6.2 mL) were then added, followed by the addition of several drops of concentrated Hydrochloric Acid. The reaction mixture was then heated to reflux for 90 minutes. The reaction mixture was then allowed to cool to room temperature and filtered through celite. Ethanol was removed via rotary vaporization. The crude reaction was then suspended in water and filtered. After drying 1.4 g of **2.S-6** as an off-white solid was obtained (78 % yield). **Spectral data.** ^{1}H NMR (400 MHz, DMSO-d_6) δ 10.11 (s, 1H), 8.24 – 8.15 (m, 2H), 7.90 (d, J = 7.7 Hz, 1H), 7.72 (t, J = 7.9 Hz, 1H), 7.06 (s, 1H), 6.87 – 6.75 (m, 2H), 4.85 (s, 2H), 1.99 (s, 3H); ^{19}F NMR (376 MHz, dmso) δ -61.08; HRMS-ESI (*m/z*): $[M + H]^+$ calcd for $C_{15}H_{13}F_3N_2O$, 295.1053; found 295.1061.

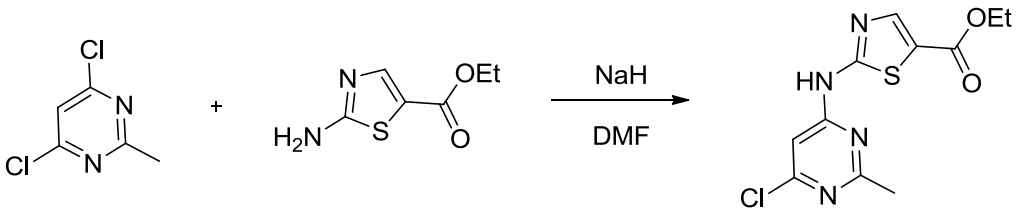

2.S-7

Synthesis of 2.S-7: ethyl 2-aminothiazole-5-carboxylate (1.0 g, 5.8 mmol) and 4,6-dichloro-2-methylpyrimidine (0.95 g, 5.8 mmol) were added to an oven dried flask. Dimethylformamide (20 mL) was then added. The reaction mixture was then cooled to 0^{o} C, and sodium hydride (0.510 g, 12.8 mmol) was added. The reaction was allowed to warm to room temperature and stir for an additional 3 hours. Excess base was quenched using ammonium chloride. The reaction was then suspended in water and filtered. After drying, **2.S-7** was obtained as a white solid (1.4g, 81% yield). **Spectral data.** ^{1}H NMR (400 MHz, DMSO-d_6) δ 12.30 (s, 1H), 8.07 (s, 1H), 6.88 (s, 1H), 4.24 (q, J = 7.1 Hz, 2H), 2.54 (s, 3H), 1.26 (t, J = 7.1 Hz, 3H); ^{13}C NMR (126 MHz, dmso) δ 167.85, 162.83, 161.96, 159.07, 157.88, 145.84, 122.02, 104.11, 61.22, 25.61,14.70; HRMS-ESI (*m/z*): $[M + H]^+$ calcd for $C_{11}H_{11}ClN_4O_2S$, 299.0364; found 299.0371.

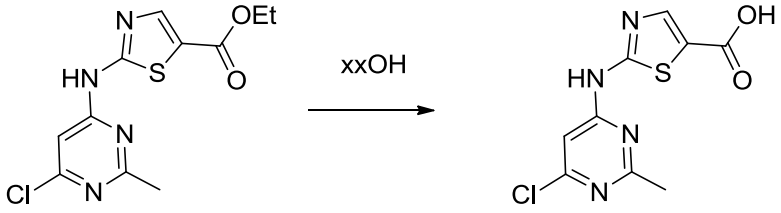

2.S-7 **2.S-8**

Synthesis of 2.S-8: Compound **2.S-7** (1.4 g, 4.7 mmol) and sodium hydroxide (1.5 g, 37.5 mmol) were added to an oven-dried round bottom flask. Methanol (11 mL) and water (4 mL) were then added. The reaction was stirred at room temperature for 48 hours. Methanol was then removed under reduced pressure. The crude reaction mixture was then suspended in 1 N HCl and filtered. After drying **2.S-8** (0.95 g, 75 % yield) was obtained as a white solid. **Spectral data.** ^{1}H NMR (500 MHz, DMSO-d6) δ 8.03 (s, 1H), 6.97 (s, 1H), 2.56 (s, 3H); ^{13}C NMR (126 MHz, dmso) δ 167.79, 163.39, 162.56, 158.94, 157.97, 145.28, 123.38, 104.03, 40.46, 40.29, 40.21, 40.13, 40.05, 39.96, 39.79, 39.62, 39.46, 25.57; HRMS-ESI (*m/z*): $[M + H]^+$ calcd for $C_9H_7ClN_4O_2S$, 271.0051; found 271.0055.

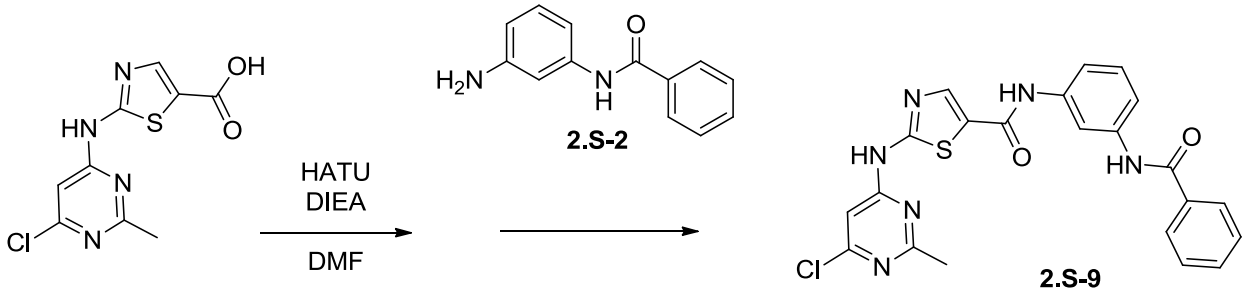

Synthesis of 2.S-9: Acid **2.S-8** (0.051 g, 0.188 mmol), aniline **2.S-2** (0.040 g, 0.188 mmol), and HATU (0.079 g, 0.207 mmol) were added to an oven-dried round bottom flask. Dimethylformamide (0.9 mL) was then added, followed by DIEA (0.073 g, 0.565 mmol). The reaction was allowed to stir at room temperature overnight. The reaction was then diluted in ethyl acetate (100 mL), and washed with water followed by brine. The organic layer was then dried over sodium sulfate. The crude reaction mixture was then purified via silica gel chromatography using a Biotage Isolera One (linear gradient 40 → 100% EtOAc in hexanes) to yield 0.075 g of compound **2.S-9** as a white solid (86 % yield).. ^{1}H NMR (500 MHz, DMSO-d6) δ 12.20 (s, 1H), 10.28 (s, 1H), 10.24 (s, 1H), 8.36 (s, 1H), 8.26 (t, J = 2.1 Hz, 1H), 7.99 – 7.92 (m, 2H), 7.61 – 7.40 (m, 5H), 7.30 (t, J = 8.1 Hz, 1H), 6.92 (s, 1H), ^{13}C NMR (126 MHz, dmso) δ 167.85, 165.98, 161.76, 160.03, 158.94, 157.96, 141.12, 139.86, 139.36, 135.38, 131.99, 129.12, 128.80, 128.12, 116.38, 116.23, 113.03, 103.88, 25.64; $[M + H]^+$ calcd for $C_{22}H_{17}ClN_6O_2S$, 465.0985; found 465.0899.

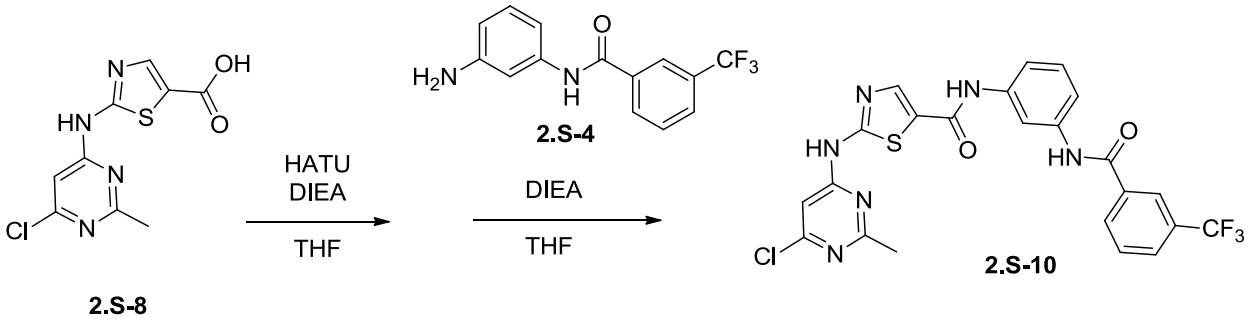

Synthesis of 2.S-10: Acid **2.S-8** (0.075 g, 0.277 mmol), aniline **2.S-4** (0.078 g, 0.277 mmol), and HATU (0.116 g, 0.305 mmol) were added to an oven-dried round bottom flask. Dimethylformamide (1.4 mL) was then added, followed by DIEA (0.143 g, 1.1 mmol). The reaction was allowed to stir at room temperature overnight. The reaction was then diluted in ethyl acetate (100 mL), and washed with water followed by brine. The organic layer was then dried over sodium sulfate. The crude reaction mixture was then purified via silica gel chromatography using a Biotage Isolera One (linear gradient 40 → 100% EtOAc in hexanes) to yield 0.035 g of compound **2.S-10** as a white solid (24 % yield). **Spectral data.** ^{1}H NMR (500 MHz, DMSO-*d*6) δ 12.20 (s, 1H), 10.51 (s, 1H), 10.27 (s, 1H), 8.37 (s, 1H), 8.31 – 8.24 (m, 3H), 7.95 (d, *J* = 7.8 Hz, 1H), 7.77 (t, *J* = 7.8 Hz, 1H), 7.47 (dd, *J* = 16.4, 8.0 Hz, 2H), 7.32 (t, *J* = 8.1 Hz, 1H), 6.93 (s, 1H), 2.58 (s, 3H); ^{19}F NMR (471 MHz, dmso) δ -61.09; HRMS-ESI (*m/z*): $[M + H]^+$ calcd for $C_{23}H_{16}ClF_3N_6O_2S$, 533.0769; found 533.0778.

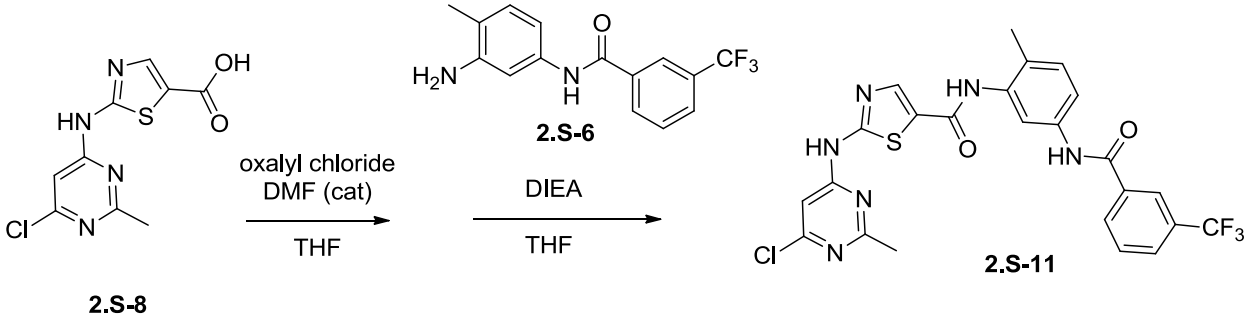

Synthesis of 2.S-11: Acid **2.S-8** (0.9 g, 3.3 mmol) was added to an oven-dried round bottom flask. Tetrahydrofuran (11 mL) was then added. The reaction was cooled to 0^{o} C. Oxalyl chloride (0.5 g, 4.0 mmol) was added, followed by a drop of dimethylformamide. The reaction was allowed to warm to room temperature and stir for an additional twenty minutes. The crude mixture was then concentrated under reduced pressure. The crude reaction mixture was then again dissolved in tetrahydrofuran (11mL). Aniline **2.S-6** (1.0 g, 3.3 mmol) was then added followed by DIEA (0.43 g, 3.3 mmol). The reaction was then allowed to stir overnight at room temperature. The crude reaction mixture was then purified via silica gel chromatography using a Biotage Isolera

One (linear gradient 40 → 100% EtOAc in hexanes) to yield 0.250 g of compound **2.S-11** as a white solid (14 % yield). **Spectral data.** ^{1}H NMR (400 MHz, DMSO-d_6) δ 12.19 (s, 1H), 10.45 (s, 1H), 9.90 (s, 1H), 8.30 – 8.11 (m, 3H), 7.93 (d, *J* = 7.8 Hz, 1H), 7.86 – 7.71 (m, 2H), 7.56 (dd, *J* = 8.2, 2.3 Hz, 1H), 7.24 (d, *J* = 8.3 Hz, 1H), 6.91 (s, 1H), 2.56 (s, 3H), 2.19 (s, 3H); ^{19}F NMR (376 MHz, dmso) δ -61.10; HRMS-ESI (*m/z*): $[M + H]^+$ calcd for $C_{24}H_{18}ClF_3N_6O_2S$, 547.0925; found 547.0924.

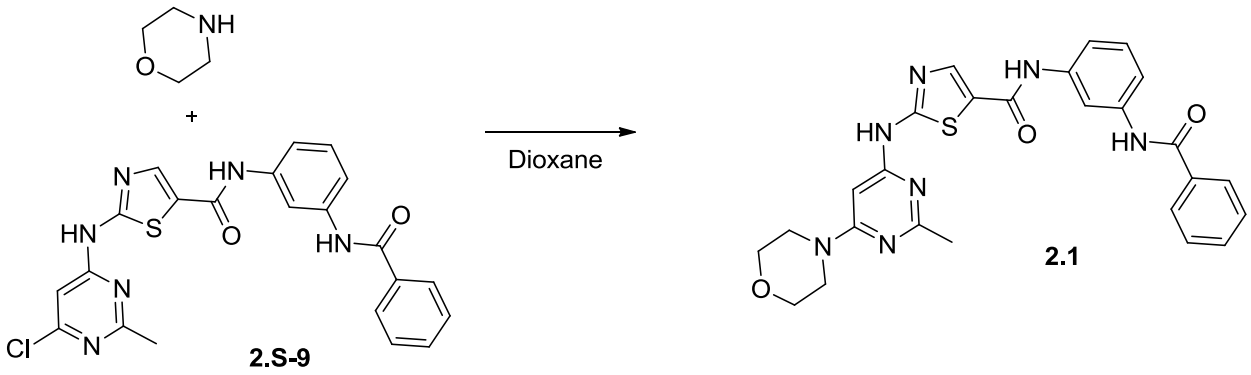

Synthesis of 2.1: To an oven dried flask was added **2.9** (0.040 mg, 0.086 mmol). Dioxane (0.29 mL) was then added, followed by morphiline (0.150 mg, 1.72 mmol). The reaction was then heated to 85 ^{o}C overnight. The reaction was allowed to cool to room temperature. Dioxane was removed under reduced pressure. The crude mixture was then suspended in ether and filtered. The crude solid was then washed with ether twice to afford the product as 5 mg of a light tan solid (11% yield). ^{1}H NMR (400 MHz, DMSO-d_6) δ 11.48 (s, 1H), 10.24 (s, 1H), 10.10 (s, 1H), 8.27 – 8.19 (m, 3H), 7.97 – 7.90 (m, 3H), 7.66 – 7.36 (m, 2H), 7.27 (t, *J* = 8.1 Hz, 1H), 6.03 (s, 1H), 3.79 (s, 2H), 3.46 (t, *J* = 4.8 Hz, 6H), 2.40 (s, 3H); ^{13}C NMR (126 MHz, dmso) δ 165.95, 165.62, 163.11, 163.05, 160.38, 157.41, 141.17, 139.82, 139.54,135.39, 131.98, 129.06, 128.80, 128.12, 127.27, 116.22, 116.15, 112.99, 83.18, 66.20, 63.75, 44.37, 43.28, 26.03; HRMS-ESI (*m/z*): $[M + H]^+$ calcd for $C_{26}H_{25}N_7O_3S$, 514.1812; found 516.1816.

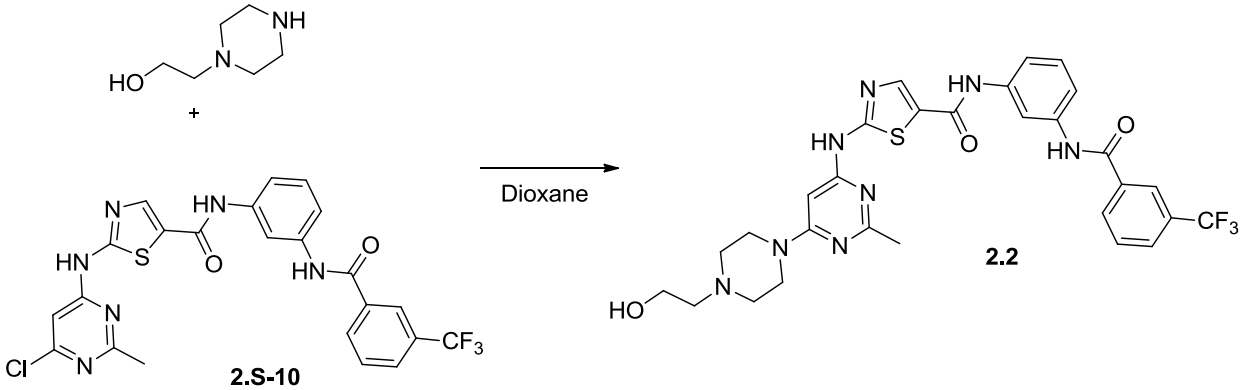

Synthesis of 2.2: Compound **2.S-10** (0.035 g, 0.066 mmol) was added to an oven-

dried round bottom flask. Dioxane (0.5 mL) was added. 1-(2-hydroxyethyl)piperazine (0.086 g, 0.657 mmol) was then added. The reaction was heated to reflux overnight. The reaction mixture was then concentrated under reduced pressure. The crude mixture was then purified using reverse-phase HPLC to afford **2.2** as a white solid (5 mg, 12% yield). **Spectral data.** ^{1}H NMR (400 MHz, DMSO-d_6) δ 11.47 (s, 1H), 10.48 (s, 1H), 10.14 (s, 1H), 8.26 (s, 2H), 8.30 – 8.15 (m, 2H), 7.94 (d, *J* = 7.9 Hz, 1H), 7.76 (t, *J* = 7.8 Hz, 1H), 7.49 – 7.39 (m, 2H), 7.29 (t, *J* = 8.1 Hz, 1H), 6.04 (s, 1H), 3.58 – 3.53 (m, 8H), 2.40 (s, 3H); ^{19}F NMR (471 MHz, dmso) δ -61.07; HRMS-ESI (*m/z*): $[M + H]^+$ calcd for $C_{29}H_{29}F_3N_8O_3S$, 627.2108; found 627.2107.

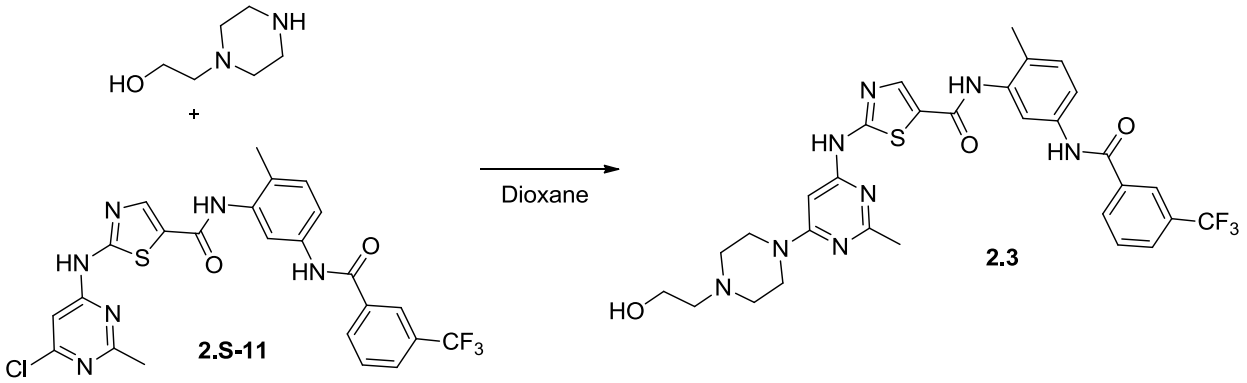

Synthesis of 2.3: Compound **2.S-11** (0.250 g, 0.457 mmol) was added to an oven-dried round bottom flask. Dioxane (1.5 mL) was added. 1-(2-hydroxyethyl)piperazine (1.190 g, 9.14 mmol) was then added. The reaction was heated to reflux overnight. The reaction mixture was then concentrated under reduced pressure. The crude mixture was then purified using reverse-phase Biotage C18 column to afford **2.3** as a white solid (25 mg, 9% yield). **Spectral data.** ^{1}H NMR (400 MHz, DMSO-d_6) δ 11.42 (s, 1H), 10.43 (s, 1H), 9.74 (s, 1H), 8.29 – 8.20 (m, 2H), 8.17 (s, 1H), 7.93 (d, *J* = 8.0 Hz, 1H), 7.82 – 7.71 (m, 2H), 7.55 (dd, *J* = 8.3, 2.2 Hz, 1H), 7.22 (d, *J* = 8.4 Hz, 1H), 6.02 (s, 1H), 4.44 (s, 1H), 3.48 (m, 4H), 3.28 (s, 8H), 2.38 (s, 3H), 2.18 (s, 3H); ^{19}F NMR (376 MHz, dmso) δ -61.09; HRMS-ESI (*m/z*): $[M + H]^+$ calcd for $C_{30}H_{31}F_3N_8O_3S$, 641.2265; found 641.2279.

SPECTRAL DATA FOR COMPOUNDS 2.S-2 – 2.3

2.S-2: 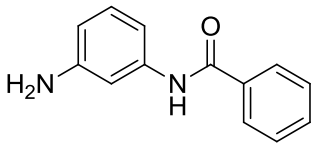

2.S-2 ^{1}H:

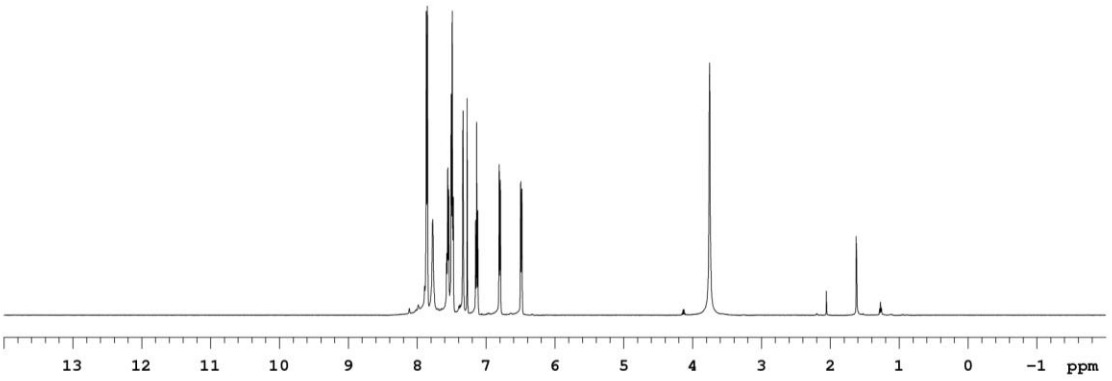

2.S-2 ^{13}C:

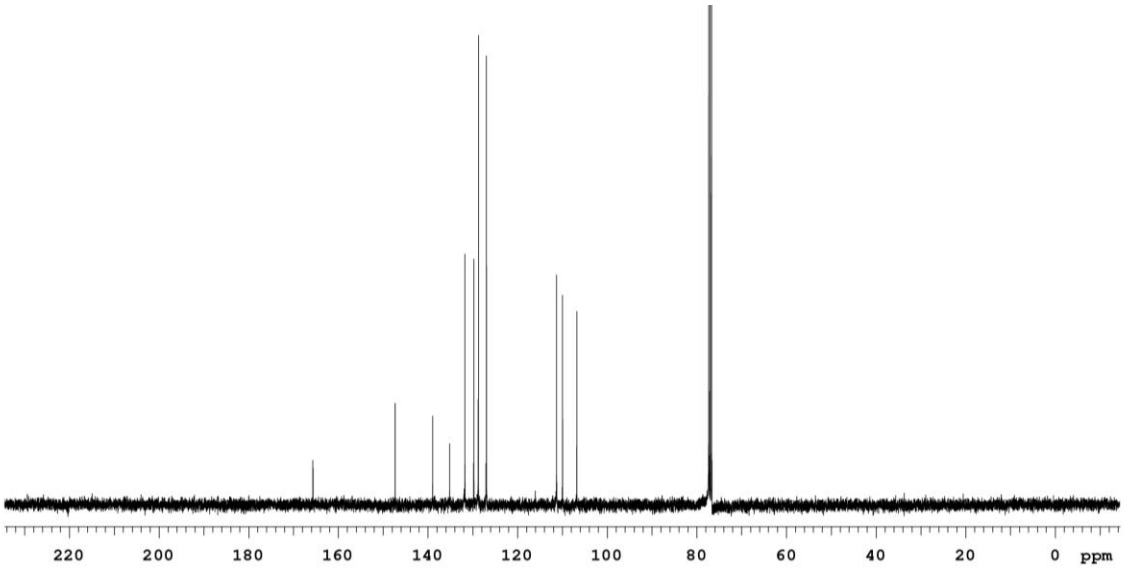

2.S-3: 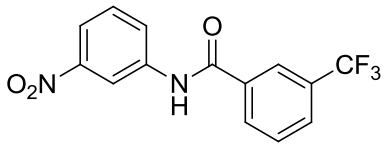

2.S-3 ^{1}H:

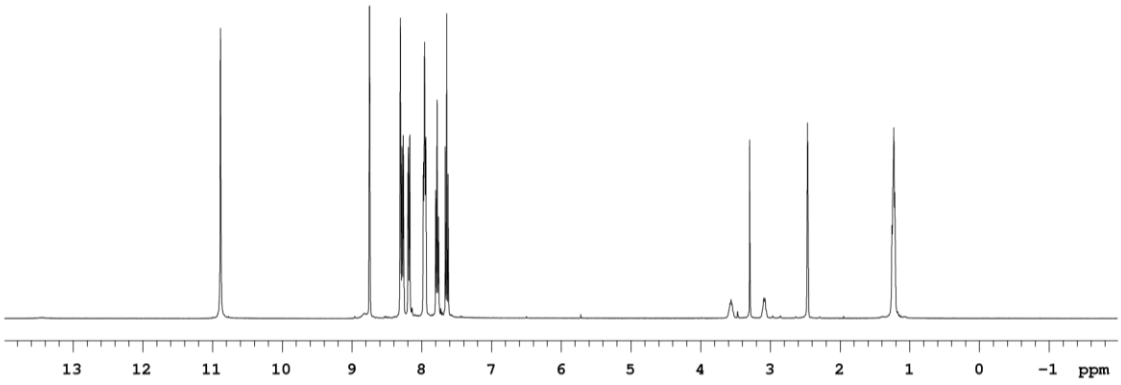

2.S-3 ^{19}F:

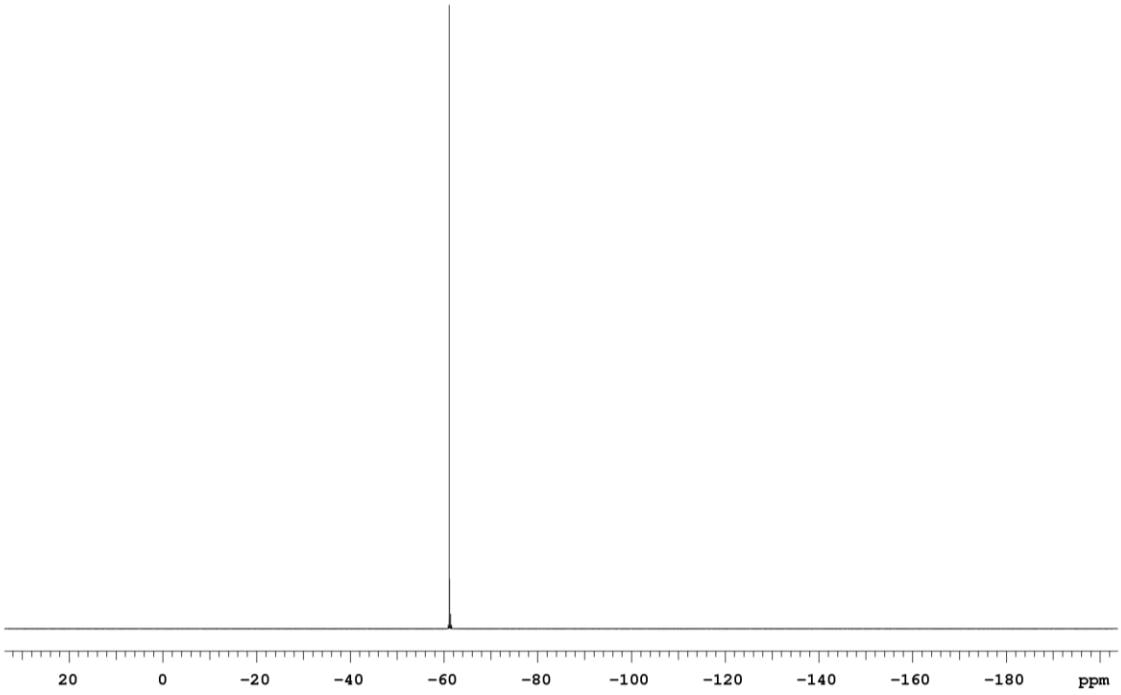

2.S-4: 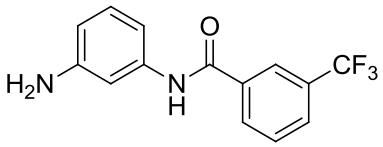

2.S-4 ^{1}H:

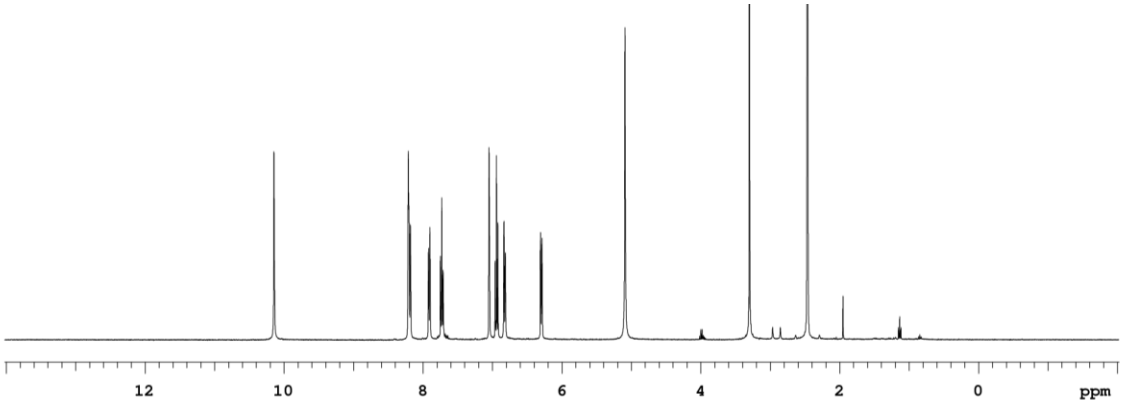

2.S-4 ^{19}F:

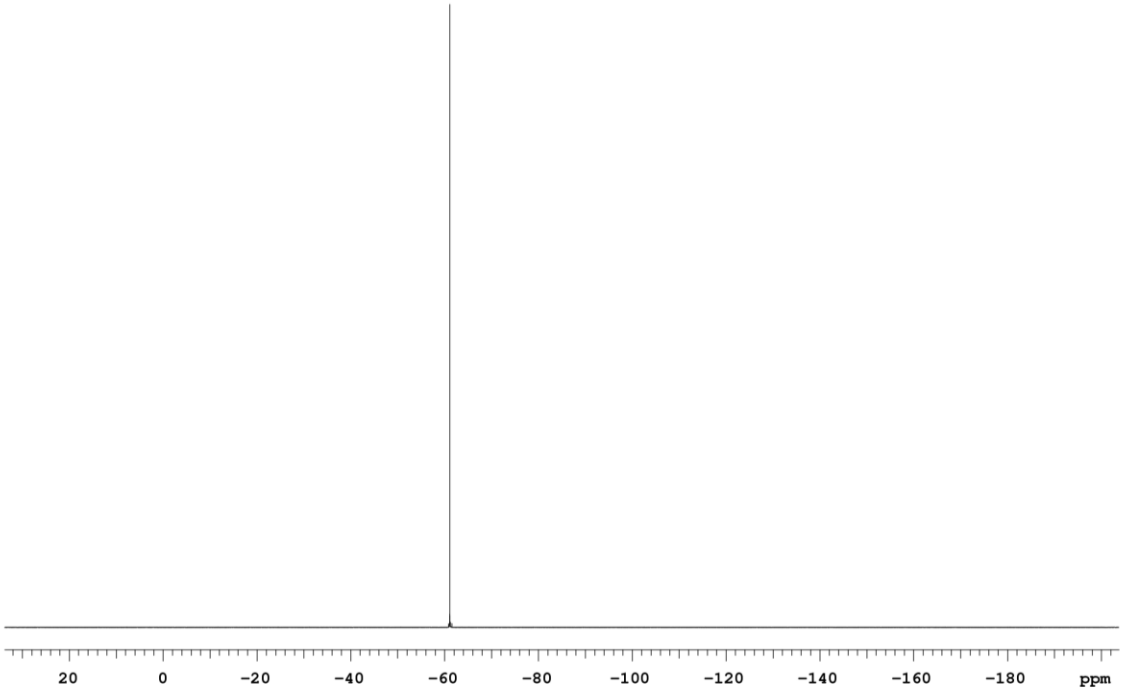

2.S-5: 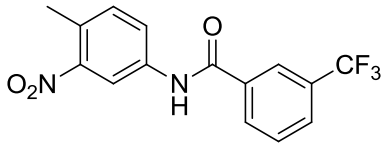

2.S-5 ^{1}H:

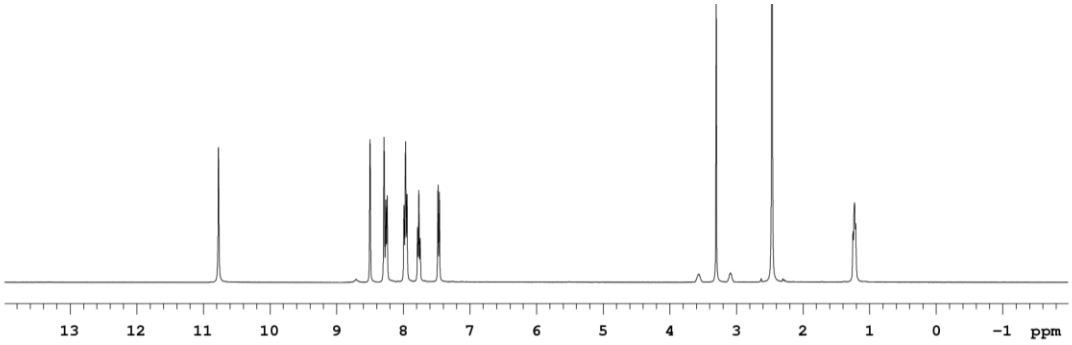

2.S-5 ^{19}F:

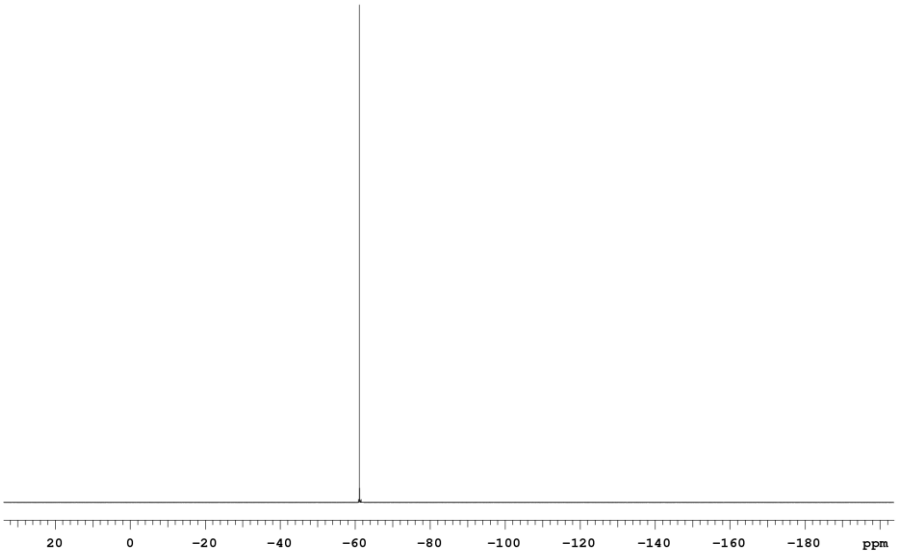

2.S-6: 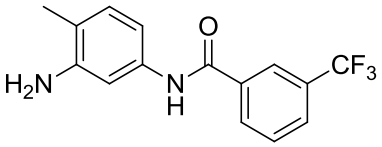

2.S-6 ^{1}H:

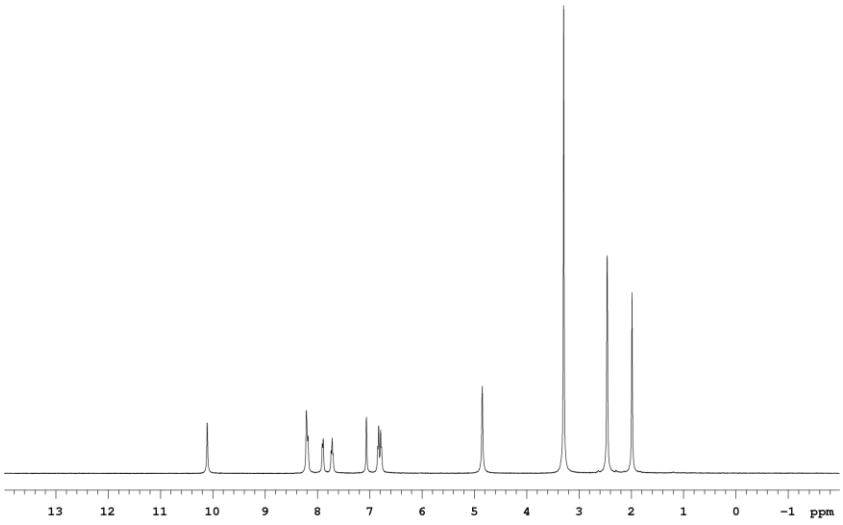

2.S-6 ^{19}F:

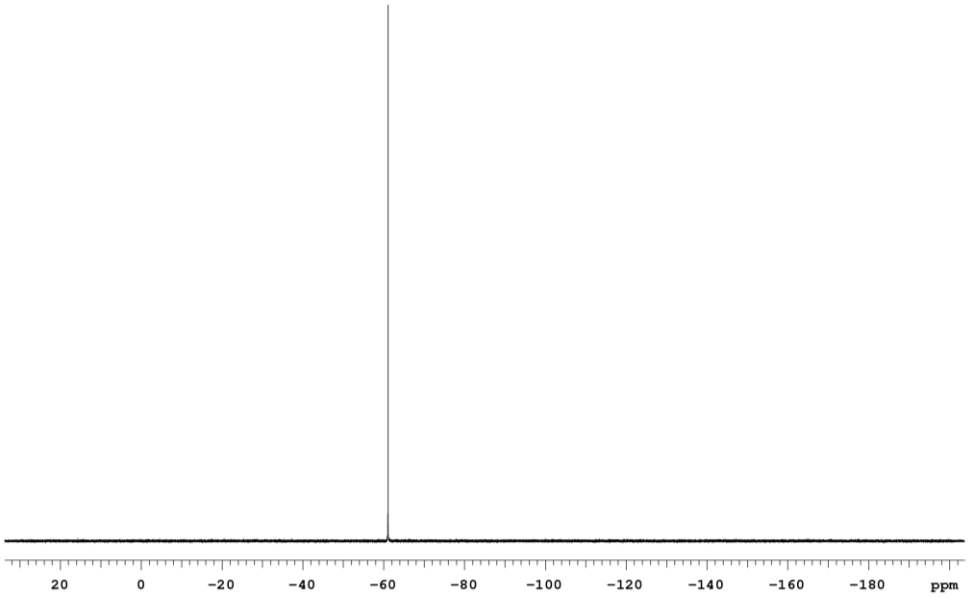

2.S-7:

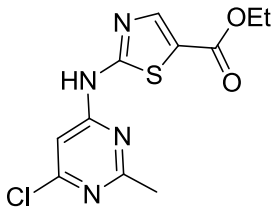

2.S-7 ^{1}H:

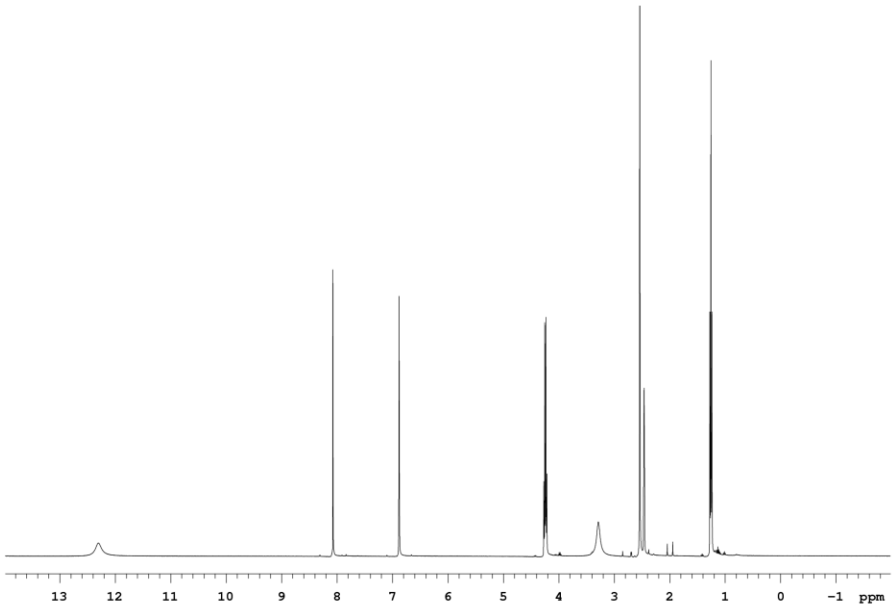

2.S-7 ^{13}C:

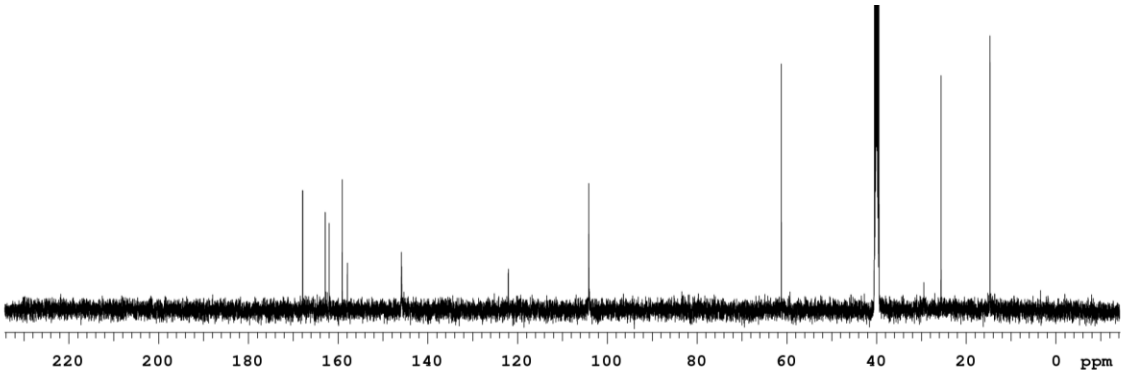

2.S8:

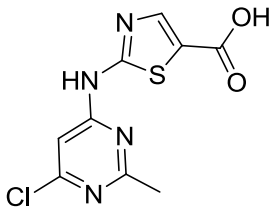

2.S8 ^{1}H:

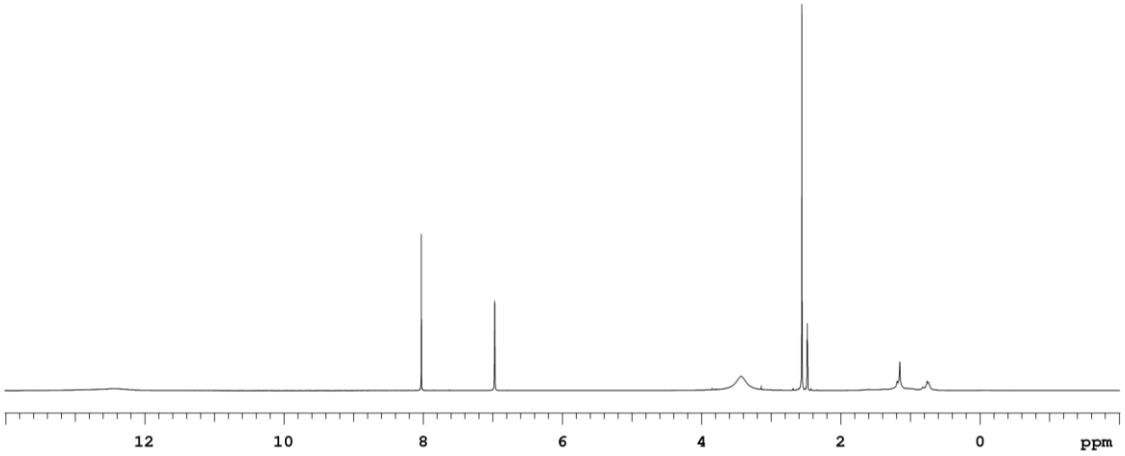

2.S8 ^{19}F:

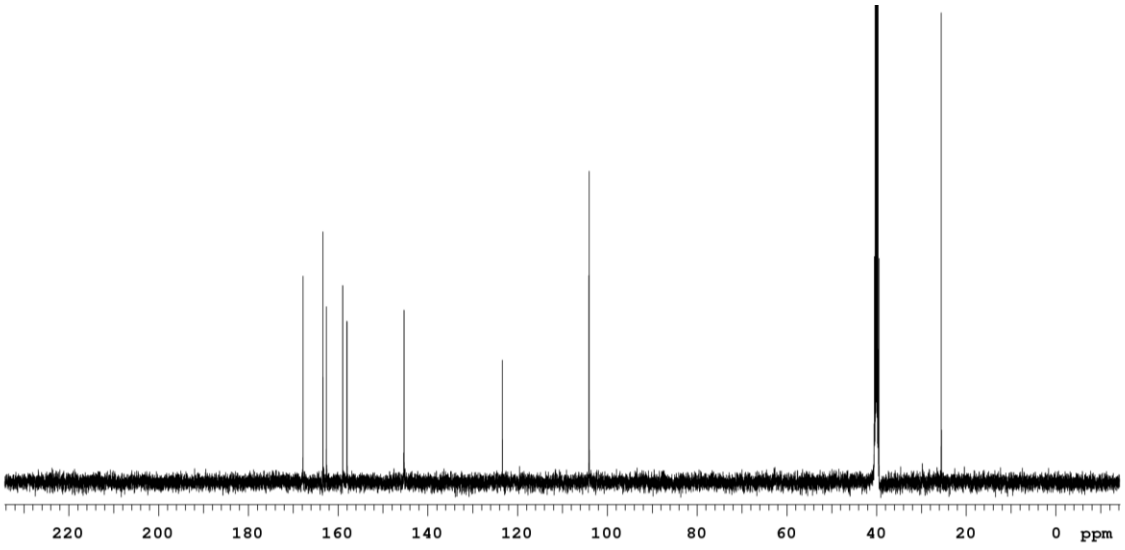

2.S-9:

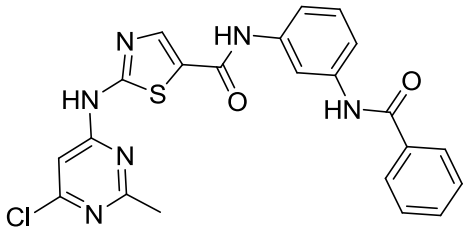

2.S-9 ^{1}H:

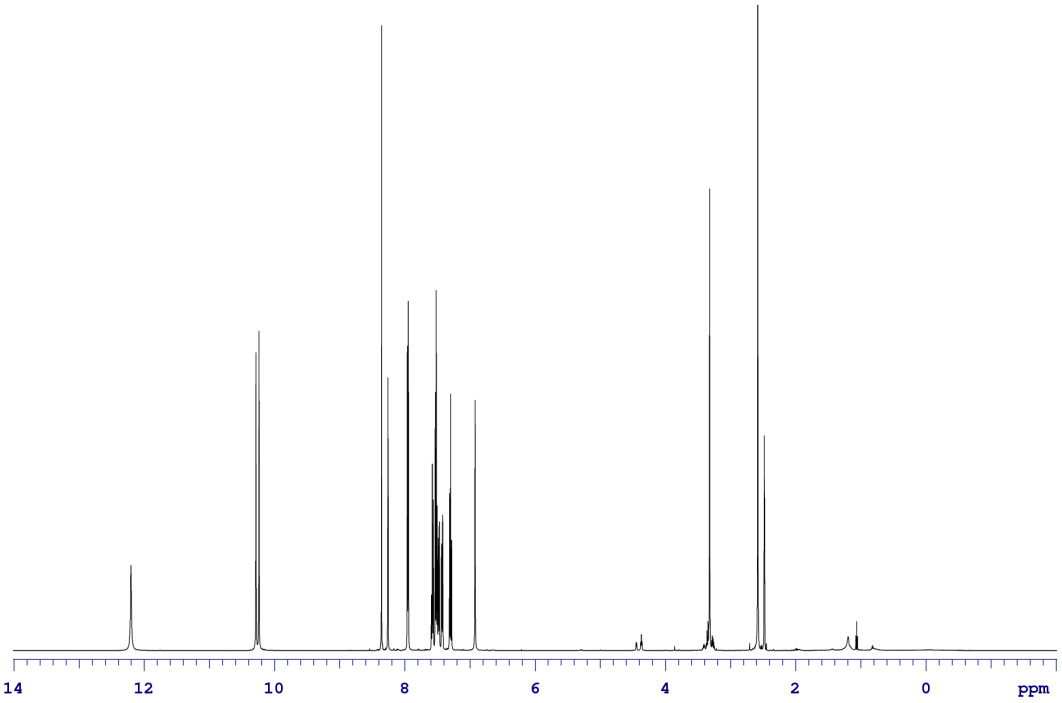

2.S-9 ^{13}C:

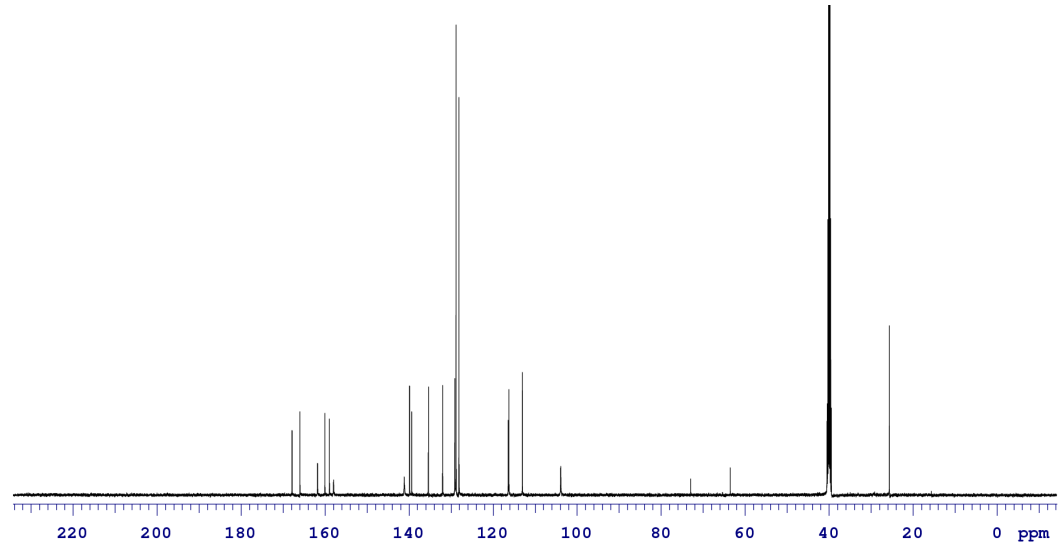

2.S-10:

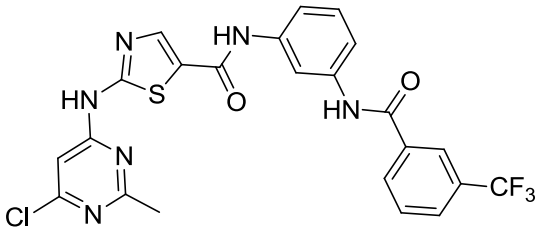

2.S-10 ^{1}H:

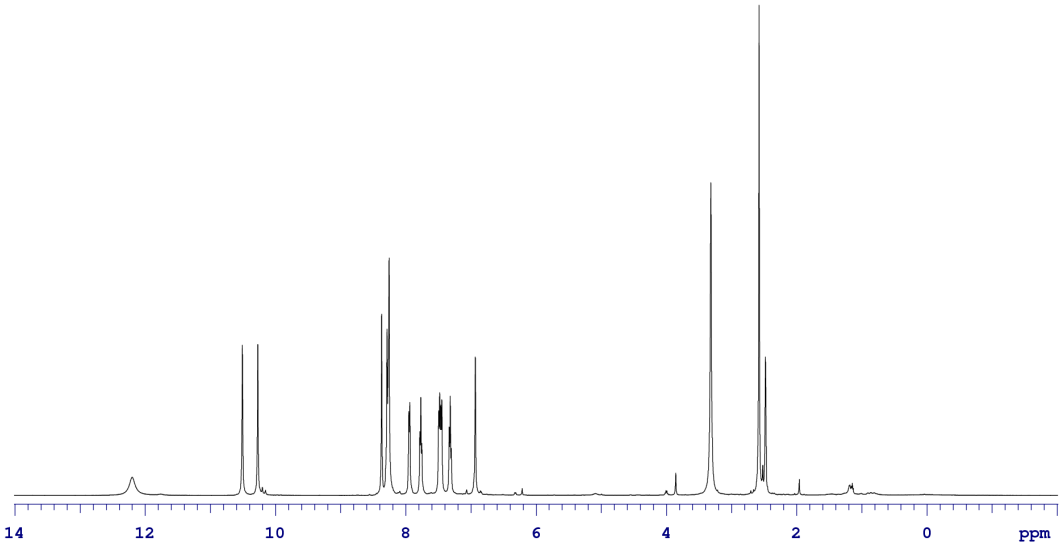

2.S-10 ^{19}F:

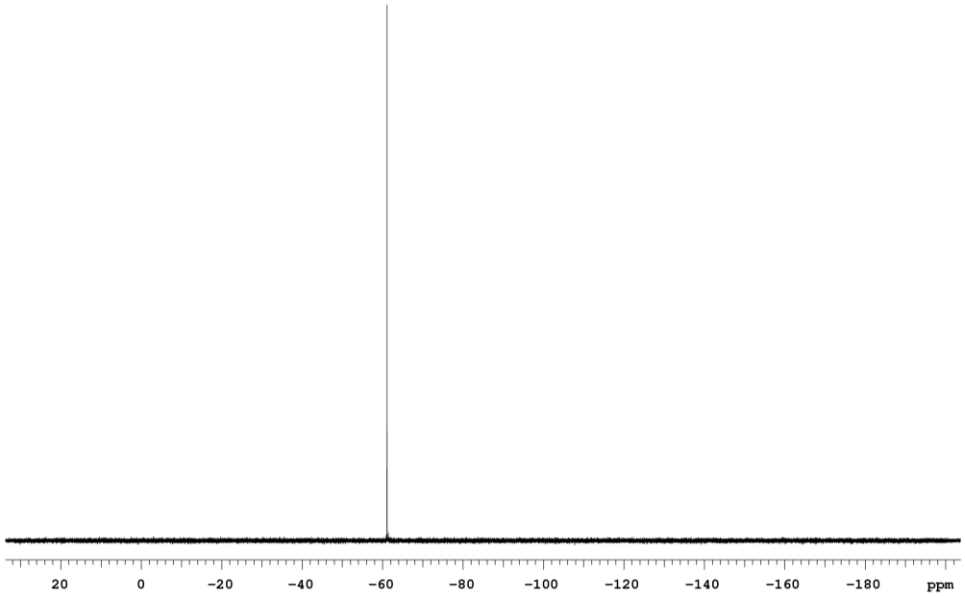

2.1:

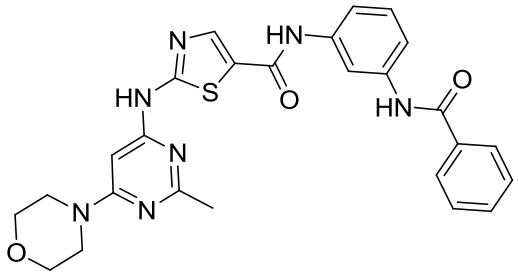

2.1 ^{1}H:

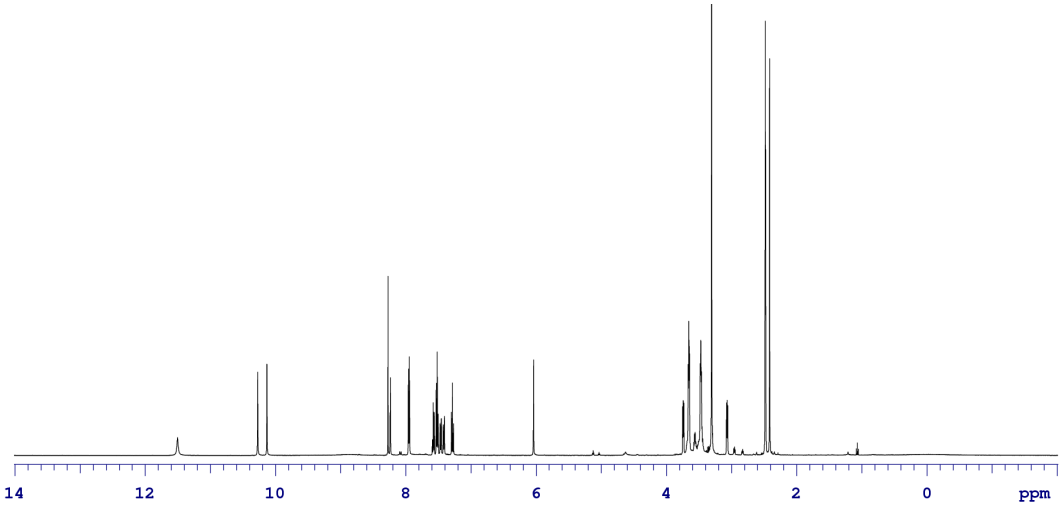

2.1 ^{13}C:

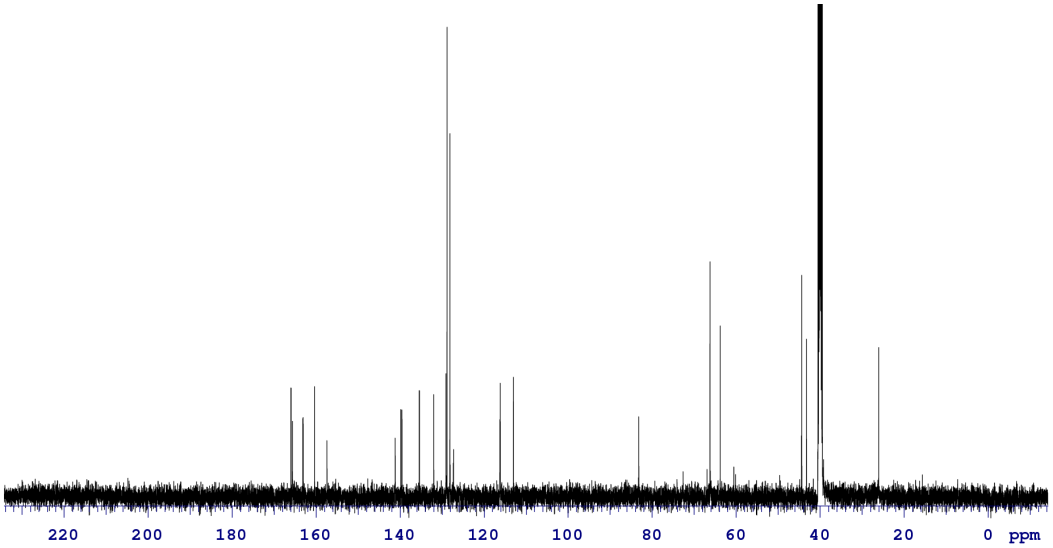

2.2:

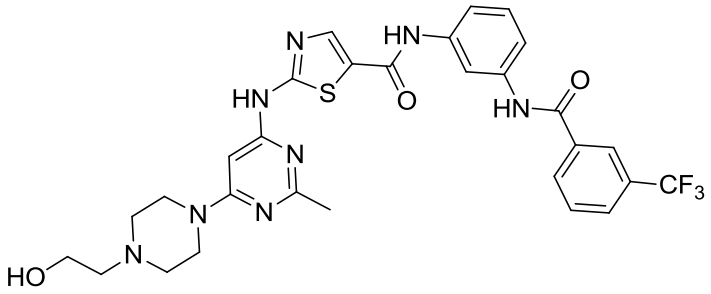

2.2 ^{1}H:

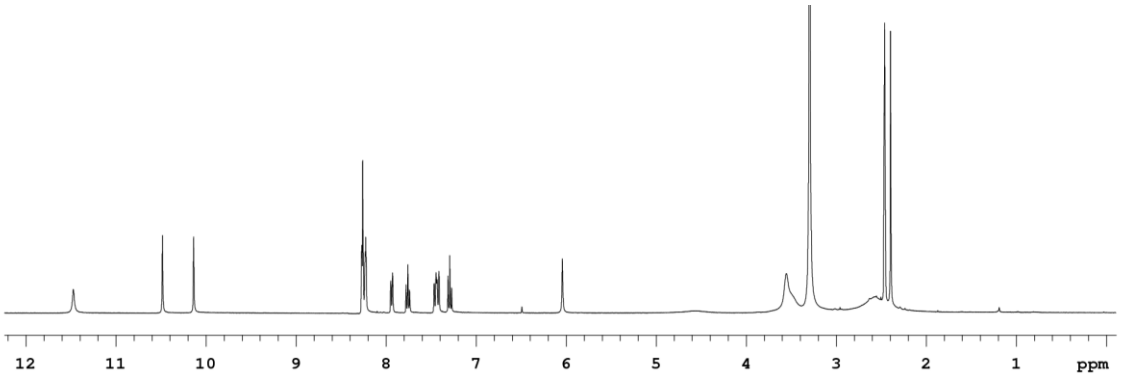

2.2 ^{19}F:

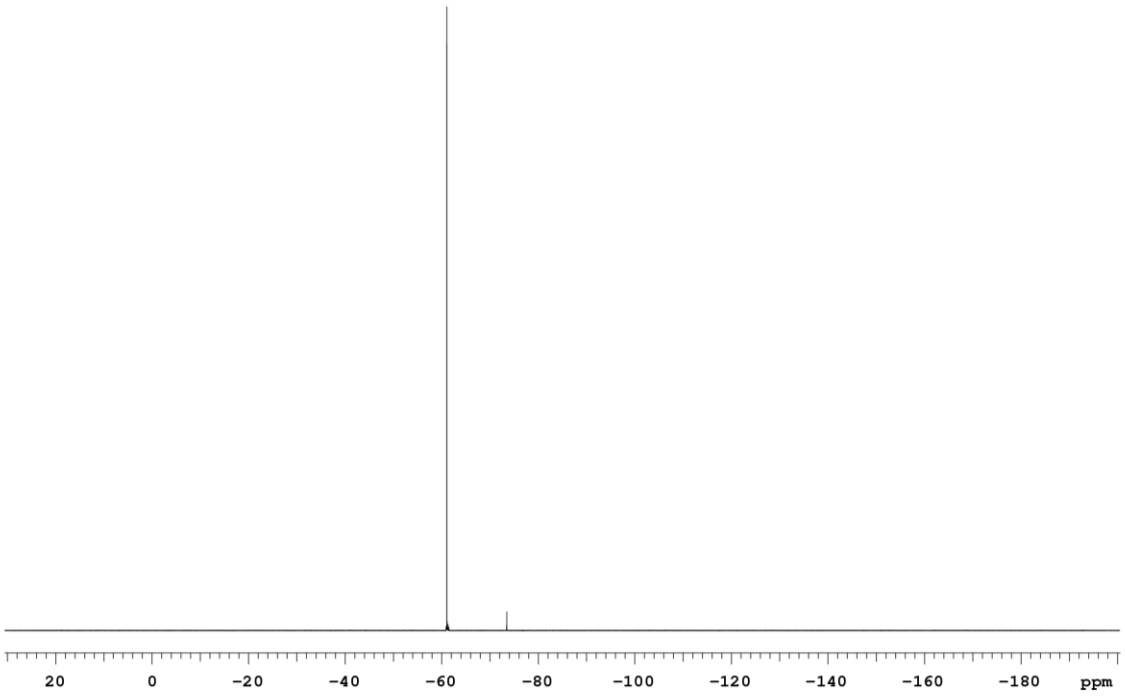

2.S11:

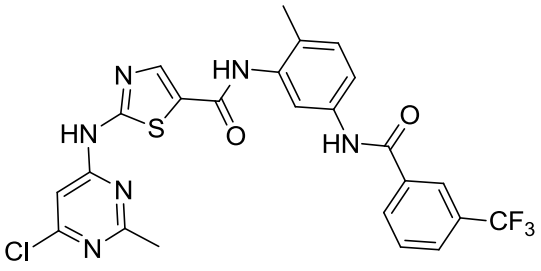

2.S-11 ^{1}H:

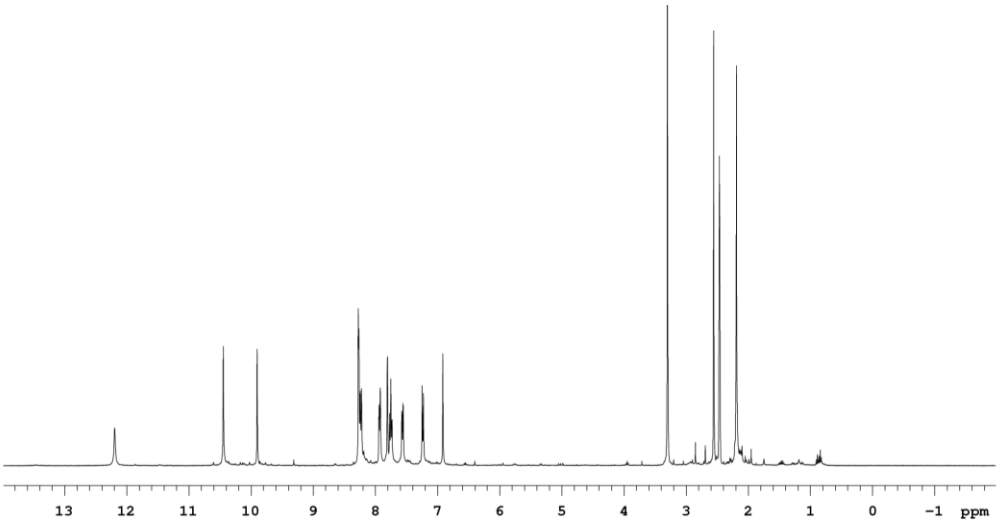

2.S-11 ^{19}F:

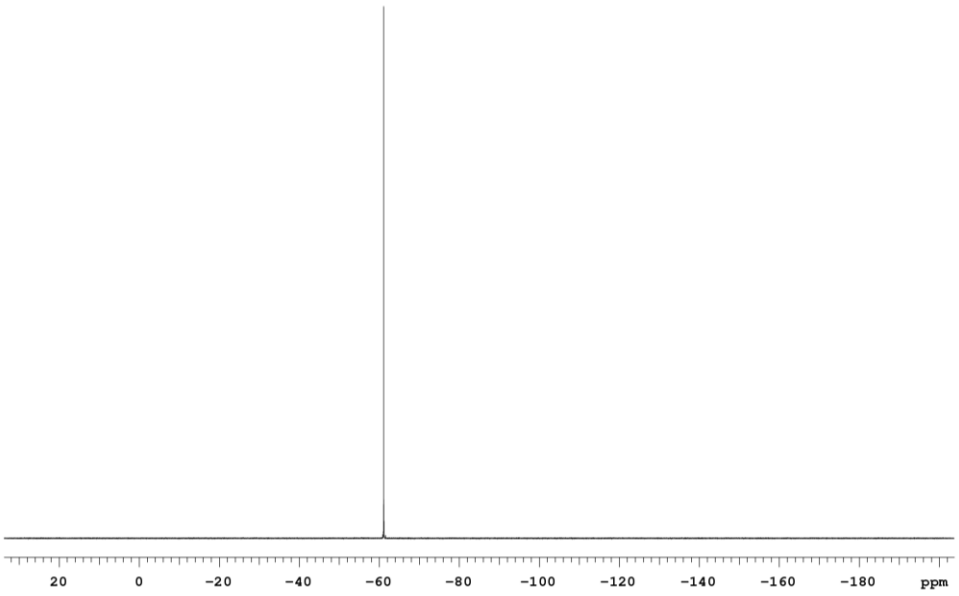

2.3:

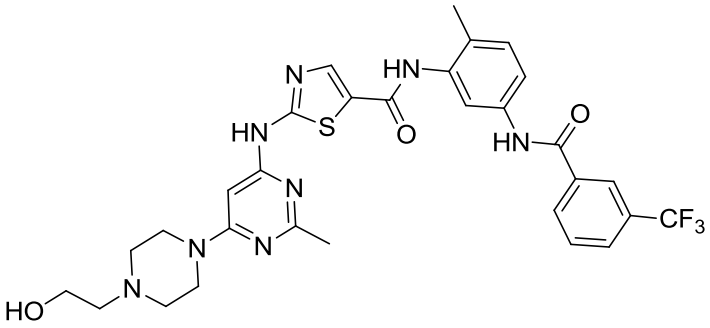

2.3 ^{1}H:

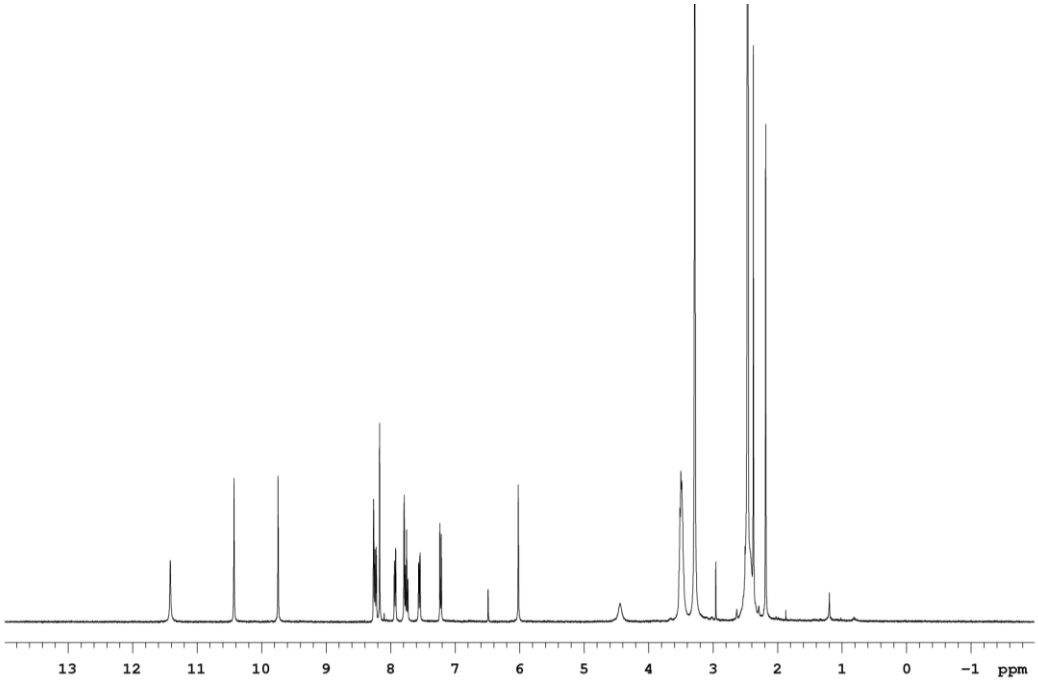

2.3 ^{19}F:

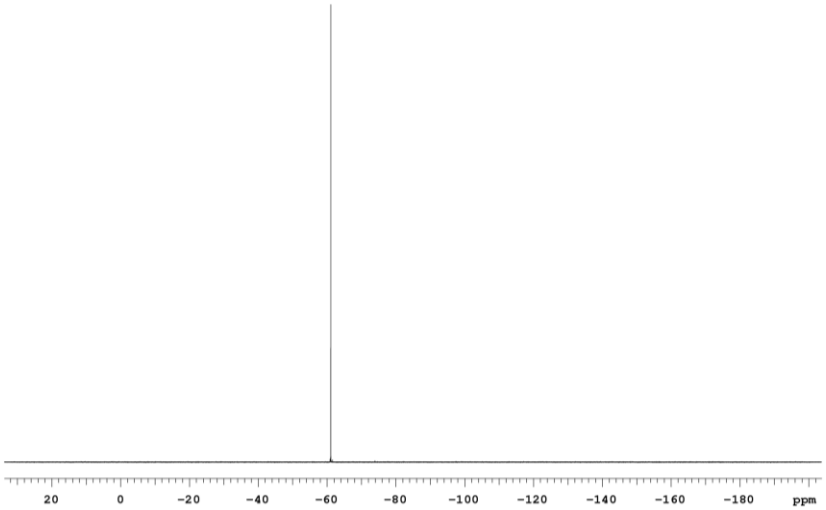

BIOCHEMICAL CHARACTERIZATION

General procedure for determination of inhibitor K_i. A continuous fluorescence assay[1] was used to determine K_i. Reaction volumes of 100 µL were used in 96-well plates. 85 µL of enzyme in buffer was added to each well. 2.5 µL of the appropriate inhibitor dilution (typically 5000, 1666, 555, 185, 61, 20, 6.8, 2.2, 0.76, 0 µM in DMSO) was then added. 2.5 µL of a substrate peptide ("compound 3" as described in Wang et al)[1] solution (1.8 mM in DMSO) was added. The reaction was initiated with 10 µL of ATP (1 mM in water), and reaction progress was immediately monitored at 405 nm (ex. 340 nm) for 10 minutes. Reactions had final concentrations of 30 nM enzyme, 45 µM peptide substrate, 100 µM ATP, 100 µM Na_3VO_4, 100 mM Tris buffer (pH 8), 10 mM $MgCl_2$, 0.01% Triton X-100.The initial rate data collected was used for determination of K_i values. For K_i determination, the kinetic values were obtained directly from nonlinear regression of substrate-velocity curves in the presence of various concentrations of the inhibitor. The equation Y = Bottom + (Top – Bottom)/(1 + 10^X – LogEC50), X = log(concentration) and Y = binding; was used in the nonlinear regression.

Analytical data for c-Src K_i determination. Each inhibitor K_i value was determined using at least three independent experiments; a representative inhibition curve is shown.

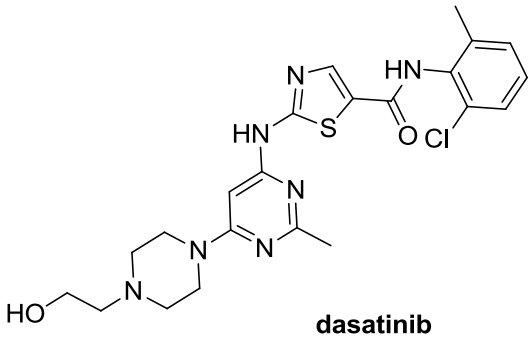

dasatinib

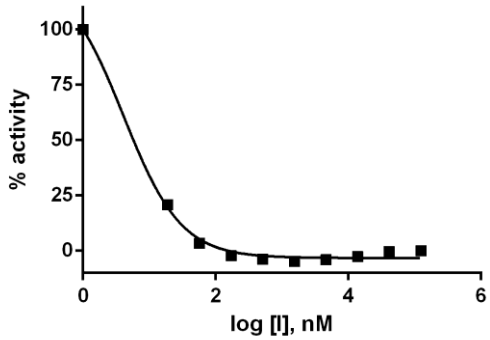

Avg $K_i \leq 0.6$ nM

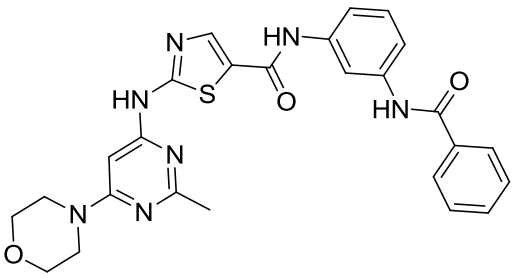

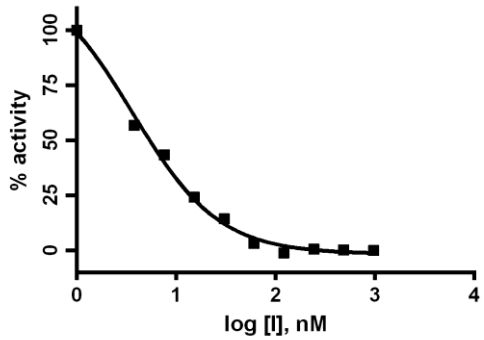

2.1 Avg K_i ≤ 0.6 nM

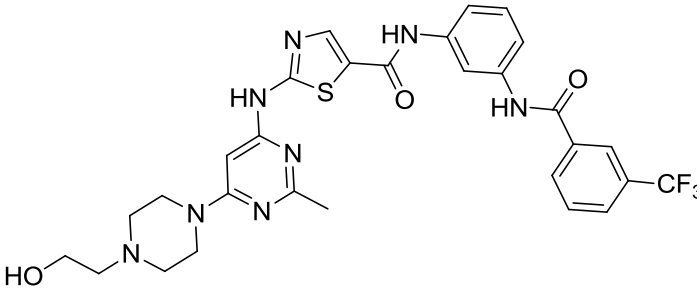

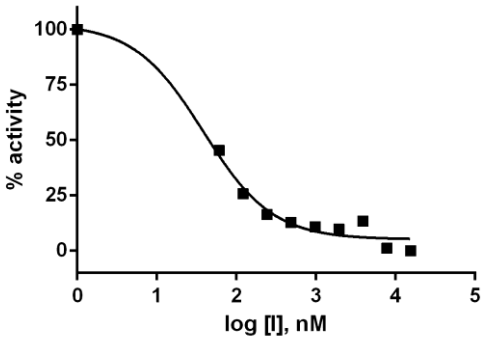

2.2 Avg K_i ≤ 0.6 nM

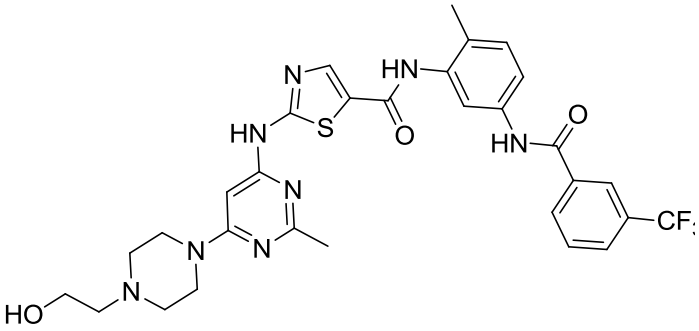

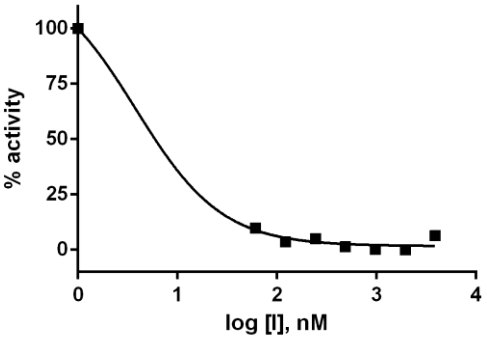

2.3 Avg K_i ≤ 0.6 nM

Analytical data for c-Src T341I K_i determination. Each inhibitor K_i value was determined using at least three independent experiments, a representative inhibition curve is shown.

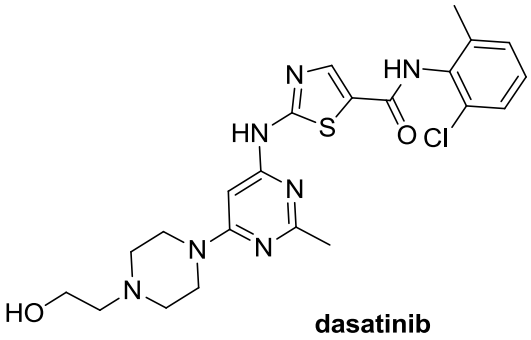

dasatinib

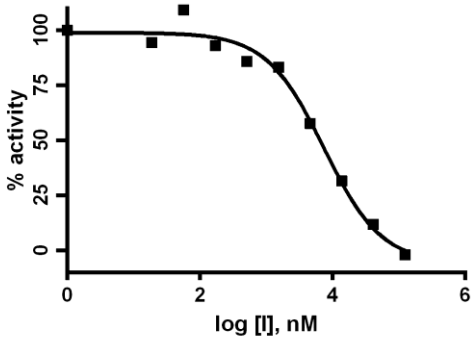

[ATP] = 25 µM

Avg K_i = 1,586 ± 427 nM

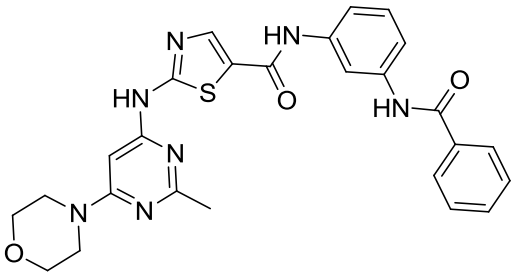

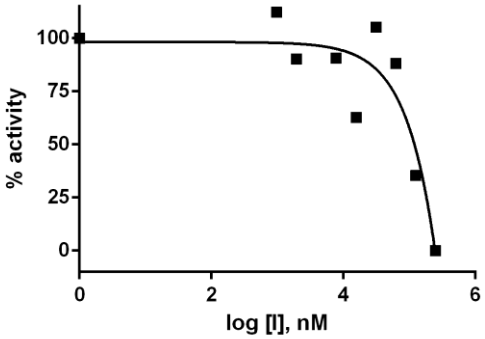

2.1; [ATP] = 10 µM

Avg K_i ≥ 40,500 nM

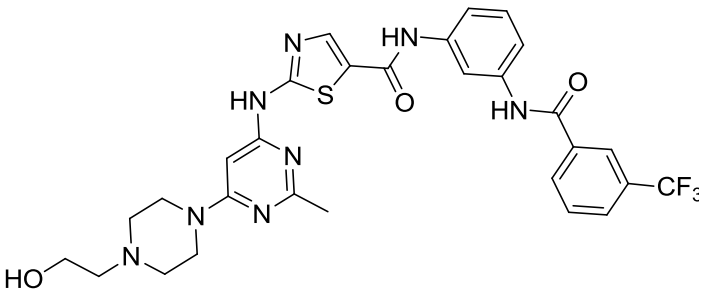

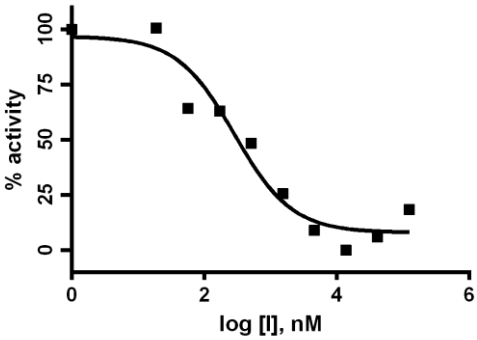

2.2; [ATP] = 25 µM

Avg K_i = 56 ± 14

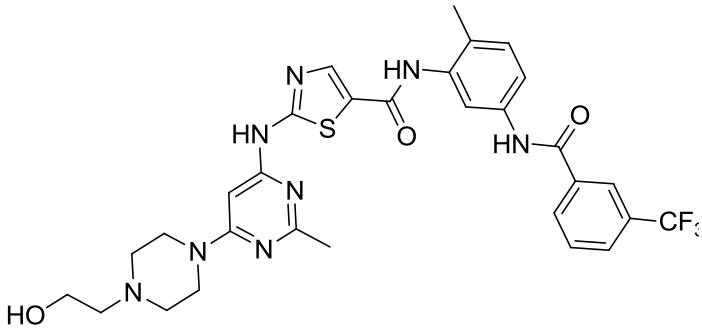

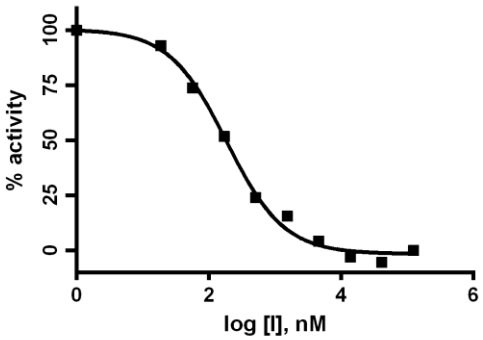

2.3; [ATP] = 500µM

Avg K_i = 1.9 ± 0.3

Analytical data for c-Src T341M K_i determination. Each inhibitor K_i value was determined using at least three independent experiments, a representative inhibition curve is shown.

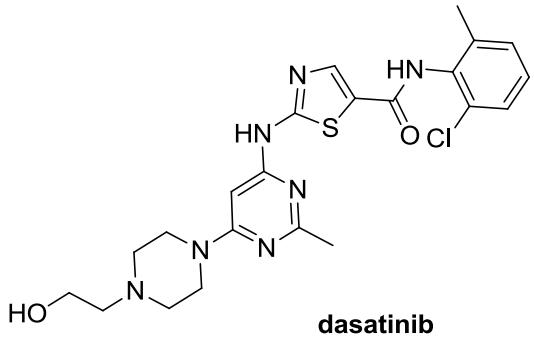

dasatinib

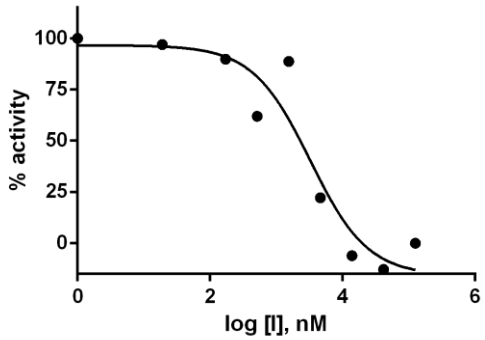

[ATP] = 25 µM

Avg K_i = 3,300

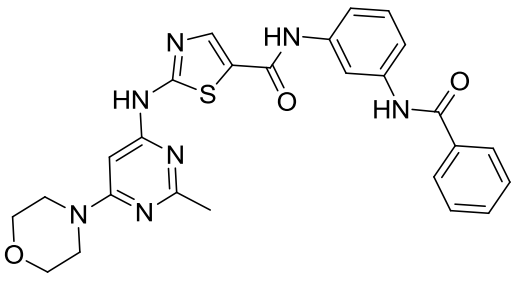

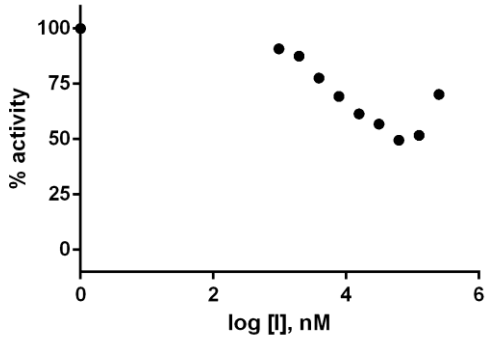

2.1; [ATP] = 100 µM

Avg K_i ≥ 20,000

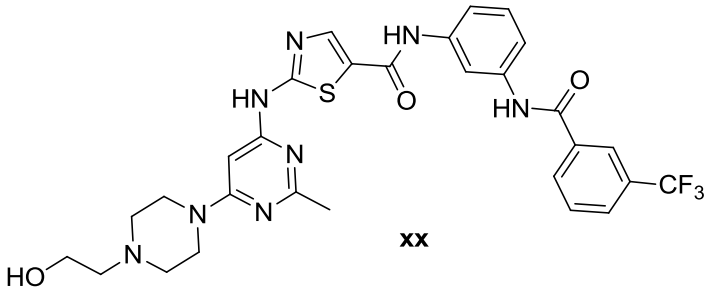

xx

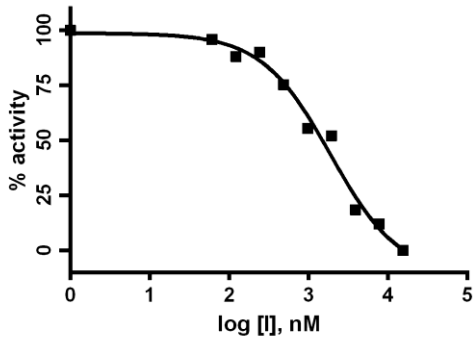

2.2; [ATP] = 25 μM

Avg K_i = 404 ± 76 nM

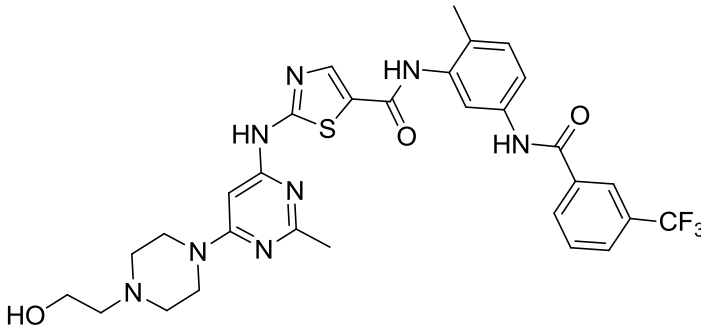

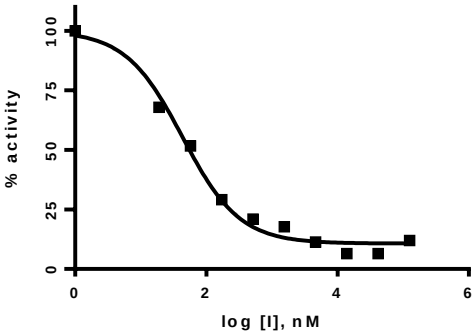

2.3

Avg K_i = 3.1 ± 1.7 nM

Analytical data for c-Abl K_i determination. Each inhibitor K_i value was determined using at least three independent experiments, a representative inhibition curve is shown.

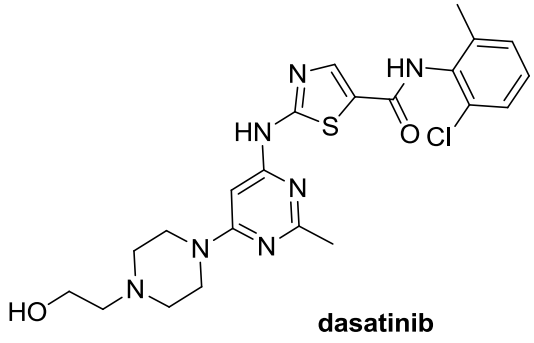

dasatinib

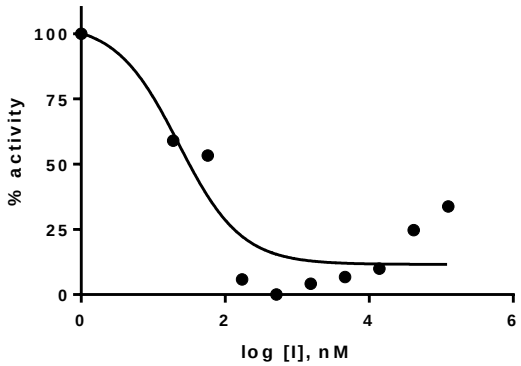

[ATP] = 5 mM

Avg K_i ≤ 3.4 nM

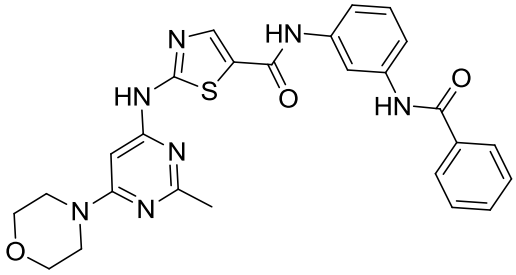

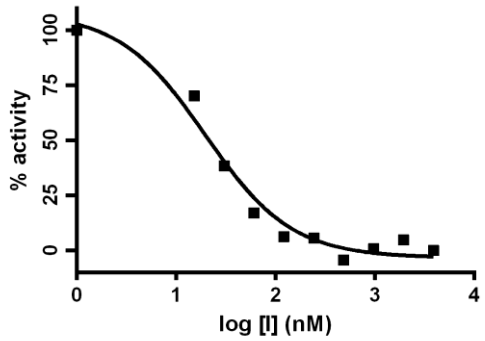

2.1; [ATP] = 5 mM

Avg K_i ≤ 3.4 nM

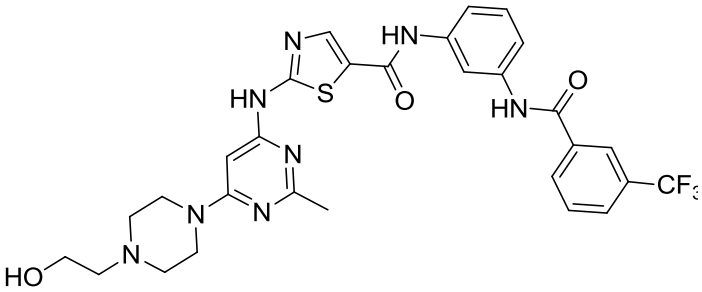

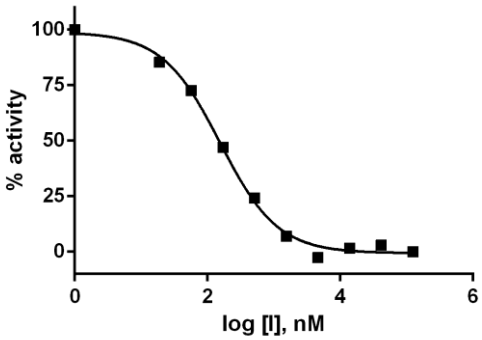

2.2; [ATP] = 5 mM

Avg K_i ≤ 3.4 nM

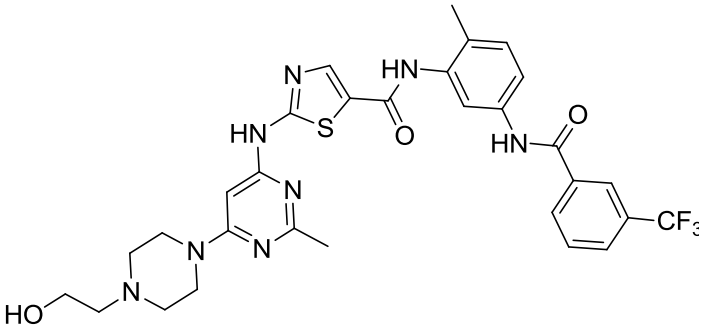

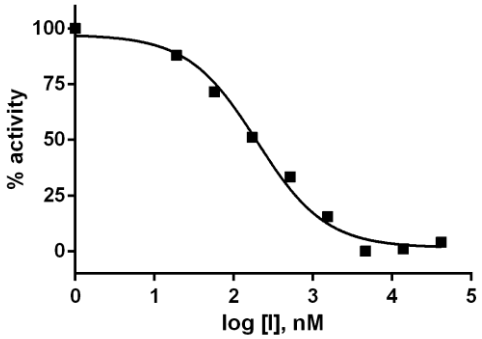

2.3; [ATP] = 5 mM

Avg K_i ≤ 3.4 nM

DiscoveRx K_d determination. Dissociation constants for compounds **2.2**, **2.3** and dasatinib were determined at DiscoveRx.

A. Tabulated K_d data.

Compound	Src	Abl	Abl T315I-nonphosphorylated	Abl T315I-phosphorylated
dasatinib*	0.21	0.029	890	
2.2	0.53	2.2	>40,000	
2.3	2.7	2.9	66	

B. Representative binding curves.

Src

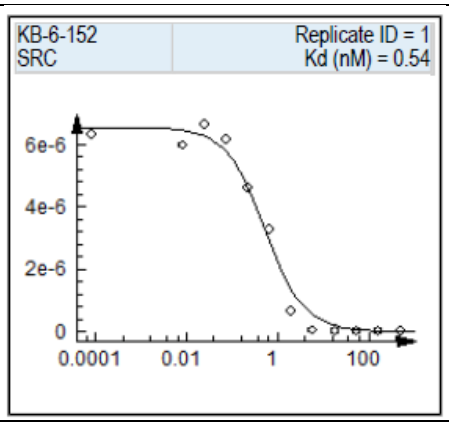

2.2

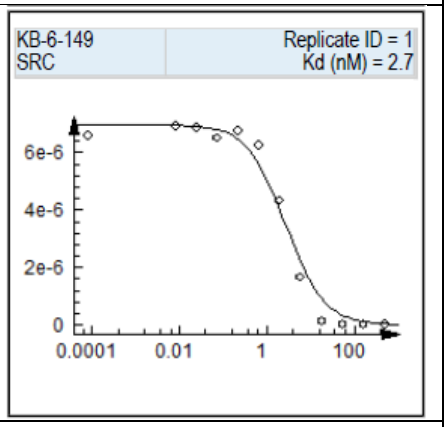

2.3

Abl

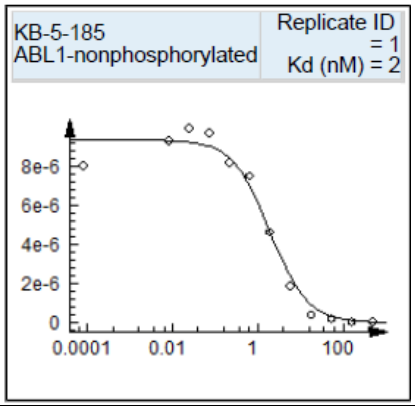

2.2

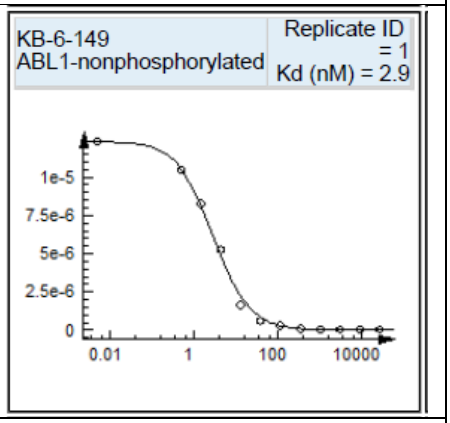

2.3

Abl T315I-nonphosphorylated	
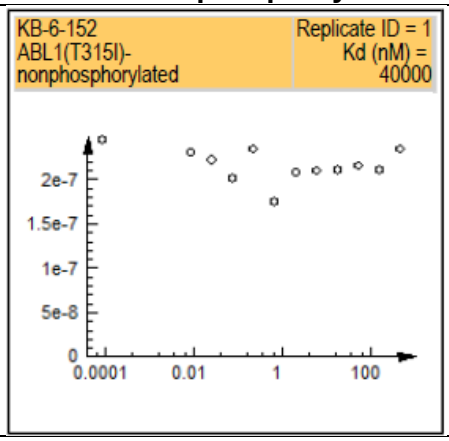	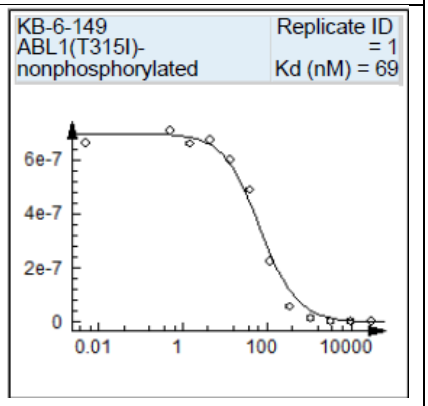
2.2	**2.3**

Abl T315I-phosphorylated	
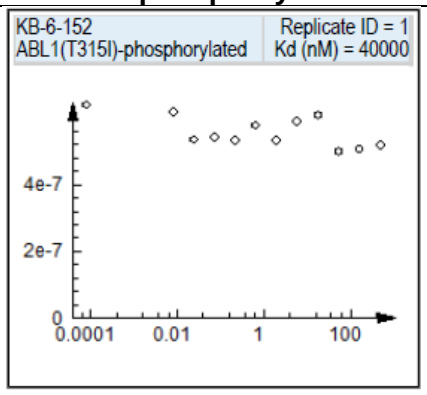	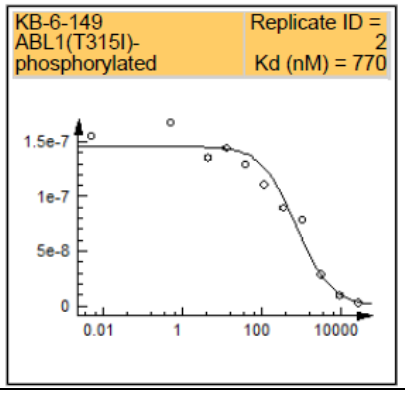
2.2	**2.3**

KINOMEscan selectivity profiling

Kinome profiling for compound **2.1** was performed by KINOMEScan (DiscoveRx, Fremont, CA). The compound was profiled at a concentration of 1 μM.

A. 2.1 TREEspot analysis:

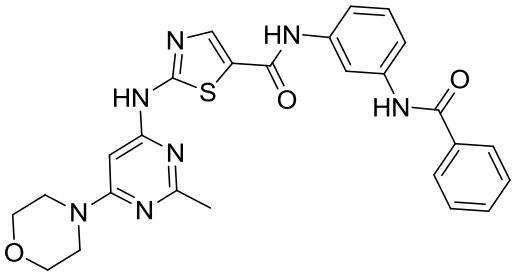

2.1

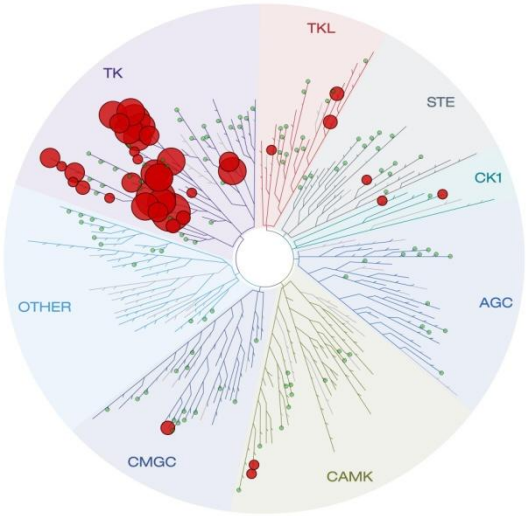

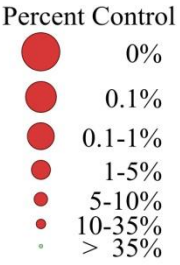

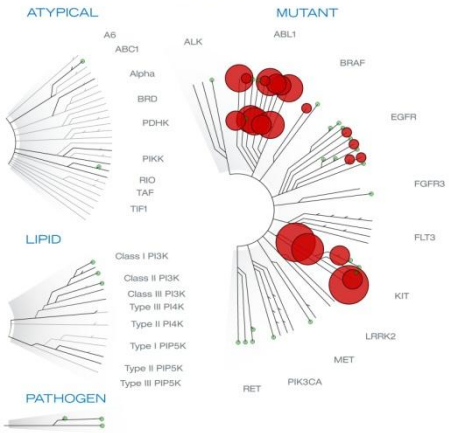

B. S-Scores for 2.1:

S(35) = 0.25

C. Tabulated data for compound 2.1:

KINOMEscan Gene Symbol	Percent Control
ABL1 (E255K)-phosphorylated	1.4
ABL1 (F317I)-nonphosphorylated	0.3
ABL1 (F317I)-phosphorylated	40
ABL1 (F317L)-nonphosphorylated	0.65
ABL1 (F317L)-phosphorylated	32
ABL1 (H396P)-nonphosphorylated	1
ABL1 (H396P)-phosphorylated	0.9
ABL1 (M351T)-phosphorylated	30
ABL1 (Q252H)-nonphosphorylated	1.9
ABL1 (Q252H)-phosphorylated	1.6
ABL1 (T315I)-nonphosphorylated	100
ABL1 (T315I)-phosphorylated	84
ABL1 (Y253F)-phosphorylated	0.35
ABL1-nonphosphorylated	0.15
ABL1-phosphorylated	0.6
ABL2	0.5
ACVR1	100
ACVR1B	100
ACVR2A	100
ACVR2B	93
ACVRL1	100
ADCK3	100
AKT1	100
AKT2	98
ALK	100
AURKA	69
AURKB	100
AXL	91
BLK	0.25
BMPR2	82
BMX	28
BRAF	56
BRAF (V600E)	32
BRK	51
BTK	68
CDK11	100
CDK2	89
CDK3	94
CDK7	100
CDK9	86
CHEK1	100
CSF1R	0.2
CSK	15
CSNK1D	100
CSNK1E	16
CSNK1G2	32
DCAMKL1	98
DDR1	0.2
DDR2	2.3
DMPK	75
DMPK2	90
DYRK1B	76
EGFR	85
EGFR (E746-A750del)	70
EGFR (G719C)	16
EGFR (G719S)	32
EGFR (L747-E749del, A750P)	55
EGFR (L747-S752del, P753S)	58
EGFR (L747-T751del,Sins)	34
EGFR (L858R)	97
EGFR (L858R,T790M)	59
EGFR (L861Q)	38
EGFR (S752-I759del)	32
EGFR (T790M)	64
EPHA1	100
EPHA2	3.3
EPHA3	18
EPHA4	2
EPHA5	2.4
EPHA6	100
EPHA7	80
EPHA8	0.9
EPHB1	7.9
EPHB2	17
EPHB3	100
EPHB4	14
EPHB6	6.4

ERBB2	89	MAP4K3	96
ERBB3	87	MAP4K4	100
ERBB4	51	MAP4K5	86
ERK1	100	MAPKAPK2	100
FAK	93	MARK3	94
FGFR1	100	MEK1	100
FGFR2	99	MEK2	93
FGFR3	100	MEK3	91
FGFR4	100	MEK4	100
FGR	1.3	MEK5	12
FLT1	3.6	MET	100
FRK	0.25	MKNK1	100
FYN	0.3	MKNK2	100
GAK	43	MLK1	87
GCN2 (Kin.Dom.2,S808G)	100	MRCKA	78
GSK3B	92	MRCKB	100
HCK	1.4	MST4	81
IGF1R	100	NLK	78
IKK-alpha	100	p38-alpha	36
IKK-beta	100	p38-beta	6
INSR	60	PAK1	100
JAK2 (JH1domain-catalytic)	97	PAK2	87
JAK3 (JH1domain-catalytic)	98	PAK4	100
JNK1	100	PCTK1	100
JNK2	82	PDGFRA	6.6
JNK3	94	PDGFRB	0
KIT	0	PDPK1	100
KIT (A829P)	94	PFCDPK1 (P.falciparum)	100
KIT (D816H)	62	PFPK5 (P.falciparum)	82
KIT (D816V)	3.2	PIK3C2B	77
KIT (L576P)	0.1	PIK3CA	90
KIT (V559D)	0	PIK3CG	89
KIT (V559D,T670I)	59	PIM1	100
KIT (V559D,V654A)	3.2	PIM2	88
KIT-autoinhibited	5.6	PIM3	100
LCK	0.4	PKAC-alpha	100
LIMK1	95	PKMYT1	96
LIMK2	83	PKNB (M.tuberculosis)	64
LKB1	100	PLK1	100
LOK	92	PLK3	100
LYN	0.9	PLK4	62
MAP3K4	100	PRKCE	100
MAP4K2	98	RAF1	47

RET	44	TESK1	81
RET (M918T)	78	TGFBR1	100
RET (V804L)	95	TGFBR2	66
RET (V804M)	100	TIE2	100
RIOK2	95	TNIK	99
RIPK2	25	TNK2	100
ROCK1	64	TNNI3K	5.1
ROCK2	64	TRKA	62
RSK2 (Kin.Dom.1-N-terminal)	89	TSSK1B	100
SIK	19	TXK	48
SIK2	19	TYK2 (JH1domain-catalytic)	100
SLK	100	ULK2	94
SNARK	71	VEGFR2	51
SRC	0.1	WEE1	100
SRMS	85	YANK3	90
SRPK3	100	YES	0.45
STK36	100	ZAK	5.6
SYK	100	ZAP70	100
TEC	11		

Luceome selectivity profiling

Kinome profiling for compound dasatinib **2.2** and **2.3** was performed by KinaseSeeker™ (Luceome Biotechnologies, Tucson, AZ). The compounds were all profiled at a final inhibitor concentration of 500 nM.

A. TREEspot analyses:

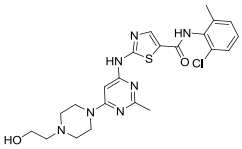

dasatinib

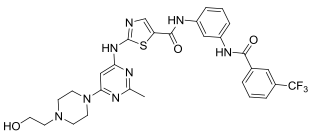

2.2

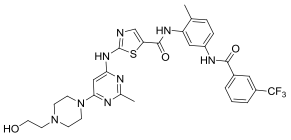

2.3

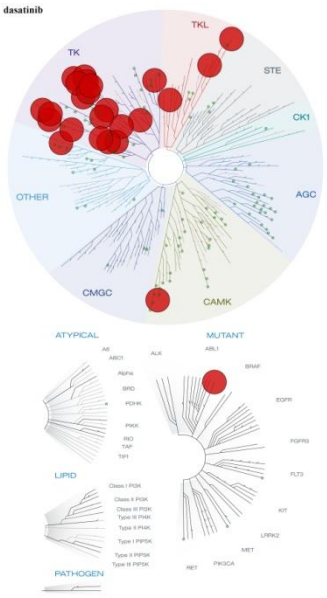

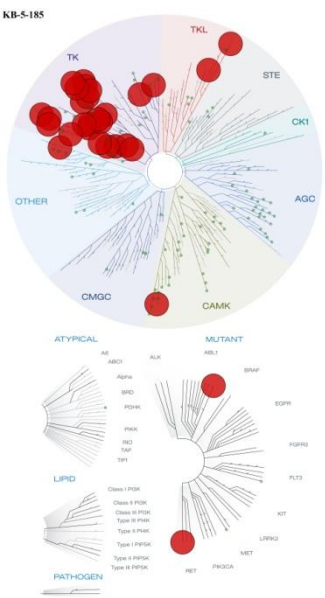

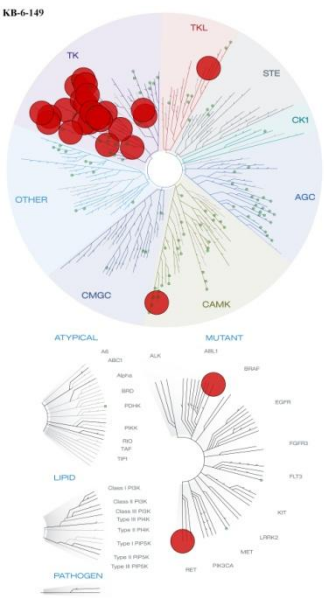

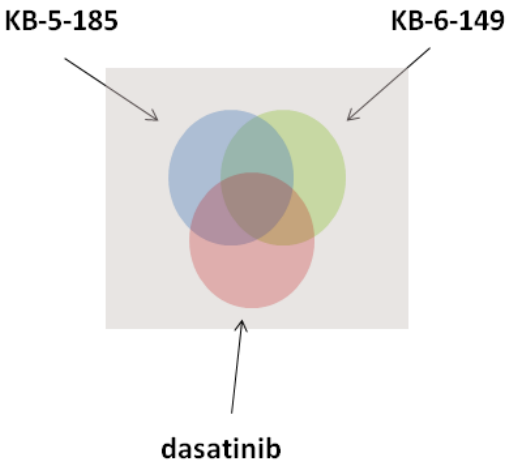

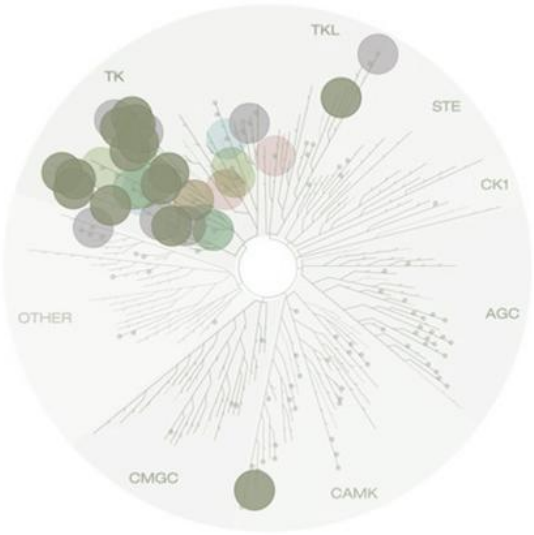

B. S(35) Scores for compounds:

dasatinib = 0.20

compound **2.2** = 0.23

compound **2.3** = 0.20

C. Tabulated Luceome selectivity profiling data for dasatinib, 2.2, and 2.3:

Kinase	% control		
	dasatinib	**2.2**	**2.3**
ABL1	1.9	4.2	10.9
ABL2	50.7	6.1	12.2
AKT1	95.1	97.5	100
AKT2	100	100	100
AKT3	73.3	92.2	100
AMPK-alpha1	93	100	100
AMPK-alpha2	67.8	70.6	100
AURKA	100	100	93.9
AURKB	100	100	100
AURKC	80.7	86.2	94.1
AXL	27.4	30.5	100
BIKE	100	97	100
BLK	0	0	6.2
BTK	35.5	73.9	26.4
CAMK1	100	100	100
CAMK1D	99.3	88.2	100
CAMK1G	100	100	97.2
CAMK2A	85.8	95.6	100
CAMK2B	68.4	92.6	100
CAMK2D	79.8	100	100
CAMKK1	75	78	100
CAMKK2	78.9	100	100
CHEK1	90.9	100	100
CSNK1D	100	100	100
CLK1	100	100	100
CLK2	100	100	100
CSK	31.3	78.9	11.5
DAPK1	100	100	97.4
DAPK2	100	100	100
DAPK3	100	100	100
DDR1	84.8	85.6	1.1
DDR2	51.8	49.2	9.1
DMPK	100	100	100
EPHA1	1.1	3.3	7.9
EPHA2	1.3	1.1	68.9
EPHA3	5.8	2.3	11.7
EPHA4	0	0	2.7

EPHB2	0	0	4.4
EPHB3	35.2	81.1	47.6
EPHB4	1.8	2.1	4
FGFR2	100	67.9	30.1
FLT1	100	4.8	6.7
FGFR1	57.2	62.2	56.7
FLT3	36.8	41.5	91.5
FYN	3.8	0.7	53.7
GSK3A	100	67.7	100
HCK	16.6	4.2	10
IGF1R	75.7	64	94.5
IKK-epsilon	100	100	100
INSR	100	100	64.2
ITK	42.3	50	100
LIMK1	50	82.1	63.9
LYN	5.9	5.9	54.1
MARK1	100	100	100
MARK2	100	100	100
MARK3	100	100	100
MARK4	100	100	100
MELK	92	100	95.9
MET	100	100	97
MLK1	38.4	40.9	100
MLK3	18.3	22.6	96.6
MST2	83.3	61.5	97.6
MUSK	86.4	20.6	60.6
MYLK	75.4	94.8	100
MYLK2	100	97	100
PKMYT1	46.9	59.9	100
p38-delta	100	100	100
PAK1	100	100	100
PDGFRA	21.3	31.9	79.1
PDGFRB	38.4	37.5	57.8
PDK1	100	100	100
PHKG1	95.7	99.5	98.2
PIM1	96.1	100	97.5
PIM2	97.4	89.6	100
PKAC-alpha	95.1	96.3	97.7
PRKACB	78.1	96.7	100
PRKCD	100	100	92.3
PRKCE	100	100	100
PRKCG	100	100	100
PRKCH	100	100	100

PRKCQ	92.4	100	100
PRKG1	100	100	97.4
PKN3	92	83.8	67
PRKX	72.8	89.3	100
PLK4	12.4	0	100
PRKD2	100	100	97.9
PRKD3	100	100	100
PTK2	100	100	100
PTK2B	100	95.2	100
PTK6	33.8	0.1	27
RET	92.2	1	11.9
RIPK2	0.1	37.2	51.8
RSK1(Kin.Dom.1-N-terminal)	92.5	100	100
RSK3(Kin.Dom.1-N-terminal)	100	94.6	100
RSK2(Kin.Dom.1-N-terminal)	100	100	99.1
RPS6KA4(Kin.Dom.1-N-terminal)	100	87.2	100
RPS6KA5(Kin.Dom.1-N-terminal)	88.3	96.7	100
RSK4(Kin.Dom.1-N-terminal)	100	100	100
SGK2	74.3	91.3	96.4
SGK3	100	100	100
QSK	57	95.1	95
SLK	100	96.2	95.3
SNARK	81.3	89.8	100
SNF1LK	12.9	28.8	10
SNF1LK2	41.3	74	47.9
SRC	8.8	10.6	16
STK16	79.4	75	100
STK33	100	100	100
SYK	73.3	89.9	100
TBK1	39.5	35.7	100
TEC	41.6	86	28.8
TESK1	49.1	94.1	78.3
TESK2	45.1	93.7	50.4
TIE1	100	27.4	64.9
TIE2	100	33.3	15.2
TNK2	24.8	91.9	39.6
TNNI3K	25.9	12.7	20.1
TRKB	100	70.6	54.8
TRKC	100	77.8	48.3
TXK	16.2	32.5	18
VEGFR2	100	15.2	49.3

YANK2	100	100	88.2
YES	8	0	12.7
YSK1	100	100	98.6

2.5 References

(1) Wang, Q.; Cahill, S. M.; Blumenstein, M.; Lawrence, D. S. *Journal of the American Chemical Society* **2006**, *128*, 1808-1809.

(2) Liu, Y.; Gray, N. S. *Nat Chem Biol* **2006**, *2*, 358-364.

(3) Okram, B.; Nagle, A.; AdriÃ¡n, F. J.; Lee, C.; Ren, P.; Wang, X.; Sim, T.; Xie, Y.; Wang, X.; Xia, G.; Spraggon, G.; Warmuth, M.; Liu, Y.; Gray, N. S. *Chemistry & Biology* **2006**, *13*, 779-786.

(4) Das, J.; Chen, P.; Norris, D.; Padmanabha, R.; Lin, J.; Moquin, R. V.; Shen, Z.; Cook, L. S.; Doweyko, A. M.; Pitt, S.; Pang, S.; Shen, D. R.; Fang, Q.; de Fex, H. F.; McIntyre, K. W.; Shuster, D. J.; Gillooly, K. M.; Behnia, K.; Schieven, G. L.; Wityak, J.; Barrish, J. C. *Journal of Medicinal Chemistry* **2006**, *49*, 6819-6832.

(5) Lombardo, L. J.; Lee, F. Y.; Chen, P.; Norris, D.; Barrish, J. C.; Behnia, K.; Castaneda, S.; Cornelius, L. A. M.; Das, J.; Doweyko, A. M.; Fairchild, C.; Hunt, J. T.; Inigo, I.; Johnston, K.; Kamath, A.; Kan, D.; Klei, H.; Marathe, P.; Pang, S.; Peterson, R.; Pitt, S.; Schieven, G. L.; Schmidt, R. J.; Tokarski, J.; Wen, M.-L.; Wityak, J.; Borzilleri, R. M. *Journal of Medicinal Chemistry* **2004**, *47*, 6658-6661.

(6) Tokarski, J. S.; Newitt, J. A.; Chang, C. Y. J.; Cheng, J. D.; Wittekind, M.; Kiefer, S. E.; Kish, K.; Lee, F. Y. F.; Borzillerri, R.; Lombardo, L. J.; Xie, D.; Zhang, Y.; Klei, H. E. *Cancer Research* **2006**, *66*, 5790-5797.

(7) Nagar, B.; Bornmann, W. G.; Pellicena, P.; Schindler, T.; Veach, D. R.; Miller, W. T.; Clarkson, B.; Kuriyan, J. *Cancer Research* **2002**, *62*, 4236-4243.

(8) Davis, M. I.; Hunt, J. P.; Herrgard, S.; Ciceri, P.; Wodicka, L. M.; Pallares, G.; Hocker, M.; Treiber, D. K.; Zarrinkar, P. P. *Nat Biotech* **2011**, *29*, 1046-1051.

(9) Branford, S.; Melo, J. V.; Hughes, T. P. *Blood* **2009**, *114*, 5426-5435.

(10) Shah, N. P.; Tran, C.; Lee, F. Y.; Chen, P.; Norris, D.; Sawyers, C. L. *Science* **2004**, *305*, 399-401.

(11) von Bubnoff, N.; Schneller, F.; Peschel, C.; Duyster, J. *The Lancet* **2002**, *359*, 487-491.

(12) Shah, N. P.; Nicoll, J. M.; Nagar, B.; Gorre, M. E.; Paquette, R. L.; Kuriyan, J.; Sawyers, C. L. *Cancer Cell* **2002**, *2*, 117-125.

(13) Huang, W.-S.; Metcalf, C. A.; Sundaramoorthi, R.; Wang, Y.; Zou, D.; Thomas, R. M.; Zhu, X.; Cai, L.; Wen, D.; Liu, S.; Romero, J.; Qi, J.; Chen, I.; Banda, G.; Lentini, S. P.; Das, S.; Xu, Q.; Keats, J.; Wang, F.; Wardwell, S.; Ning, Y.; Snodgrass, J. T.; Broudy, M. I.; Russian, K.; Zhou, T.; Commodore, L.; Narasimhan, N. I.; Mohemmad, Q. K.; Iuliucci, J.; Rivera, V. M.; Dalgarno, D. C.; Sawyer, T. K.; Clackson, T.; Shakespeare, W. C. *Journal of Medicinal Chemistry* **2010**, *53*, 4701-4719.

(14) Jester, B. W.; Cox, K. J.; Gaj, A.; Shomin, C. D.; Porter, J. R.; Ghosh, I. *Journal of the American Chemical Society* **2010**, *132*, 11727-11735.

(15) Patricelli, M. P.; Szardenings, A. K.; Liyanage, M.; Nomanbhoy, T. K.; Wu, M.; Weissig, H.; Aban, A.; Chun, D.; Tanner, S.; Kozarich, J. W. *Biochemistry* **2006**, *46*, 350-358.

(16) Kuma, Y.; Sabio, G.; Bain, J.; Shpiro, N.; MÃ¡rquez, R.; Cuenda, A. *Journal of Biological Chemistry* **2005**, *280*, 19472-19479.

CHAPTER 3

Rational design of c-helix out inhibitors

This chapter continues to address the question of "*How does binding an "inactive" fold influence kinase inhibitor selectivity?"* The focus of this chapter is on inhibitors that bind the c-helix out inactive conformation of protein kinases (For an in-depth introduction to c-helix out inhibitors see Chapter 1.5) Unlike DFG-out inhibitors there is no known general method for converting a DFG-in inhibitor to a c-helix out inhibitor. A careful analysis reveals key differences between inhibitors which respectively bind the DFG-out and c-helix out inactive kinase forms, and a general method for selectively targeting the c-helix out fold was developed (Figure 3.1).

3.1 Introduction

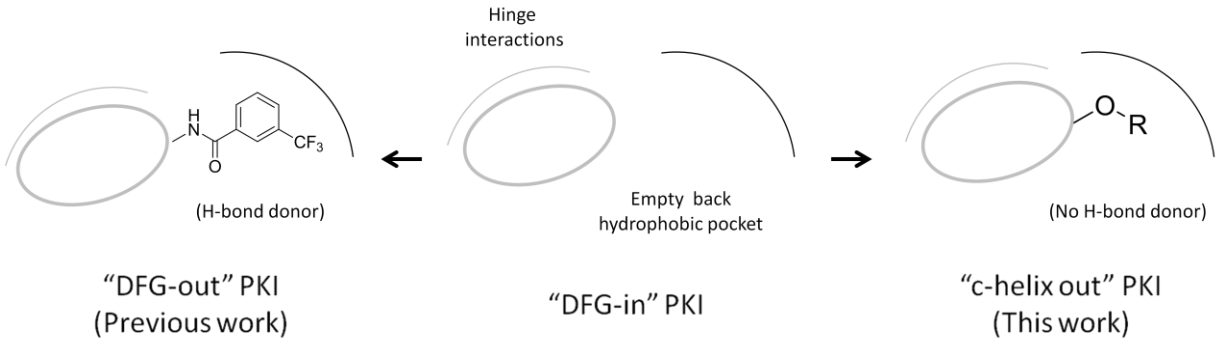

Figure 3.1. General strategy for conversion of a DFG-in to c-helix out inhibitor.

Binding the c-helix out conformation has an unknown influence on kinase inhibitor selectivity. In order to investigate this possibility it was decided that a general method for the synthesis of c-helix out kinase inhibitors would be useful. There is no method for creating c-helix out inhibitors analogous to the DFG-in to DFG-out conversion described

in Chapter 1.4. In an effort toward convertin a DFG-in inhibitor to a c-helix out inhibitor the general chemical features of the binding mode were analyzed.

3.2 Results and discussion

In general, c-helix out kinase inhibitors contain a chemical feature which encroaches upon the back of the ATP-pocket which forces the alpha-c helix out of its usual catalytically active position. DFG-out kinase inhibitors also occupy this back region. In order to bias inhibitor design toward binding the c-helix out conformation a comparison of DFG-out and c-helix out inhibitor binding modes was conducted (Figure 3.2). It was observed that DFG-out kinase inhibitors routinely have a hydrogen bond donor interaction with the conserved glutamate of the c-helix. It was hypothesized that elimination of this feature would bias inhibitor binding to the c-helix out conformation. A series of dasatinib derivatives were created based upon this assumption (Figure 3.3).

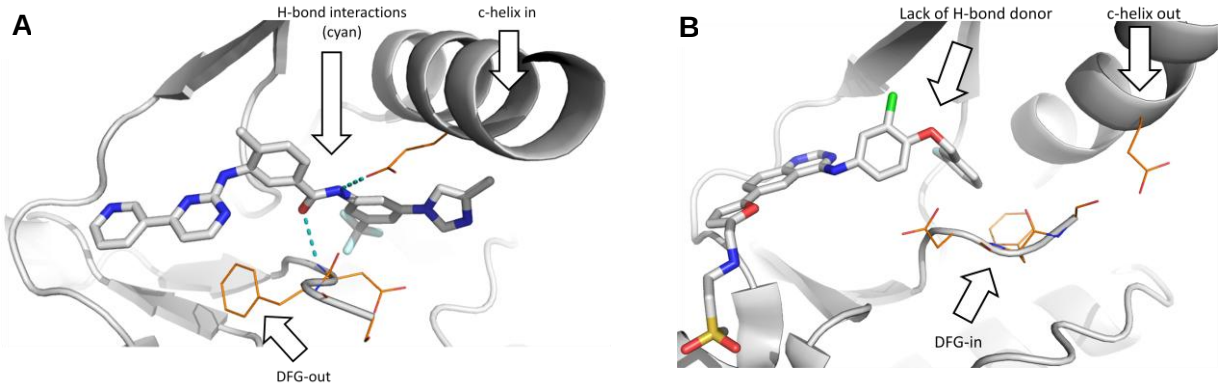

Figure 3.2. General chemical features of DFG-out and c-helix out kinase inhibitors. A) Co-crystal structure of imatinib bound to Abl kinase in the DFG-out conformation with key hydrogen bonds displayed in cyan. PDB: 1IEP B) Co-crystal structure of lapatinib bound to EGFR in the c-helix out conformation. PDB: 1XKK.

In order to initially characterize the impact that these substitutions had on inhibitor potency activity-based kinase assays were conducted (Figure 3.3). All compounds tested displayed excellent potency for the selected kinases. It is of some interest that all compounds were strong inhibitors of Abl because the c-helix out conformation has not been previously observed for this kinase. When tested against a commonly observed resistance mutation, all compounds displayed negligible inhibition, even less so than dasatinib.

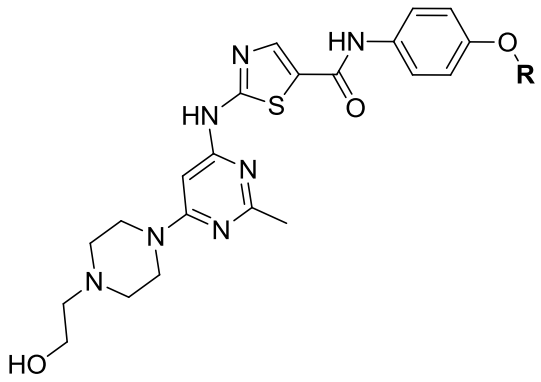

R =

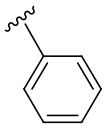

3.1

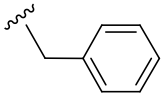

3.2

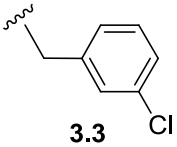

3.3

Compound	K_i (nM) c-Src	Abl	Src T341M	Src T341I
3.1	≤ 0.6	<0.2	ni	ni
3.2	≤ 0.6	<0.2	ni	ni
3.3	≤ 0.6	<0.2	ni	ni
dasatinib	≤ 0.6	<0.2	3,300	1,586

Figure 3.3. Structures and biochemical inhibition assays for compounds **3.1-3.3**. n.i. = no inhibition up to 125 µM inhibitor.

Our laboratory has previously observed that incorporation of a methyl substituent in the central phenyl ring of dasatinib analogs confers significant potency for kinases bearing the "gatekeeper mutation". A compound which included this feature was synthesized (compound **3.4**) and was subsequently subjected to inhibition assays (Figure 3.4). Gratifyingly, a significant increase in potency in inhibition of the both gatekeeper mutants was observed.

Despite the promising biochemical inhibition profile of compound **3.4** there was no evidence supporting that it binds the c-helix out conformation as it was intended to. Therefore co-crystallization with the kinase domains both Src and Abl with all new compounds was attempted. Compound **3.1** provided acceptable crystals that diffracted at 2.45 Å and 2.9 Å respectively for Src and Abl. The structure of Src bound to compound **3.1** is shown in Figure 3.5. As expected, the density for the DFG motif clearly corresponds with what would be expected from a DFG-in conformation, additionally the c-helix is swung outward in order to accommodate the phenoxy substituent. It is noteworthy that this is the first observation of Abl kinase in the c-helix out conformation.

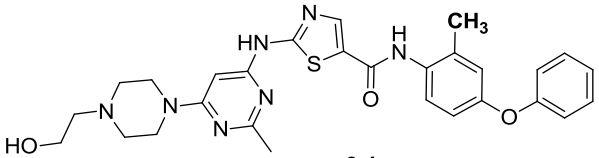

3.4

Compound	K_i (nM) Src	Abl	Src T341M	Src T341I
3.4	<0.6	<0.2	n.d.	32

Figure 3.4. Activity-based kinase inhibition assays for compound **3.4**.

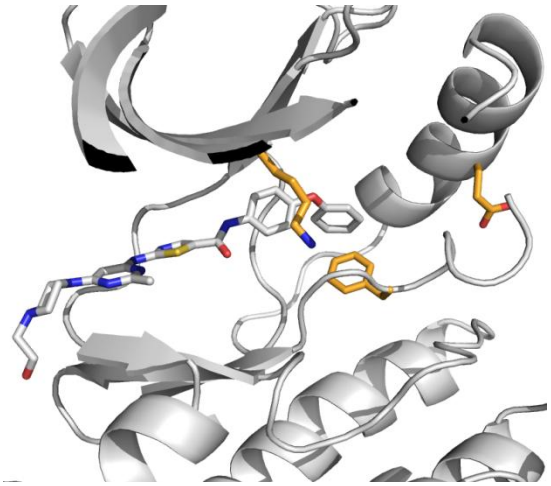

Figure 3.5. Co-crystal structures of compound **3.1** bound to Src kinase. Data kindly provided by Frank Kwarcinski (Soellner lab).

Structural validation of compound **3.1** binding Abl in a c-helix out conformation implied that the selectivity of this set of inhibitors may be lower than other known c-helix out inhibitors. Compound **3.4** was subjected profiling against a diverse panel of 131 kinases using a single point binding assay[1] (Figure 3.6). Compound **3.4** was found to be more selective than dasatinib (S(35) score = 0.16 and 0.20 respectively; S(35) is defined as the number of kinases that displayed ≤ 35% of competitor probe remaining bound). The most pronounced difference in the profiles **3.4** and dasatinib was loss of inhibition of the Eph family kinases for the c-helix out compound. These data generally suggest that the inhibitor binding of the c-helix out conformation may be a valid strategy to increase selectivity.

The cellular performance of compound **3.4** was assessed in the MDA-MB-231 breast cancer cell line. This cell line is triple-negative for expression of the estrogen receptor, progesterone receptor and Her2/neu. The triple-negative phenotype accounts for 15 percent of all types of breast cancer[2] and has clinically been observed to have increased tumor size, likelihood of death, distant metastases and recurrence relative to non-triple-negative tumors[3-6]. The triple-negative tumors are also more difficult to treat because of the absence of the receptor targets, therefore new therapy options would be beneficial.

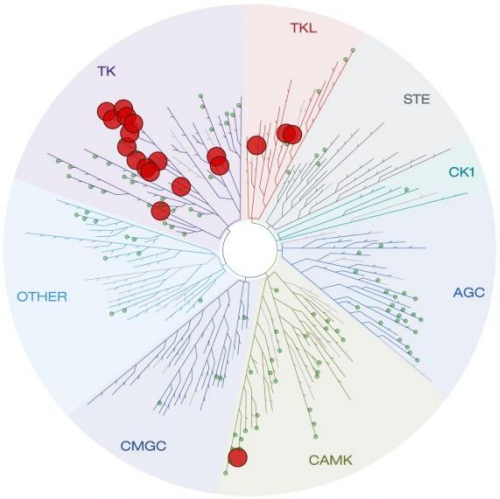

Figure 3.6. Kinome selectivity profile for compound **3.4** using a single point binding assay. Compound **3.4** was screened at 500 nM. Red circles indicate >65 % binding, and small green dots indicate kinases included in the panel that did not display any binding. For a tabulated list of binding data see experimental section.

Promisingly, compound **3.4** performed similarly to dasatinib (Table 3.1) in two-dimensional cell culture. It has been observed that 3-dimensional cell culture can provide results that more closely align with what would be seen *in vivo*[7], and so **3.4** was tested under these conditions. It was reassuring to see that compound **3.4** also appreciably inhibited cell growth under these conditions as well.

Compound	**MDA-MB-231 (2D) GI_{50} (μM)**	**MD-MB-231 (3D) % inhibition (1 uM cpd)**
3.4	8.3	48.0
dasatinib	6.5	50.7

Table 3.1. Treatment of breast cancer cells using **3.4** and dasatinib. Data kindly provided by Michael Steffey (Soellner lab).

3.3 Conclusions

This chapter describes a method developed to transform a DFG-in kinase inhibitor to a c-helix out kinase inhibitor. Application of this method allowed for a comparison of the selectivity of DFG-in and c-helix out inhibitors derived from the same chemical scaffold. It appears that targeting the c-helix out inactive conformation does improve inhibitor selectivity, which is in contrast to the findings described in Chapter 2 with DFG-out inhibitors, Thus, the development of general strategy described above will likely be valuable for further generation of c-helix out kinase inhibitors.

3.4 Experimental section

GENERAL SYNTHETIC METHODS. Unless otherwise noted, all reagents were obtained via commercial sources and used without further purification. Tetrahydrofuran (THF) and dichloromethane (CH_2Cl_2) were dried over alumina under a nitrogen atmosphere. All ^{1}H and ^{13}C NMR spectra were measured with a Varian MR400, VNMRS 500 or Inova 500 spectrometer. Mass Spectrometry (HRMS) was carried out by the University of Michigan Mass Spectrometry Facility (J. Windak, director).

SYNTHESIS OF COMPOUNDS 3.S1-3.4

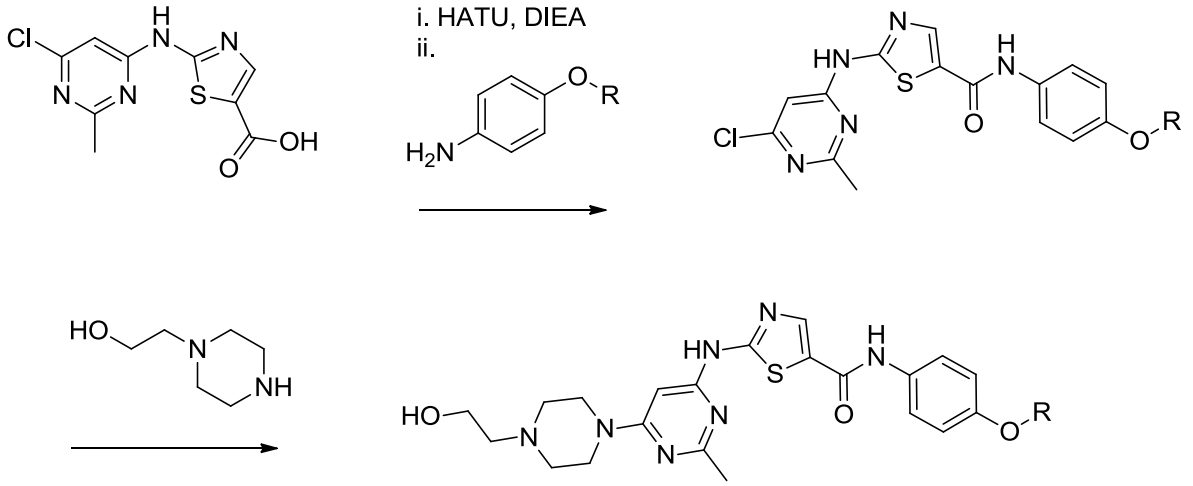

Scheme 3.S-1. Representative synthetic routes for final compounds 3.1 –3.4.

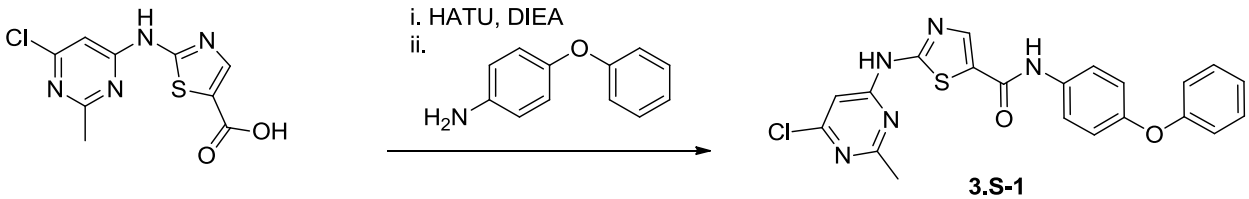

Synthesis of 3.S-1: 2-((6-chloro-2-methylpyrimidin-4-yl)amino)thiazole-5-carboxylic acid (44 mg, 0.162 mmol) and HATU (68 mg, 0.178 mmol) were added to an oven-dried round bottom flask. N,N-dimethylformamide (0.8 mL) was then added, followed by diisopropylethylamine (0.085 mL, 0.486 mmol). The reaction was allowed to stir at room

temperature for 45 min. 4-phenoxyaniline (30 mg, 0.162 mmol) was then added, and the reaction was allowed to stir overnight at room temperature. The reaction mixture was then precipitated by addition of water. The crude mixture was filtered, and the solid that was collected was then subjected to silica gel chromatography using a 30 → 100% ethyl acetate in hexanes gradient. Product **3.S-1** was isolated as tan solid. **Spectral data.** ^{1}H NMR (400 MHz, DMSO-d_6) δ 12.20 (s, 1H), 10.19 (s, 1H), 8.29 (s, 1H), 7.68 (d, J = 8.4 Hz, 2H), 7.35 (t, J = 7.8 Hz, 2H), 7.09 (t, J = 7.4 Hz, 1H), 7.04 – 6.89 (m, 5H), 2.57 (s, 3H). ^{13}C NMR (100 MHz, DMSO-d_6): ^{13}C NMR (126 MHz, dmso) δ 167.88, 161.69, 159.87, 158.96, 157.94, 157.63, 152.65, 141.04, 134.94, 130.44, 123.55, 122.32, 119.71, 118.50, 118.32, 103.85, 25.65; HRMS-ESI (*m/z*): $[M + H]^+$ calcd for $C_{21}H_{16}ClN_5O_2S$, 438.0786; found 438.0792.

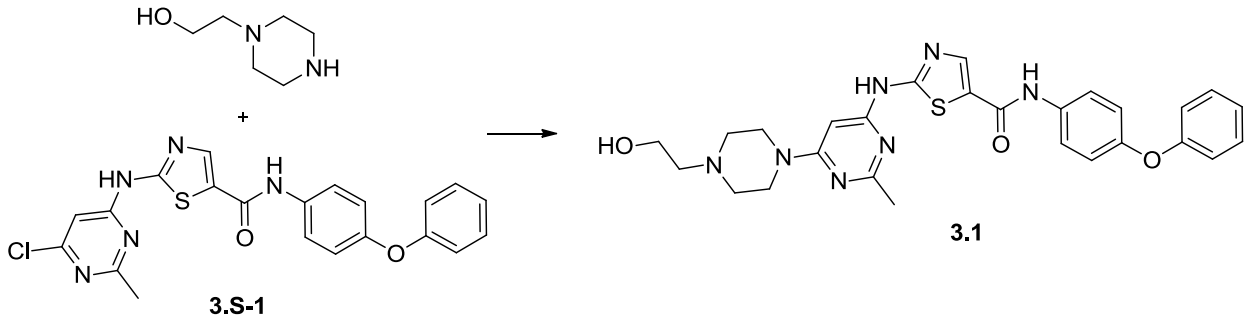

Synthesis of 3.1: Compound **3.S-1** (10 mg, 0.023 mmol) was added to an oven-dried round bottom flask. Dioxane (0.228 mL) was then added, followed by 1-(2-hydroxyethyl)piperazine) (0.028 mL, 0.228 mmol). The reaction was then refluxed overnight. The reaction was then allowed to cool to room temperature, and the dioxane was removed under reduced pressure. The crude residue was the purified using reverse-phase HPLC using a 5→95% acetonitrile in water gradient. Product **3.1** was isolated as 3 mg of a white solid (25% yield). **Spectral data.** ^{1}H NMR (400 MHz, DMSO-d_6) δ 11.46 (s, 1H), 10.08 (s, 1H), 8.21 (s, 1H), 7.72 – 7.64 (m, 2H), 7.35 (dd, J = 8.6, 7.3 Hz, 2H), 7.08 (t, J = 7.4 Hz, 1H), 7.04 – 6.92 (m, 4H), 6.03 (s, 1H), 3.29 (s, 3H), 3.21 (s, 0H), 2.39 (s, 4H), 0.79 (s, 0H). ^{13}C NMR (126 MHz, dmso) δ 165.66, 163.01, 162.75, 160.24, 157.71, 157.41, 152.43, 141.04, 135.20, 130.42, 127.11, 123.49, 122.18, 119.73, 118.44, 83.18, 52.83; 26.04. HRMS-ESI (*m/z*): $[M + H]^+$ calcd for $C_{27}H_{29}N_7O_3S$, 532.2125; found 532.2118.

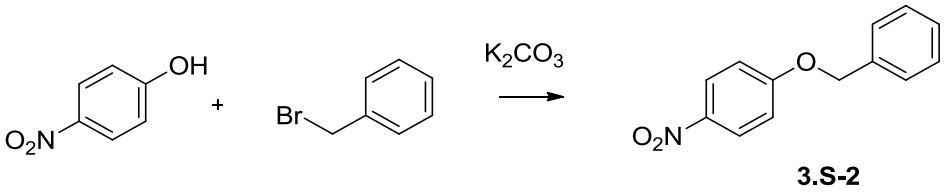

Synthesis of 3.S-2: 4-nitrophenol (2.3 g, 16.5 mmol) and potassium carbonate (4.57 g, 33.1 mmol) were added to an oven-dried round bottom flask. N,N-dimethylformamide (30 mL) was then added followed by benzyl bromide (2.0 mL, 16.5 mmol). The reaction mixture was then heated to 40^{o} C overnight. The reaction mixture was then added to

120 mL of water. After filtration **3.S-2** was obtained as a light yellow solid (3.5 g, 15.3 mmol, 92% yield). **Spectral data.** ^{1}H NMR (400 MHz, Chloroform-*d*) δ 8.23 – 8.13 (m, 2H), 7.47 – 7.31 (m, 5H), 7.06 – 6.97 (m, 2H), 5.15 (s, 2H). ^{13}C NMR (125 MHz, Chloroform-*d*): δ 163.73, 141.66, 135.54, 128.83, 128.53, 127.54, 125.94, 114.89, 70.70; HRMS-EI (*m/z*): calcd for $C_{13}H_{11}NO_3$, 229.0739; found 229.0744.

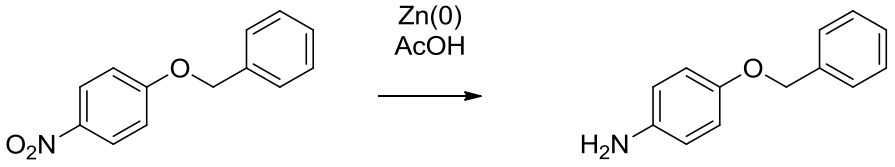

3.S-2 **3.S-3**

Synthesis of 3.S-3: Compound **3.S-2** (2.0 g, 8.7 mmol) and zinc (2.74 g, 42 mmol) were added to an oven-dried round bottom flask. Tetrahydrofuran (44 mL) was then added, followed by acetic acid (2 mL, 35 mmol). The reaction was stirred overnight under N_2. The crude mixture was then filtered through celite. Tetrahydrofuran was removed under reduced pressure. The crude mixture was then subjected to silica gel chromatography (0→85% ethyl acetate in hexanes) to afford 1.24 g (6.22 mmol) of **3.S-3** as a dark red oil (71% yield). **Spectral data.** ^{1}H NMR (500 MHz, Chloroform-*d*) δ 7.47 – 7.29 (m, 5H), 6.86 – 6.80 (m, 2H), 6.70 – 6.63 (m, 2H), 5.01 (s, 2H), 3.45 (s, 2H). ^{13}C NMR (126 MHz, Chloroform-*d*) δ 147.23, 135.48, 132.76, 123.73, 123.02, 122.72, 111.59, 111.32, 66.03; HRMS-ESI (*m/z*): $[M + H]^+$ calcd for $C_{13}H_{13}NO$, 200.1070; found 200.1071.

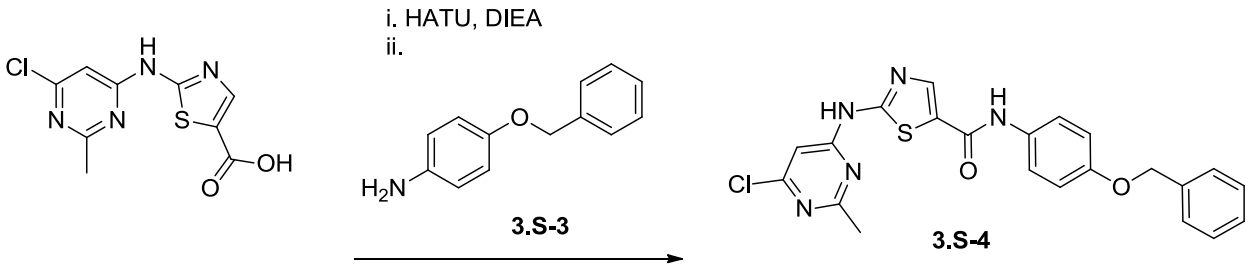

3.S-3 **3.S-4**

Synthesis of 3.S-4: 2-((6-chloro-2-methylpyrimidin-4-yl)amino)thiazole-5-carboxylic acid (18 mg, 0.075 mmol) and HATU (116 mg, 0.305 mmol) were added to an oven-dried round bottom flask. N,N-dimethylformamide (1.385 mL) was then added, followed by diisopropylethylamine (0.194 mL, 1.1 mmol). The reaction was allowed to stir at room temperature for 45 min. **3.S-3** (55 mg, 0.277 mmol) was then added, and the reaction was allowed to stir overnight at room temperature. The reaction mixture was then precipitated by addition of water. The crude mixture was filtered, and the solid that was collected was then subjected to silica gel chromatography using a 30 → 100% ethyl acetate in hexanes gradient. Product **3.S-4** was isolated as a tan solid. **Spectral data.** ^{1}H NMR (500 MHz, DMSO-d_6) δ 12.21 (s, 1H), 10.08 (s, 1H), 8.28 (s, 1H), 7.62 – 7.55

(m, 2H), 7.39 (ddd, *J* = 32.4, 24.7, 7.2 Hz, 5H), 7.05 – 6.97 (m, 2H), 6.93 (s, 1H), 5.09 (s, 2H), 2.60 (s, 3H). ^{13}C NMR (126 MHz, dmso) δ 167.87, 161.54, 159.67, 158.93, 157.96, 155.08, 140.68, 137.59, 132.35, 128.84, 128.23, 128.12, 122.26, 115.27, 103.85, 69.81, 25.64; HRMS-ESI (*m/z*): $[M + H]^+$ calcd for $C_{22}H_{18}ClN_5O_2S$, 452.0942; found 452.0938.

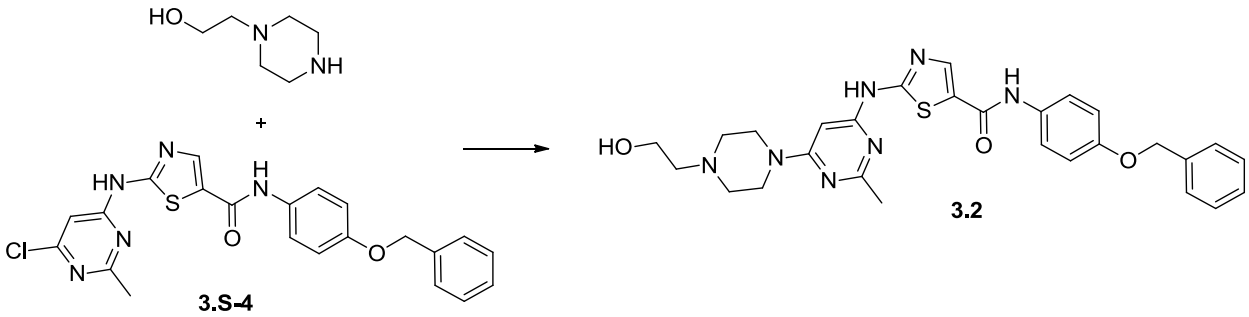

Synthesis of 3.2: Compound **3.S-4** (18 mg, 0.04 mmol) was added to an oven-dried round bottom flask. Dioxane (0.200 mL) was then added, followed by 1-(2-hydroxyethyl)piperazine) (0.049 mL, 0.398 mmol). The reaction was then refluxed overnight. The reaction was then allowed to cool to room temperature, and the dioxane was removed under reduced pressure. The crude residue was the purified using reverse-phase HPLC using a 5→95% acetonitrile in water gradient. Product **3.2** was isolated as a white solid. **Spectral data.** HRMS-ESI (*m/z*): $[M + H]^+$ calcd for $C_{28}H_{31}N_7O_3S$, 546.2282; found 546.2277.

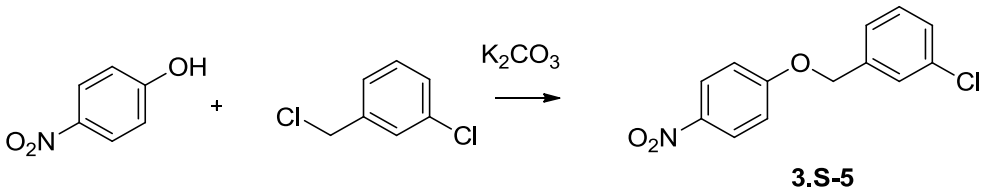

Synthesis of 3.S-5: 4-nitrophenol (2.3 g, 16.5 mmol) and potassium carbonate (4.57 g, 33.1 mmol) were added to an oven-dried round bottom flask. N,N-dimethylformamide (30 mL) was then added followed by 3-chlorobenzyl chloride (2.1 mL, 16.5 mmol). The reaction mixture was then stirred at room temperature overnight. The reaction mixture was diluted in ether. The organic solution was washed twice with water, followed by a brine wash. The organic solution was dried over sodium sulfate. The solvent was removed under reduced pressure. The crude residue was subjected to silica gel chromatography (5→25% ethyl acetate in hexanes) to afford 1.0 g of **3.S-5** as a yellow solid (23% yield). **Spectral data.** ^{1}H NMR (500 MHz, Chloroform-*d*) δ 8.26 – 8.20 (m, 2H), 7.45 (s, 1H), 7.42 – 7.25 (m, 4H), 7.04 (d, *J* = 9.2 Hz, 2H), 5.15 (s, 2H). ^{13}C NMR (126 MHz, Chloroform-*d*) δ 163.29, 141.85, 137.51, 134.76, 130.10, 128.65, 127.45,

125.99, 125.38, 114.83, 69.75; HRMS-EI (*m/z*): calcd for $C_{13}H_{10}ClNO_3$, 263.0349; found 263.0359.

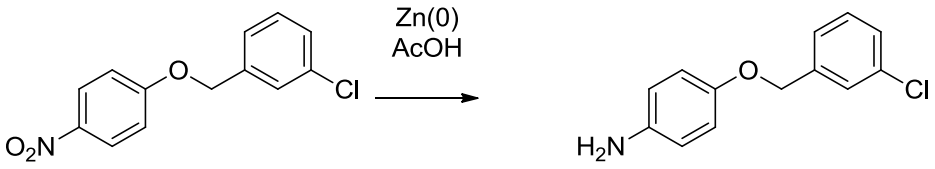

3.S-5 **3.S-6**

Synthesis of 3.S-6: Compound **3.S-5** (1.0 g, 3.8 mmol) and zinc (1.19 g, 18.2 mmol) were added to an oven-dried round bottom flask. Tetrahydrofuran (19 mL) was then added, followed by acetic acid (2 mL, 35 mmol). The reaction was stirred overnight under N_2. The crude mixture was then filtered through celite. Tetrahydrofuran was removed under reduced pressure. The crude mixture was then subjected to silica gel chromatography (5→25% ethyl acetate in hexanes) to afford 1.24 g (6.22 mmol) of **3.S-6** as a light red oil (71% yield). **Spectral data.** ^{1}H NMR (400 MHz, Chloroform-*d*) δ 7.41 (dt, *J* = 2.3, 1.1 Hz, 1H), 7.27 (q, *J* = 1.7 Hz, 3H), 6.83 – 6.74 (m, 2H), 6.67 – 6.58 (m, 2H), 4.94 (s, 2H), 3.18 (s, 3H). ^{13}C NMR (126 MHz, Chloroform-*d*) δ 151.63, 140.45, 139.62, 134.40, 129.79, 127.91, 127.43, 125.38, 116.37, 116.05, 69.94; HRMS-ESI (*m/z*): $[M + H]^+$ calcd for $C_{13}H_{12}ClNO$, 234.0680; found 234.0680.

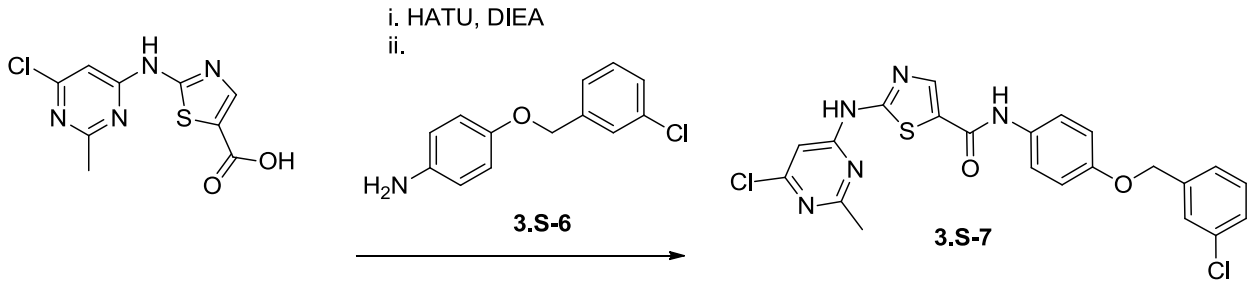

Synthesis of 3.S-7: 2-((6-chloro-2-methylpyrimidin-4-yl)amino)thiazole-5-carboxylic acid (13 mg, 0.047 mmol) and HATU (20 mg, 0.052 mmol) were added to an oven-dried round bottom flask. N,N-dimethylformamide (0.235 mL) was then added, followed by diisopropylethylamine (0.025 mL, 0.141 mmol). The reaction was allowed to stir at room temperature for 45 min. Compound **3.S-6** (11 mg, 0.047 mmol) was then added, and the reaction was allowed to stir overnight at room temperature. The reaction mixture was then precipitated by addition of water. The crude mixture was filtered, and the solid that was collected was then subjected to silica gel chromatography using a 30 → 100% ethyl acetate in hexanes gradient. The product **3.S-7** was isolated as a white solid. **Spectral data.** ^{1}H NMR (400 MHz, DMSO-d_6) δ 12.19 (s, 1H), 10.07 (s, 1H), 8.26 (s, 1H), 7.57 (d, *J* = 8.5 Hz, 2H), 7.48 (s, 1H), 7.38 (d, *J* = 6.8 Hz, 3H), 6.98 (d, *J* = 8.5 Hz, 2H), 6.91 (s, 1H), 5.08 (s, 2H), 2.57 (s, 3H). ^{13}C NMR (126 MHz, dmso) δ 167.88, 161.56, 159.70,

158.93, 157.95, 154.79, 140.74, 140.22, 133.54, 132.54, 130.81, 128.85, 128.16, 127.73, 126.62, 122.27, 115.31, 103.85, 68.85, 25.67.; HRMS-ESI (*m/z*): $[M + H]^+$ calcd for $C_{22}H_{17}Cl_2N_5O_2S$, 486.0553; found 486.0546.

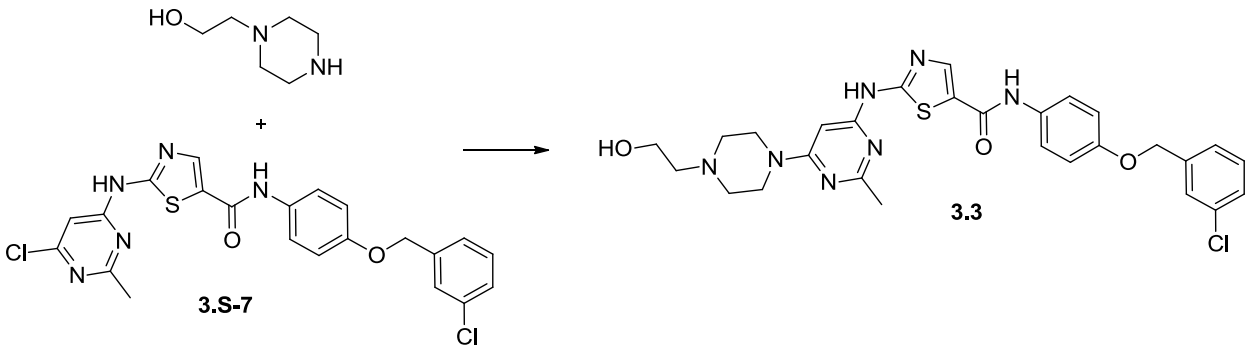

Synthesis of 3.3: Compound **3.S-7** (10 mg, 0.023 mmol) was added to an oven-dried round bottom flask. Dioxane (0.230 mL) was then added, followed by 1-(2-hydroxyethyl)piperazine) (0.028 mL, 0.228 mmol). The reaction was then refluxed overnight. The reaction was then allowed to cool to room temperature, and the dioxane was removed under reduced pressure. The crude residue was the purified using reverse-phase HPLC using a 5→95% acetonitrile in water gradient. **Spectral data.** HRMS-ESI (*m/z*): $[M + H]^+$ calcd for $C_{28}H_{30}ClN_7O_3S$, 580.1892; found 580.1895.

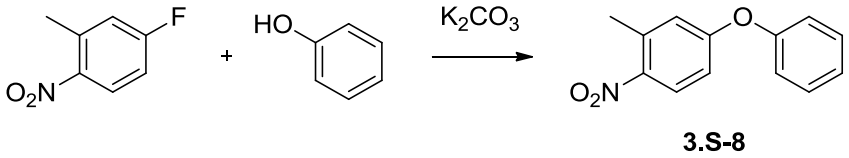

Synthesis of 3.S-8: 4-fluoro-2-methyl-1-nitrobenzene (1 g, 6.45 mmol), phenol (0.61 g, 6.45 mmol), and potassium carbonate (2.67 g, 19.34 mmol) were added to an oven-dried flask. N,N-dimethylformamide (21.5 mL) was then added and the reaction mixture was heated to 85^{o}C overnight. The reaction mixture was cooled to room temperature and subsequently diluted with ethyl acetate. The organic solution was then washed with neutral water twice, followed by one wash with brine. The organic layer was then dried over sodium sulfate. The solvent was then removed under reduced pressure. The product was isolated as 2.1 g (86% yield) of an oil. **Spectral data.** ^{1}H NMR (400 MHz, Chloroform-*d*) δ 8.07 – 7.99 (m, 1H), 7.46 – 7.30 (m, 2H), 7.22 (dt, *J* = 7.2, 1.3 Hz, 1H), 7.10 – 7.00 (m, 2H), 6.87 – 6.74 (m, 2H), 2.58 (s, 3H). ^{13}C NMR (126 MHz, Chloroform-

d) δ 161.62, 154.86, 143.45, 137.10, 130.24, 127.46, 125.17, 120.53, 120.43, 115.05, 21.42; HRMS-EI (*m/z*): calcd for $C_{13}H_{11}NO_3$, 229.0739; found 229.0736.

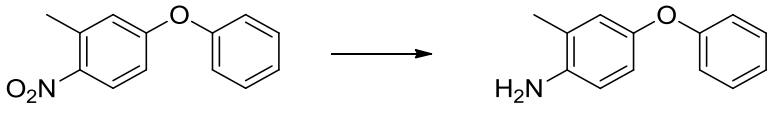

3.S-8 **3.S-9**

Synthesis of 3.S-9: Compound **3.S-8** (0.96 g, 4.19 mmol) was added to an oven-dried round bottom flask. Ethanol (16.75 mL) and water (4.2 mL) were then added followed by iron (1.17 g, 21 mmol). Several drops of concentrated hydrochloric acid were then added, and the reaction was refluxed for 90 minutes. After cooling to room temperature the crude reaction was filtered through celite. Ethanol was removed under reduced pressure. The crude residue was dissolved in ethyl acetate, and the organic solution was washed with water. The organic layer was then dried over sodium sulfate. The crude residue was subjected to silica gel chromatography (0→40% Ethyl acetate in hexanes). Removal of the organic solvent provided (0.37 g, 1.86 mmol) of product **3.S-9** as a dark brown oil (44% yield). **Spectral data.** ^{1}H NMR (400 MHz, Chloroform-*d*) δ 7.32 – 7.21 (m, 2H), 6.99 (td, *J* = 7.4, 1.1 Hz, 1H), 6.95 – 6.88 (m, 2H), 6.81 – 6.70 (m, 2H), 6.64 (d, *J* = 8.4 Hz, 1H), 3.50 (s, 2H), 2.14 (s, 3H). ^{13}C NMR (126 MHz, Chloroform-*d*) δ 159.03, 148.37, 140.89, 129.50, 123.97, 122.30, 121.95, 118.67, 117.18, 115.85, 17.60; HRMS-ESI (*m/z*): $[M + H]^+$ calcd for $C_{13}H_{13}NO$, 200.1070; found 200.1075.

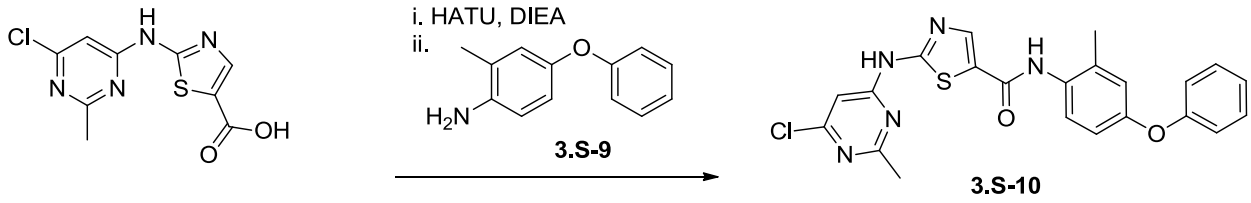

3.S-10

Synthesis of 3.S-10: 2-((6-chloro-2-methylpyrimidin-4-yl)amino)thiazole-5-carboxylic acid (75 mg, 0.28 mmol) and HATU (116 mg, 0.305 mmol) were added to an oven-dried round bottom flask. N,N-dimethylformamide (1.4 mL) was then added, followed by diisopropylethylamine (0.194 mL, 1.108 mmol). The reaction was allowed to stir at room temperature for 45 min. Compound **3.S-9** (59 mg, 0.28 mmol) was then added, and the reaction was allowed to stir overnight at room temperature. The reaction mixture was then dissolved in ethyl acetate and the organic solution was washed with water twice, followed by a brine wash. The crude mixture was then subjected to silica gel chromatography using a 0 → 100% ethyl acetate in hexanes gradient. Product **3.S-10** was isolated as a tan solid. **Spectral data.** ^{1}H NMR (400 MHz, DMSO-d_6) δ 12.18 (s, 1H), 9.80 (s, 1H), 8.25 (s, 1H), 7.42 – 7.32 (m, 2H), 7.28 (d, *J* = 8.6 Hz, 1H), 7.11 (td, *J*

= 7.4, 1.2 Hz, 1H), 7.04 – 6.87 (m, 4H), 6.82 (dd, *J* = 8.6, 2.8 Hz, 1H), 2.56 (s, 3H), 2.18 (s, 3H).

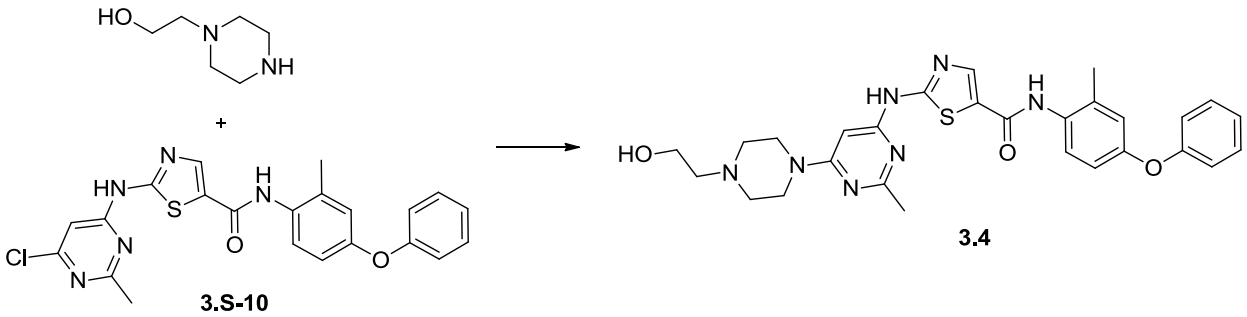

Synthesis of 3.4: Compound **3.S-10** (40 mg, 0.089 mmol) was added to an oven-dried round bottom flask. Dioxane (0.9 mL) was then added, followed by 1-(2-hydroxyethyl)piperazine) (0.11 mL, 0.885 mmol). The reaction was then refluxed overnight. The reaction was then allowed to cool to room temperature, and the dioxane was removed under reduced pressure. The crude residue was the purified using reverse-phase HPLC using a 5→95% acetonitrile in water gradient. Product **3.4** was isolated as 7 mg of a white solid (15% yield). **Spectral data.** ^{13}C NMR (126 MHz, dmso) δ 165.78, 162.82, 162.68, 160.73, 157.38, 157.17, 154.90, 140.95, 136.59, 131.75, 130.52, 128.77, 123.89, 120.66, 118.93, 116.62, 83.25, 70.16, 59.70, 52.45, 43.03, 25.95, 18.38; HRMS-ESI (*m/z*): $[M + H]^+$ calcd for $C_{28}H_{30}ClN_7O_3S$, 546.2282; found 546.2286.

Analytical data for compounds 3.S-1 – 3.4

3.S-1:

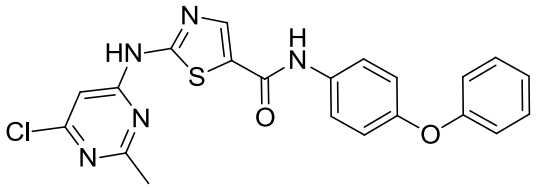

3.S-1 ^{1}H:

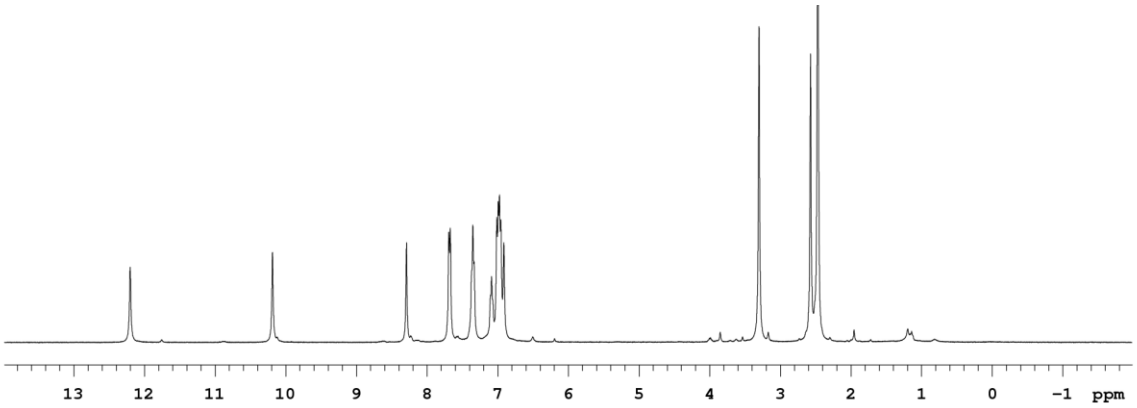

3.S-1 ^{13}C:

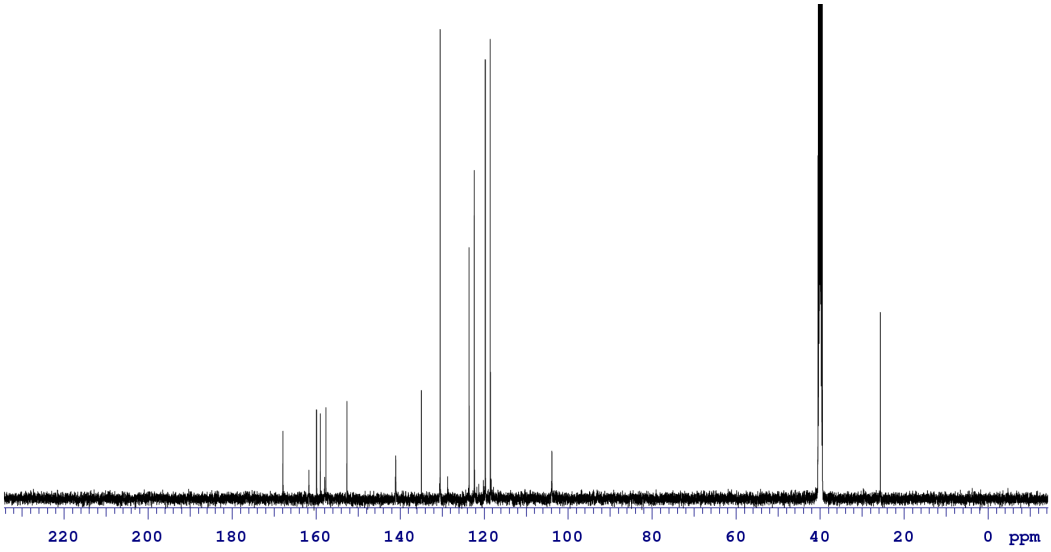

3.1:

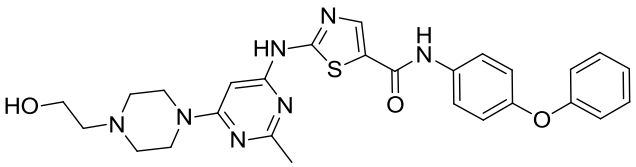

3.1 ^{1}H:

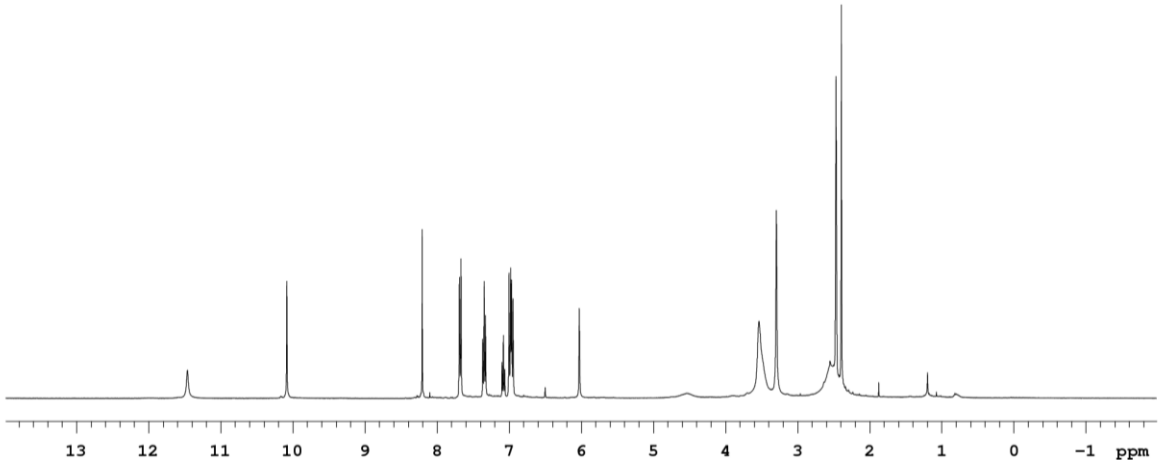

3.1 ^{13}C:

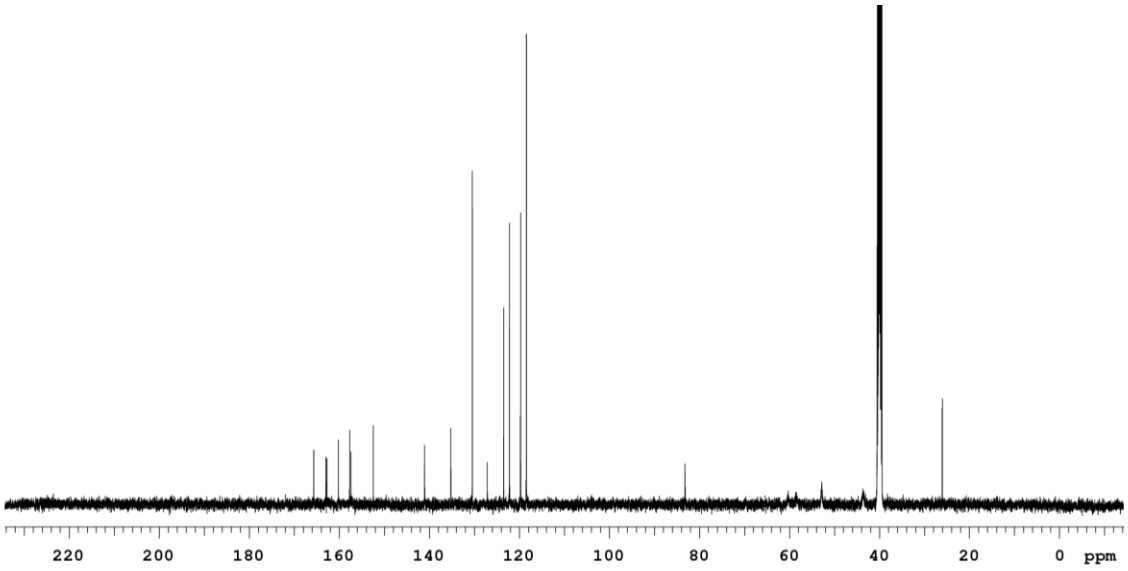

3.S-2:

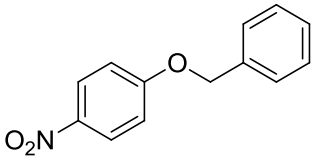

3.S-2 ^{1}H:

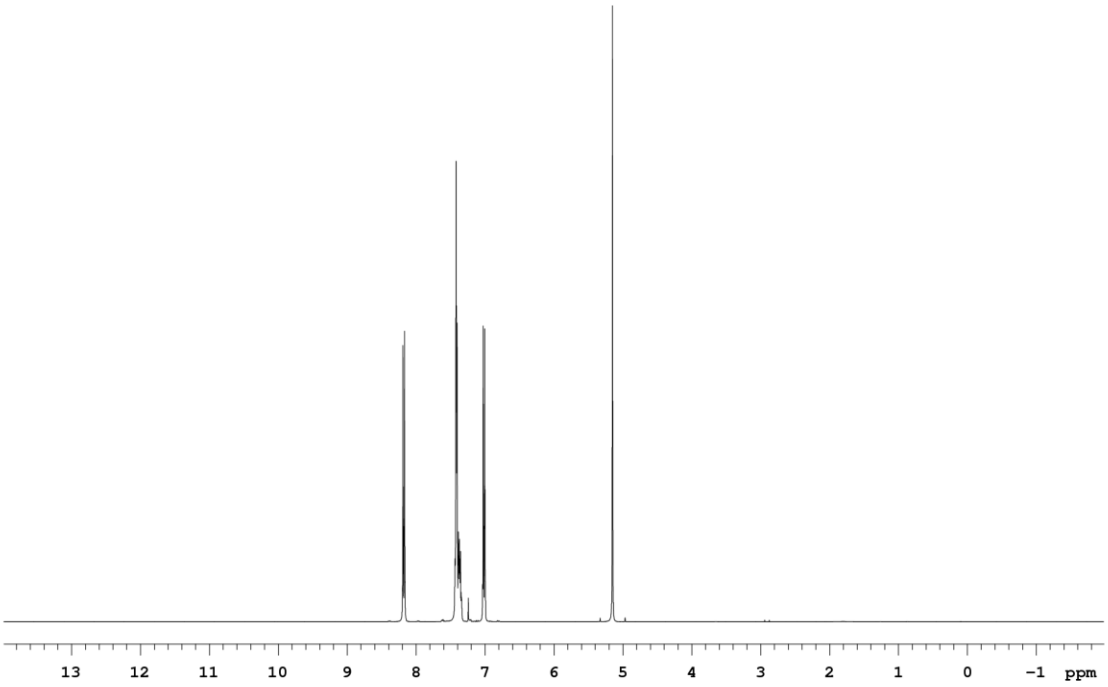

3.S-2 ^{13}C:

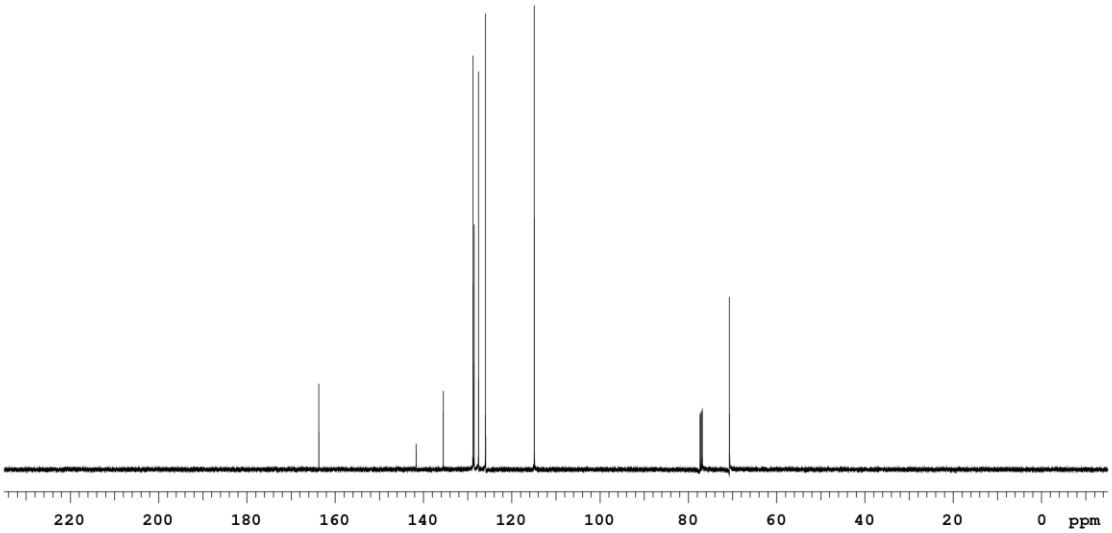

3.S-3:

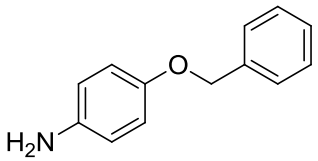

3.S-3 ^{1}H:

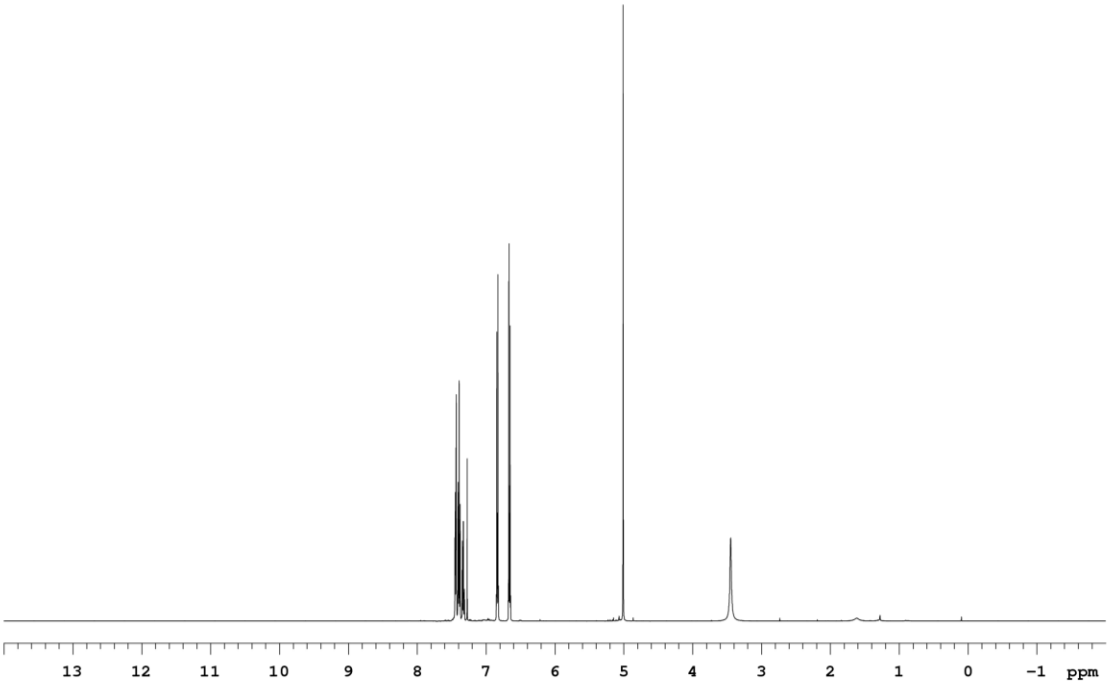

3.S-3 ^{13}C:

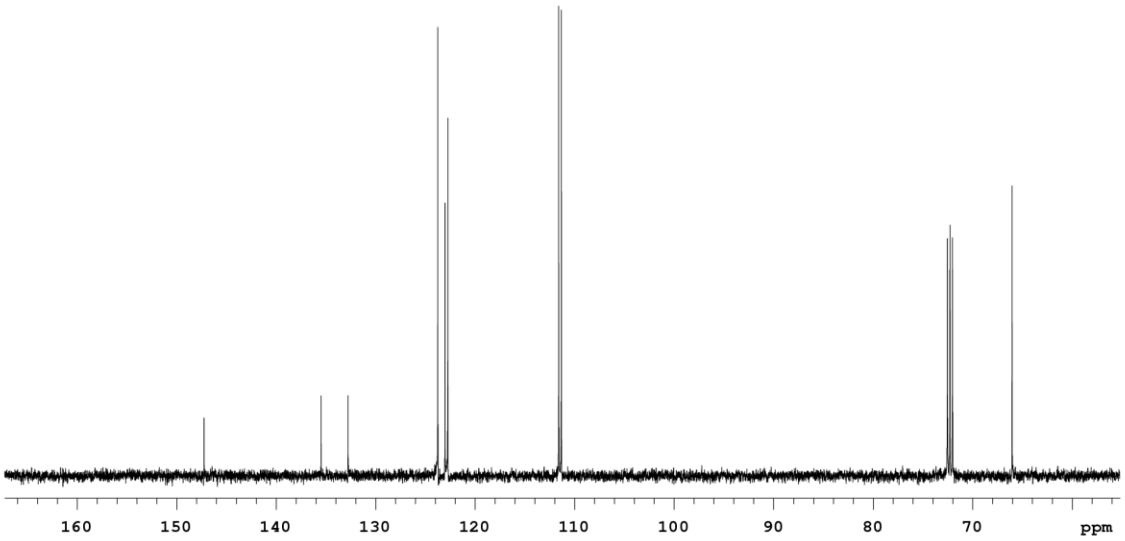

3.S-4:

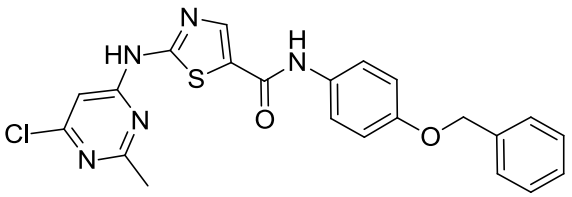

3.S-4 ^{1}H:

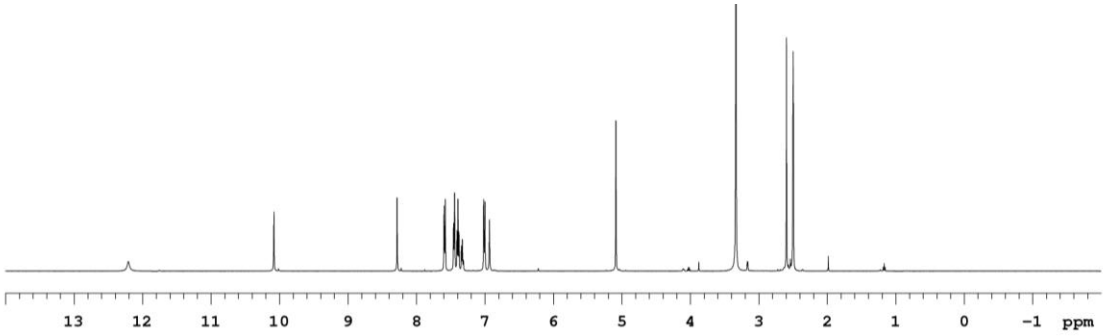

3.S-4 ^{13}C:

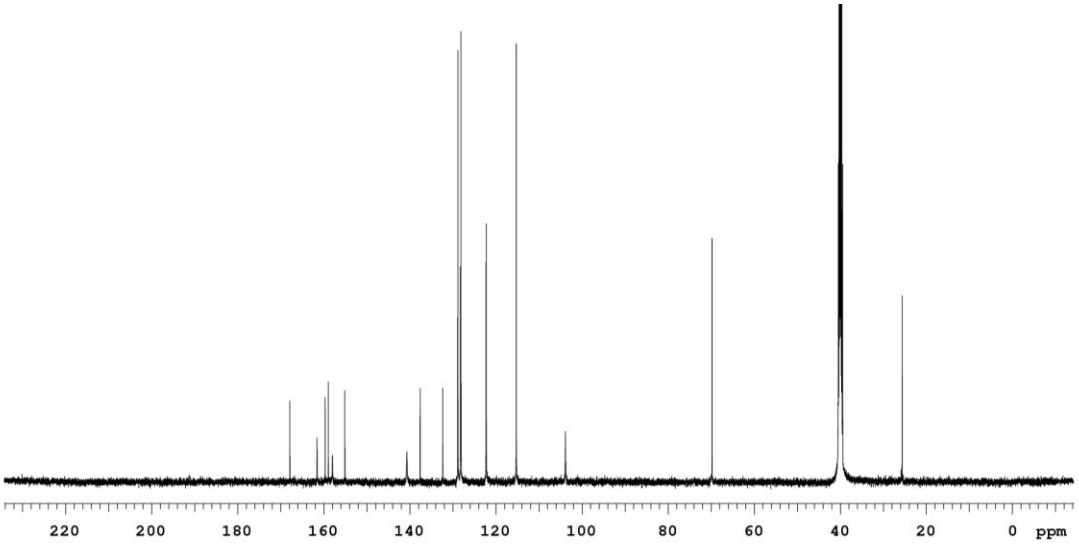

3.2:

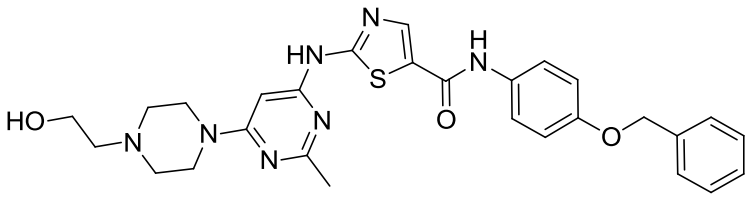

S3.2 ^{1}H:

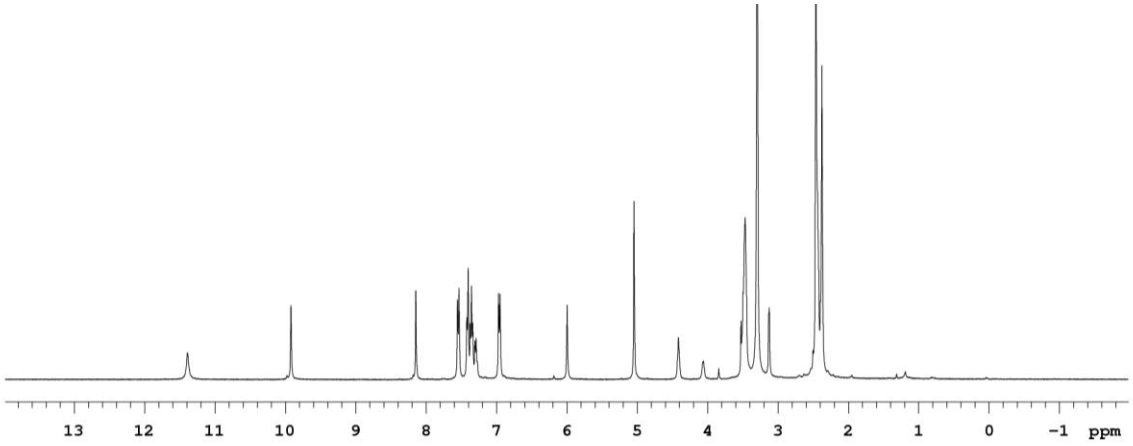

3.2 ^{13}C:

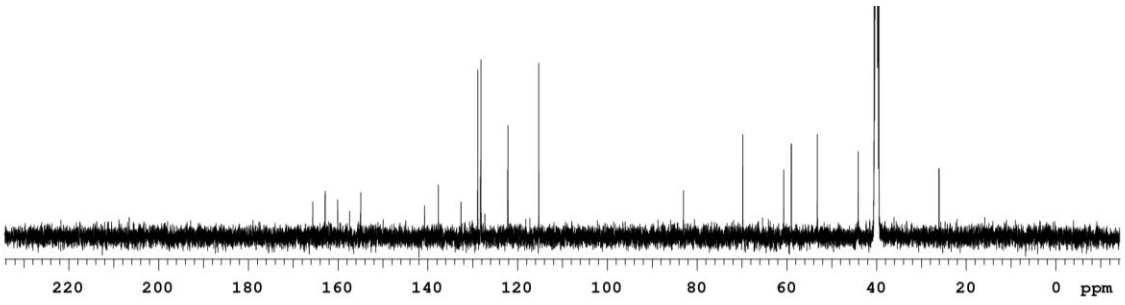

3.S-5:

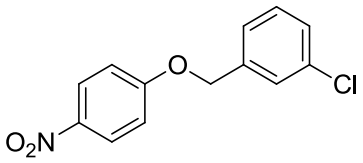

3.S-5 ^{1}H:

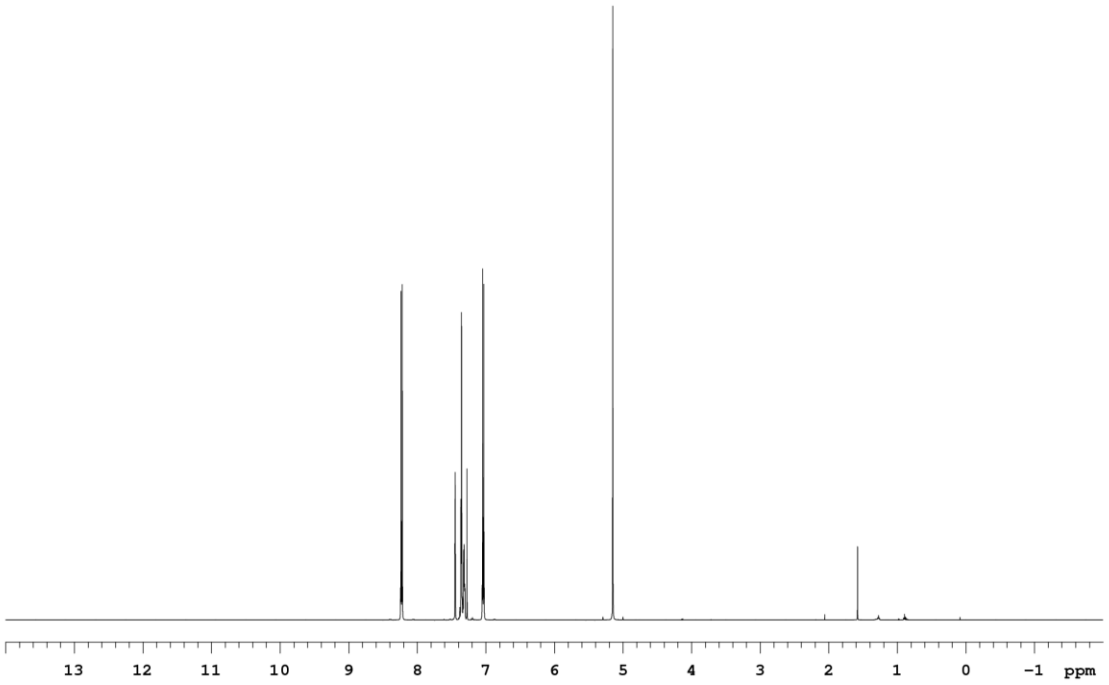

3.S-5 ^{13}C:

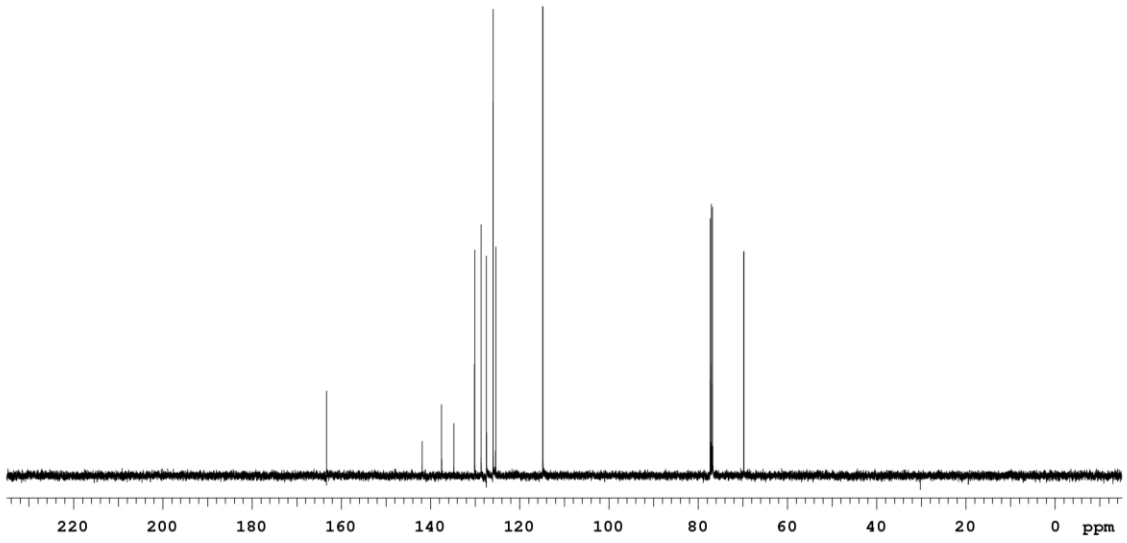

3.S-6:

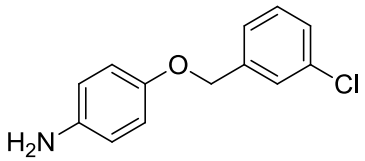

3.S-6 ^{1}H:

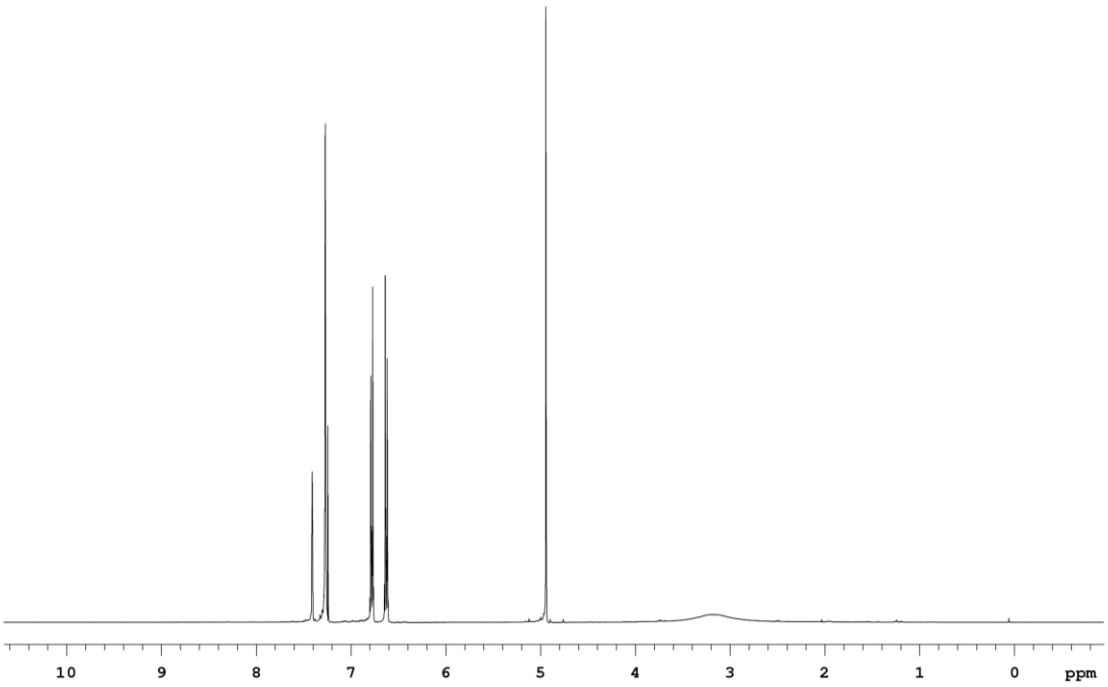

3.S-6 ^{13}C:

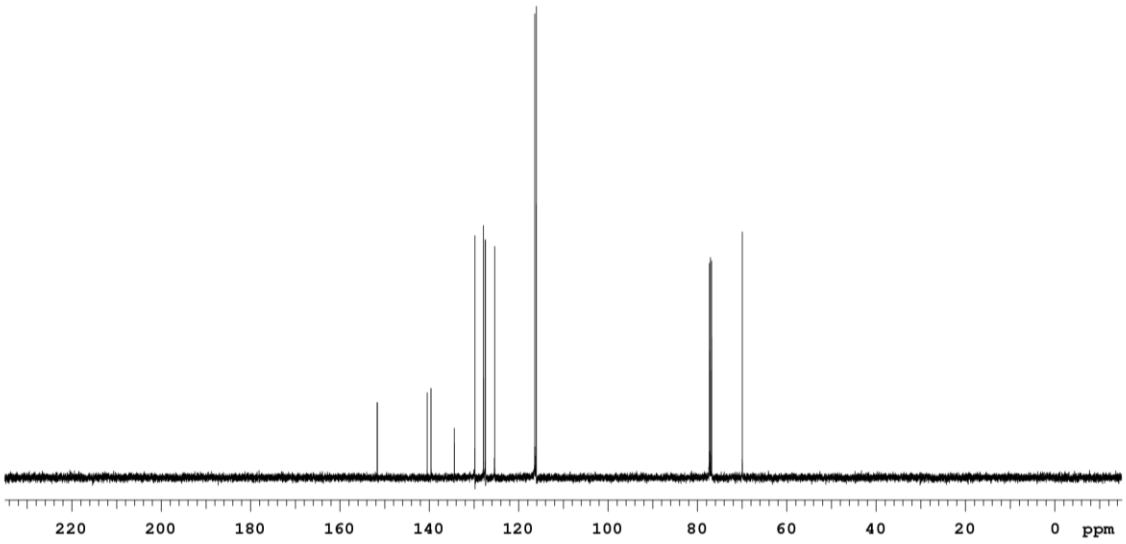

3.S-7:

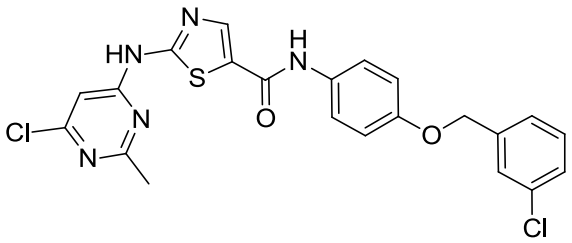

3.S-7 ^{1}H:

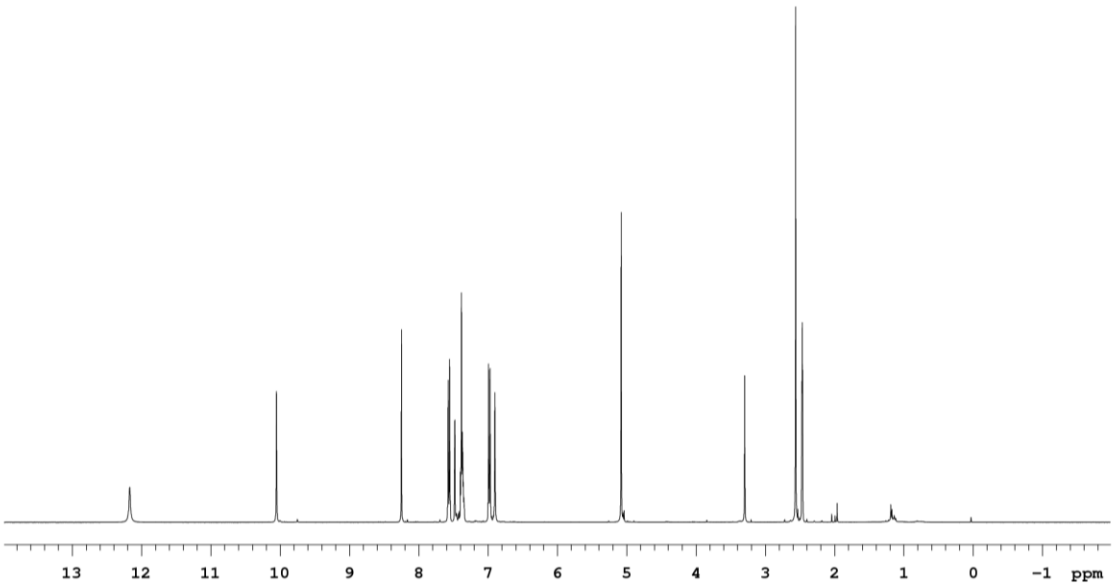

3.S-7 ^{13}C:

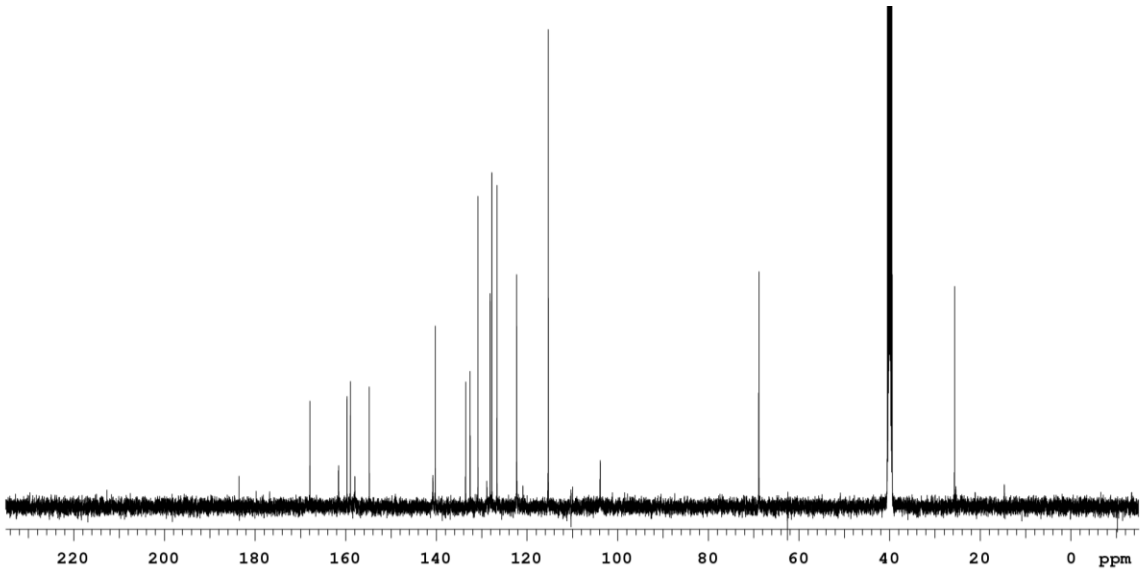

3.3: 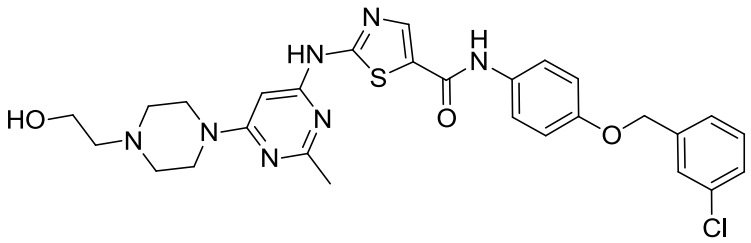

3.3 ^{1}H:

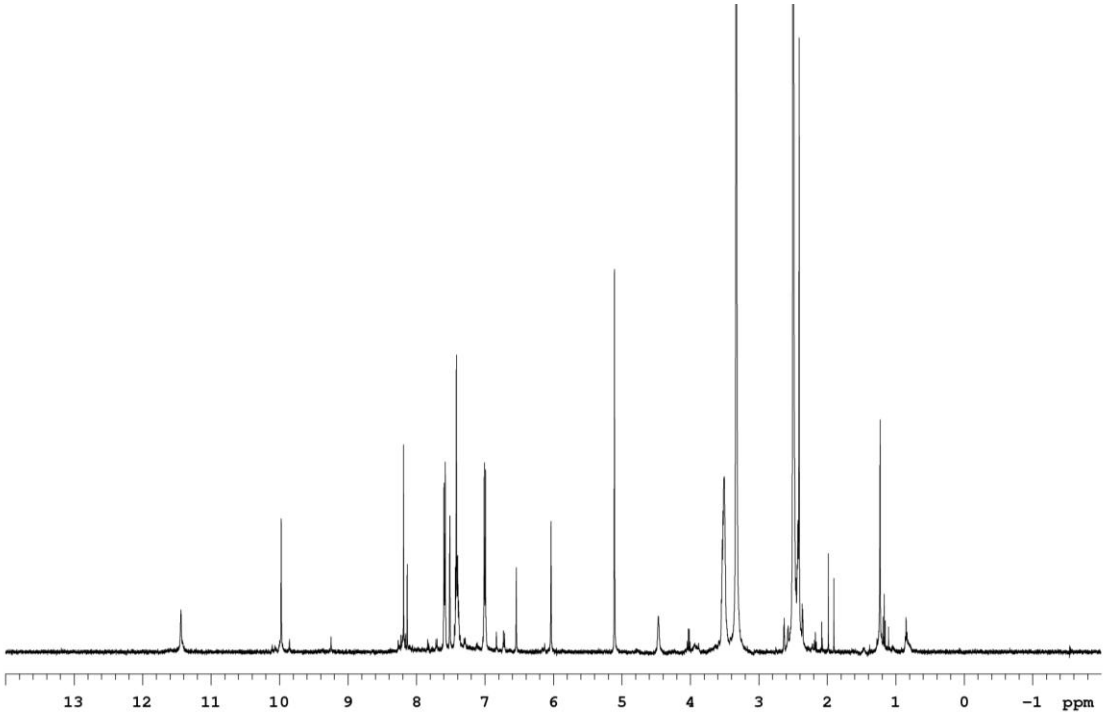

3.S-8:

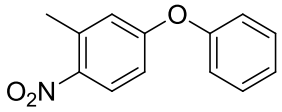

S3 ^{1}H:

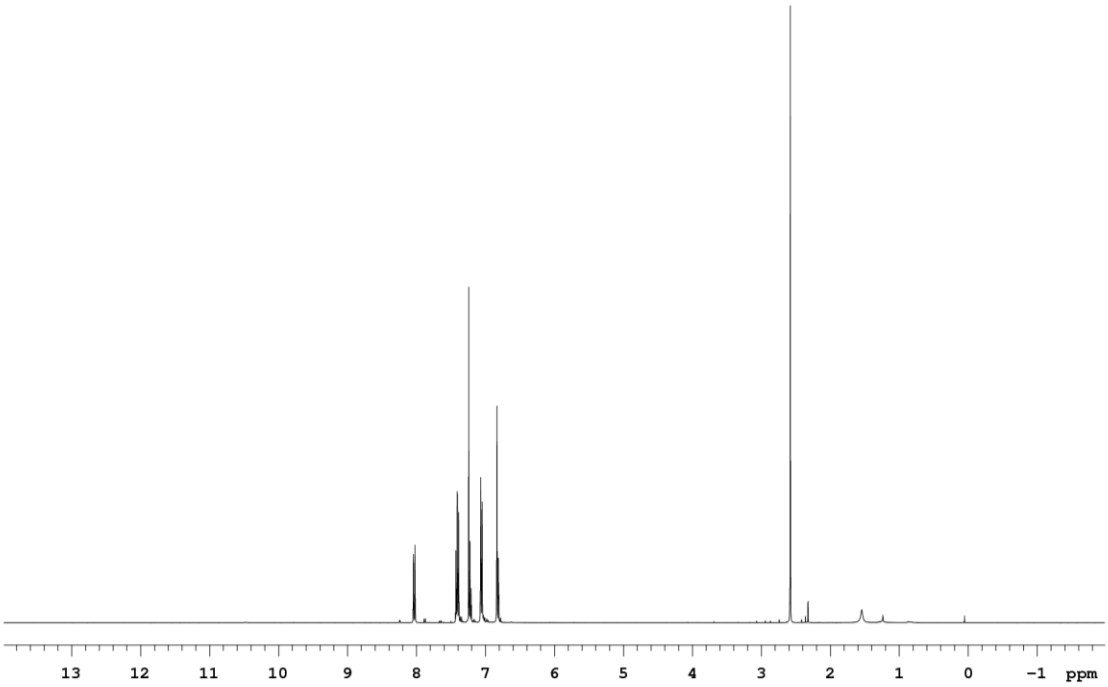

S3 ^{13}C:

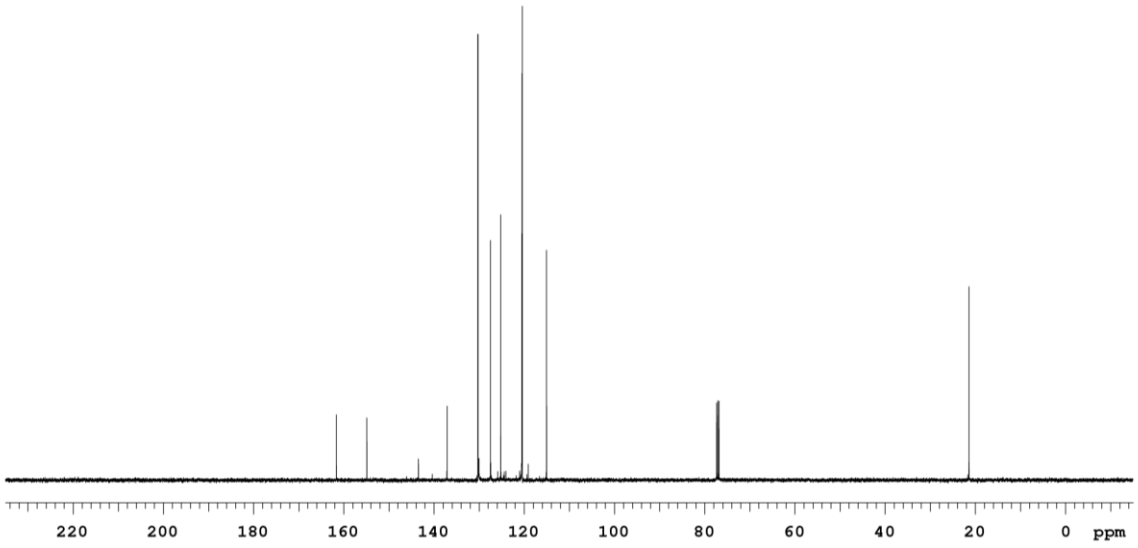

3.S-9: 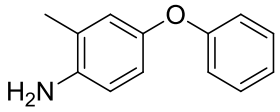

3.S-9 ^{1}H:

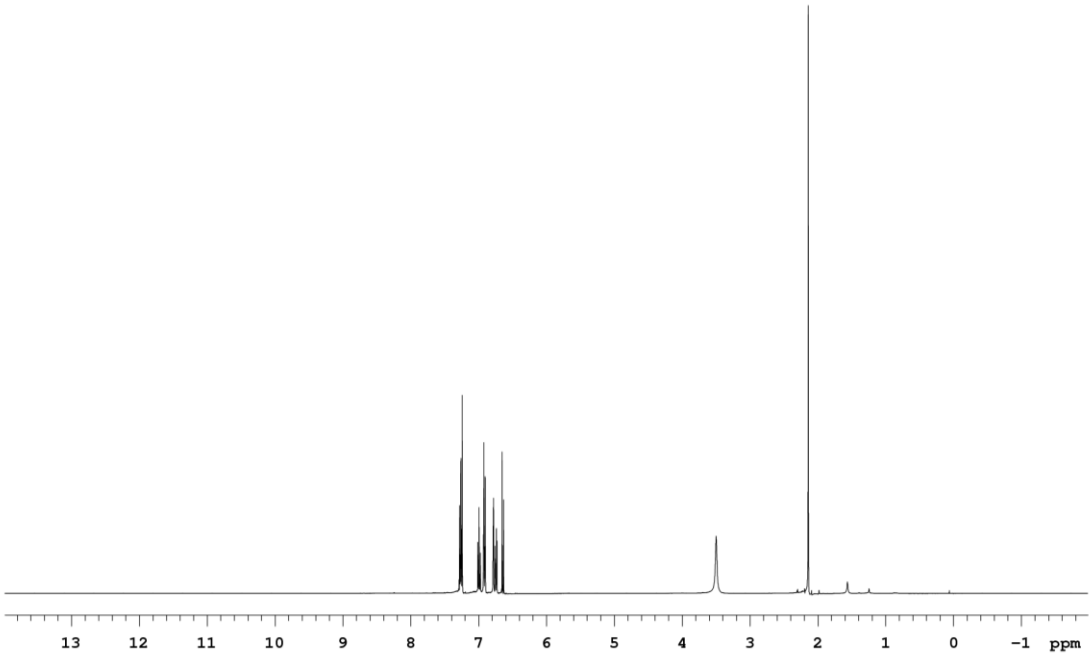

3.S-9 ^{13}C:

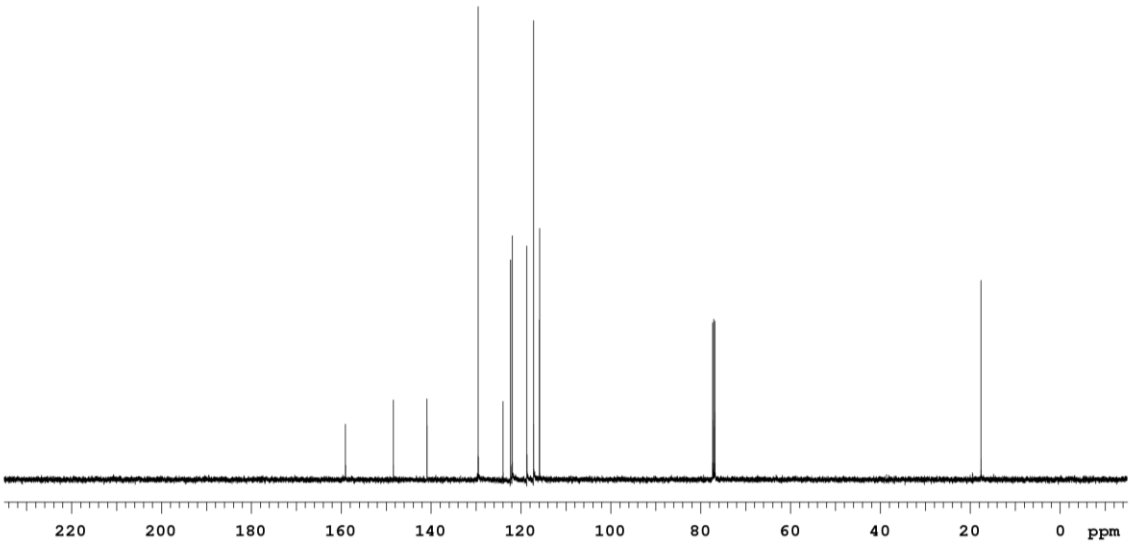

3.S-10:

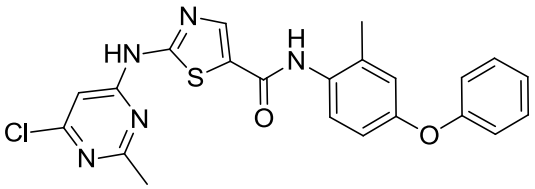

3.S-10 ^{1}H:

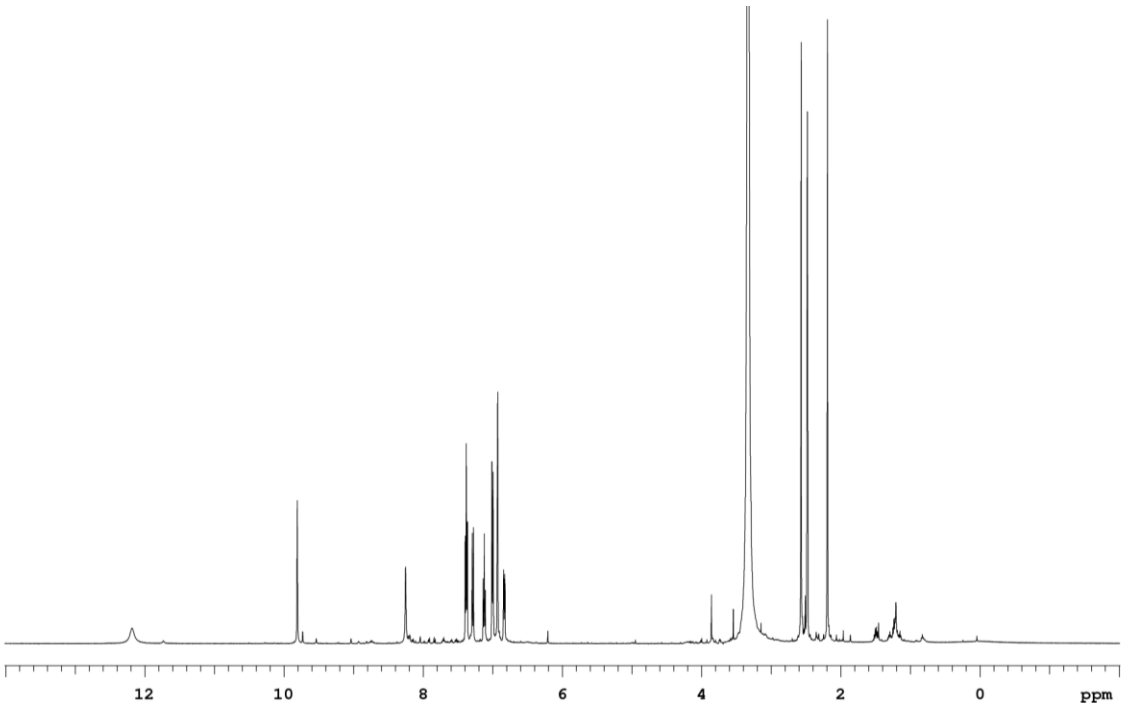

3.S-10 ^{13}C:

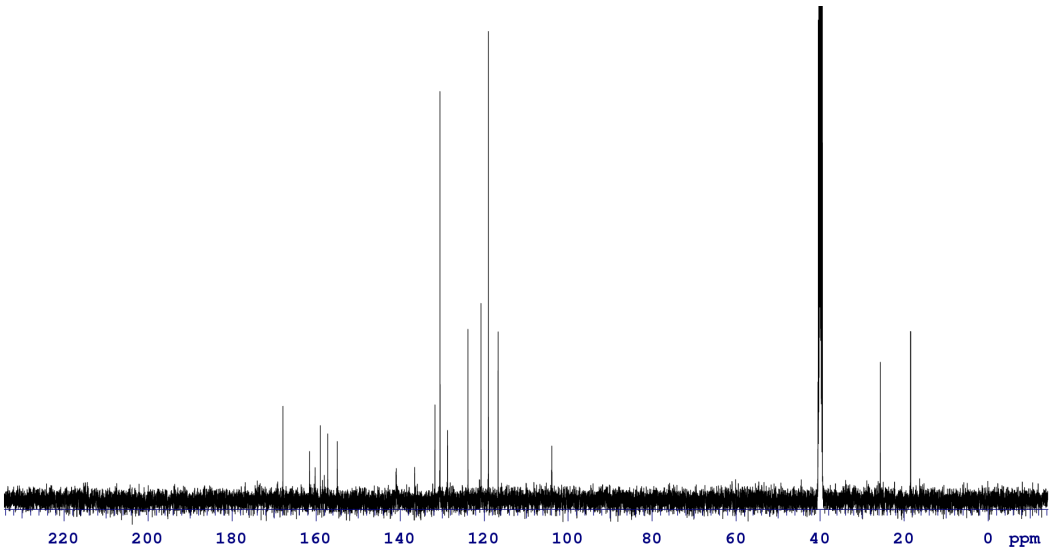

3.4:

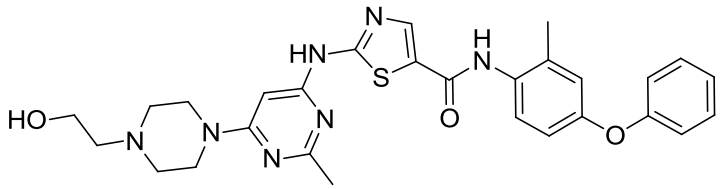

S3 ^{1}H:

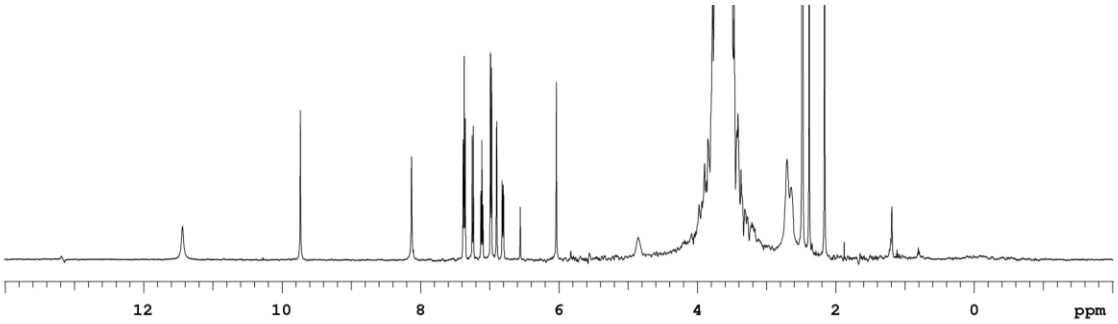

S3 ^{13}C:

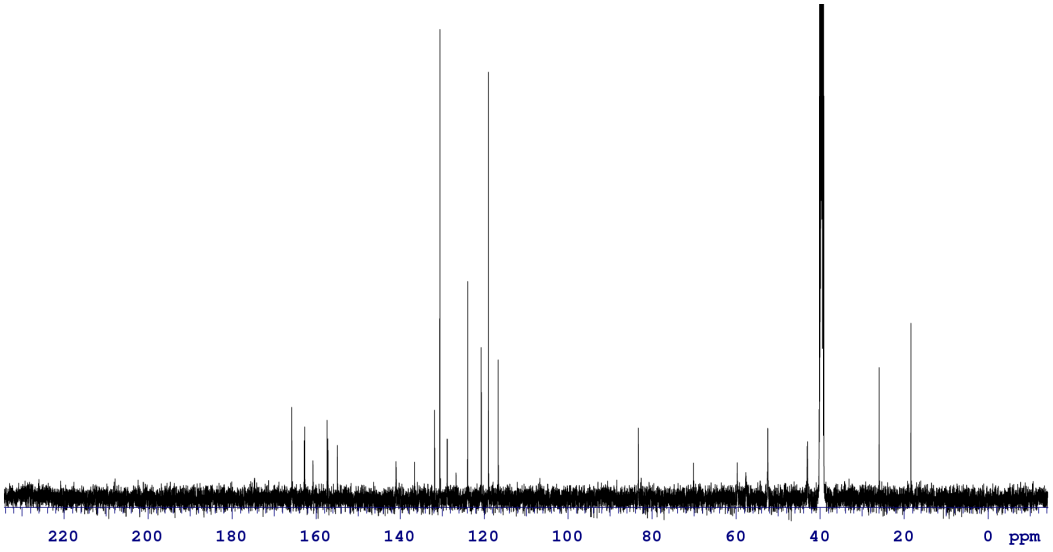

Biochemical and cellular characterization

General procedure for determination of inhibitor K_i. A continuous fluorescence assay[8] was used to determine K_i. Reaction volumes of 100 µL were used in 96-well plates. 85 µL of enzyme in buffer was added to each well. 2.5 µL of the appropriate inhibitor dilution (typically 5000, 1666, 555, 185, 61, 20, 6.8, 2.2, 0.76, 0 µM in DMSO) was then added. 2.5 µL of a substrate peptide ("compound 3" as described in Wang et al)[8] solution (1.8 mM in DMSO) was added. The reaction was initiated with 10 µL of ATP (1 mM in water), and reaction progress was immediately monitored at 405 nm (ex. 340 nm) for 10 minutes. Reactions had final concentrations of 30 nM enzyme, 45 µM peptide substrate, 100 µM ATP, 100 µM Na_3VO_4, 100 mM Tris buffer (pH 8), 10 mM $MgCl_2$, 0.01% Triton X-100.The initial rate data collected was used for determination of K_i values. For K_i determination, the kinetic values were obtained directly from nonlinear regression of substrate-velocity curves in the presence of various concentrations of the inhibitor. The equation Y = Bottom + (Top – Bottom)/(1 + 10^X – LogEC50), X = log(concentration) and Y = binding; was used in the nonlinear regression.

Analytical data for c-Src K_i determination. Each inhibitor K_i value was determined using at least three independent experiments; a representative inhibition curve is shown.

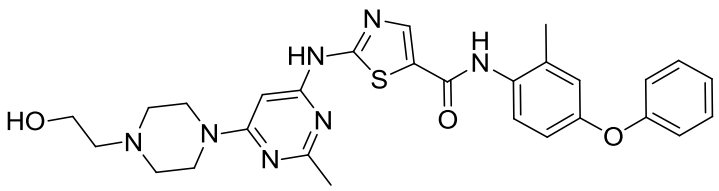

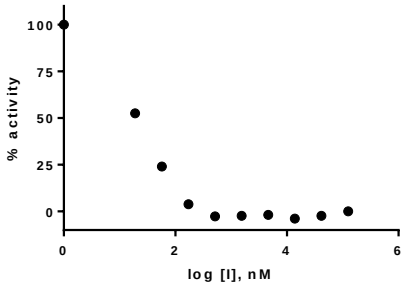

3.4 Avg K_i ≤ 0.6 nM

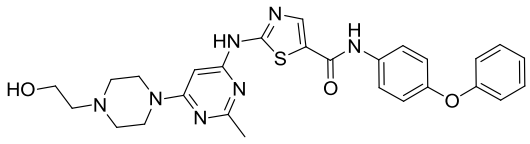

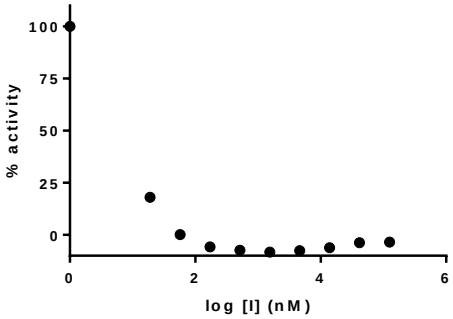

3.1 Avg K_i ≤ 0.6 nM

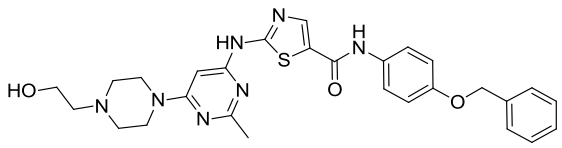

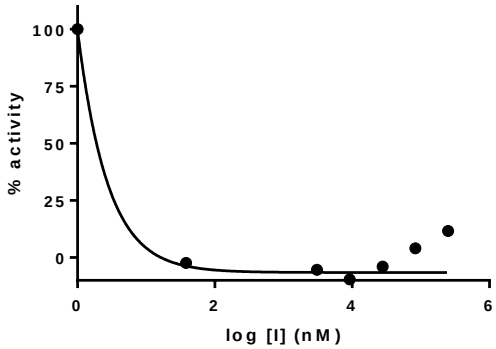

3.2 Avg $K_i \leq 0.6$ nM

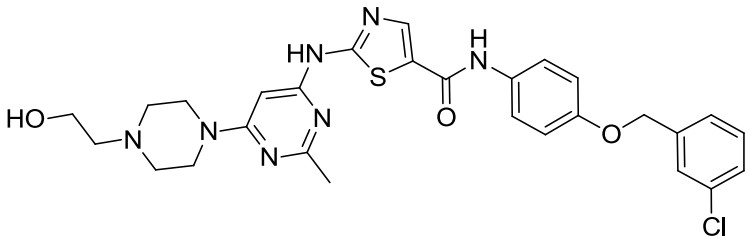

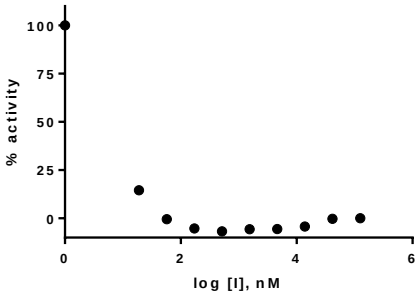

3.3 Avg $K_i \leq 0.6$ nM

Analytical data for c-Abl K_i determination. Each inhibitor K_i value was determined using at least three independent experiments, a representative inhibition curve is shown.

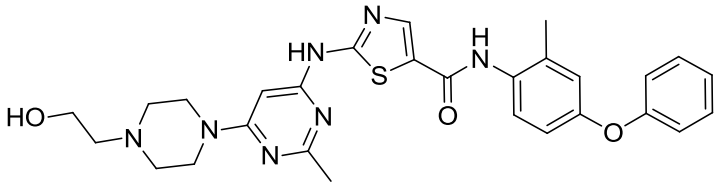

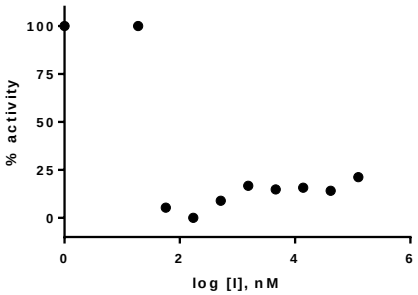

3.4 Avg $K_i \leq 0.6$ nM

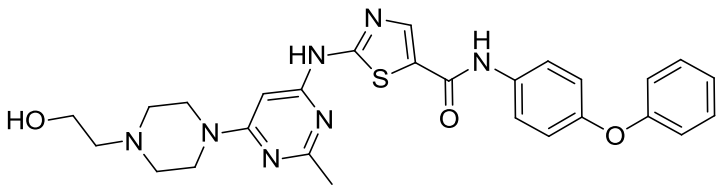

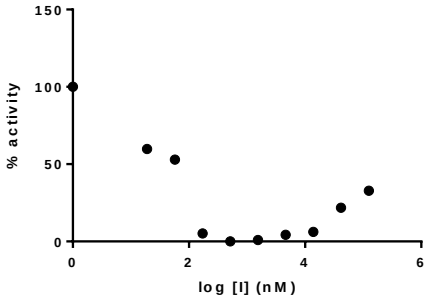

3.1 Avg $K_i \leq 0.6$ nM

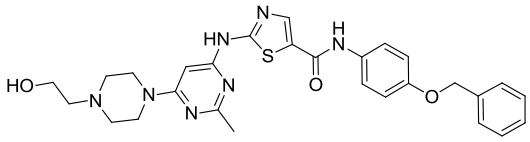

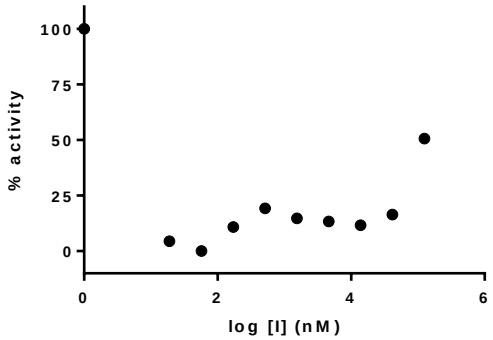

3.2 Avg $K_i \leq 0.6$ nM

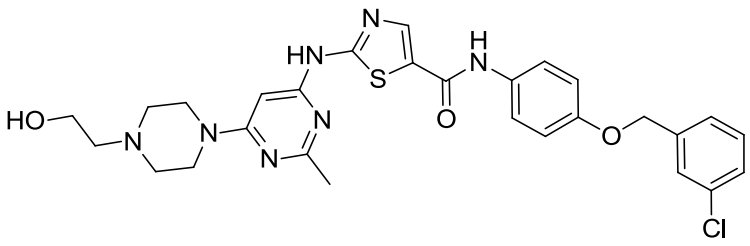

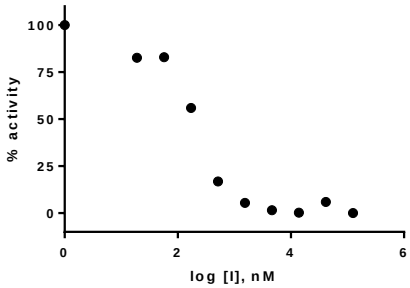

3.3 Avg $K_i \leq 0.6$ nM

Analytical data for Src T341I K_i determination. Each inhibitor K_i value was determined using at least three independent experiments, a representative inhibition curve is shown.

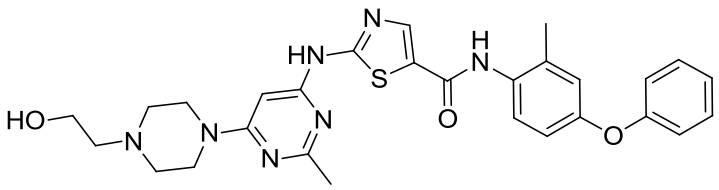

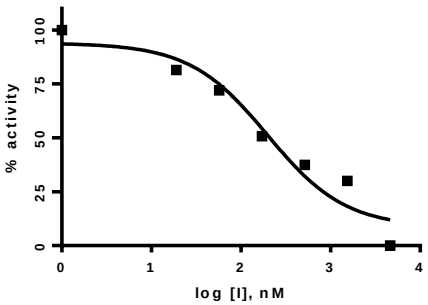

3.4 Avg K_i = 32 nM

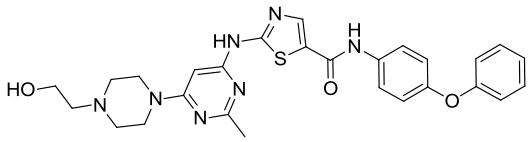

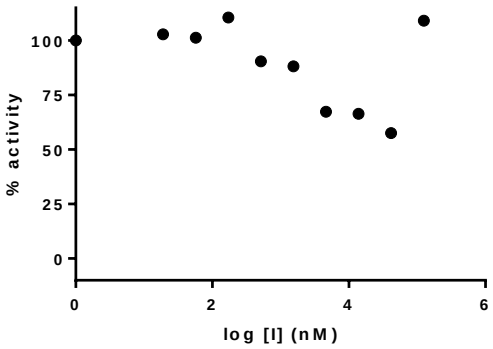

3.1

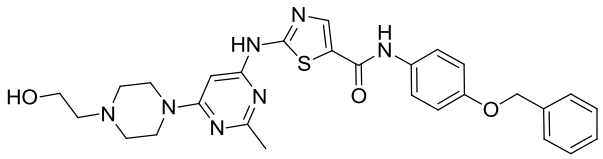

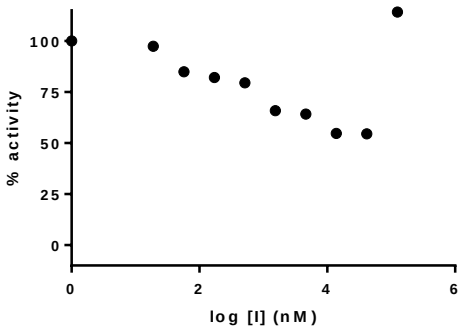

3.2

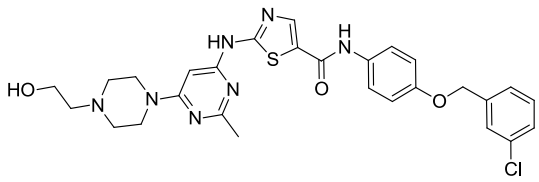

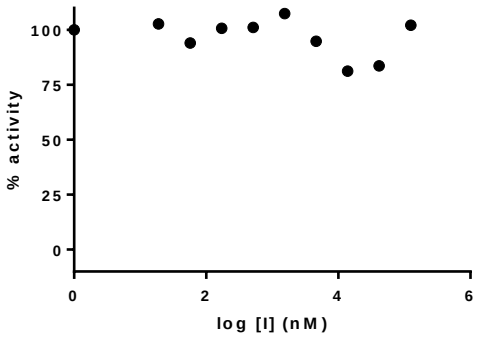

3.3

Analytical data for Src T341M K_i determination. Each inhibitor K_i value was determined using at least three independent experiments, a representative inhibition curve is shown.

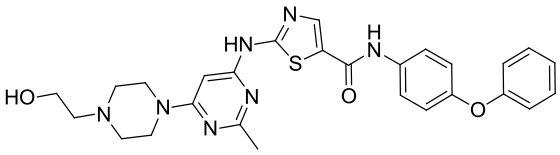

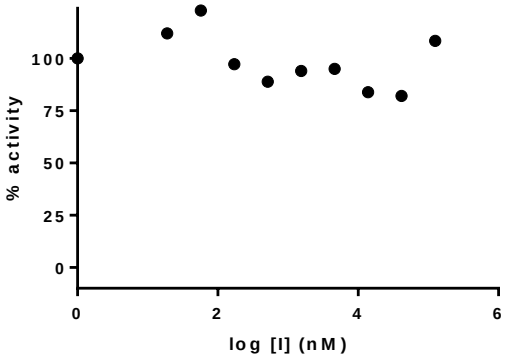

3.1

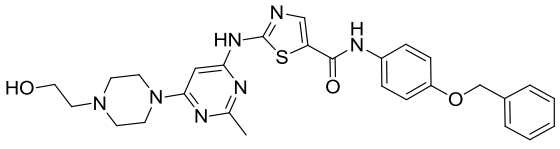

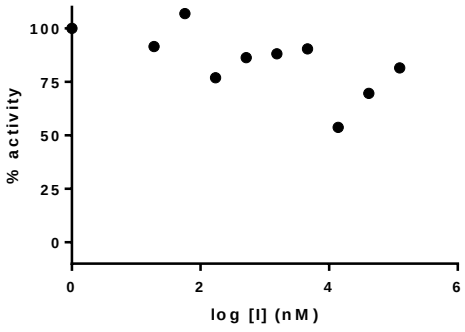

3.2

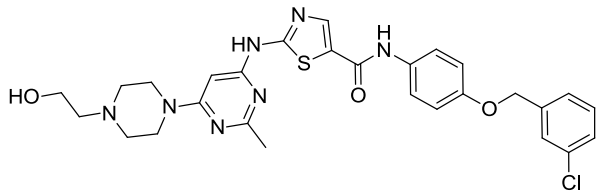

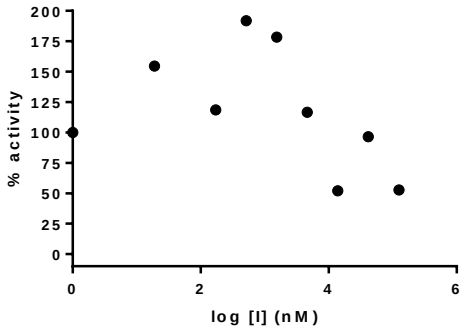

3.3

DiscoveRx Kd determination

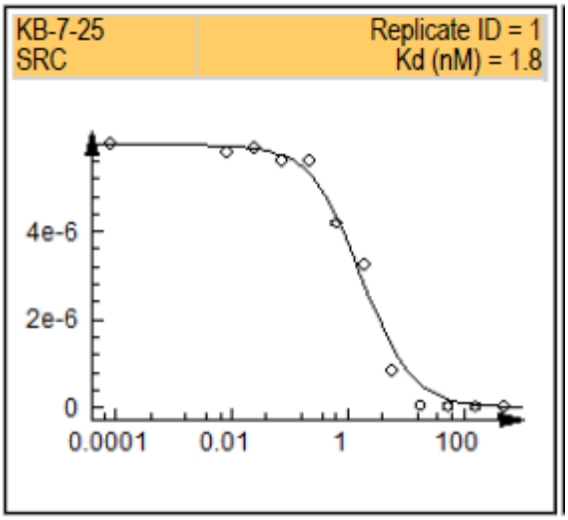

3.4

Luceome profiling

Kinome profiling for compound **3.4** was performed by KinaseSeeker™ (Luceome Biotechnologies, Tucson, AZ). The compound was profiled at a final concentration of 500 nM.

A. TREEspot analysis:

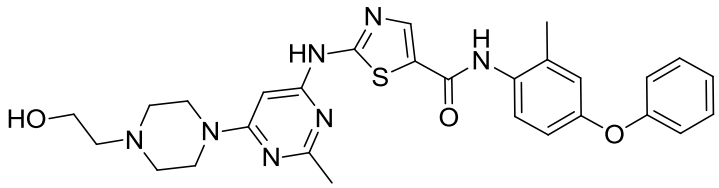

3.4

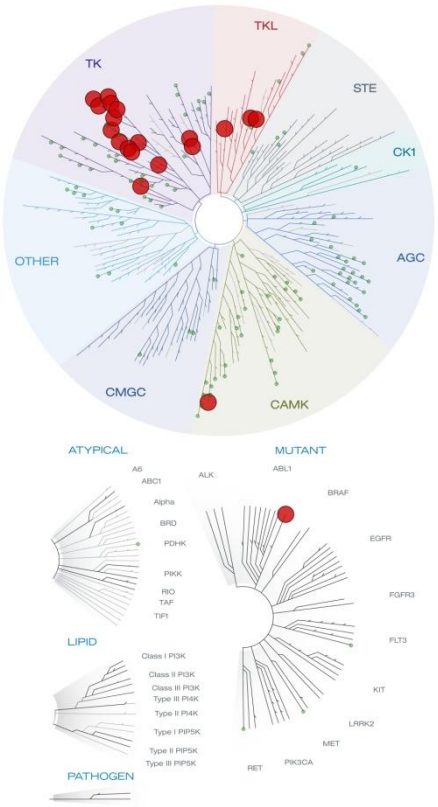

B. S-Scores:

S (35) = 0.16

C. Tabulated data:

KINOMEscan Gene Symbol	Entrez Gene Symbol	Percent Control
ABL1-phosphorylated	ABL1	8.1
ABL2	ABL2	9
AKT1	AKT1	100
AKT2	AKT2	100
AKT3	AKT3	100
AMPK-alpha1	PRKAA1	100
AMPK-alpha2	PRKAA2	100
AURKA	AURKA	91.4
AURKB	AURKB	100
AURKC	AURKC	96
AXL	AXL	100
BIKE	BMP2K	100
BLK	BLK	6.6
BTK	BTK	15.5
CAMK1	CAMK1	100
CAMK1D	CAMK1D	100
CAMK1G	CAMK1G	93
CAMK2A	CAMK2A	100
CAMK2B	CAMK2B	100
CAMK2D	CAMK2D	100
CAMKK1	CAMKK1	100
CAMKK2	CAMKK2	100
CHEK1	CHEK1	100
CSNK1D	CSNK1D	100
CLK1	CLK1	100
CLK2	CLK2	100
CSK	CSK	6.1
DAPK1	DAPK1	100
DAPK2	DAPK2	100
DAPK3	DAPK3	100
DDR1	DDR1	18.6
DDR2	DDR2	28.9
DMPK	DMPK	100
EPHA1	EPHA1	14
EPHA2	EPHA2	96.1
EPHA3	EPHA3	63.7
EPHA4	EPHA4	77.4
EPHB2	EPHB2	100
EPHB3	EPHB3	100

EPHB4	EPHB4	92.9
FGFR2	FGFR2	100
FLT1	FLT1	95.7
FGFR1	FGFR1	100
FLT3	FLT3	95.1
FYN	FYN	21
GSK3A	GSK3A	100
HCK	HCK	12.7
IGF1R	IGF1R	100
IKK-epsilon	IKBKE	100
INSR	INSR	97.6
ITK	ITK	100
LIMK1	LIMK1	8.1
LYN	LYN	34.4
MARK1	MARK1	100
MARK2	MARK2	100
MARK3	MARK3	100
MARK4	MARK4	100
MELK	MELK	100
MET	MET	100
MLK1	MLK1	100
MLK3	MLK3	100
MST2	MST2	100
MUSK	MUSK	100
MYLK	MYLK	100
MYLK2	MYLK2	98.8
PKMYT1	PKMYT1	100
p38-delta	MAPK13	100
PAK1	PAK1	90.6
PDGFRA	PDGFRA	74.9
PDGFRB	PDGFRB	38.8
PDK1	PDK1	100
PHKG1	PHKG1	63.9
PIM1	PIM1	99
PIM2	PIM2	100
PKAC-alpha	PRKACA	98.2
PRKACB	PRKACB	100
PRKCD	PRKCD	100
PRKCE	PRKCE	100
PRKCG	PRKCG	100
PRKCH	PRKCH	100
PRKCQ	PRKCQ	96.6
PRKG1	PRKG1	94.8

PKN3	PKN3	88.4
PRKX	PRKX	100
PLK4	PLK4	100
PRKD2	PRKD2	100
PRKD3	PRKD3	100
PTK2	PTK2	100
PTK2B	PTK2B	100
PTK6	PTK6	6.2
RET	RET	100
RIPK2	RIPK2	2.7
RSK1(Kin.Dom.1-N-terminal)	RPS6KA1	100
RSK3(Kin.Dom.1-N-terminal)	RPS6KA2	100
RSK2(Kin.Dom.1-N-terminal)	RPS6KA3	100
RPS6KA4(Kin.Dom.1-N-terminal)	RPS6KA4	96.5
RPS6KA5(Kin.Dom.1-N-terminal)	RPS6KA5	100
RSK4(Kin.Dom.1-N-terminal)	RPS6KA6	100
SGK2	SGK2	100
SGK3	SGK3	100
QSK	KIAA0999	91.1
SLK	SLK	98.8
SNARK	SNARK	100
SNF1LK	SNF1LK	23.9
SNF1LK2	SNF1LK2	84
SRC	SRC	9.2
STK16	STK16	100
STK33	STK33	100
SYK	SYK	100
TBK1	TBK1	97
TEC	TEC	22.2
TESK1	TESK1	67.8
TESK2	TESK2	23.4
TIE1	TIE1	100
TIE2	TIE2	100
TNK2	TNK2	61.3
TNNI3K	TNNI3K	77.6
TRKB	TRKB	100
TRKC	TRKC	100
TXK	TXK	41.5
VEGFR2	VEGFR2	100
YANK2	YANK2	100
YES	YES1	6.3
YSK1	STK25	100

3.5 References

(1) Jester, B. W.; Cox, K. J.; Gaj, A.; Shomin, C. D.; Porter, J. R.; Ghosh, I. *Journal of the American Chemical Society* **2010**, *132*, 11727-11735.

(2) Cleator, S.; Heller, W.; Coombes, R. C. *The Lancet Oncology* **2007**, *8*, 235-244.

(3) Dent, R.; Trudeau, M.; Pritchard, K. I.; Hanna, W. M.; Kahn, H. K.; Sawka, C. A.; Lickley, L. A.; Rawlinson, E.; Sun, P.; Narod, S. A. *Clinical Cancer Research* **2007**, *13*, 4429-4434.

(4) Bauer, K. R.; Brown, M.; Cress, R. D.; Parise, C. A.; Caggiano, V. *Cancer* **2007**, *109*, 1721-1728.

(5) Rakha, E. A.; El-Sayed, M. E.; Green, A. R.; Lee, A. H. S.; Robertson, J. F.; Ellis, I. O. *Cancer* **2007**, *109*, 25-32.

(6) Reis-Filho, J. S.; Tutt, A. N. J. *Histopathology* **2008**, *52*, 108-118.

(7) Tibbitt, M. W.; Anseth, K. S. *Biotechnology and Bioengineering* **2009**, *103*, 655-663.

(8) Wang, Q.; Cahill, S. M.; Blumenstein, M.; Lawrence, D. S. *Journal of the American Chemical Society* **2006**, *128*, 1808-1809.

CHAPTER 4

A rational and modular approach to bisubstrate inhibition of protein kinases

This chapter addresses the *"How much selectivity may be gained by exploiting structural features outside of the canonical ATP-pocket?"* theme. The substrate site of Src kinase is targeted using a derivative of an optimal peptide substrate in a bisubstrate inhibition approach. It is shown that this strategy results in the most selective bisubstrate kinase inhibitor reported. Furthermore, the strategy appears to be modular and is used to develop a bisubstrate inhibitor of PDGFR kinase. Herein we report, using c-Src kinase as a model, a general bisubstrate inhibition approach in which modification of the peptide sequence drives the selectivity, which ultimately results in a potent and selective inhibitor of a kinase of interest.

4.1 Introduction

In Chapter 1.6 it is suggested that targeting the highly variable substrate binding site should provide kinase inhibitors with good selectivity. Substrate-competitive inhibitors frequently suffer from poor potency. It was decided to pursue a bisubstrate inhibition approach because it promises potency from the ATP-competitive fragment and selectivity from the substrate-competitive fragment.

4.2 Results and discussion

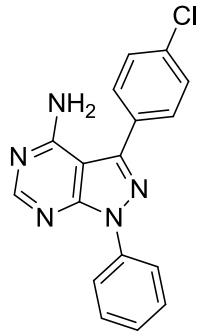

4.1

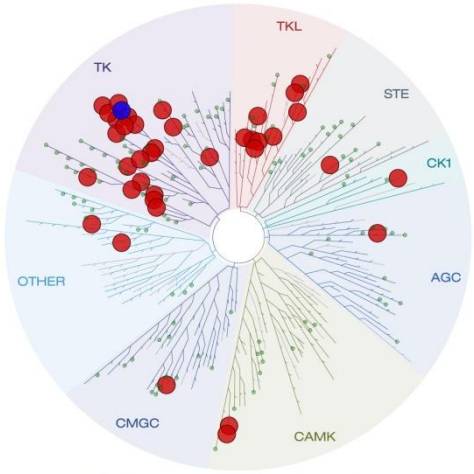

Figure 4.1.. a) Structure of compound **4.1**. b) Selectivity profile of compound **4.1** using a single-point binding assay. The compound was screened at 10 µM. Red circles are indicative of inhibitor binding to a given kinase > 35% control. Green circles indicate kinases included in the panel that did not display binding. c-Src is highlighted in blue.

For the design of the bisubstrate inhibition strategy it was desired to have an ATP-competitive inhibitor which targeted the model kinase c-Src, but would also be relatively promiscuous. An N1-phenyl pyrazolopyrimidine scaffold was selected because it fit the set criteria. Compound **4.1**[1] was screened against a diverse panel of 200 kinases (KINOMEscan[2], Figure 4.1). It was found that the compound bound a significant portion of the panel with appreciable affinity (52 kinases were ≥ 65% displaced from an immobilized ligand, see Experimental Section), thus it was deemed that this scaffold would be a considerable challenge in terms of attempting to improve its selectivity through application of a bisubstrate inhibition approach.

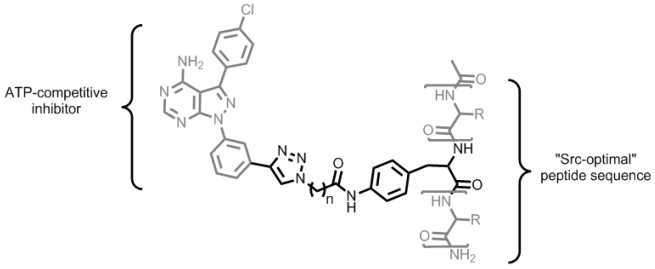

Figure 4.2. General structure for bisubstrate inhibitors. For full structures see Experimental Section.

Based upon previous work with Ser/Thr kinases[3], it was envisioned that the selectivity of the promiscuous ATP-competitive inhibitor could be modulated via covalent linkage to a substrate-competitive peptide. It was necessary to decide how to conjugate the two respective components of the bisubstrate inhibitor, and a click-chemistry[4] approach was

evaluated toward this end (Figure 4.2). The ATP-competitive pyrazolopyrimidine N1-phenyl ring was modified to contain an alkyne handle[5], and a peptide that was representative of a Src-optimal substrate sequence[6] was modified such that the phosphorylatable tyrosine residue was replaced with 4-aminophenylalanine[7] which could be acylated with an azido linker (See experimental section for peptide sequence).

Compound	Linker length (n =)	c-Src IC_{50} (nM)
4.2	3	159
4.3	5	< 30
4.4	7	121

Table 4.1. Optimization of linker length for a c-Src bisubstrate inhibitor. Inhibitors were characterized using a continuous fluorescence assay. Assay conditions: 5 mM ATP, 45 µM peptide substrate.

The linker length between the two fragments has been previously demonstrated to significantly influence the potency of bisubstrate inhibitors[8]. Molecular modeling was conducted using a structural overlay of a pyrazolopyrimidine bound to c-Src and a bisubstrate inhibitor bound c-Abl (c-Src has no reported structure with a ligand bound in the substrate-binding site) (Figure 4.S-1). The modeling indicated a distance of 11 Å between the two points of attachment of the proposed bisubstrate fragments. Linker lengths which bracketed the predicted optimal distance were evaluated. The short investigation of linker length revealed that affinity was greatly impacted by this feature (Table 4.1). The observed optimal linker length of n = 5 was in good agreement with what was expected from modeling.

Bisubstrate inhibition should result in a synergistic increase in potency relative to the two individual nonconjugated components. Inhibition of c-Src by the respective ATP-competitive and substrate-competitive fragments was evaluated to determine if synergistic inhibition was achieved in the merged product (Table 4.2).

Compound	Binding mode	c-Src IC_{50} (µM)
4.1	ATP-competitive	>250
4.5	Substrate-competitive	8.37

Table 4.2: Biochemical characterization of the individual fragments of a bisubstrate inhibitor designed for c-Src. Inhibitors were characterized using a continuous fluorescence assay. Assay conditions: 5 mM ATP, 45µM peptide substrate.

It was observed that the ATP-competitive compound (**4.1**) bound extremely poorly, which was not surprising given the high concentration of ATP used in the assay. The substrate-competitive fragment (**4.5**) bound with low micromolar affinity, which was

expected for an inhibitor of this type under the given assay conditions. Altogether these data indicate that covalent conjugation of the individual components of the bisubstrate inhibitor results in a dramatic synergistic increase in potency.

The high potency of bisubstrate inhibitor **4.3** did not allow for precise determination of its affinity for c-Src using an activity based assay, so it was decided to pursue alternate means of characterization. Affinity for a tight binding ligand which has been fluorophore-labeled can be easily determined using TR-FRET. Inhibitor **4.3** was labeled on its N-terminus with a fluorescent small molecule (Cy-5, see experimental section for full structure) to provide affinity probe **4.6**. The K_d of the affinity probe was determined using TR-FRET and displayed low nanomolar affinity for c-Src (Figure 4.3).

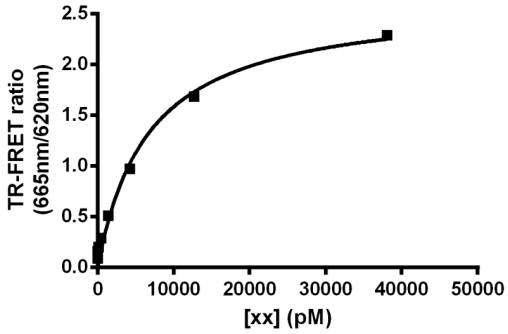

Figure 4.3. Measurement of the affinity of a fluorescently labeled bisubstrate probe 4.7 for c-Src. Binding was determined using a TR-FRET assay. A representative run is shown. The probe was found to have an affinity of K_d = 6.3 ± 1.6 nM.

Fluorophore labeling of inhibitors is widely known to potentially modify the potency relative to the unlabeled counterpart. Therefore, a competition assay using probe **4.6** was used to determine the affinity of inhibitor **4.3** for c-Src (Table 4.3). It was found that the unlabeled inhibitor **4.3** was approximately ten times more potent than affinity probe **4.6**. To validate the binding assay a known ATP-competitive c-Src inhibitor, PP2, was also subjected to affinity determination. The observed value was similar to those previously reported and to an affinity value obtained using a commercially available kinase tracer (see Supporting Information). It was also of interest to determine if this assay would be useful for characterizing substrate-competitive inhibitors. Using substrate-competitive inhibitor **MEB-4-151** in the TR-FRET assay yielded an affinity value very similar to what is obtained using activity based assays. We therefore propose that this inhibitor could be useful for finding other substrate-competitive small molecules.

After the affinity of inhibitor **4.3** was adequately characterized it was desired that the selectivity be determined. It was initially hypothesized that the substrate-competitive fragment would drive the selectivity of a bisubstrate inhibitor, and this needed to be validated. The peptide sequence used for the bisubstrate inhibitor **4.3** was derived from a substrate that is readily phosphorylated by c-Src but not by the structurally homologous kinase c-Abl. Based upon the known substrate selectivity, it was expected that compound **4.3** would be a poor inhibitor of c-Abl. Biochemical assays revealed that compound **4.3** inhibits c-Abl with an IC_{50} = 1,168 nM (see experimental section). The observed data were in good agreement with the proposed hypothesis; the compound inhibited c-Src with much greater affinity than c-Abl.

Competitor	K_d (nM)
4.3	0.28
PP2	22
MEB-4-151	15, 566

Table 4.3. Inhibitor K_d determination using probe **4.7**.

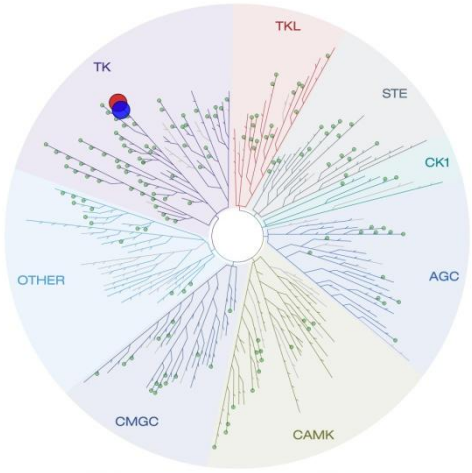

Figure 4.4. Selectivity profile for compound **4.3** at 115 nM against a panel of 200 kinases. determined using a binding assay (see supporting information for details). Only kinases that displayed ≤ 35% control are displayed.

There are few reports in which a bisubstrate inhibitor's selectivity profile has been determined using a large kinase panel, and in general those that have been subjected to thorough evaluation display only modest improvement in selectivity relative to the parent components. In an effort to adequately determine the degree of selectivity that could be achieved using the described strategy compound **4.3** was submitted for selectivity profiling against a diverse panel of 200 kinases (KinaseSeeker[9], Figure 4.4). Compound **4.3** was found to be highly selective, with only two kinases found to be significantly bound (≤ 35% control), the target kinase, c-Src, and a related Src family kinase, Yes. It is noteworthy that three other SFKs (Fyn, Blk, Hck) were found to be modestly bound (≤ 55% control) which would be expected by the redundant substrate preference of this

family. To our knowledge this is the most selective SFK inhibitor, bisubstrate or otherwise, reported to date (S (35) = 0.010).

Given the high selectivity of **4.3**, further interrogation of the source of selectivity was a reasonable next inquiry. It was proposed that the selectivity is due to interactions between the substrate-binding site of the enzyme and residues within the peptide fragment. Inhibitor **4.3** was truncated to provide a bisubstrate inhibitor which contained only a 4-aminophenylalanine residue (Figure 4.5). Biochemical characterization of compound **4.7** revealed it to be much less selective than its related bisubstrate counterpart. Compound **4.7** displayed significant inhibition of c-Abl and Hck (neither of which were >65% displaced in the selectivity panel). Altogether these data are suggestive that additional interactions within the substrate binding site are necessary to obtain high levels of both potency and selectivity.

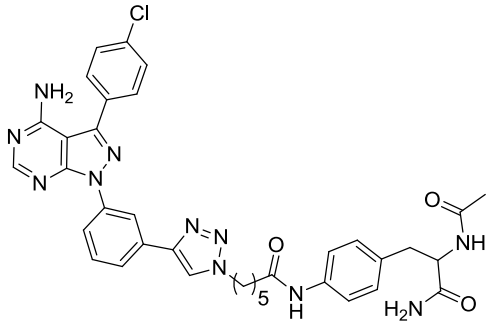

xx

	IC_{50} (nM)		
Cpd	**c-Src**	**Hck**	**Abl**
4.7	1,182	555	1,134

Figure 4.5. Structure and biochemical characterization of a truncated c-Src bisubstrate inhibitor **4.7**. Inhibitors were characterized using a continuous fluorescence assay. Assay conditions: 100 µM ATP, 45 µM peptide substrate.

	IC_{50} (µM)		
Compound (target)	**c-Src**	**Blk**	**PDGFRB**
4.3 (c-Src)	0.016	0.13	2.0
4.8 (PDGFRB)	>10	1.3	0.35

Table 4.4. Biochemical characterization of a bisubstrate inhibitor designed to bind PDGFRB. For assay details see supporting information.

It was determined that the selectivity of compound **4.3** is driven by interactions within the substrate binding site, therefore it should be possible to tune the selectivity of the inhibitor by replacing the peptide fragment with a sequence that is representative for an optimal substrate for another kinase. In an effort to determine the modularity of this strategy another kinase found to be tightly bound by the parent pyrazolopyrimidine fragment was chosen to be targeted, PDGFRB (99.5% displacement from an immobilized ligand using 10 µM inhibitor **4.1**, see supporting information). The same inhibitor development strategy was employed with the exception of the replacement of a substrate-competitive inhibitor whose sequence was based upon a reported substrate[10] to provide compound **4.8** (see experimental

section for sequence). Significantly, compound **4.8** displayed good selectivity for PDGFR over c-Src, with no notable inhibition of c-Src up to 10 μM (Table 4.4).

Clinically used kinase inhibitors commonly become ineffective upon a cancer patient's development of a resistance mutation. One of the most commonly observed mutations is the "gatekeeper" mutation in the ATP-binding site[11,12]. This mutation results in loss of a key hydrogen bond required for the binding of most kinase inhibitors and also sterically occludes inhibitor binding. It was hypothesized that bisubstrate inhibitors would be less impacted relative to their ATP-competitive counterparts due to having additional interactions outside of the ATP pocket. Therefore we compared dasatinib[13], a dual Src-Abl ATP-competitive inhibitor approved for treatment of patients whom develop resistance mutations in CML, to bisubstrate inhibitor **4.3** with respect to the T338I gatekeeper mutation in c-Src. Both inhibitors displayed decreased potency relative to the wild type kinase. Despite dasatinib being approximately six times more potent for the wild type kinase (see Supporting Information), it was found that inhibitor **4.3** was thirty times more potent versus the gatekeeper mutation (Figure 4.6) which represents a relative 180-fold potency shift. It is therefore proposed that the bivalent nature of inhibitor **4.3** makes it less susceptible to mutations in the ATP-binding site. To our knowledge this is the first examination of the influence of the gatekeeper mutation on a bisubstrate inhibitor which has an ATP-competitive fragment that would be predicted to clash with this residue (for an example of a bisubstrate inhibitor which evades T338I see reference [14]).

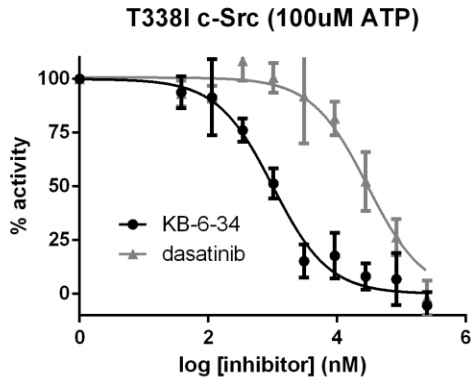

	KB-6-34	dasatinib
EC50	1009	29699

Figure 4.6. ATP-competitive vs. bisubstrate-competitive inhibition of a clinically observed resistance mutation. IC_{50}s were determined using the activity assay described in the Experimental section.

In order for a kinase inhibitor to be valuable as a cellular probe it must have adequate membrane permeability. In general, the utility of peptides has suffered considerably because of their poor cell permeability; therefore it was not surprising to observe that

the c-Src selective bisubstrate inhibitor **4.3** had little effect in cell-based assays (See experimental section). Fortunately, several strategies have been developed to increase peptide permeability including incorporation of a poly-Arg tag. Compound **4.3** was modified to include a poly-Arg tag at its N-terminus to provide compound **4.3-R9**. Addition of the Arg9 tag had little impact on its performance in biochemical inhibition assays (See experimental section). Treatment of HT29 cells with compound **4.3-R9** resulted in dose-dependent growth inhibition (GI_{50} = 36 μM, See experimental section). Therefore, it is postulated that any inhibitor developed using the described strategy has good potential for application in whole-cell experiments.

4.3 Conclusions

Bisubstrate kinase inhibition has been of great interest due to the promise of selectivity offered by interactions with the substrate-binding site, but examples of such inhibitors that have been subjected to a large and diverse selectivity panel are rare. This work describes a rational approach to provide highly potent and selective bisubstrate kinase inhibitors in a modular fashion. Using c-Src as a model kinase, a bisubstrate inhibitor has been created which displays significantly higher potency than the respective individual components. It was also found that these bisubstrate inhibitors perform better than ATP-competitive inhibitors against a clinically observed resistance mutation. Importantly, when this inhibitor was subjected to a panel of 200 diverse kinases, only two kinses (c-Src and the related Src family kinase, Yes) showed significant affinity for the compound. It is also shown that replacing the peptide fragment with a sequence that is representative of a PDGFRB kinse substrate provides an inhibitor that potently inhibits PDGFRB but not c-Src, which is suggestive selectivity is driven by the peptidic substrate-competitive fragment. Furthermore, it is also shown that inhibitors generated using this strategy can be made cell permeable, which is encouraging for their application in whole-cell experiments.

4.5 Experimental section

SUPPLEMENTAL FIGURES

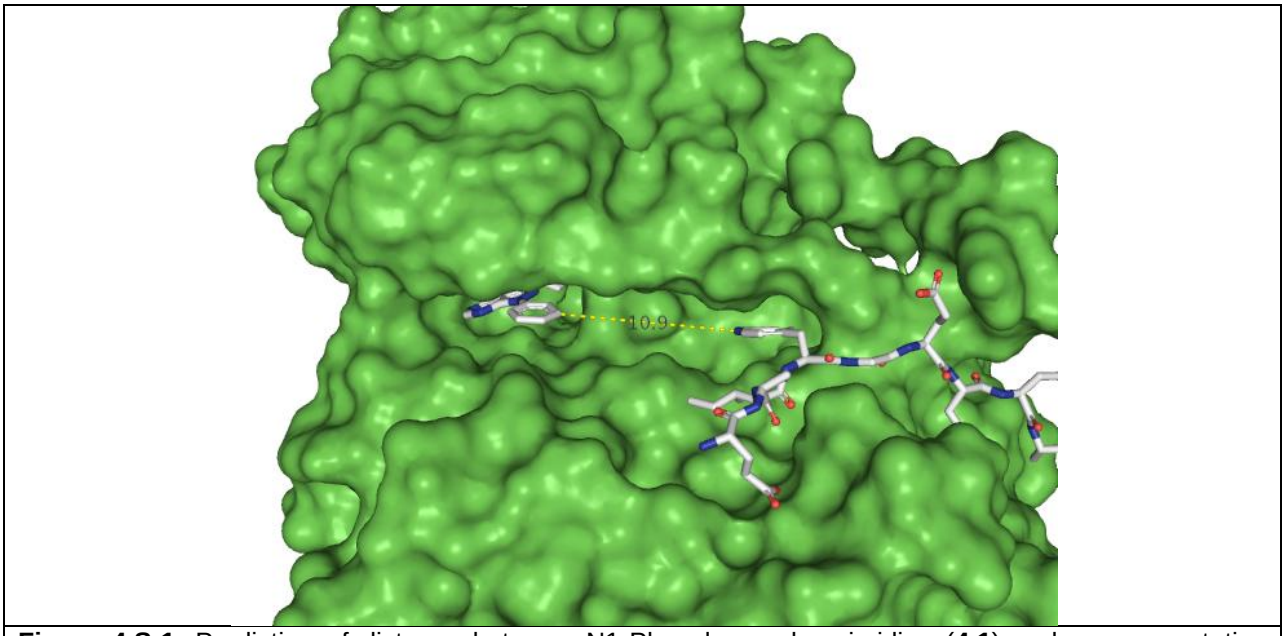

Figure 4.S-1. Prediction of distance between N1-Phenylpyrazolopyrimidine (**4.1**) and a representative substrate peptide bound to a kinase based upon a molecular model. Pyrazolopyrimidine binding was modeled based upon a structure of PP2 bound to c-Src kinase (PDB 3GEQ). Peptide substrate binding was modeled based upon a structure of a bisubstrate inhibitor bound to c-Abl (PDB 2G1T), only the peptidic portion of the inhibitor is shown for clarity. The image shown was rendered using PyMol.

GENERAL SYNTHETIC METHODS. Unless otherwise noted, all reagents were obtained via commercial sources and used without further purification. Mass Spectrometry (HRMS) was carried out by the University of Michigan Mass Spectrometry Facility (J. Windak, director).

SYNTHESIS OF COMPOUNDS 4.S-1 - 4.9

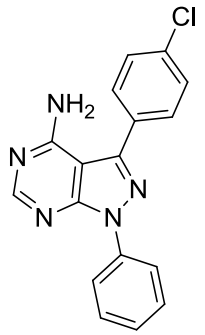

Synthesis of **4.1**: **4.1** was synthesized as previously described.[1]

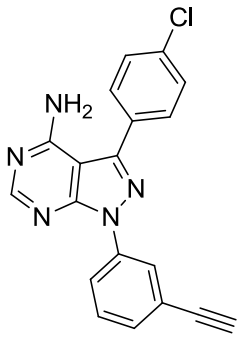

Synthesis of **4.S-1**: **4.S-1** was synthesized as previously described.[5]

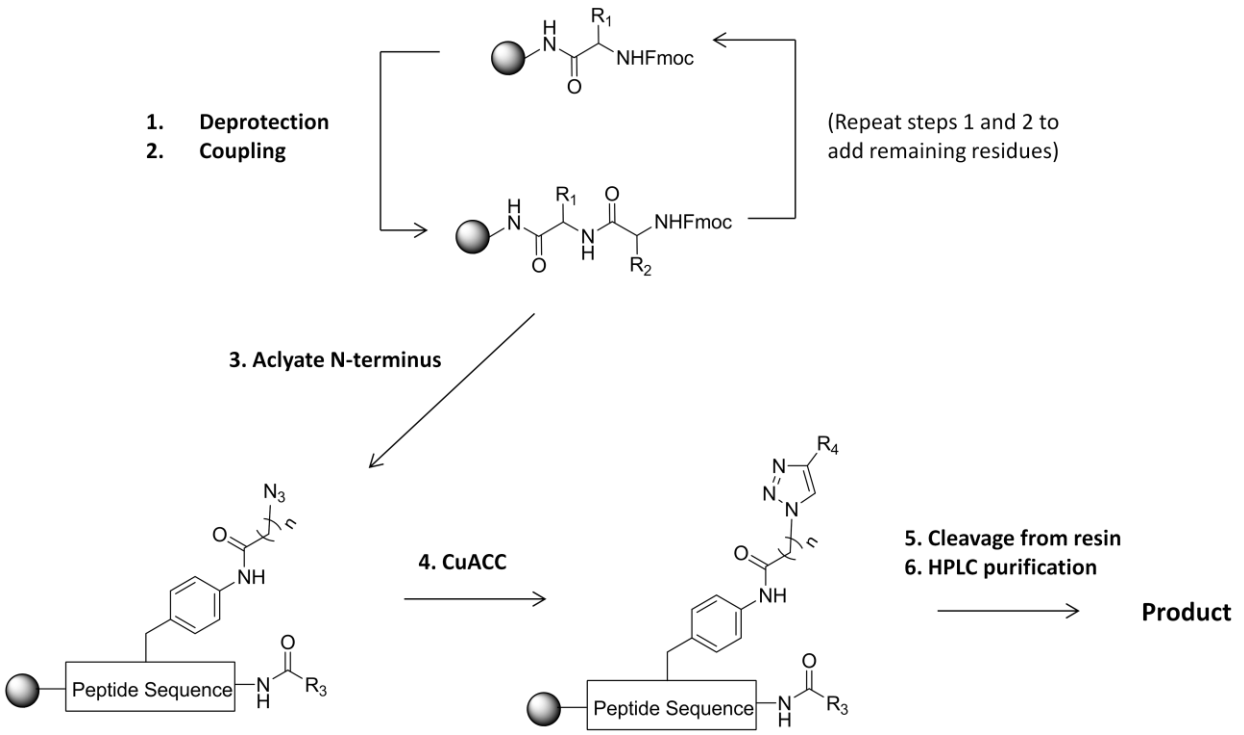

Scheme 4.S-1. General synthetic scheme for bisubstrate competitive kinase inhibitors using solid phase peptide synthesis.

Peptide synthesis: Standard solid phase Fmoc peptide synthesis using rink amide resin was performed. Briefly, to a 10 ml peptide synthesis vessel was added 0.1 mmol of rink amide resin and 4 ml of deprotection solution (20% piperidine in NMP). The reaction was sealed and agitated for 30 min. The reaction solution was then removed via filtration and the resin was rinsed three times with NMP. Separately, a solution of 0.3 mmol amino acid and 0.3 mmol HBTU in activator solution (5 % DIEA in NMP) was prepared; this solution was added to the vessel loaded with the pre-swelled rink amide resin. The vessel was sealed and agitated using a mechanical shaker for 30 min. The reaction solution was removed via filtration and the crude resin was rinsed three times with NMP. To the vessel containing the crude resin was added 4 ml deprotection solution (20% piperidine in NMP). The vessel was sealed and agitated using a mechanical shaker for 30 min. The reaction solution was drained and the crude resin was rinsed three times using NMP. The coupling-deprotection sequence was repeated with the amino acids necessary to afford the final desired peptides. After the final Fmoc deprotection, the terminal amine was acetylated using “Cap-mix A” (80% tetrahydrofuran, 10% acetic anhydride, 10% pyridine).

Solid phase copper-catalyzed cycloadditions: To a 10 mL peptide synthesis vessel which was loaded with 0.1 mmol of resin (prepared as described in previous step) was added 0.3 mmol copper (I) iodide and 4 ml of a 25% diisopropylamine solution in NMP.

The reaction mixture was then agitated overnight at room temperature using a mechanical shaker. The reaction solution was drained and the crude resin was rinsed three times respectively using water, then NMP, and finally chloroform. The products were cleaved using a trifluoroacetic acid (TFA) solution (90% TFA, 5% water, 5% triisopropylsilane). TFA was then removed under reduced pressure. The crude reaction mixture was then dissolved in DMSO and purified using reverse phase HPLC (10% -> 85% acetonitrile in water).

Synthesis of Probe 4.6. The general protocol for peptide synthesis was followed with the exception being that a dye containing an acid handle for coupling was used to Cap the N-terminus.

I. ANALYTICAL DATA FOR COMPOUNDS 4.2–4.9.

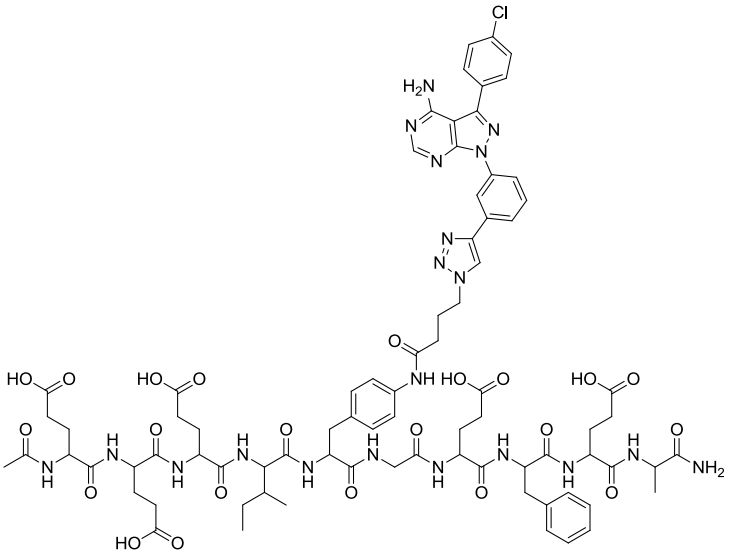

Spectral data for compound 4.2. HRMS-QTOF ESI+ (*m/z*): $[M + H]^+$ calcd for $C_{79}H_{95}ClN_{20}O_{22}$, 1711.6691; found 1711.6655.

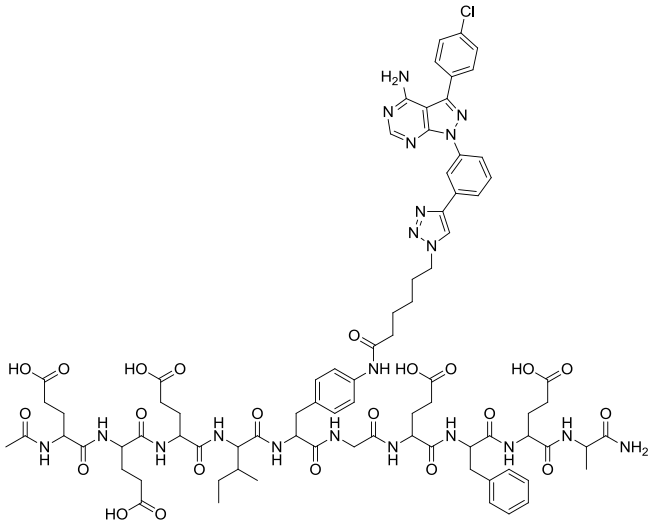

Spectral data for compound 4.3. HRMS-QTOF ESI+ (*m/z*): $[M + 2H]^{++}$ calcd for $C_{81}H_{99}ClN_{20}O_{22}$, 870.3538; found 870.3510.

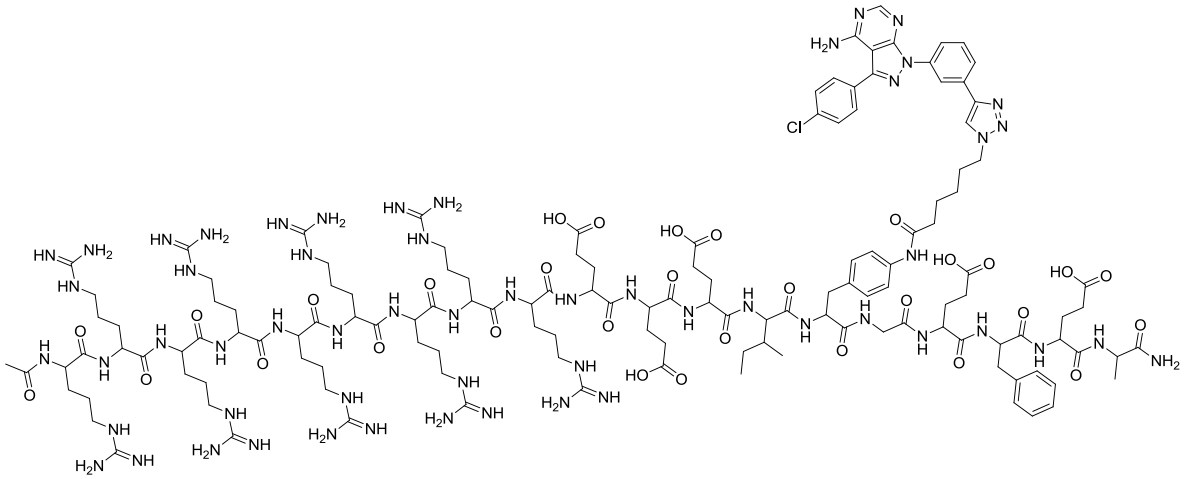

Spectral data for compound 4.3-R9. HRMS-MALDI (*m/z*): $[M - 3Arg + H]^+$ calcd for $C_{121}H_{182}ClN_{48}O_{28}$, 2790.3981, found 2790.558.

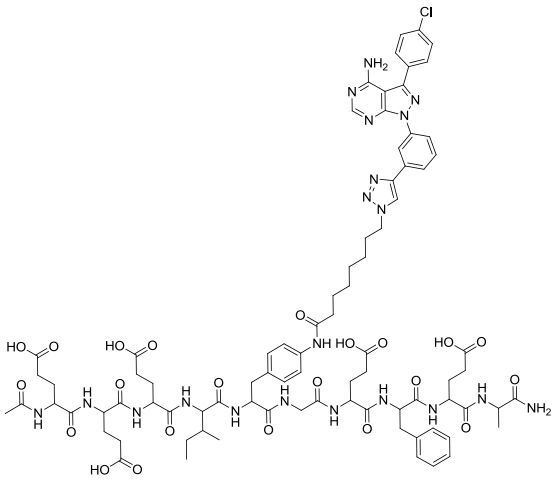

Spectral data for compound 4.4. HRMS-QTOF ESI+ (*m/z*): $[M + 2H]^{++}$ calcd for $C_{83}H_{103}ClN_{20}O_{22}$, 884.3695; found 884.3687.

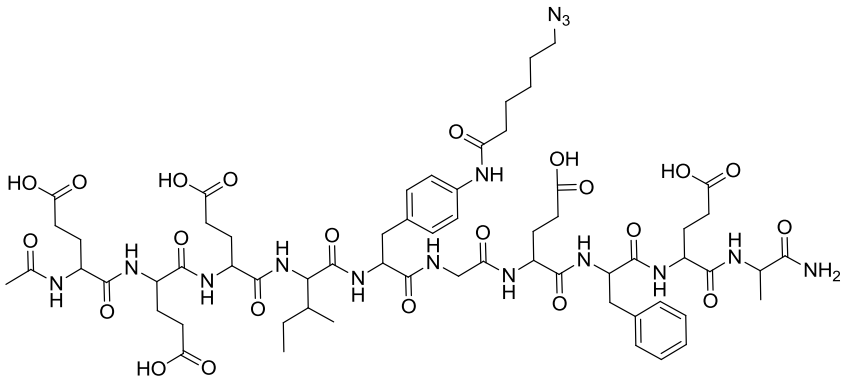

Spectral data for compound 4.5. HRMS-QTOF ESI+ (*m/z*): $[M + H]^+$ calcd for $C_{62}H_{87}N_{15}O_{22}$, 1394.6223; found 1394.6251.

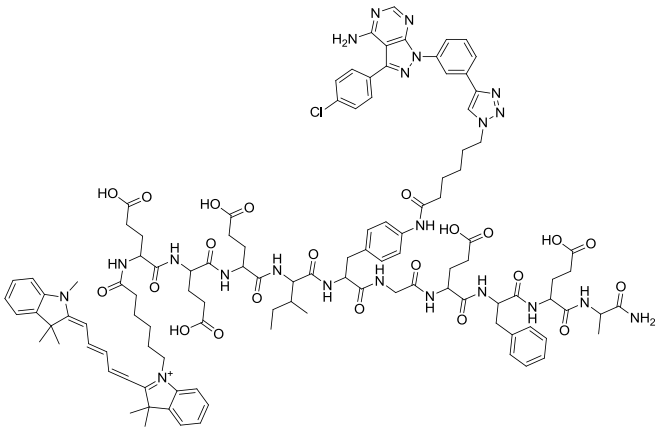

Spectral data for compound 4.6. HRMS-QTOF ESI+ (*m/z*): $[M + 2H]^{++}$ calcd for C111H133ClN22O22, 1081.9939; found 1081.9893.

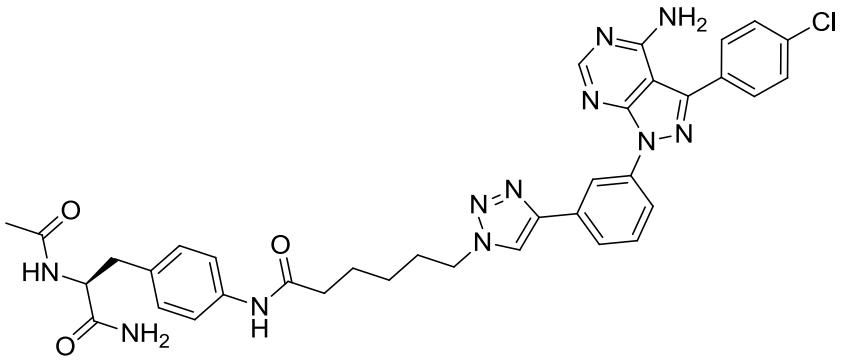

Spectral data for compound 4.7. HRMS-QTOF ESI+ (*m/z*): $[M + H]^+$ calcd for $C_{36}H_{36}ClN_{11}O_3$, 706.2764, found 706.2755.

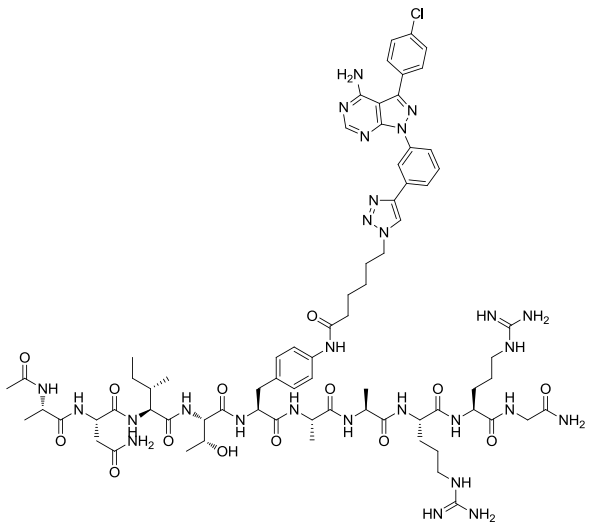

Spectral data for compound 4.8. HRMS-QTOF ESI+ (*m/z*): $[M + 2H]^{++}$ calcd for $C_{73}H_{102}ClN_{27}O_{14}$, 808.8967; found 808.8958.

BIOCHEMICAL AND CELLULAR CHARACTERIZATION

A. General procedure for determination of inhibitor IC_{50}.

A continuous fluorescence assay[15] was used to determine IC_{50}. Reaction volumes of 100 µL were used in 96-well plates. 85 µL of enzyme in buffer was added to each well. 2.5 µL of the appropriate inhibitor dilution (typically 5000, 1666, 555, 185, 61, 20, 6.8, 2.2, 0.76, 0 µM in DMSO) was then added. 2.5 µL of a substrate peptide ("compound 3" as described in Wang et al[16]) solution (1.8 mM in DMSO) was added. The reaction was initiated with 10 µL of ATP (1 mM in water), and reaction progress was immediately monitored at 405 nm (ex. 340 nm) for 10 minutes. Reactions had final concentrations of 30 nM enzyme, 45 µM peptide substrate, 100 µM Na_3VO_4, 100 mM Tris buffer (pH 8), 10 mM $MgCl_2$, 0.01% Triton X-100; the concentration of ATP varied from 0.1 – 5 mM, and the concentrations are specified for each experiment in the following section. The initial rate data collected was used for determination of IC_{50} values. For IC_{50} determination, the kinetic values were obtained directly from nonlinear regression of substrate-velocity curves in the presence of various concentrations of the inhibitor. The equation Y=Bottom + (Top-Bottom)/(1+10^(X-LogEC50)) was used in the nonlinear regression.

B. Analytical data for c-Src IC_{50} determination.

Each inhibitor IC_{50} value was determined using at least three independent experiments; a representative inhibition curve is shown.

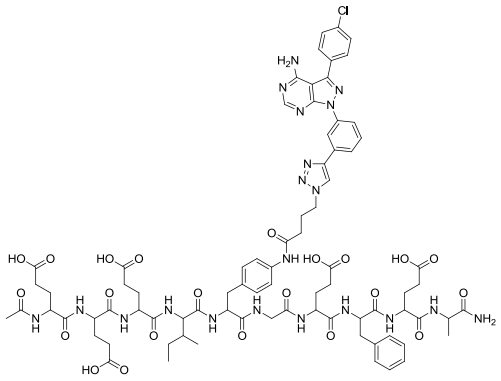

4.2

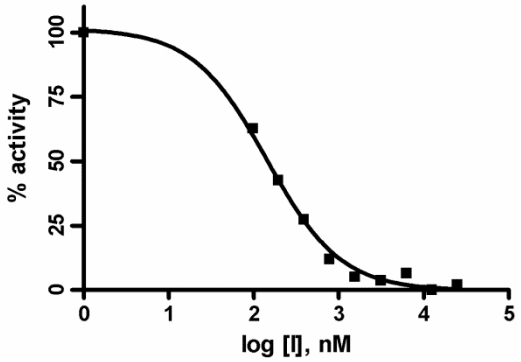

Avg IC_{50} = 159 ± 28 nM
[ATP] = 5 mM

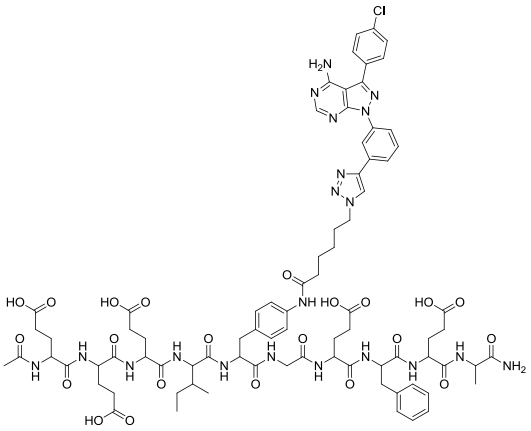

4.3

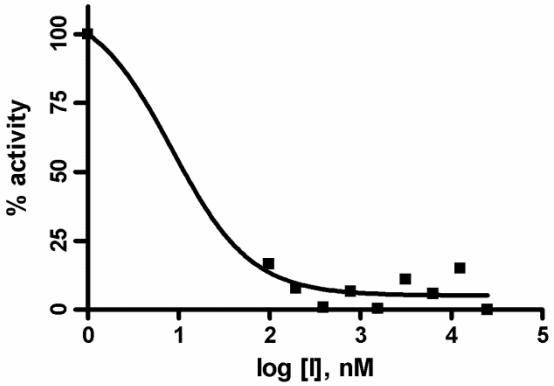

Avg IC_{50} ≤ 8.4 nM
[ATP] = 5 mM

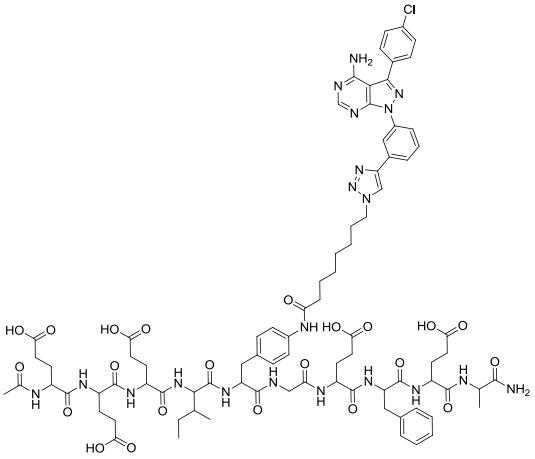

4.4

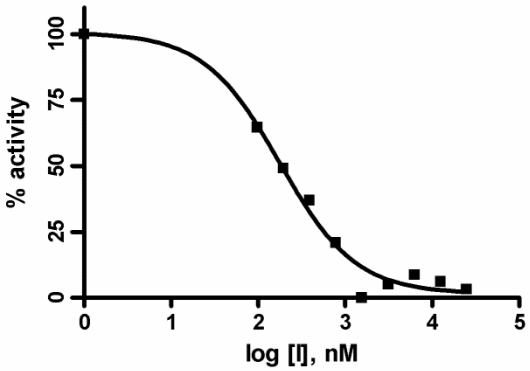

Avg IC_{50} = 121 ± 50 nM
[ATP] = 5 mM

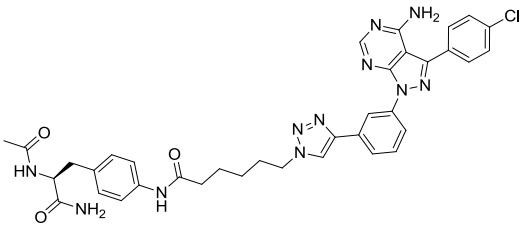

4.7

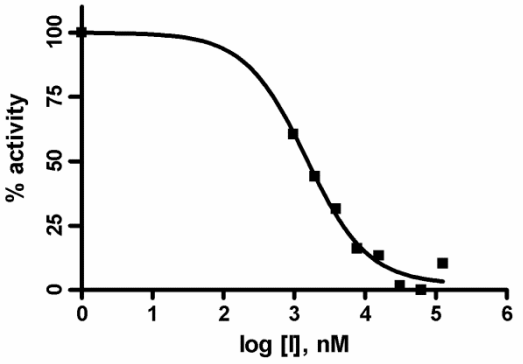

Avg IC_{50} = 1,182 ± 275 nM
[ATP] = 100 µM

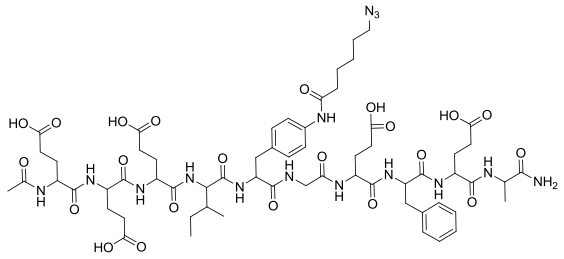

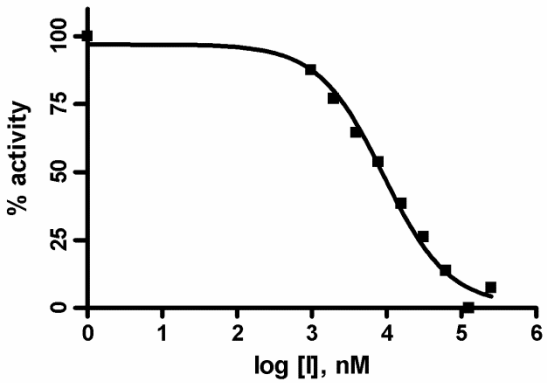

4.5

Avg IC_{50} = 8,372 ± 861 nM
[ATP] = 5 mM

C. Analytical data for T338I c-Src IC_{50} determination. Each inhibitor IC_{50} value was determined using at least three independent experiments; a representative inhibition curve is shown.

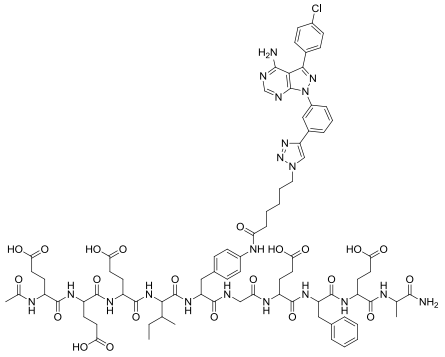

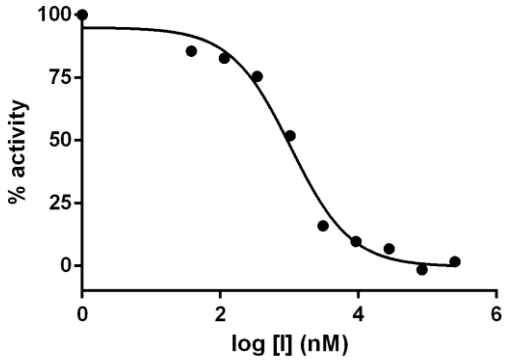

4.3

Avg IC_{50} = 953 ± 82 nM
[ATP] = 100 µM

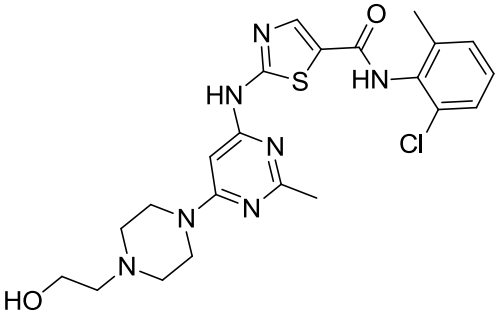

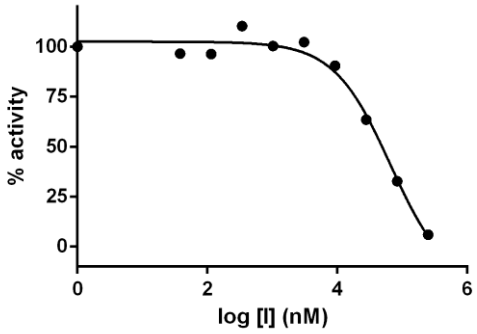

dasatinib

Avg IC_{50} = 50,395 ± 18,520 nM
[ATP] = 100 µM

D. Analytical data for Hck IC_{50} determination. Each inhibitor IC_{50} value was determined using at least three independent experiments; a representative inhibition curve is shown.

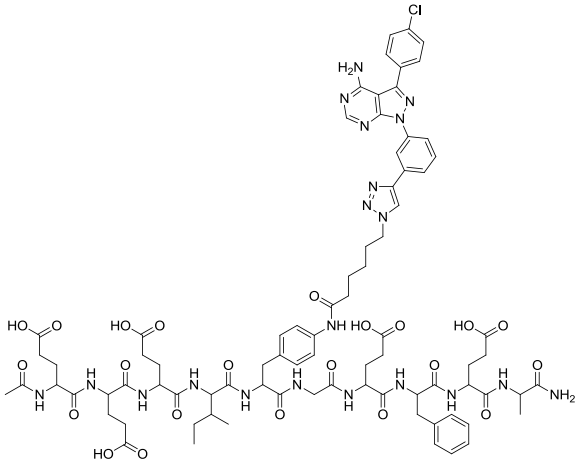

4.3

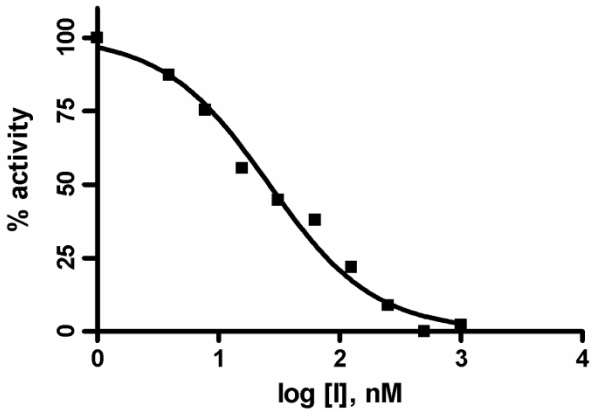

Avg IC_{50} = 37 ± 14 nM
[ATP] = 5 mM

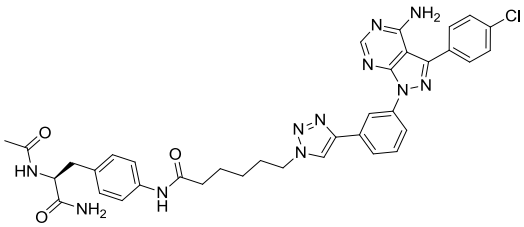

4.7

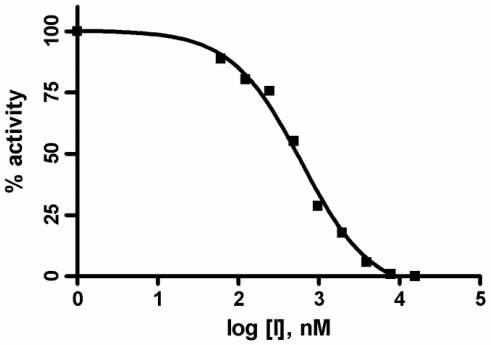

Avg IC_{50} = 555 ± 73 nM
[ATP] = 100 µM

E. Analytical data for c-Abl IC_{50} determination. Each inhibitor IC_{50} value was determined using at least three independent experiments; a representative inhibition curve is shown.

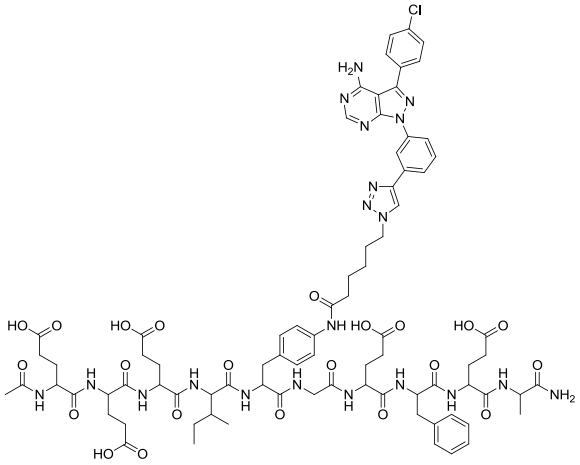

4.3

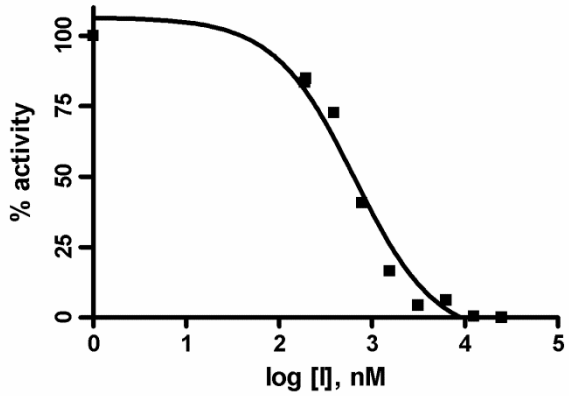

Avg IC_{50} = 1,168 ± 731 nM
[ATP] = 5 mM

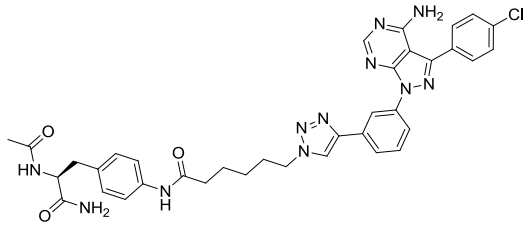

4.7

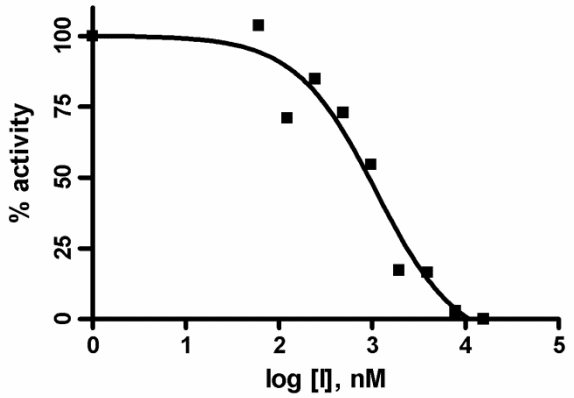

Avg IC_{50} = 1,134 ± 374 nM
[ATP] = 100 µM

F. General procedure for determination of K_d for Cy-5 labeled bisubstrate inhibitor (4.6).

A Time Resolved FRET (TR-FRET) assay was used to determine K_d. Well volumes of 20 µL were used in 384-well plates. 10 µL of a solution of 6xHis-enzyme and Eu3+ labeled Anti-6xHis antibody in buffer was added to each well. 5 µL of the appropriate probe dilution in buffer (typically 5000, 1666, 555, 185, 61, 20, 6.8, 2.2, 0.76, 0 nM in buffer) was then added. 5 µl buffer was then added. The plate was then centrifuged for 30 seconds at 4,000 rpm. The plate was then allowed to incubate at room temperature for 30 minutes in an area devoid of light. TR-FRET emission was then determined respectively at 650 and 620 nM (ex. 360 ± 40 nm). A 570 ± 100 nm emission filter was used. 20 measurements were collected per data point with 100 µsec of delay time and 200 µsec of data collection. Wells had final concentrations of 5 nM enzyme, 2 nM Eu3+ labeled Anti-6xHis antibody, 50 mM Tris buffer (pH 8.0), 100 mM NaCl, 0.1% BSA, an varying concentrations of probe **4.6**,. For K_d determination, the kinetic values were obtained directly from nonlinear regression of probe-binding curves. The equation Y=Bmax*X/(Kd+X) was used in the nonlinear regression.

G. Analytical data for c-Src Kd determination of 4.6.

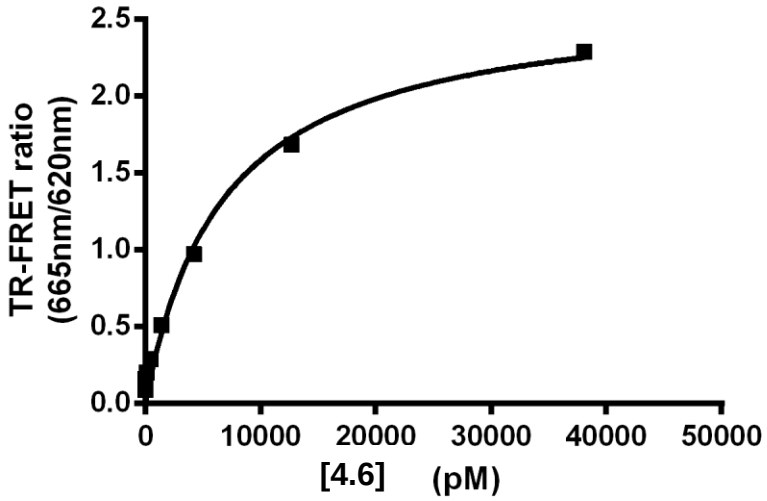

Probe **4.6** Avg K_d = 6.3 ± 1.6 nM

H. General procedure for competition-assay based determination of inhibitor K_d.

A Time Resolved FRET (TR-FRET) competition assay was used to determine K_d. Reaction volumes of 20 µL were used in 384-well plates. 10 µL of a solution of 6xHis-enzyme and Eu3+ labeled Anti-6xHis antibody in buffer was added to each well. 5 µL solution of probe **4.6** in buffer was added (final concentrations for individual experiments

are specified below). 5 µL of the appropriate inhibitor dilution (typically 5000, 1666, 555, 185, 61, 20, 6.8, 2.2, 0.76, 0 nM in buffer) was then added. The plate was then centrifuged for 30 seconds at 4,000 rpm. The plate was then allowed to incubate at room temperature for 30 minutes in an area devoid of light. TR-FRET emission was then determined respectively at 650 and 620 nM (ex. 360 ± 40 nm). A 570 ± 100 nm emission filter was used. 20 measurements were collected per data point with 100 µsec of delay time and 200 µsec of data collection. Reactions had final concentrations of 5 nM enzyme, 2 nM Eu3+ labeled Anti-6xHis antibody, 50 mM Tris buffer (pH 8.0), 100 mM NaCl, 0.1% BSA. For K_d determination, the kinetic values were obtained directly from nonlinear regression of probe-binding curves in the presence of various concentrations of the competing ligand. The equation Y=Bottom + (Top-Bottom)/(1+10^(X-LogEC50)) was used in the nonlinear regression.

I. Analytical data for c-Src inhibitor K_d determination using probe 4.6. Each ligand EC_{50} value was determined using at least three independent experiments; a representative binding curve is shown.

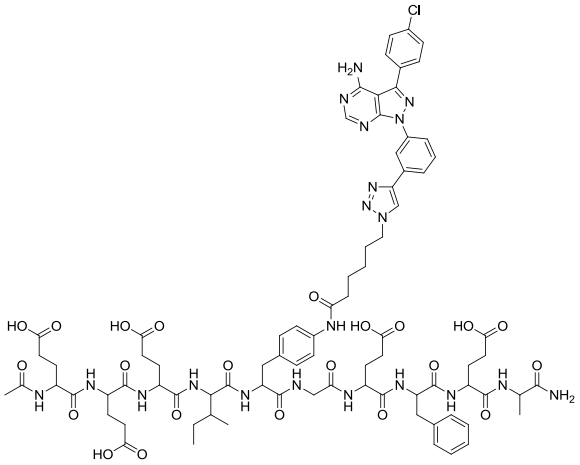

4.3

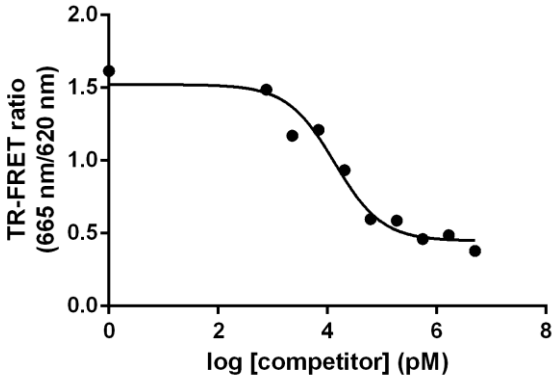

Avg K_d = 280 ± 76 pM
[fluorescent probe **4.6**] = 400 nM

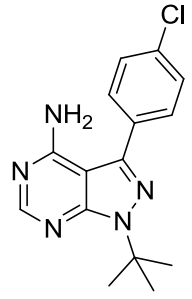

PP2

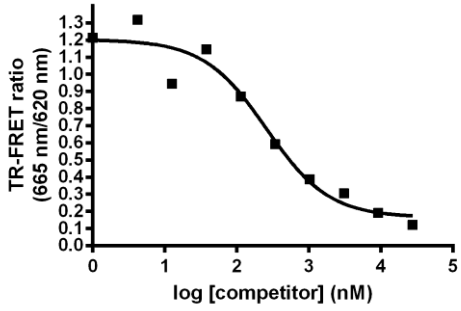

Avg K_d = 22 ± 7 nM
[fluorescent probe **4.6**] = 40 nM

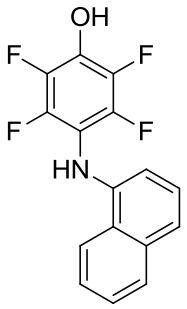

MEB-4-151

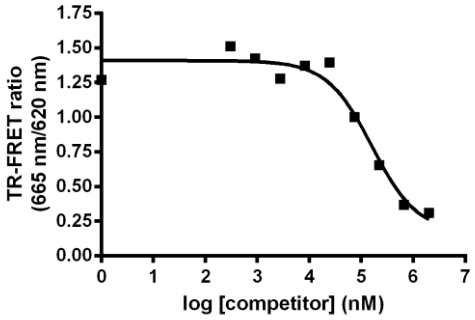

Avg K_d = 15,567 ± 4,304 nM
[fluorescent probe **4.6**] = 40 nM

J. Analytical data for c-Src inhibitor K_d determination using kinase Tracer 236. A modified protocol which employed kinase Tracer 236 (final concentrations for individual experiments are specified below)**.** Each ligand EC_{50} value was determined using at least three independent experiments; a representative binding curve is shown.

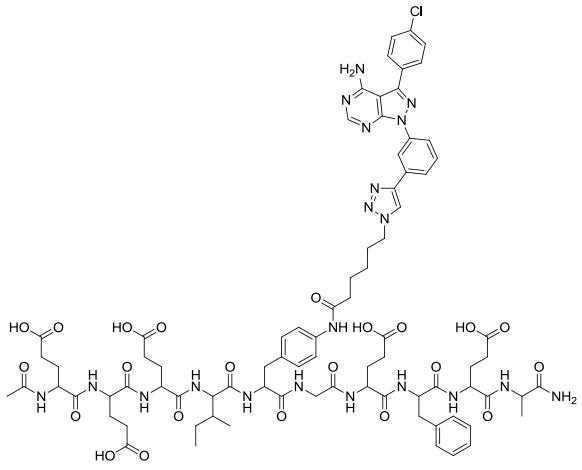

4.3

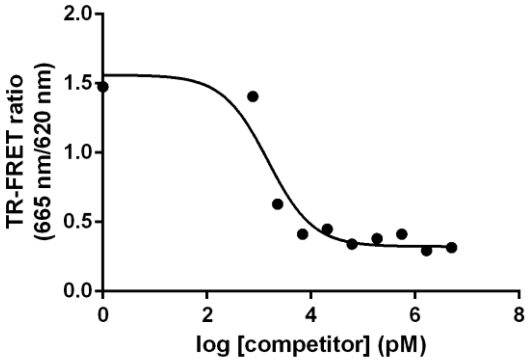

Avg K_d = 187 pM
[tracer 236] = 250 nM

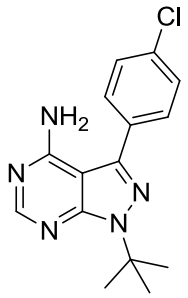

PP2

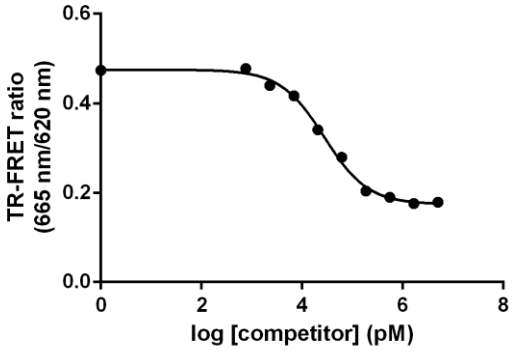

Avg K_d = 8.9 ± 2.7 nM
[tracer 236] = 50 nM

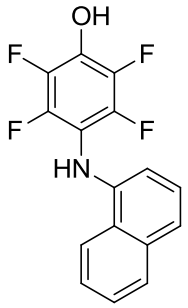

MEB-4-151

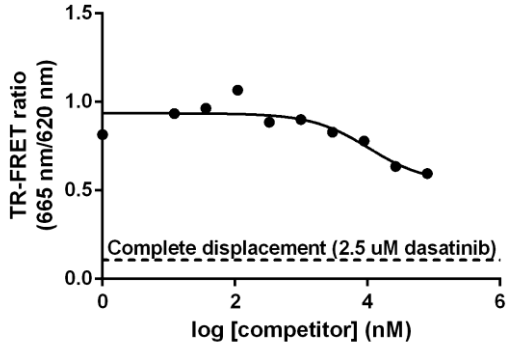

Avg K_d > 330,000
[tracer 236] = 50 nM

K. Cancer cell growth inhibition assays.

General procedure:

1. **Cell culture and seeding**: Cells are dispersed from flasks and collected by centrifugation (125xg for 5 minutes at room temperature). An aliquot of the resuspended cells is mixed with trypan blue solution and the cell number is quantified using a hemacytometer. In general, depending on the growth rate of the untreated cells, the cells will be plated at 5.0 – 7.5 x 10^3 cells per well. 100 µL of the cell mixture will be added to each well so the concentration should be 10X the cells per well in cells per mL. The cells are plated into sterile, clear bottom 96 well plates and cultured under normal growth conditions overnight prior to dosing with compound.
2. **Dosing**: The 100% DMSO compound stocks need to be prepared to 100X the final concentration that is desired in the assay. 3 µL of the DMSO stock solution is then added to 297 µL of the cell growth media to give a DMSO concentration of 1%. The cell media is removed by aspiration for adherent cells and replaced with 100 µL per well of the cell growth media containing the compound. In general each compound concentration is dosed in triplicate wells. The plates are returned to normal culture conditions for 24 – 72 hours.
3. **Assay**: After the required incubation period the plates are removed from the incubator and 10 µL per well of WST-1 reagent is added. The plates are returned to the incubator and the color change is visually monitored for 0.5 – 2 hours. When sufficient color change has occurred the plates are shaken on a plate shaker for 60 seconds and read in the appropriate plate reader.
4. **Data Analysis**: The reference absorbance reading is subtracted from the formazan absorbance and the data is plotted as a percentage of the vehicle (1% DMSO alone). Data analysis and curve fitting was performed using Graphpad Prism. For each cell line, there were n = 3 data points for each concentration. Each dose response curve was performed at least twice, providing n ≥ 6 for each data point.

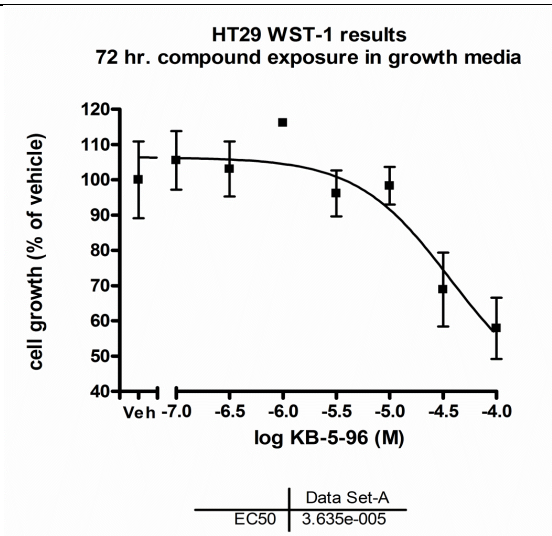

Figure 4.S-2. Treatment of HT-29 colon cancer cells with 4.3-R9.

Luceome IC_{50} determination

IC_{50}s for compounds **4.3 and 4.8** were determined using KinaseLite™ (Luceome Biotechnologies, Tucson AZ).

A. Tabulated Luceome IC_{50} data:

	IC_{50} (μM)		
Test Compound	**SRC**	**BLK**	**PDGFRB**
4.3	0.016 ± 0.005	0.13 ± 0.021	2.0 ± 1
4.8	>10	1.3 ± 0.1	0.35 0.07

B. Representative Luceome IC_{50} curves:

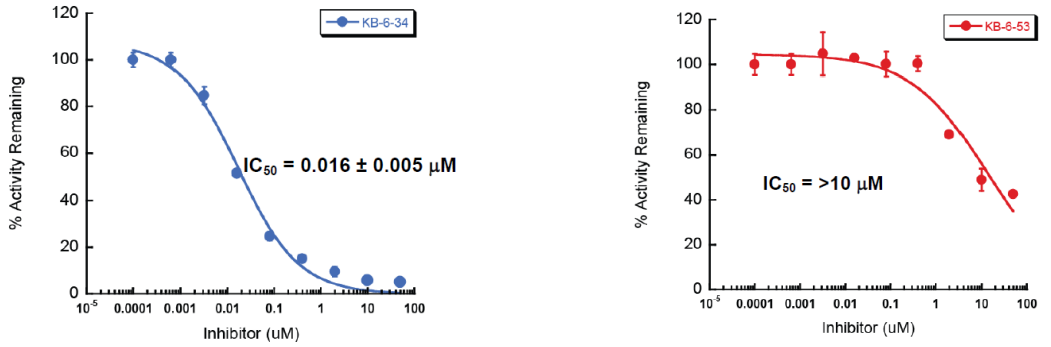

Figure 4.S-3. Representative Src IC_{50} plots for A) Cpd 4.3 and B) Cpd 4.8

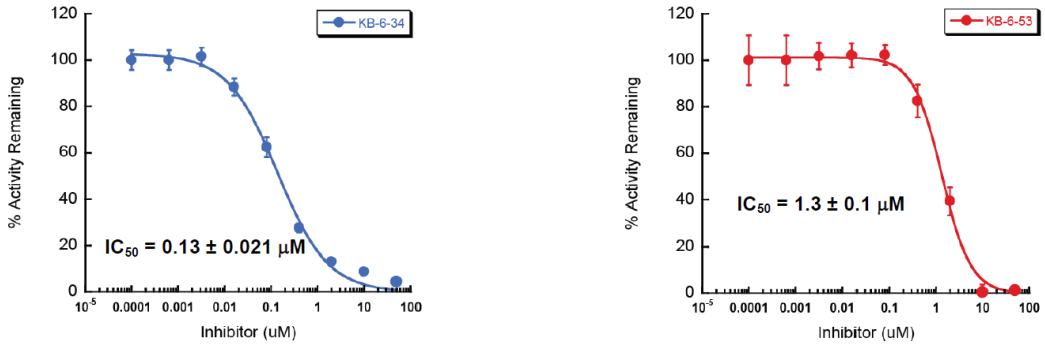

Figure 4.S-4. Representative Blk IC_{50} plots for A) Cpd 4.3 and B) Cpd 4.8

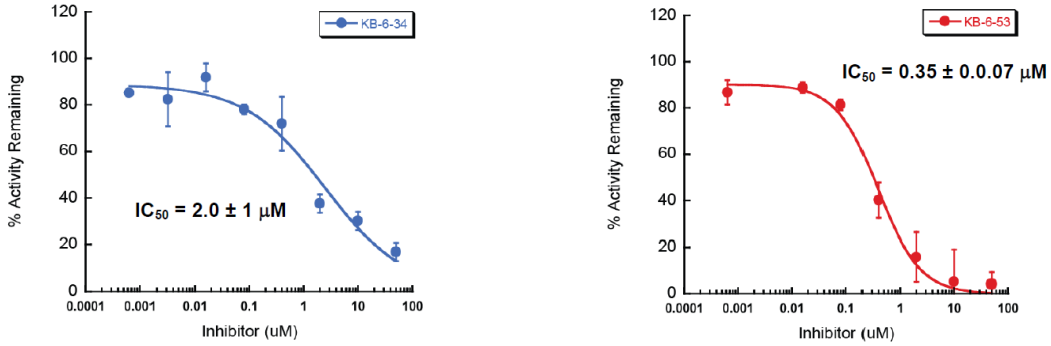

Figure 4-S-5. Representative PDGFRB IC_{50} plots for A) Cpd 4.3 and B) Cpd 4.8

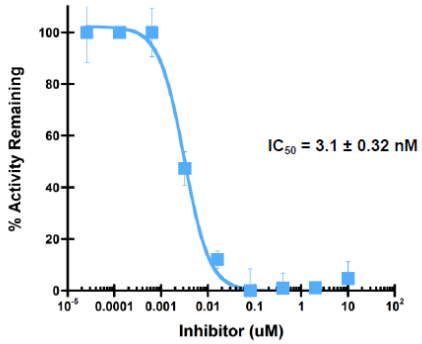

Figure 4.S-6. Representative Src IC_{50} plot for dasatinib.

KINOMEscan profiling

Kinome profiling for compound **4.1** was performed by KINOMEscan (DiscoveRx, Fremont, CA). The compound was profiled at a concentration of 10 μM.

A. 4.1 TREEspot analysis:

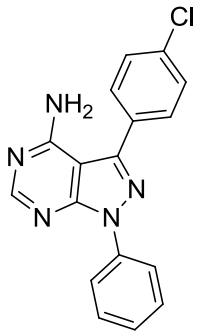

4.1

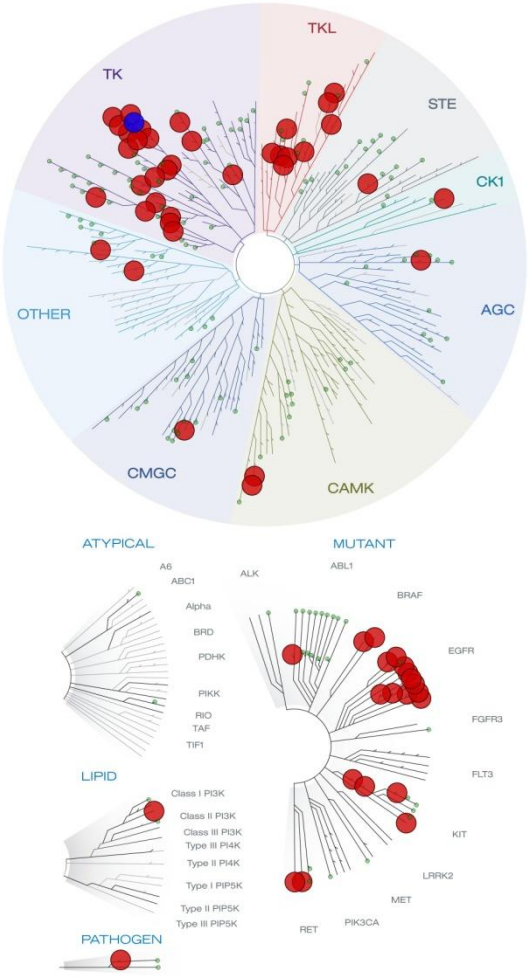

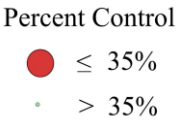

B. S-Scores for 4.1:

S(35) = 0.252

C. Tabulated data for compound 4.1:

KINOMEscan Gene Symbol	% control
ABL1(E255K)-phosphorylated	36
ABL1(F317I)-nonphosphorylated	100
ABL1(F317I)-phosphorylated	76
ABL1(F317L)-nonphosphorylated	100
ABL1(F317L)-phosphorylated	44
ABL1(H396P)-nonphosphorylated	20
ABL1(H396P)-phosphorylated	52
ABL1(M351T)-phosphorylated	90
ABL1(Q252H)-nonphosphorylated	73
ABL1(Q252H)-phosphorylated	51
ABL1(T315I)-nonphosphorylated	100
ABL1(T315I)-phosphorylated	87
ABL1(Y253F)-phosphorylated	57
ABL1-nonphosphorylated	59
ABL1-phosphorylated	49
ABL2	27
ACVR1	20
ACVR1B	62
ACVR2A	50
ACVR2B	8.6
ACVRL1	15
ADCK3	64
AKT1	99
AKT2	99
ALK	100
AURKA	90
AURKB	94
AXL	69
BLK	0.75
BMPR2	100
BMX	37
BRAF	22
BRAF(V600E)	18
BRK	3.2
BTK	66
CDK11	44
CDK2	83
CDK3	100
CDK7	97
CDK9	76
CHEK1	100
CSF1R	40
CSK	92
CSNK1D	85
CSNK1E	0.35
CSNK1G2	78
DCAMKL1	99
DDR1	28
DDR2	61
DMPK	81
DMPK2	21
DYRK1B	79
EGFR	4.4
EGFR(E746-A750del)	8.2
EGFR(G719C)	0.45
EGFR(G719S)	1.6
EGFR(L747-E749del, A750P)	6.4
EGFR(L747-S752del, P753S)	6.2
EGFR(L747-T751del,Sins)	6.6
EGFR(L858R)	9.6
EGFR(L858R,T790M)	80
EGFR(L861Q)	5.7
EGFR(S752-I759del)	6.2
EGFR(T790M)	33
EPHA1	13
EPHA2	51
EPHA3	66
EPHA4	44
EPHA5	54
EPHA6	64
EPHA7	100
EPHA8	15
EPHB1	75
EPHB2	66
EPHB3	16
EPHB4	60
EPHB6	31
ERBB2	56
ERBB3	48
ERBB4	31
ERK1	92
FAK	92
FGFR1	92
FGFR2	86
FGFR3	100

FGFR4	100	MET	100
FGR	5.2	MKNK1	100
FLT1	83	MKNK2	100
FRK	5.8	MLK1	96
FYN	7	MRCKA	55
GAK	4.7	MRCKB	70
GCN2(Kin.Dom.2,S808G)	90	MST4	80
GSK3B	100	NLK	13
HCK	3.3	p38-alpha	90
IGF1R	100	p38-beta	73
IKK-alpha	100	PAK1	100
IKK-beta	100	PAK2	78
INSR	81	PAK4	99
JAK2(JH1domain-catalytic)	97	PCTK1	100
JAK3(JH1domain-catalytic)	92	PDGFRA	38
JNK1	94	PDGFRB	0.5
JNK2	84	PDPK1	96
JNK3	91	PFCDPK1(P.falciparum)	13
KIT	1	PFPK5(P.falciparum)	80
KIT(A829P)	86	PIK3C2B	100
KIT(D816H)	96	PIK3CA	91
KIT(D816V)	6.8	PIK3CG	12
KIT(L576P)	1.8	PIM1	100
KIT(V559D)	0.5	PIM2	77
KIT(V559D,T670I)	79	PIM3	100
KIT(V559D,V654A)	37	PKAC-alpha	37
KIT-autoinhibited	89	PKMYT1	65
LCK	0.5	PKNB(M.tuberculosis)	100
LIMK1	77	PLK1	100
LIMK2	85	PLK3	91
LKB1	88	PLK4	67
LOK	81	PRKCE	100
LYN	21	RAF1	20
MAP3K4	89	RET	7.6
MAP4K2	94	RET(M918T)	3.6
MAP4K3	96	RET(V804L)	82
MAP4K4	97	RET(V804M)	97
MAP4K5	100	RIOK2	100
MAPKAPK2	100	RIPK2	0.25
MARK3	83	ROCK1	77
MEK1	65	ROCK2	83
MEK2	65	RSK2(Kin.Dom.1-N-terminal)	79
MEK3	96	SIK	12
MEK4	100	SIK2	18
MEK5	7.9	SLK	77

SNARK	79	TNNI3K	75
SRC	0.15	TRKA	69
SRMS	74	TSSK1B	91
SRPK3	100	TXK	1.1
STK36	33	TYK2(JH1domain-catalytic)	100
SYK	80	ULK2	98
TEC	100	VEGFR2	100
TESK1	23	WEE1	100
TGFBR1	68	YANK3	78
TGFBR2	3.1	YES	11
TIE2	89	ZAK	33
TNIK	83	ZAP70	100
TNK2	52		

Luceome selectivity profiling

Kinome profiling for compound **4.3** was performed by KinaseSeeker™ (Luceome Biotechnologies, Tucson, AZ). The compound was profiled at a concentration of 115 nM.

A. Compound 4.3 TREEspot analysis:

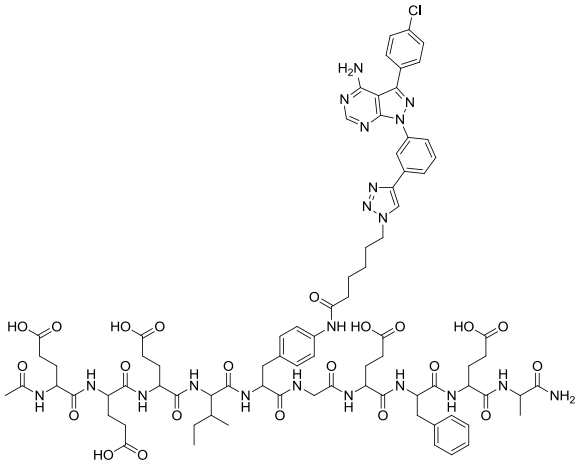

4.3

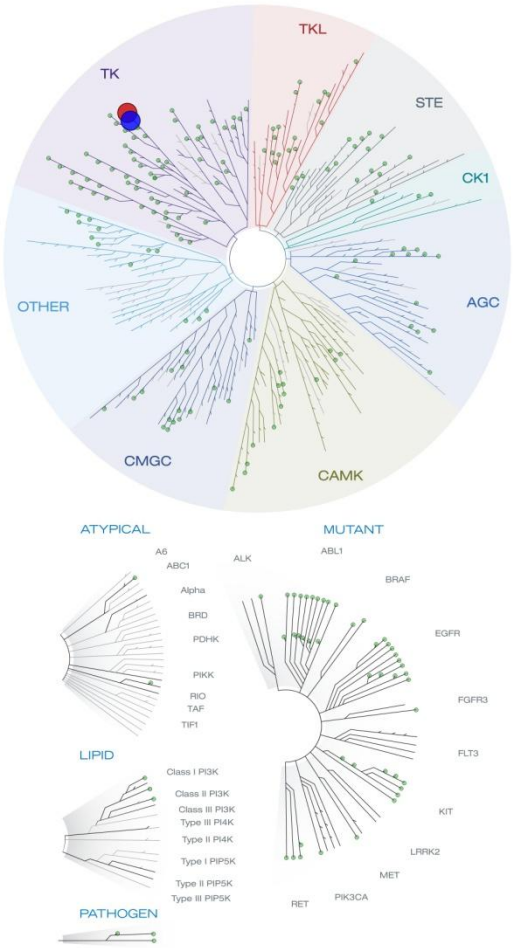

Percent Control

≤ 35%

> 35%

B. S-Scores for 4.3:

S(35) = 0.010

C. Tabulated Luceome selectivity profiling data for compound 4.3:

Kinase	Family	% Activity Remaining
ABL1	TK	100.0
ABL2	TK	96.5
AKT1	AGC	100.0
AKT1(FL)	AGC	96.8
AKT2	AGC	98.4
AKT2(S474A)	AGC	94.7
AKT2(S474D)	AGC	94.9
AKT2(T309A,S474A)	AGC	94.4
AKT2(T309D,S474D)	AGC	90.9
AKT3	AGC	100.0
AMPK-a1	CAMK	99.7
AMPK-a2	CAMK	100.0
AURKA	Other	100.0
AURKB	Other	100.0
AURKC	Other	96.3
AXL	TK	100.0
BIKE	Other	96.5
BLK	TK	42.4
BTK	TK	100.0
CAMK1	CAMK	99.9
CAMK1D	CAMK	99.1
CAMK1G	CAMK	100.0
CAMK2A	CAMK	100.0
CAMK2B	CAMK	97.1
CAMK2D	CAMK	100.0
CAMKK1	Other	100.0
CAMKK2	Other	100.0
CHEK1	CAMK	96.9
CK1D	CK1	100.0
CLK1	CMGC	100.0
CLK2	CMGC	100.0
CSK	TK	95.3
DAPK1	CAMK	100.0
DAPK2	CAMK	100.0
DAPK3	CAMK	97.4
DDR1	TK	95.0
DDR2	TK	96.3
DMPK	AGC	100.0
EPHA1	TK	100.0
EPHA2	TK	100.0
EPHA3	TK	100.0
EPHA4	TK	100.0
EPHB2	TK	100.0
EPHB3	TK	90.3
EPHB4	TK	98.9
FGFR2	TK	100.0
FLT1	TK	100.0
FLT2	TK	92.5
FLT3	TK	100.0
FYN	TK	37.7
GSK3a	CMGC	100.0
HCK	TK	54.7
IGF1R	TK	92.1
IKK-e	Other	97.3
INSR	TK	100.0
ITK	TK	100.0
LIMK1	TKL	100.0
LYN	TK	78.4
MARK1	CAMK	90.1
MARK2	CAMK	100.0
MARK3	CAMK	100.0
MARK4	CAMK	100.0
MELK	CAMK	100.0
MET	TK	100.0
MLK1	TKL	100.0
MLK3	TKL	100.0
MST2	STE	81.0
MUSK	TK	100.0
MYLK	CAMK	88.0
MYLK2	CAMK	100.0
p38-g	CMGC	97.0
PAK1	STE	100.0
PAK1(T423A)	STE	100.0
PAK1(T423E)	STE	99.2
PDGFRA	TK	100.0
PDGFRB	TK	100.0
PDK1	AGC	100.0
PHKG1	CAMK	90.0
PIM1	CAMK	88.3
PIM2	CAMK	100.0
PKAC-a	AGC	98.9
PKAC-b	AGC	100.0
PKC-d	AGC	94.9
PKC-e	AGC	98.7
PKC-g	AGC	100.0

PKC-h	AGC	100.0
PKC-t	AGC	84.0
PRKD2	CAMK	100.0
PRKD3	CAMK	93.3
PKG1	AGC	100.0
PKN3	AGC	74.7
PLK4	Other	96.5
PKX	AGC	100.0
PTK2	TK	100.0
PTK2B	TK	92.7
PTK6	TK	76.7
RET	TK	91.9
RIPK2	TK	95.5
RPS6KA1/RSK1	AGC	94.4
RPS6KA2/RSK3	AGC	100.0
RPS6KA3/RSK2	AGC	100.0
RPS6KA4/MSK2	AGC	82.4
RPS6KA5/MSK1	AGC	98.0
RPS6KA6/RSK4	AGC	98.8
SGK2	AGC	95.1
SGK3	AGC	100.0
SNF1LK	CAMK	87.7
SNF1LK2	CAMK	84.9
SIK3	CAMK	96.3
SLK	STE	100.0
SNARK	CAMK	77.1
SRC	TK	15.9
STK16	Other	78.5
STK33	CAMK	97.5
SYK	TK	98.7
TBK1	Other	100.0
TEC	TK	100.0
TESK1	TKL	100.0
TESK2	TKL	85.7
TIE1	TK	100.0
TIE2	TK	95.0
TNK2	TK	100.0
TNNI3K	TKL	97.6
TRKB	TK	97.0
TRKC	TK	100.0
TKX	TK	63.4
VEGFR2	TK	100.0
YANK2	AGC	100.0
YES1	TK	17.4
YSK1	STE	88.2

4.5 References

(1) Ko, K. S.; Steffey, M. E.; Brandvold, K. R.; Soellner, M. B. *ACS Medicinal Chemistry Letters* **2013**, *4*, 779-783.

(2) Davis, M. I.; Hunt, J. P.; Herrgard, S.; Ciceri, P.; Wodicka, L. M.; Pallares, G.; Hocker, M.; Treiber, D. K.; Zarrinkar, P. P. *Nat Biotech* **2011**, *29*, 1046-1051.

(3) van Wandelen, L. T. M.; van Ameijde, J.; Mady, A. S. A.; Wammes, A. E. M.; Bode, A.; Poot, A. J.; Ruijtenbeek, R.; Liskamp, R. M. J. *ChemMedChem* **2012**, *7*, 2113-2121.

(4) Kolb, H. C.; Finn, M. G.; Sharpless, K. B. *Angew. Chem., Int. Ed.* **2001**, *40*, 2004.

(5) Brandvold, K. R.; Steffey, M. E.; Fox, C. C.; Soellner, M. B. *ACS Chemical Biology* **2012**, *7*, 1393-1398.

(6) Songyang, Z.; Carraway, K. L.; Eck, M. J.; Harrison, S. C.; Feldman, R. A.; Mohammadi, M.; Schlessinger, J.; Hubbard, S. R.; Smith, D. P.; Eng, C.; Lorenzo, M. J.; Ponder, B. A. J.; Mayer, B. J.; Cantley, L. C. *Nature* **1995**, *373*, 536-539.

(7) Parang, K.; Till, J. H.; Ablooglu, A. J.; Kohanski, R. A.; Hubbard, S. R.; Cole, P. A. *Nat Struct Mol Biol* **2001**, *8*, 37-41.

(8) Hines, A. C.; Parang, K.; Kohanski, R. A.; Hubbard, S. R.; Cole, P. A. *Bioorganic Chemistry* **2005**, *33*, 285-297.

(9) Jester, B. W.; Cox, K. J.; Gaj, A.; Shomin, C. D.; Porter, J. R.; Ghosh, I. *Journal of the American Chemical Society* **2010**, *132*, 11727-11735.

(10) Chan, P. M.; Keller, P. R.; Connors, R. W.; Leopold, W. R.; Miller, W. T. *FEBS letters* **1996**, *394*, 121-125.

(11) Shah, N. P.; Nicoll, J. M.; Nagar, B.; Gorre, M. E.; Paquette, R. L.; Kuriyan, J.; Sawyers, C. L. *Cancer Cell* **2002**, *2*, 117-125.

(12) Azam, M.; Seeliger, M. A.; Gray, N. S.; Kuriyan, J.; Daley, G. Q. *Nat Struct Mol Biol* **2008**, *15*, 1109-1118.

(13) Das, J.; Chen, P.; Norris, D.; Padmanabha, R.; Lin, J.; Moquin, R. V.; Shen, Z.; Cook, L. S.; Doweyko, A. M.; Pitt, S.; Pang, S.; Shen, D. R.; Fang, Q.; de Fex, H. F.; McIntyre, K. W.; Shuster, D. J.; Gillooly, K. M.; Behnia, K.; Schieven, G. L.; Wityak, J.; Barrish, J. C. *Journal of Medicinal Chemistry* **2006**, *49*, 6819-6832.

(14) Georghiou, G.; Kleiner, R. E.; Pulkoski-Gross, M.; Liu, D. R.; Seeliger, M. A. *Nat Chem Biol* **2012**, *8*, 366-374.

(15) Wang, Q.; Cahill, S. M.; Blumenstein, M.; Lawrence, D. S. *Journal of the American Chemical Society* **2006**, *128*, 1808-1809.

(16) Castanedo, G.; Clark, K.; Wang, S.; Tsui, V.; Wong, M.; Nicholas, J.; Wickramasinghe, D.; Marsters Jr, J. C.; Sutherlin, D. *Bioorganic & Medicinal Chemistry Letters* **2006**, *16*, 1716-1720.

CHAPTER 5

Development of a highly selective c-Src kinase inhibitor

This chapter additionally addresses the "*How much selectivity may be gained by exploiting structural features outside of the canonical ATP-pocket?"* theme. This chapter regards targeting features proximal to the ATP-pocket. Using a tethering approach similar to that described in Chapter 4 it is discovered that building toward the p-loop region of c-Src provides a highly selective inhibition. This selective probe is also used to demonstrate that dual Src-Abl inhibition is ineffective in some breast cancer cell lines.

5.1 Introduction

The non-receptor tyrosine kinase c-Src plays a vital role in many facets of cell physiology, regulating diverse processes including cell division, motility, adhesion, angiogenesis, and survival.[1,2] c-Src was the first proto-oncogene to be identified and is frequently over-expressed in cancers[2]. Furthermore, the extent of this over-expression typically correlates with malignant potential and patient survival.[1,2] Recently, c-Src was identified as the major resistance factor to Herceptin, a first line therapy for Her2+ breast cancer.[3] Despite the significant attention devoted to c-Src inhibitor discovery, there are no highly selective probes for c-Src suitable for chemical genetic experiments in native systems.[4,5,6]

To fully understand the role of c-Src in oncogenesis, specific probes of c-Src function are required. Herein, we describe the development of the first highly selective and cell-permeable inhibitor of c-Src. Our approach involves modifying an existing non-selective inhibitor to interact with an adjacent pocket formed by the phosphate-binding loop of c-Src. This approach represents an underutilized method for improving kinase inhibitor selectivity that is likely generalizable across many kinase families.[7] We have developed

This chapter has been published, in part, under the same title. Referenece: Brandvold, K.R.; Steffey, M.E.; Fox, C.C.; Soellner, M.B. *ACS Chem Biol*, **2012**, 7, 1393-1398.

the most selective c-Src inhibitor to date and, using this inhibitor, we demonstrate that selective inhibition of c-Src is significantly more efficacious than multi-kinase inhibition in cell culture. Finally, using our probe we show that inhibition of a common off-target kinase of c-Src inhibitors, c-Abl, is pro-oncogenic in a breast cancer cell model.

5.2 Results and discussion

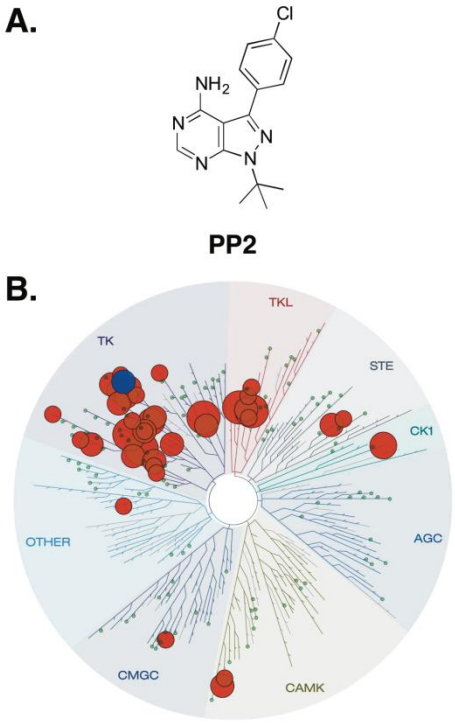

Figure 5.1 A. Structure of PP2. **B.** Kinome dendrogram of PP2 selectivity profiling at 10 µM. c-Src is colored blue and off-target kinases of PP2 are colored red. Dendrogram was generated using TREEspot software tool with 10% cutoff. Green circles denote kinases kinases included in panel that show no binding below cutoff. Dendrogram reprinted with permission from KINOMEscan.

We started our work by examining PP2, a well-known inhibitor reported to be highly selective for c-Src.[8] The description of PP2 as selective arises from a 2007 report in which several kinase inhibitors were profiled against a panel of 73 kinases, most of which were Ser/Thr kinases.[9] Despite over 1,000 subsequent biological studies using PP2 as a tool, no broader kinome profiling of PP2 has been reported. To test PP2's selectivity more definitively, the inhibitor was screened against a diverse panel of 200 kinases using an in vitro ATP-site competition binding assay (KINOMEScan[10]) at a concentration of 10 µM. In contrast to previous reports,[9]

PP2 is classed as non-selective from these data (S35 = 0.41, Figure 5.1). S35 is calculated by dividing the number of kinases with less than 35% of control by the total number of kinases tested. In the KINOMEScan panel, 56 kinases showed greater than 95% displacement from an immobilized ligand by PP2 (24 kinases had >99% displacement). Based on our results, PP2 is less selective than dasatinib, a well-studied and promiscuous tyrosine kinase inhibitor (in this

panel S35 = 0.27).[11] Given this lack of selectivity, interpretation of the results from the numerous reports using PP2 in biological studies are complicated by inhibition of many other kinases. For example, PP2 has been used to demonstrate that c-Src activity modulates ErbB2 and ErbB3 phosphorylation state in breast cancer.[12] However, our profiling shows that PP2 significantly inhibits both ErbB2 and ErbB3. For the complete profiling data for PP2, see the Supporting Information.

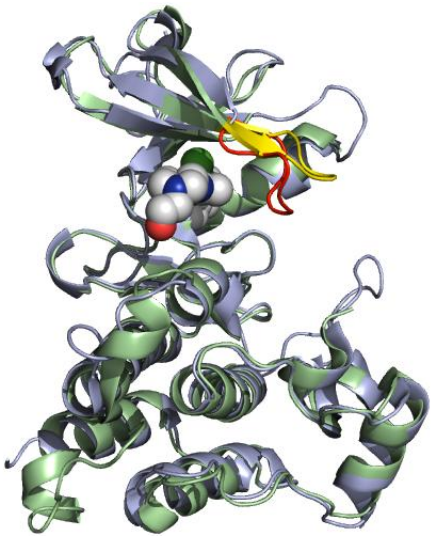

Figure 5.2. Alignment of structures with dasatinib bound to c-Src (PDB code: 3QLG) and c-Abl (2GQG). c-Src is colored light green with P-loop of c-Src highlighted yellow. c-Abl is colored light blue with P-loop of c-Abl highlighted red. Dasatinib is shown in space fill model.

Based on co-crystal structures of PP2 bound to c-Src and Src-family kinases,[13,14] we hypothesized that PP2 could be modified to obtain a selective inhibitor. Specifically, a pocket formed by the phosphate-binding loop (P-loop, also known as the glycine-rich loop) was identified in c-Src that did not appear in homologous kinases, including c-Abl (for molecular models of this pocket, see the Supporting Information). c-Abl is a tyrosine kinase with high sequence similarity to c-Src (69% across the entire kinase domain) and nearly identical ATP-binding pockets. No clinical or pre-clinical inhibitors of c-Src have been reported that do not also inhibit c-Abl.[11] Therefore, c-Abl was chosen as our initial test for inhibitor selectivity. From our analyses of co-crystal structures of dasatinib bound to both c-Src and c-Abl, c-Src has a more “open” P-loop compared to c-Abl (Figure 2). Likewise, in co-crystal structures of imatinib with c-

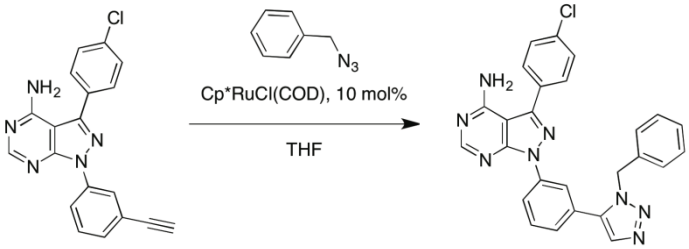

1
K_i, c-Src = 1,450 nM
K_i, c-Abl = 7,150 nM

2
K_i, c-Src = 207 nM
K_i, c-Abl = >125,000 nM

Scheme 5.1. Synthesis and biochemical characterization of benzyl triazole compound **5.2**.

Table 5.1. Summary of K_i values obtained for compounds **5.1–5.6**.

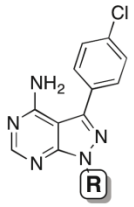

Compound	R =	K_i c-Src (nM)	K_i c-Abl (nM)
1	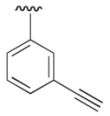	1,450	7,150
2	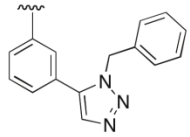	207	>125,000
3	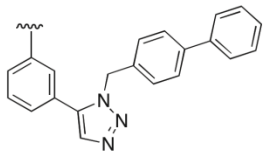	>60,000	N.D.
4	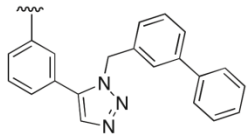	44	>125,000
5	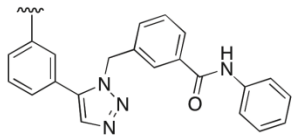	37,000	N.D.
6	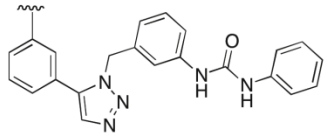	>60,000	N.D.

Src and c-Abl the P-loop of c-Src is “open” while the P-loop of c-Abl is “closed” (Supporting Information Figure S1).

To obtain molecules that could interact with the P-loop pocket of c-Src, a PP2 analog containing an aryl alkyne handle was synthesized. PP2~alkyne (**5.1**) is a modest inhibitor of c-Src (K_i = 1.4 μM). Based on our proposed molecular docking model (see Supporting Information Figure S2), PP2~alkyne scaffold was elaborated using benzyl azide and

either Cu- or Ru-based click chemistry[15] to form 1,4- or 1,5-disubstituted benzyl triazoles, respectively. Consistent with our model, the 1,4-disubstituted benzyl triazole is not an effective inhibitor of c-Src (see Supporting Information), while the 1,5-disubstituted benzyl triazole (**5.2**) has increased binding affinity for c-Src (K_i = 207 nM). Significantly, compound **5.2** did not inhibit c-Abl activity up to 125 μM (Scheme 5.1).

In an effort to further improve potency, a limited number of analogs (compounds 5.3–5.6) were synthesized (Table 5.1). From this series of compounds, meta-substituted

biphenyl 4 was the only compound that had improved binding (lower K_i) to c-Src. Compound **5.4** is a potent inhibitor (K_i = 44 nM) of c-Src and does not inhibit c-Abl up to 125 µM. The binding affinity of compound 4 for c-Src is comparable to that of PP2 (K_i = 33 nM). However, PP2 is also an effective c-Abl inhibitor (K_i = 325 nM).

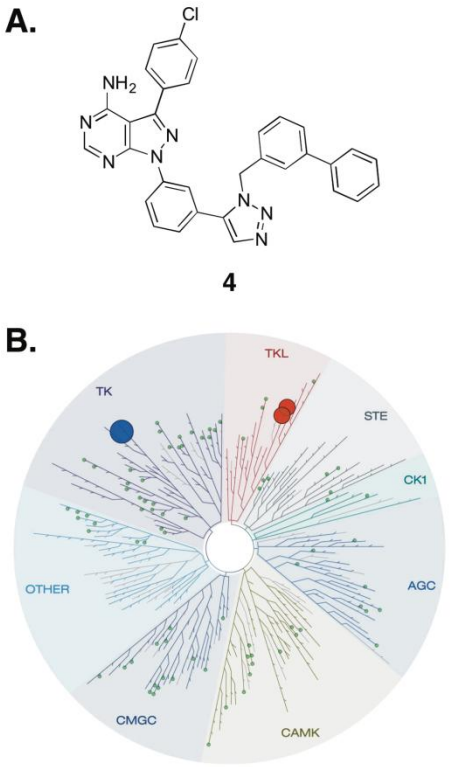

Figure 5.3. A. Structure of compound **4**. **B.** Kinome dendrogram of compound **4** selectivity profiling at 10 µM. c-Src is colored blue and off-target kinases of compound **4** are colored red. Dendrogram was generated using TREEspot software tool with 10% cutoff. Green circles denote kinases kinases included in panel that show no binding below cutoff. Dendrogram reprinted with permission from KINOMEscan.

Compound **5.4** was screened against a diverse kinase panel (KINOMEscan[10]) using an in vitro ATP-site competition binding assay at a concentration of 10 µM (Figure 5.3). From this panel, we found that compound 4 was remarkably selective. Only three kinases (c-Src, c-Raf, and B-Raf) exhibited >95% displacement from an immobilized ligand by compound **5.4** (only c-Src had >99% displacement). Detailed selectivity profiling results can be found in the Supporting Information.

Using this same method,[10] K_d measurements were obtained for c-Src and 6 homologous kinases that are members of the Src kinase family and not found in the panel (Table 5.2). Obtaining selectivity across this conserved kinase family has been a challenging task with only a handful of compounds identified that can discriminate between them.[16,17] The K_d for c-Src (86 nM) was in good agreement with the K_i we obtained in our biochemical activity assay. Compound **5.4** is selective between Src family members, with >2-fold selectivity over both Lck and Fgr, 8-fold selectivity over c-Yes, and >40-fold selectivity over Lyn, Hck, and Fyn (Table 5.2).

Interactions with the P-loop of kinases have previously been reported to modulate selectivity in kinase–ligand interactions.[18-20] Typically, these interactions are not due to the primary sequence of the P-loop, but rather due to distributed contributions throughout the kinase catalytic domain.[19] To probe the selectivity of compound 4, the P-loop of c-Src (residues 273-281, chicken c-Src numbering) was replaced with the P-loop residues of c-Abl. Compound **5.4** bound c-Src-TM (Q275G, C277Q, F278Y) with similar potency to that of wild-type c-Src (K_i = 175 nM). This suggests that the primary sequence of the P-loop is not solely responsible for the observed selectivity. Studies aimed at better understanding compound **5.4**'s impressive selectivity are in progress.

Table 5. 2. K_d values obtained by KINOMEscan for Src family kinases with compound **5.4**.

kinase	K_d (nM)
c-Src	86
Lck	160
Fgr	240
Yes	720
Lyn	3200
Hck	4400
Fyn	>40,000

To serve as an effective probe in biological studies, the probe must function in cells. Compound **5.4** was incubated with murine embryonal fibroblast (MEF) cells exogenously expressing full-length c-Src. The change in phosphorylation of c-Src Tyr-416 was measured using specific antibodies in a sandwich ELISA.[21] In this assay, compound **5.4** has an IC50 = 1.9 μM indicating that our probe is cell permeable and inhibits c-Src activity in cells (See experimental section).

In the kinome profiling of compound **5.4**, B-Raf and c-Raf were inhibited along with c-Src. To assess whether compound **5.4** has Raf inhibitory activity in cellulo, phosphorylation changes in Erk, a downstream substrate of B-Raf and c-Raf, were measured. In SK-BR-3 cells stimulated with EGF to activate the Raf pathway, treatment of 100 μM compound **5.4** had no effect on p-Erk levels (see Experimental Section). From these results, we assume that cellular inhibition of B-Raf and/or c-Raf is not significant.[22]

We were interested in whether selective c-Src inhibition would be as efficacious as multi-kinase inhibition.[23] To test this, our selective probe **5.4** was compared to the non-

selective inhibitor PP2. PP2 has a nearly identical biochemical K_i for c-Src and has been extensively used in cell culture experiments. Four different cancer cell lines were examined,[24] each of which have been shown to be growth dependent upon c-Src activity.[25] In all cancer cell lines tested, compound **5.4** is more efficacious than PP2 (Table 5.3). Addressing the debate about whether selective inhibition offers any advantage for kinase inhibitor therapeutics has been complicated by a lack of truly selective kinase inhibitors.[23] In our studies, selective inhibition leads to improved cellular efficacy.

The most profound differences between compound **5.4** and PP2 were found in cell lines derived from breast cancer tumors. Recent work has shown that, in contrast to its role in hematopoietic cancers, c-Abl activity in breast cancer is anti-oncogenic.[26] That is, inhibition of c-Abl in breast cancer increases disease progression. We hypothesized that the increased efficacy of compound **5.4** could be due, in part, to removal of c-Abl inhibition. To test this hypothesis, the efficacy of compound **5.4** was examined in 4T1 cells, which are frequently used as a late-stage model of metastatic breast cancer.

Table 5.3. Biochemical and characterization of PP2 and compound **5.4**.

	PP2	Compound **4**
K_i, c-Src	0.033 µM	0.044 µM
GI_{50}, HT-29	48 µM	11 µM
GI_{50}, SK-BR-3	> 100 µM	12 µM
GI_{50}, MCF7	> 100 µM	11 µM
GI_{50}, MDA-MB-453	14 µM	6.0 µM
GI_{50}, NIH-3T3	17 µM	> 100 µM

Schiemann and co-workers have previously demonstrated that expression of a constitutively active c-Abl gene is sufficient to prevent growth of 4T1 cells in 3D culture.[27] The efficacy of c-Src inhibitors has not previously been reported in 4T1 cell culture, however, we found that 4T1 cell growth in 3D culture is dependent upon c-Src activity using compound **5.4** (Figure 5.4). To determine whether inhibition of c-Abl can mitigate the efficacy of compound **5.4**, a highly specific inhibitor of c-Abl, GNF-2,[28] was used. When GNF-2 and compound **5.4** are dosed together, the decrease in 4T1 growth observed with compound **5.4** alone was significantly abrogated (Figure

5.4). Avoiding inhibition of off-target kinases that have anti-oncogenic activities is an important and frequently neglected advantage of selective inhibition. In addition to c-Abl, we anticipate there are other kinases inhibited by PP2 whose native activity is anti-oncogenic.

The results with 4T1 cellular inhibition highlight the potential utility of c-Src inhibitors in breast cancer therapy. Indeed, the identification of c-Src as a major resistance pathway to Herceptin therapy has re-invigorated the clinical exploration of c-Src inhibitors as a breast cancer therapy.[3] Unfortunately, there are no c-Src inhibitors in pre-clinical development or clinical use that are not also inhibitors of c-Abl.[4,11] Our data (and others[26,27]) indicate that inhibition of c-Abl should be avoided in breast cancer. Furthermore, development of highly selective c-Src inhibitors for therapeutic use should be pursued (rather than dual-Src/Abl and/or pan-kinase inhibitors).

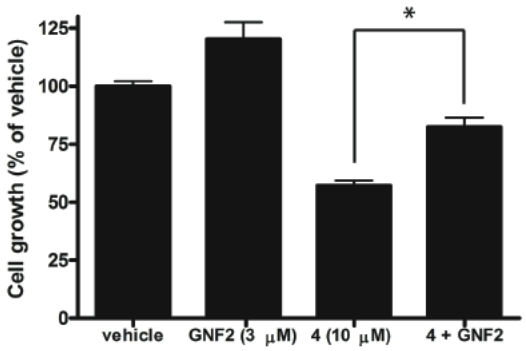

Figure 5.4. 4T1 cell proliferation in 3D culture. Growth inhibition occurs with treatment of 10 μM compound **4**. Addition of 3 μM of a specific c-Abl inhibitor (GNF-2) mitigates effects of compound **5.4. *,** p-value = <0.005.

Cancer cell profiling was performed by the National Cancer Institute (NCI 60 panel).[29] Consistent with published reports for inhibition of c-Src using genomic techniques,[25] compound **5.4** was cytostatic (and not cytotoxic). At a single concentration of 10 μM, mean growth across 57 cell lines tested was 71%. Seven cell lines showed <50% growth. There is good correlation between two of the cell lines, HT-29 and MCF7, where full dose-response curves were obtained in our laboratory (vide supra). For complete information on the NCI 60 panel with compound **5.4**, see the Supporting Information.

Along with dramatic increases in cellular efficacy against cancer cell lines, toxicity to a non-cancer cell line, NIH-3T3, was significantly reduced with selective c-Src inhibition (Table 5.2). With compound **5.4**, no growth inhibition up to 100 μM is observed while PP2 has a GI_{50} of 17 μM for NIH-3T3 cells. PP2 is actually more effective at slowing the

growth of non-cancerous NIH-3T3 cells than 3 of the 4 cancer cell lines examined. The reduced toxicity to healthy cells afforded by compound **5.4** is yet another advantage of selective inhibition.

5.3 Conclusions

Despite being the first oncogene discovered, and playing a central role in many cancer signaling pathways, there have been no reports of a truly selective c-Src inhibitor that can be used in cellular studies. Using a novel approach of extending into the P-loop pocket of c-Src, we have developed a highly selective probe for c-Src activity. Moreover, we have shown distinct advantages to selective inhibition. Studies using compound **5.4** to improve our understanding of c-Src signaling in cancer are in progress.

5.4 Experimental Section

SUPPLEMENTARY FIGURES FOR MANUSCRIPT

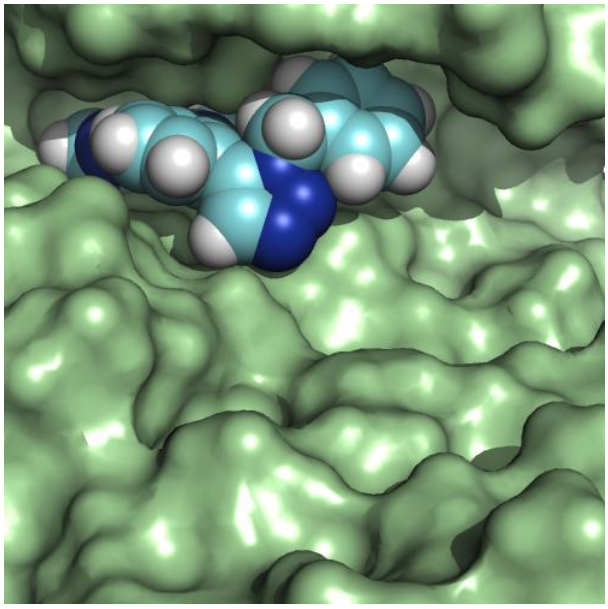

Figure 5.S1. Model image of compound **5.2** bound to c-Src (starting structure from PDB code 3DQW). Model was generated using MOE (Chemical Computing Group) software. The benzyl triazole functionality of compound **5.2** is observed to make significant interactions with the P-loop pocket of c-Src.

Table 5.S-1. Biochemical characterization of analogs designed to increase interaction in the P-loop pocket of c-Src.

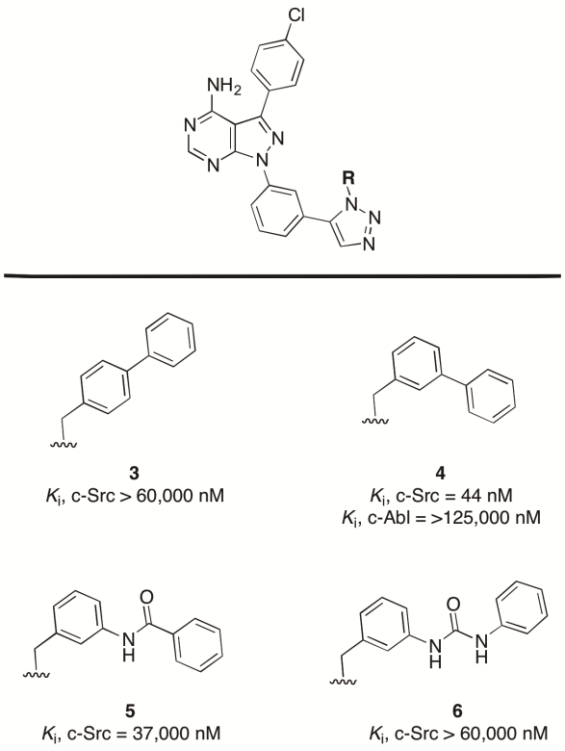

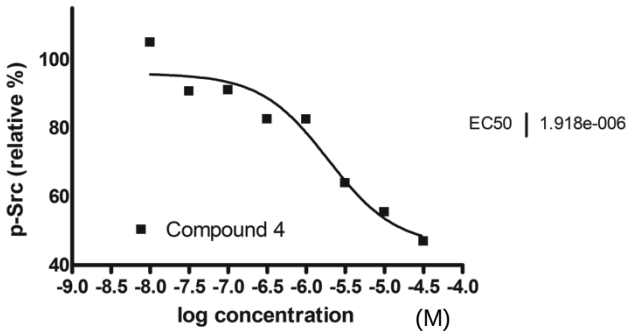

Figure 5.S-2. c-Src autophosphorylation assay. For detailed information, see Supporting Information page S52.

GENERAL SYNTHETIC METHODS. Unless otherwise noted, all reagents were obtained via commercial sources and used without further purification. Tetrahydrofuran (THF) and dichloromethane (CH_2Cl_2) were dried over alumina under a nitrogen atmosphere. All ^{1}H and ^{13}C NMR spectra were measured with a Varian MR400 or Inova 500 spectrometer. Mass Spectrometry (HRMS) was carried out by the University of Michigan Mass Spectrometry Facility (J. Windak, director).

SYNTHESIS OF COMPOUNDS 5.S-1 - 5.6

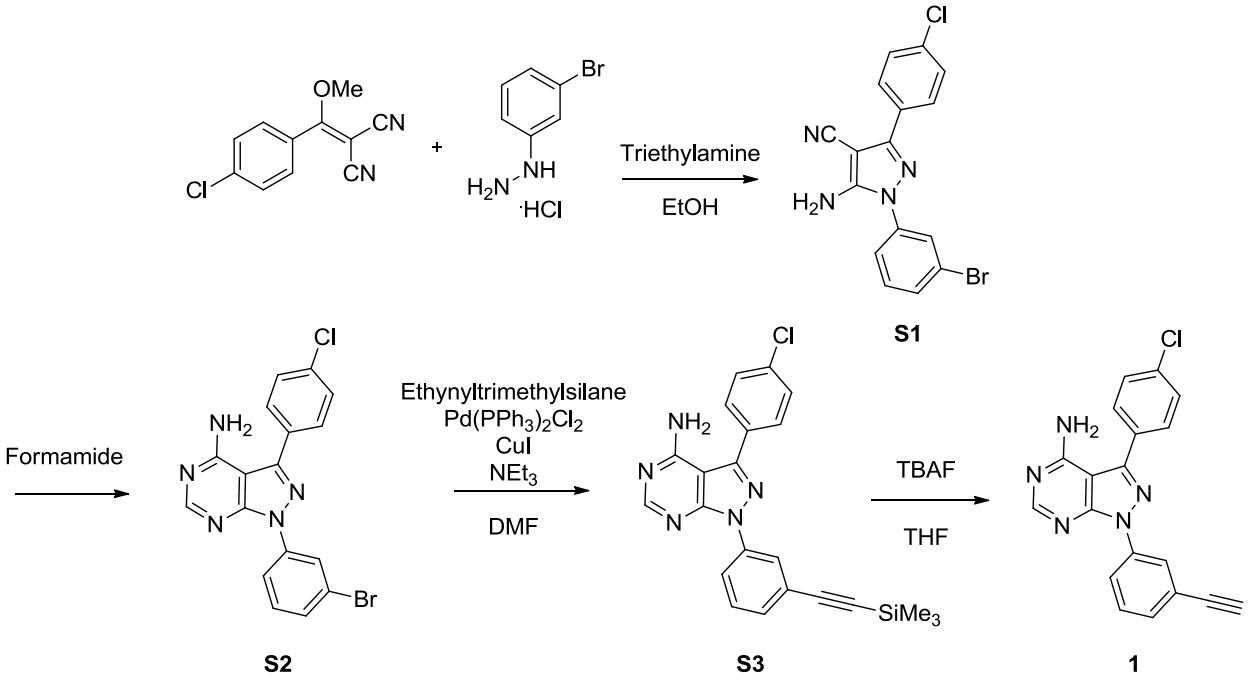

Scheme 5.S1. Synthesis of PP2~alkyne (**5-1**).

Synthesis of 5.S-1: 2-((4-chlorophenyl)(methoxy)methylene)malononitrile (4.3 g, 19.7 mmol) (prepared as described previously)[1] was added to an oven-dried flask. Ethanol (100 mL) was then added, followed by triethylamine (5.0 g, 49.2 mmol), and 3-bromophenyl hydrazine hydrochloride (4.4 g, 3.2 mmol). The reaction mixture was heated to reflux for 40 minutes. Approximately half of the solvent was then removed under reduced pressure. The reaction mixture was then suspended in water (150 mL) and filtered. After drying, the reaction afforded **5.S-1** as a tan solid (4.0 g, 54% yield). **Spectral data.** ^{1}H NMR (500 MHz, DMSO-d_6): δ 7.88-7.85, (m, 2 H), 7.51 (t, J = 8.06 Hz, 1 H), 7.68-7.65 (m, 1 H), 7.63-7.60 (m, 1 H), 7.59-7.56 (m, 2H), 7.53-7.48 (m, 1 H), 7.03 (s, 2 H); ^{13}C NMR (100 MHz, DMSO-d_6): δ 153.71, 149.87, 139.01, 134.33,

131.77, 131.36, 130.27, 129.38, 128.13, 127.47, 123.79, 122.41, 115.68, 71.85; HRMS-ESI (*m/z*): $[M + H]^+$ calcd for $C_{16}H_{10}BrClN_4$, 372.9850; found 372.9849.

Synthesis of 5.S-2: Compound **5.S-1** (4.0 g, 10.7 mmol) was added to an oven-dried flask, followed by formamide (75 mL). The reaction mixture was heated to a gentle reflux for 2.5 hours. The reaction mixture was then allowed to cool to room temperature. The product was subsequently precipitated with water (120 mL). The crude mixture was filtered to yield 3.3 g (76% yield) of compound **5.S-2** as a light tan solid. **Spectral data.** ^{1}H NMR (500 MHz, DMSO-d_6): δ 8.53 (s, 1 H), 8.41 (s, 1 H), 8.31-8.28 (m, 1 H), 7.79-7.76 (m, 2 H), 7.66-7.62 (m, 2 H), 7.50-7.57 (m, 2 H); ^{13}C NMR (100MHz, DMSO-d_6): δ 158.84, 157.21, 155.25, 145.48, 140.36, 134.50, 131.61, 131.24, 130.71, 129.65, 129.25, 123.37, 122.19, 119.86, 99.33; HRMS-ESI (*m/z*): $[M + H]^+$ calcd for $C_{17}H_{11}BrClN_5$; 399.9959, found 399.9956.

Synthesis of 5.S-3: Compound **5.S-2** (3.1 g, 7.7 mmol), $Pd(PPh_3)_2Cl_2$ (272 mg, 0.4 mmol), and CuI (74 mg, 0.4 mmol) were added to an oven-dried round-bottom flask. The reaction vessel was evacuated using a vacuum pump and subsequently filled with N_2; this was repeated for a total of three cycles. N,N-dimethylformamide (50 mL) was then added, followed by ethynyltrimethylsilane (1 g, 10 mmol) and triethylamine (2.4 g, 23.2 mmol). The reaction mixture was then heated to 60^{o}C and stirred overnight. The mixture was then allowed to cool to room temperature and was precipitated using water (250 mL). The resulting solid was filtered, and then washed with water (20 mL). The residual solid was purified via silica gel chromatography using a Biotage Isolera One (linear gradient 20% → 100% EtOAc in hexanes) to yield 2.4 g (74% yield) of compound **5.S-3** as a light tan solid. **Spectral data.** ^{1}H NMR (500 MHz, DMSO-d_6): δ 8.41 (s, 1 H), 8.35 (s, 1 H), 8.32-8.28 (m, 1 H), 7.79-7.75 (m, 2 H), 7.65-7.61 (m, 2 H), 7.56 (t, J = 8.1 Hz, 1 H), 7.44-7.41 (m, 1 H), 0.26 (s, 9 H); ^{13}C NMR (100 MHz, DMSO-d_6): δ 158.80, 157.08, 155.06, 145.25, 139.23, 134.41, 131.29, 130.67, 130.09, 129.60, 123.52, 123.33, 121.59, 104.87, 99.29, 95.34, 79.61, 0.26; HRMS-ESI (*m/z*): $[M + H]^+$ calcd for $C_{22}H_{20}ClN_5Si$, 418.1249; found 418.1254.

Synthesis of 5.1: Compound **5.S-3** (2.3 g, 6.6 mmol) was added to an oven-dried flask. Tetrahydrofuran (28 mL) was then added followed by a 1 M solution of tetrabutlyammonium fluoride in THF (6.6 mL). The reaction mixture was allowed to stir at room temperature for 1 hour. 1 N HCl (6.6 mL) was added. The organic solvent was then removed under reduced pressure. The reaction mixture was then suspended in water (100 mL), and subsequently filtered. The residual solid was rinsed twice with water (20 mL). After drying, 1.3 g (68% yield) of compound **5.1** was obtained as a light tan solid. **Spectral data.** ^{1}H NMR (500 MHz, DMSO-d_6): δ 8.42-8.40 (m, 2 H), 8.31-8.27 (m, 1 H), 7.80-7.75 (m, 2 H), 7.66-7.62 (m, 2 H), 7.60-7.56 (m, 1 H), 7.48-7.44 (m, 1 H), 4.34 (s, 1H); ^{13}C NMR (100 MHz, DMSO-d_6): δ 158.83, 157.15, 155.12, 145.27, 139.24, 134.42, 131.31, 130.71, 130.17, 129.74, 129.63, 123.89, 122.89, 121.63, 99.25,

83.30, 81.98; HRMS-ESI (*m/z*): $[M + H]^+$ calcd for $C_{19}H_{12}ClN$, 346.0854; found 346.0856.

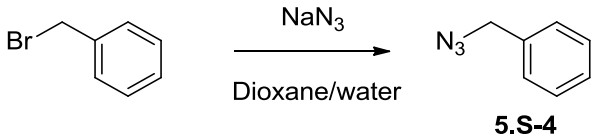

5.S-4

Synthesis of 5.S-4: Benzyl bromide (1.0 g, 5.9 mmol) was added to an oven-dried flask. Dioxane (22 mL) and water (7 mL) were added, followed by sodium azide (1.9 g, 29 mmol). The reaction mixture was heated to 65^{o}C overnight. After the reaction was cooled to room temperature dioxane was removed under reduced pressure. The aqueous phase was then extracted with ethyl acetate (7 mL) three times. The organic layers were then collected and dried over sodium sulfate. After filtration, removal of solvent afforded **5.S-4** (0.7 g, 90% yield) as a light yellow oil. **Spectral data.** ^{1}H NMR (500 MHz, $CDCl_3$): δ 7.44-7.33 (m, 5 H), 4.36 (s, 2 H); ^{13}C NMR (100 MHz, $CDCl_3$): δ 135.47, 128.89, 128.35, 128.28, 54.80; HRMS-EI (*m/z*): calcd for $C_7H_7N_3$, 133.0640; found 133.0640.

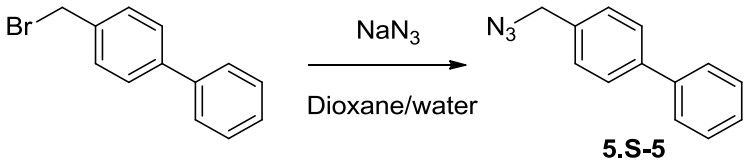

5.S-5

Synthesis of 5.S-5: 4-(bromomethyl)-1,1'-biphenyl (247 mg, 1.0 mmol) was added to an oven-dried flask. Dioxane (3.8 mL) and water (1.2 mL) were then added, followed by sodium azide (325 mg, 5.0 mmol). The reaction mixture was heated to 60^{o}C overnight. After the reaction was cooled to room temperature dioxane was removed under reduced pressure. The aqueous phase was then extracted with ethyl acetate (5 mL) three times. The organic layers were then collected and dried over sodium sulfate. After filtration, removal of solvent afforded **5.S-5** (188 mg, 90% yield) as a light yellow solid. **Spectral data.** ^{1}H NMR (400 MHz, DMSO-d_6): δ 7.69-7.62 (m, 4 H), 7.46-7.41 (m, 4 H), 7.37-7.31 (m, 1 H), 4.46 (s, 2 H); ^{13}C NMR (100 MHz, DMSO-d_6): δ 140.40, 140.03, 135.22, 129.50, 129.40, 128.04, 127.42, 127.12, 53.71; HRMS-ESI (*m/z*): calcd for $C_{13}H_{11}N_3$, 209.0953; found 209.0961.

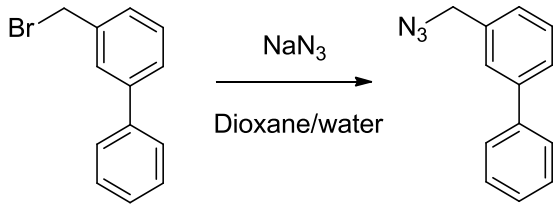

5.S-6

Synthesis of 5.S-6: 3-(bromomethyl)-1,1'-biphenyl (247 mg, 1.0 mmol) was added to an oven-dried flask. Dioxane (3.8 mL) and water (1.2 mL) were then added, followed by sodium azide (325 mg, 5.0 mmol). The reaction mixture was heated to 60^{o}C overnight. After the reaction was cooled to room temperature dioxane was removed under reduced pressure. The aqueous phase was then extracted with ethyl acetate (5 mL) three times. The organic layers were then collected and dried over sodium sulfate. After filtration, removal of solvent afforded **5.S-6** (180 mg, 86% yield) as a light yellow oil. **Spectral data.** ^{1}H NMR (500 MHz, $CDCl_3$): δ 7.64-7.58 (m, 3 H), 7.56 (s, 1 H), 7.52-7.46 (m, 3 H), 7.42-7.37 (m, 1 H), 7.35-7.31 (m, 1 H), 4.44 (s, 2 H); ^{13}C NMR (100 MHz, $CDCl_3$): δ 141.92, 140.64, 135.93, 129.29, 128.85, 127.58, 127.21, 127.13, 127.02, 126.98, 54.85; HRMS-EI (*m/z*): calcd for $C_{13}H_{11}N_3$, 209.0953; found 209.0957.

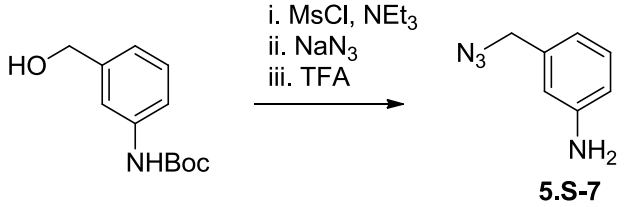

5.S-7

Synthesis of 5.S-7: tert-butyl (3-(hydroxymethyl)phenyl)carbamate[2] (1.0 g, 4.5 mmol) was added to an oven-dried flask. The reaction vessel was evacuated using a vacuum pump and subsequently filled with N_2. This procedure was repeated for a total of 3 times. Dichloromethane (22 mL) was added. The reaction mixture was cooled with an ice bath. Diethylisopropylamine (0.7 g, 5.4 mmol) was added followed by methanesulfonyl chloride (0.56 g, 4.9 mmol). The reaction mixture was allowed to stir for 5 minutes, at which time the reaction was allowed to warm to room temperature. The reaction mixture was stirred for an additional 60 minutes at room temperature. The reaction was then diluted with dichloromethane (40 mL), washed with 1 N HCl (60 mL), followed by a wash with saturated $NaHCO_3$ (60 mL). The organic layer was then dried over Na_2SO_4. The solvent was removed under reduced pressure, which resulted in a clear oil and was carried on without further purification. To the flask containing the crude intermediate was added sodium azide (1.5 g, 22.4 mmol), followed by a THF/water mixture (3:1, 20 mL). The reaction mixture was heated to 50^{o}C overnight. The reaction

mixture was then allowed to cool to room temperature. 1 N NaOH was added (5 mL). The organic solvent was removed under reduced pressure. The aqueous layer was extracted with ethyl acetate (20 mL) three times. The organic layers were combined and dried over Na_2SO_4. The solvent was removed under reduced pressure, and resulted in clear oil that was carried on without further purification. To the flask containing the crude intermediate was added DCM (20 mL) and trifluoroacetic acid (6 mL). The reaction mixture was stirred at room temperature for 60 minutes. Solvent was removed under reduced pressure. Chloroform (40 mL) was added, and solvent was again removed under reduced pressure. The resulting oil was dissolved in ethyl acetate (40 mL) and was washed with 1 N NaOH (40 mL), and then brine (40 mL). The organic layer was then dried over Na_2SO_4. The crude reaction mixture was then purified by silica gel chromatography using a Biotage Isolera One (linear gradient 0 → 100% EtOAc in hexanes) to yield 266 mg (39% yield over three steps) of compound **5.S-7** as a light orange oil. **Spectral data.** ^{1}H NMR (500 MHz, $CDCl_3$): δ 7.21-7.16 (m, 1 H), 6.75-6.66 (m, 3 H), 4.26 (s, 2 H), 3.91 (br s, 2 H); ^{13}C NMR (100 MHz, $CDCl_3$): δ 146.31, 136.56, 129.78, 118.60, 115.21, 114.82, 54.77; HRMS-EI (*m/z*): calcd for $C_7H_8N_4$, 148.0749; found 148.0749.

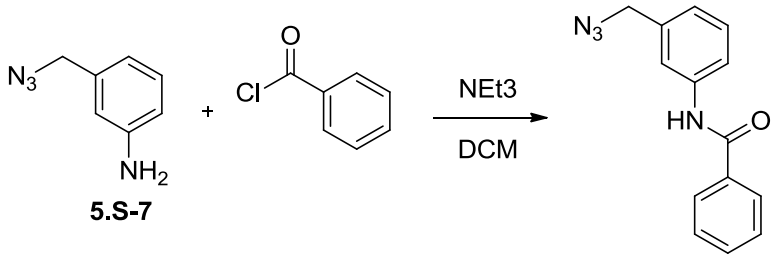

5.S-7 **5.S-8**

Synthesis of 5.S-8: 3-(azidomethyl)aniline (44 mg, 0.3 mmol) was added to an oven-dried flask. Dichloromethane (1 mL) was then added. The reaction was cooled in an ice bath. Benzoyl chloride (42 mg, 0.3 mmol) was then added, followed by triethylamine (39 mg, 0.4 mmol). The reaction was allowed to warm to room temperature and stir overnight. The reaction was then diluted with dichoromethane (20 mL) and washed with water (20 mL). The aqueous phase was then back-extracted with dichloromethane three times (20 mL each). The organic layers were collected and dried over sodium sulfate. The crude reaction mixture was then purified by silica gel chromatography using a Biotage Isolera One (linear gradient 0 → 100% EtOAc in hexanes). **5.S-8** was isolated as a yellow solid (68 mg, 85% yield). **Spectral data.** ^{1}H NMR (400 MHz, DMSO-d_6): δ 10.30 (s, 1 H), 7.95-7.91 (m, 2 H), 7.83-7.81 (m, 1 H), 7.74-7.70 (m, 1H), 7.59-7.47 (m, 3H), 7.35 (t, *J* = 7.83 Hz, 1 H), 7.09-7.05 (m, 1 H), 4.43 (s, 2 H) ; ^{13}C NMR (100 MHz, DMSO-d_6): δ 166.07, 140.00, 136.53, 135.27, 132.06, 129.42, 128.82, 128.11, 124.00,

120.47, 120.44, 54.16; HRMS-APCI (*m/z*): $[M + H]^+$ calcd for $C_{14}H_{12}N_4O$, 253.1084; found 253.1088.

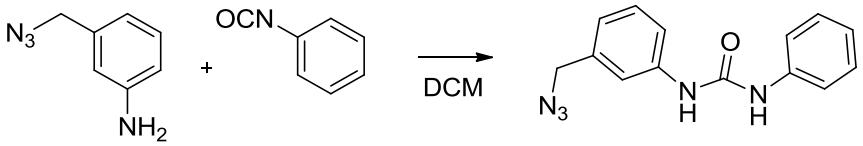

5.S-7 **5.S-9**

Synthesis of 5.S-9: 3-(azidomethyl)aniline (44 mg, 0.3 mmol) was added to an oven-dried flask. Dichloromethane (1 mL) was then added. The reaction was cooled in an ice bath. Phenylisocyanate (36 mg, 0.3 mmol) was then added. The reaction was allowed to warm to room temperature and stir overnight. Solvent was removed under reduced pressure. The crude reaction mixture was dissolved in DMSO (1 mL), and purified by reverse-phase HPLC (25 →90% acetonitrile in water) to yield 45 mg (56% yield) of the product as a white solid. **Spectral data.** ^{1}H NMR (500 MHz, DMSO-d_6): δ 8.76 (s, 1 H), 8.67 (s, 1 H), 7.53-7.51 (m, 1 H), 7.47-7.43 (m, 2 H), 7.41-7.37 (m, 1 H), 7.33-7.25 (m, 3 H), 6.99-6.94 (m, 2 H), 4.42 (s, 2 H); ^{13}C NMR (100 MHz, DMSO-d_6): δ 152.91, 140.51, 140.03, 136.67, 129.61, 129.23, 122.33, 122.19, 118.65, 118.27, 54.13; HRMS-APCI (*m/z*): $[M + H]^+$ calcd for $C_{14}H_{13}N_5O$, 268.1193; found 268.1195.

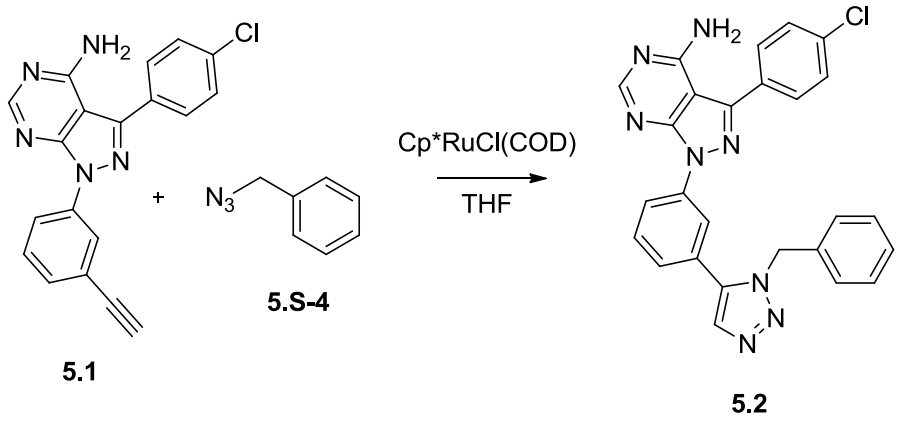

5.1 **5.S-4** **5.2**

Synthesis of 5.2: Compound **5.1** (18 mg, 0.05 mmol) and Cp*RuCl(COD) (2 mg, 0.005 mmol) were added to a flame-dried round-bottom flask. The reaction vessel was evacuated using a vacuum pump and subsequently filled with N_2, this procedure was repeated for a total of 3 times. THF (1 mL) and **5.S-4** (7 mg, 0.05 mmol) were then added. The reaction mixture was allowed to stir at room temperature overnight. THF was removed under reduced pressure. The crude mixture was then dissolved in DMSO (1 mL), and then purified by reverse-phase HPLC (linear gradient of 25 → 90% CH_3CN in H_2O) to yield 12 mg (48% yield) of compound **5.2** as a white solid. **Spectral data.** ^{1}H

NMR (500 MHz, DMSO-d_6): δ 8.37-8.30 (m, 3 H), 8.07 (s, 1 H), 7.76-7.71 (m, 2 H), 7.68-7.61 (m, 3 H), 7.47-7.42 (m, 1 H), 7.28-7.20 (m, 3 H), 7.10-7.05 (m, 2 H), 5.76 (s, 2 H); ^{13}C NMR (100 MHz, DMSO-d_6): δ 158.81, 157.09, 155.13, 145.26, 139.43, 137.55, 136.35, 134.43, 133.76, 131.30, 130.69, 130.46, 129.62, 129.10, 128.23, 127.78, 127.35, 126.69, 121.95, 120.84, 99.21, 51.70; HRMS-ESI (*m/z*): $[M + H]^+$ calcd for $C_{26}H_{19}ClN_8$, 479.1494; found 479.1489.

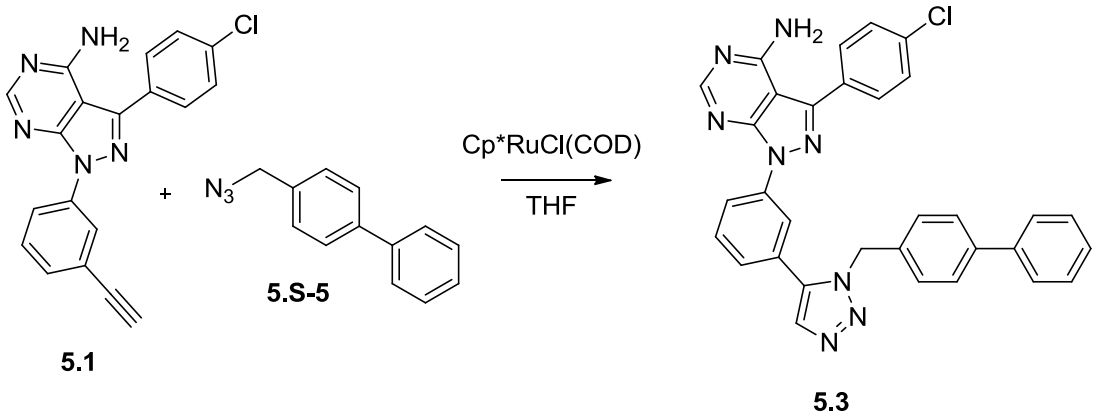

Synthesis of 5.3: Compound **5.1** (18 mg, 0.05 mmol) and Cp*RuCl(COD) (2 mg, 0.005 mmol) were added to a flame-dried round-bottom flask. The reaction vessel was evacuated using a vacuum pump and subsequently filled with N_2, this procedure was repeated for a total of 3 times. THF (1 mL) and **5.S-5** (9 mg, 0.05 mmol) were then added. The reaction mixture was allowed to stir at room temperature overnight. THF was removed under reduced pressure. The crude mixture was then dissolved in DMSO (1 mL), and then purified by reverse-phase HPLC (linear gradient of 25 → 90% CH_3CN in H_2O) to yield 10 mg (35% yield) of compound **5.3** as a white solid. **Spectral data.** ^{1}H NMR (500 MHz, DMSO-d_6): δ 8.41-8.37 (m, 1 H), 8.32 (s, 1 H), 8.30-8.28 (m, 1 H), 8.10 (s, 1 H), 7.73-7.67 (m, 3 H), 7.57-7.53 (m, 6 H), 7.52-7.49 (m, 1 H), 7.44-7.40 (m, 2 H), 7.37-7.32 (m, 1 H), 7.21-7.18 (m, 2 H), 5.79 (s, 2 H); ^{13}C NMR (100 MHz, DMSO-d_6): δ 158.81, 157.10, 155.12, 145.30, 139.99, 139.80, 139.46, 137.59, 135.49, 134.42, 133.76, 131.29, 130.66, 130.52, 129.61, 129.34, 128.10, 128.00, 127.82, 127.34, 126.97, 126.85, 122.01, 120.87, 99.24, 51.41; HRMS-ESI (*m/z*): $[M + H]^+$ calcd for $C_{32}H_{23}ClN_8$, 555.1087; found 555.1805.

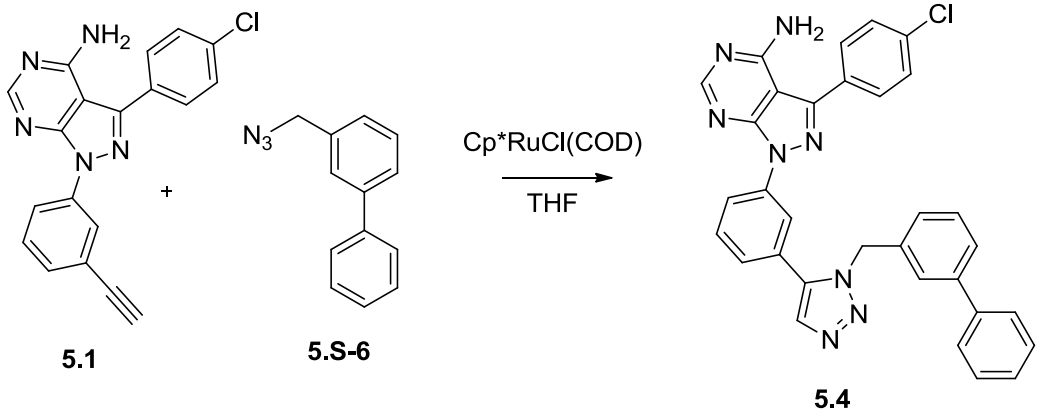

Synthesis of 5.4: Compound **5.1** (18 mg, 0.05 mmol) and Cp*RuCl(COD) (2 mg, 0.005 mmol) were added to a flame-dried round-bottom flask. The reaction vessel was evacuated using a vacuum pump and subsequently filled with N_2, this procedure was repeated for a total of 3 times. THF (1 mL) and **5.S-6** (9 mg, 0.05 mmol) were then added. The reaction mixture was allowed to stir at room temperature overnight. THF was removed under reduced pressure. The crude mixture was then dissolved in DMSO (1 mL), and then purified by reverse-phase HPLC (linear gradient of 25 → 90% CH_3CN in H_2O) to yield 12 mg (42% yield) of compound **5.4** as a white solid. **Spectral data.** ^{1}H NMR (400 MHz, DMSO-d_6): δ 8.37-8.32 (m 2H), 8.28 (s 1H), 8.90 (s 1H), 7.71-7.65 (m 3H), 7.63-7.58 (m 2H), 7.52-7.45 (m 2H) 7.39-7.25 (m 7H), 7.03-7.08 (s 1H), 5.87-5.79 (s 2H); ^{13}C NMR (100 MHz, DMSO-d_6): δ 158.79, 157.04, 155.12, 145.23, 140.90, 139.94, 139.45, 137.60, 136.98, 134.41, 133.84, 131.26, 130.63, 130.48, 129.80, 129.60, 129.23, 127.97, 127.85, 126.89, 126.77, 126.62, 126.47, 125.97, 121.88, 120.94, 99.22, 51.84; HRMS-ESI (*m/z*): $[M + H]^+$ calcd for $C_{32}H_{23}ClN_8$, 555.1807; found 555.1804.

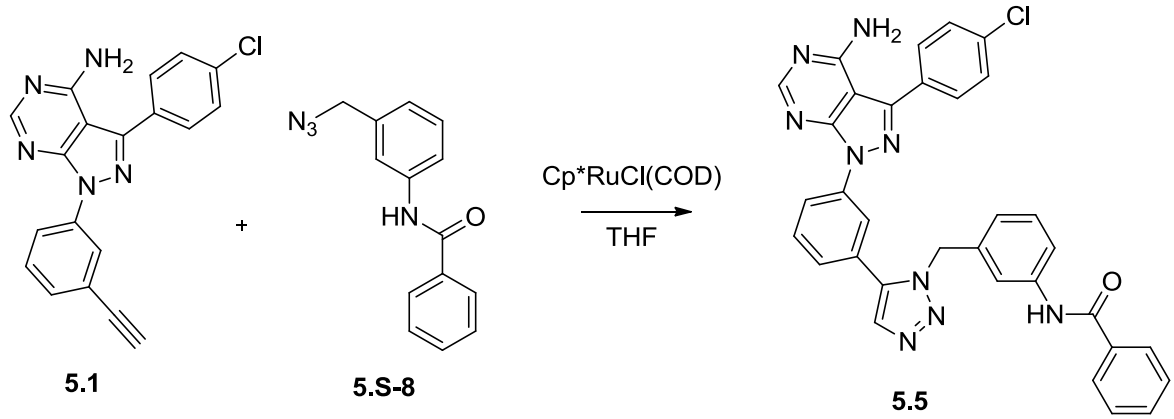

Synthesis of 5.5: Compound **5.1** (18 mg, 0.05 mmol) and Cp*RuCl(COD) (2 mg, 0.005 mmol) were added to a flame-dried round-bottom flask. The reaction vessel was evacuated using a vacuum pump and subsequently filled with N_2, this procedure was

repeated for a total of 3 times. THF (1 mL) and **5.S-8** (10 mg, 0.05 mmol) were then added. The reaction mixture was allowed to stir at room temperature overnight. THF was removed under reduced pressure. The crude mixture was then dissolved in DMSO (1 mL), and then purified by reverse-phase HPLC (linear gradient of 25 → 90% CH_3CN in H_2O) to yield 14 mg (45% yield) of compound **5.5** as a white solid. **Spectral data.** ^{1}H NMR (500 MHz, DMSO-d_6): δ 10.23 (s, 1 H), 8.38-8.33 (m, 2 H), 8.31 (s, 1 H), 8.10 (s, 1 H), 7.87-7.84 (m, 2 H), 7.73-7.66 (m, 4 H), 7.63-7.59 (m, 2 H), 7.59-7.54 (m, 2 H), 7.51-7.46 (m, 3 H), 7.22 (t, *J* = 7.82 Hz, 1 H), 6.84-6.81 (m, 1 H), 5.76 (s, 2 H); ^{13}C NMR (100 MHz, DMSO-d_6): δ 165.93, 158.79, 157.08, 155.14, 145.22, 140.10, 139.47, 137.66, 136.91, 135.18, 134.38, 133.75, 131.99, 131.30, 130.65, 130.47, 129.60, 129.34, 128.73, 128.05, 127.82, 126.73, 122.48, 121.95, 120.94, 119.92, 118.83, 99.20, 51.75; HRMS-ESI (*m/z*): $[M + H]^+$ calcd for $C_{33}H_{24}ClN_9O$, 598.1865; found 598.1866.

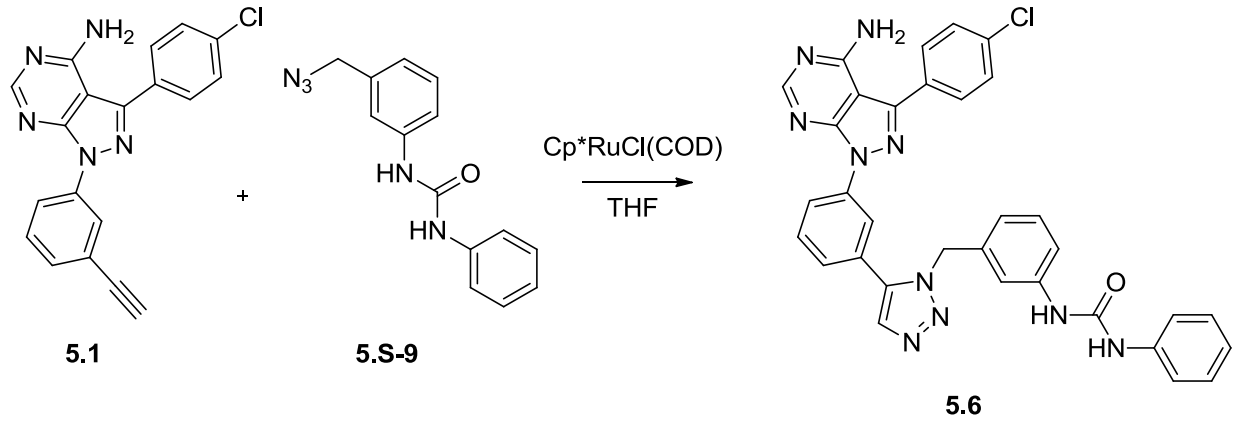

Synthesis of 5.6: Compound **5.1** (18 mg, 0.05 mmol) and Cp*RuCl(COD) (2 mg, 0.005 mmol) were added to a flame-dried round-bottom flask. The reaction vessel was evacuated using a vacuum pump and subsequently filled with N_2, this procedure was repeated for a total of 3 times. THF (1 mL) and **5.S-9** (11 mg, 0.05 mmol) were then added. The reaction mixture was allowed to stir at room temperature overnight. THF was removed under reduced pressure. The crude mixture was then dissolved in DMSO (1 mL), and then purified by reverse-phase HPLC (linear gradient of 25 → 90% CH_3CN in H_2O) to yield 14 mg (44% yield) of compound **5.6** as a white solid. **Spectral data.** ^{1}H NMR (500 MHz, DMSO-d_6): δ 8.73 (s, 1 H), 8.59 (s, 1 H), 8.38-8.32 (m, 3 H), 8.10 (s, 1 H), 7.73-7.66 (m, 3 H), 7.64-7.60 (m, 2 H), 7.49-7.46 (m, 1 H), 7.41-7.35 (m, 3 H), 7.27-7.22 (m, 2 H), 7.17-7.12 (m, 2 H), 6.97-6.92 (m, 1 H), 6.68-6.64 (m, 1 H), 5.73 (s, 2 H); ^{13}C NMR (100MHz, DMSO-d_6): δ 158.81, 157.10, 155.14, 152.73, 145.26, 140.63, 139.99, 139.46, 137.65, 137.14, 134.39, 133.75, 131.30, 130.66, 130.48, 129.61, 129.18, 127.79, 126.71, 122.25, 121.97, 120.87, 120.46, 118.56, 117.71, 116.49, 99.21, 51.70; HRMS-ESI (*m/z*): $[M + H]^+$ calcd for $C_{33}H_{25}ClN_{10}O$; 613.1974, found 613.1971.

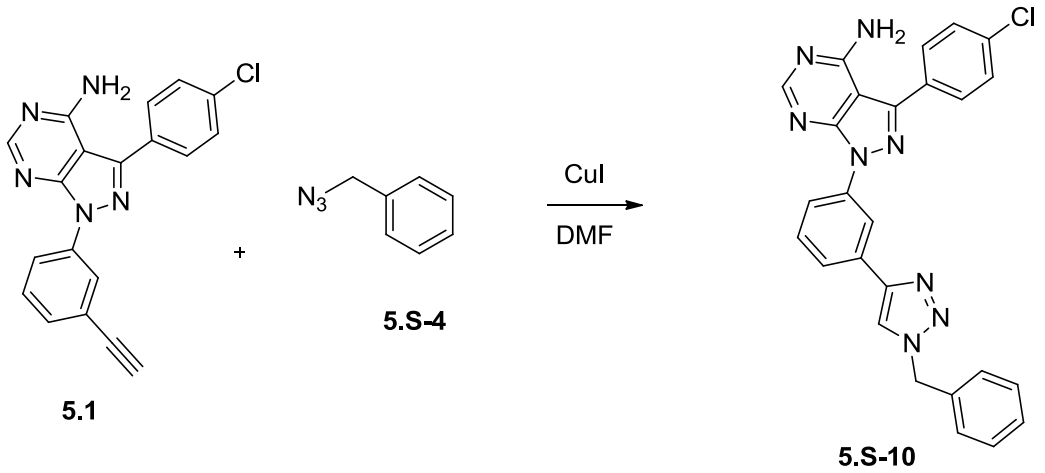

Synthesis of 5.S10: Compound **5.1** (45 mg, 145 µmol) was added to an oven dried microwave vial, followed by copper iodide and 1 ml DMF containing 2 equivalents of **5.S-4** (39 mg, 290 µmol). The reaction was heated to 75^{o}C in a microwave reactor for 45 min. After the reaction was cooled to room temperature, water (5 mL) was added to precipitate product. The reaction was then filtered, rinsed with water twice, followed by a hexanes wash. The crude precipitate was then chromatographed via silica gel chromatography using a Biotage Isolera One (linear gradient of 40→100% EtOAc in DCM) to yield 45 mg of **5.S-10** (65% yield) as a white solid. **Spectral data.** ^{1}H NMR (400 MHz, DMSO-d_6): δ 8.74 (s, 1 H), 8.68-8.65 (m, 1 H), 8.37 (s, 1 H), 8.23-8.18 (m, 1H), 7.80-7.74 (m, 3 H), 7.64-7.56 (m, 3 H), 7.40-7.28 (m, 5 H), 5.64 (s, 1 H); ^{13}C NMR (100 MHz, DMSO-d_6): δ 158.84, 157.10, 155.07, 146.53, 145.06, 139.62, 136.42, 134.36, 132.10, 131.47, 130.75, 130.22, 129.65, 129.25, 128.62, 128.34, 123.59, 122.58, 120.92, 117.91, 99.20, 53.51; HRMS-ESI (*m/z*): $[M + H]^+$ calcd for $C_{26}H_{19}ClN_8$, 479.1494; found 479.1495.

IV. SPECTRAL DATA FOR COMPOUNDS 5.1–5.6.

5.S-1:

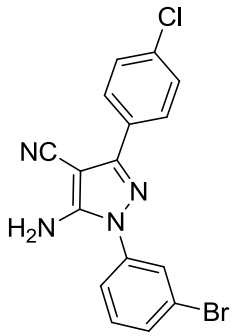

5.S-1 ^{1}H:

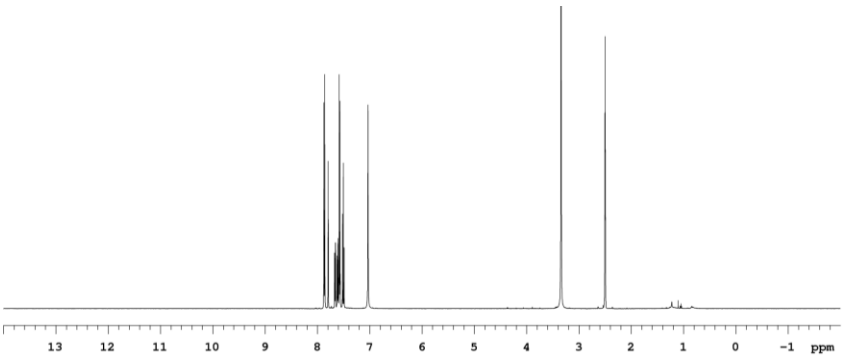

5.S-1 ^{13}C:

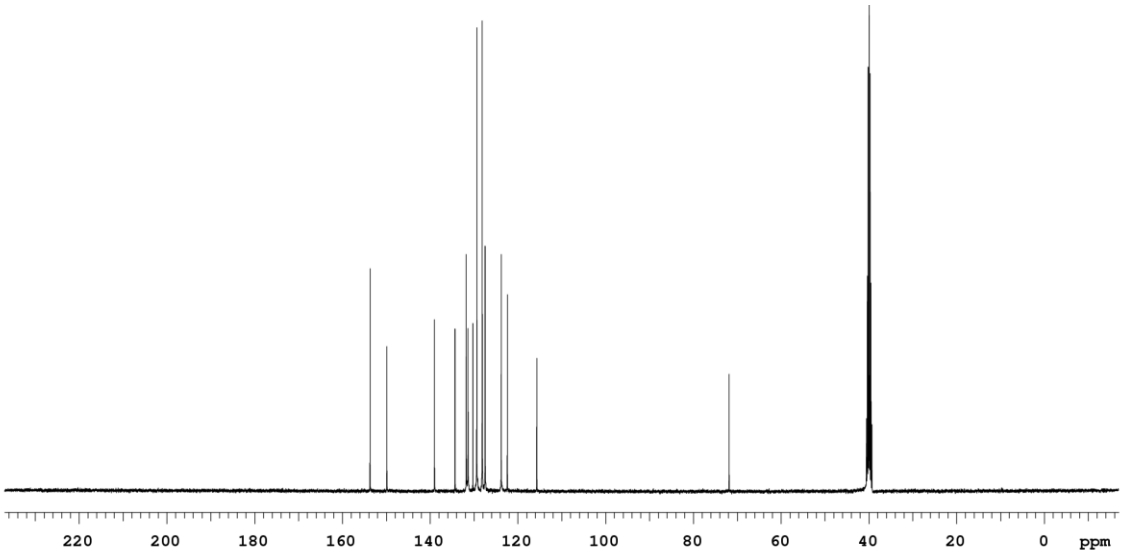

5.S-2:

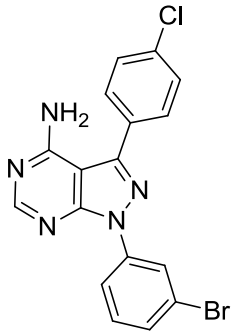

5.S-2 ^{1}H:

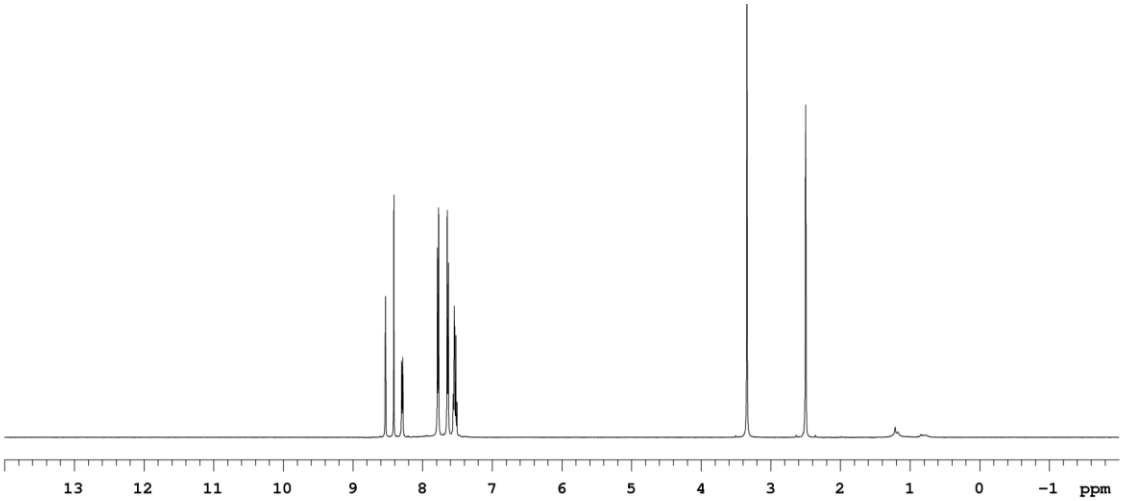

5.S-2 ^{13}C:

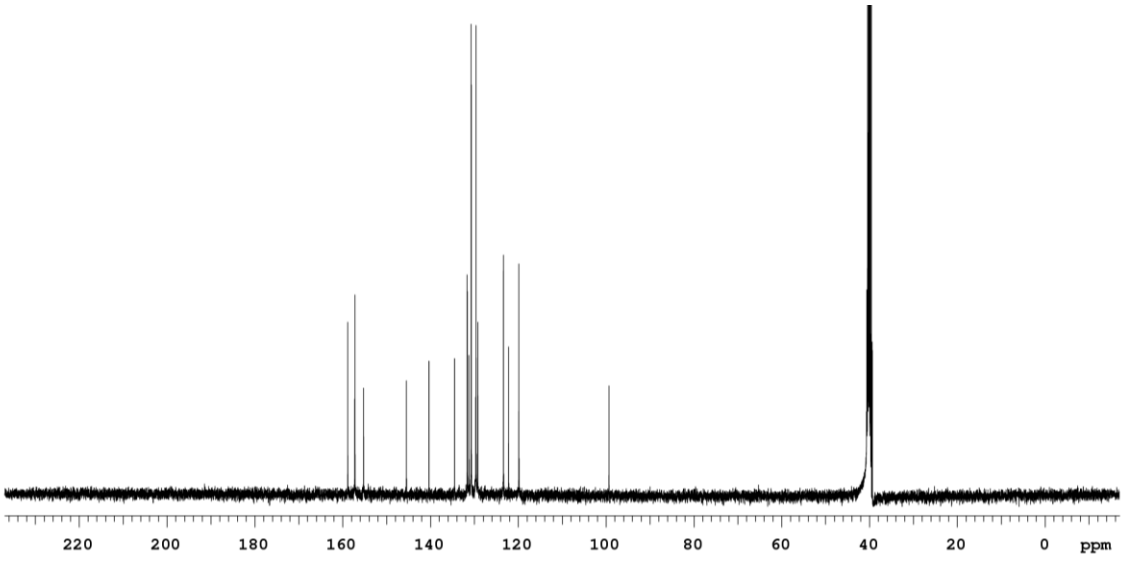

5.S-3:

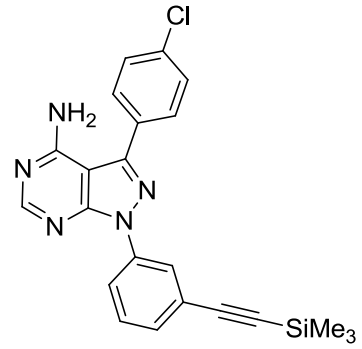

5.S-3 ^{1}H:

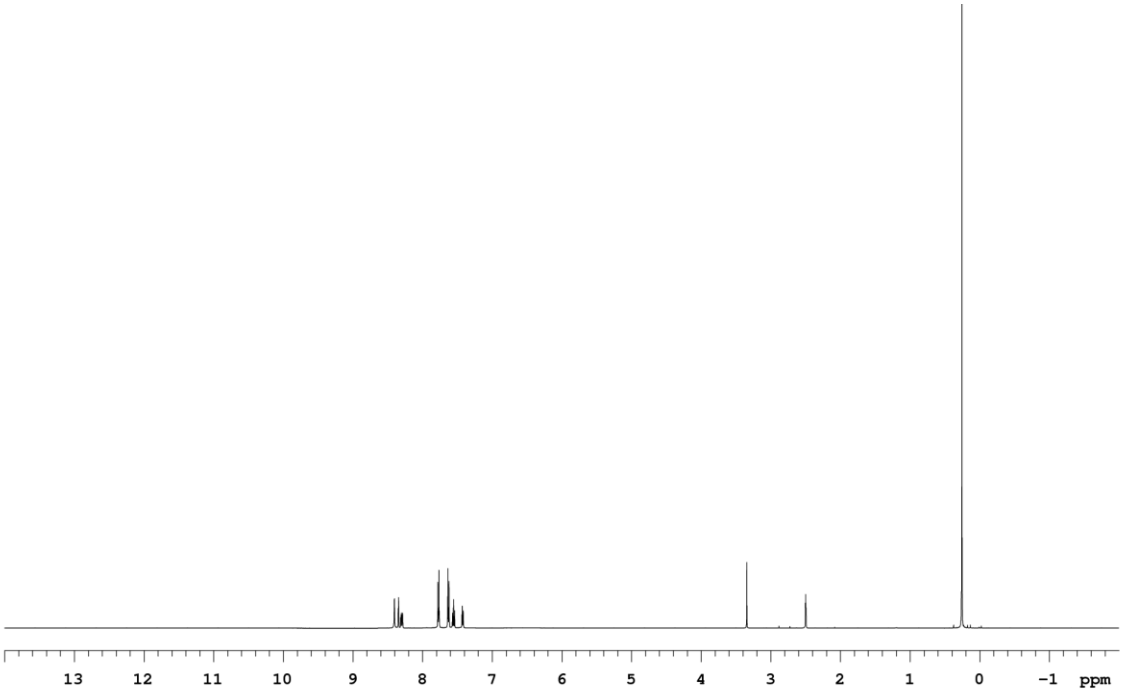

5.S-3 ^{13}C:

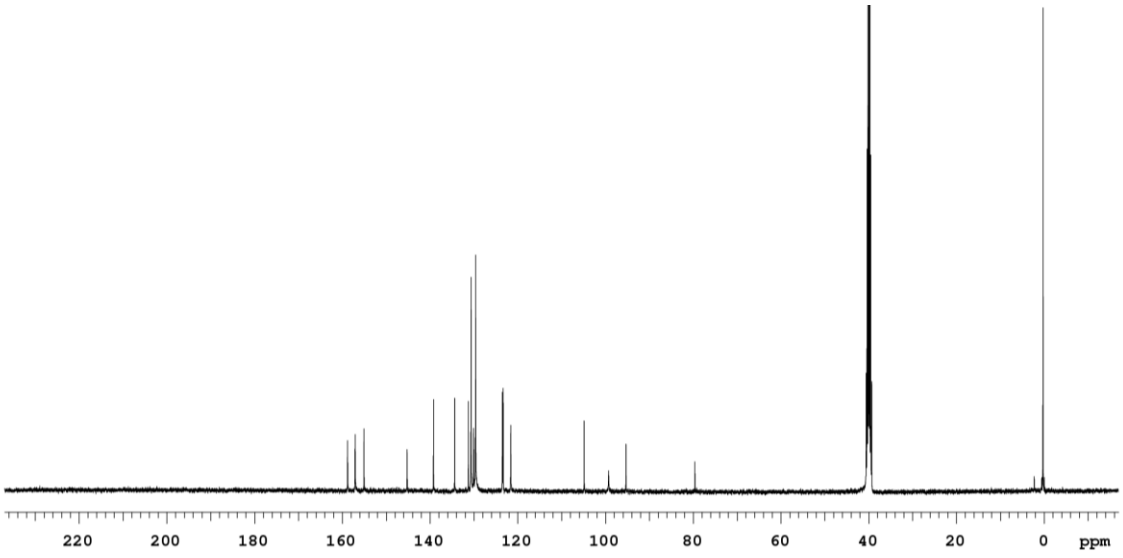

5.1:

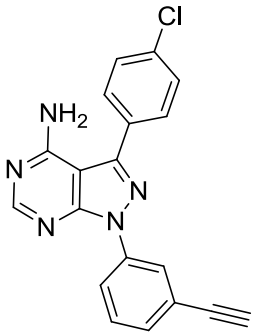

5.1 ^{1}H:

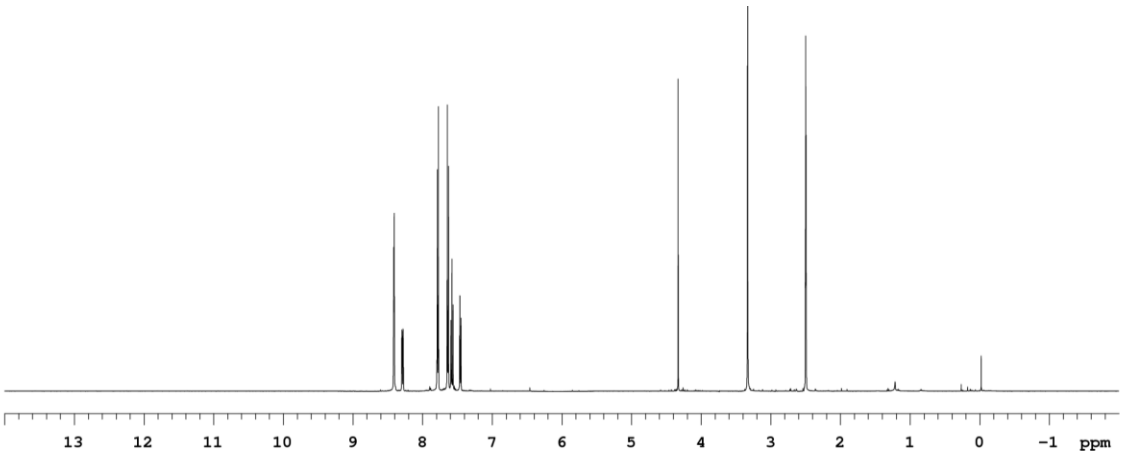

5.1 ^{13}C:

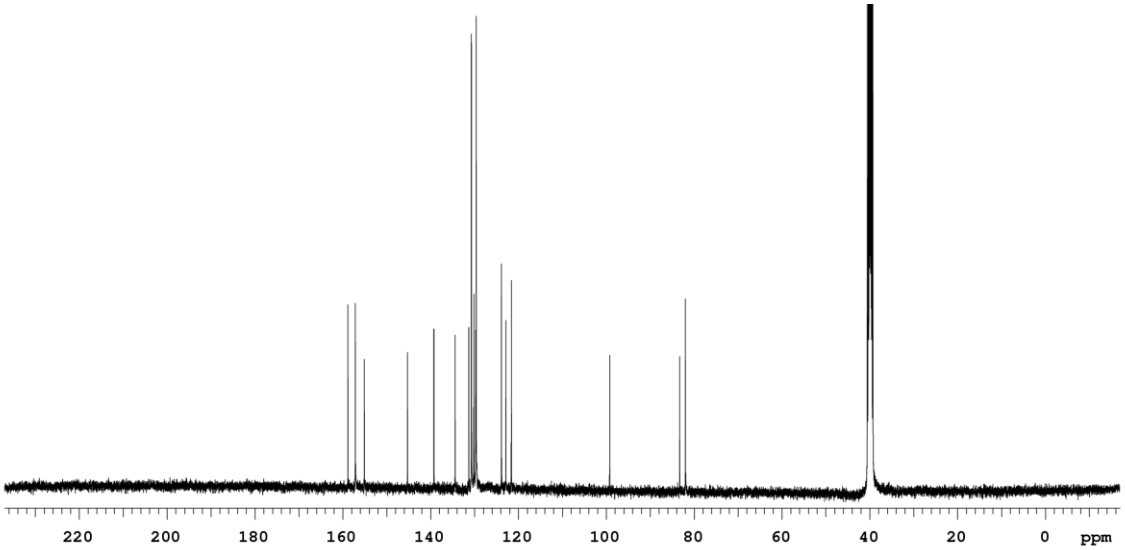

5.S-4: 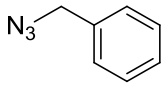

5.S-4 ^{1}H:

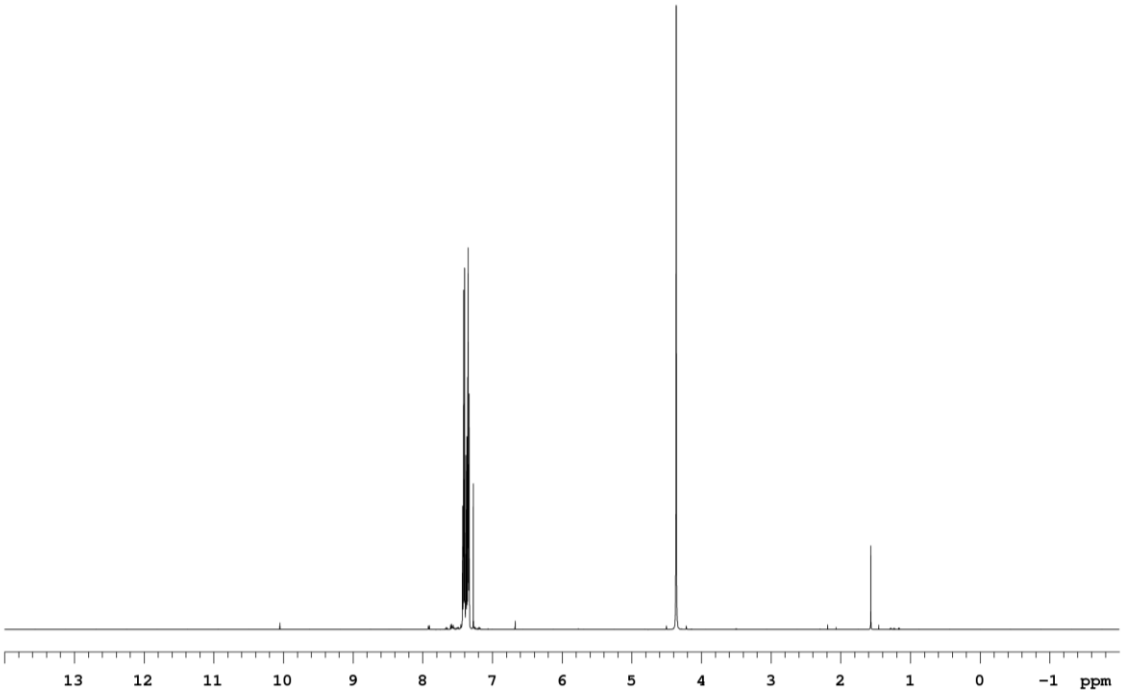

5.S-4 ^{13}C:

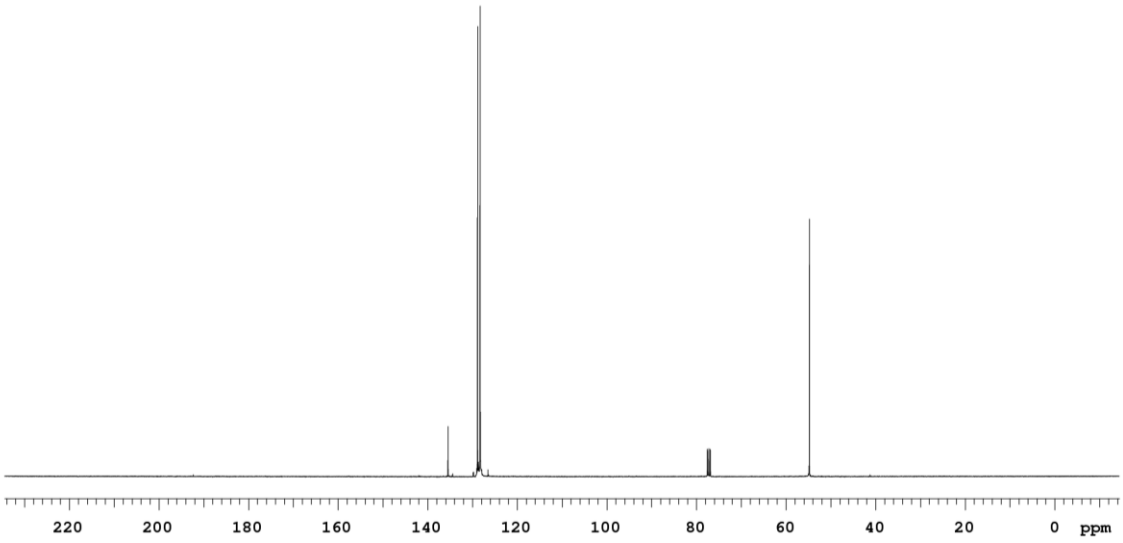

5.S-5:

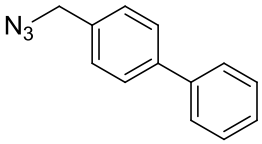

5.S-5 ^{1}H:

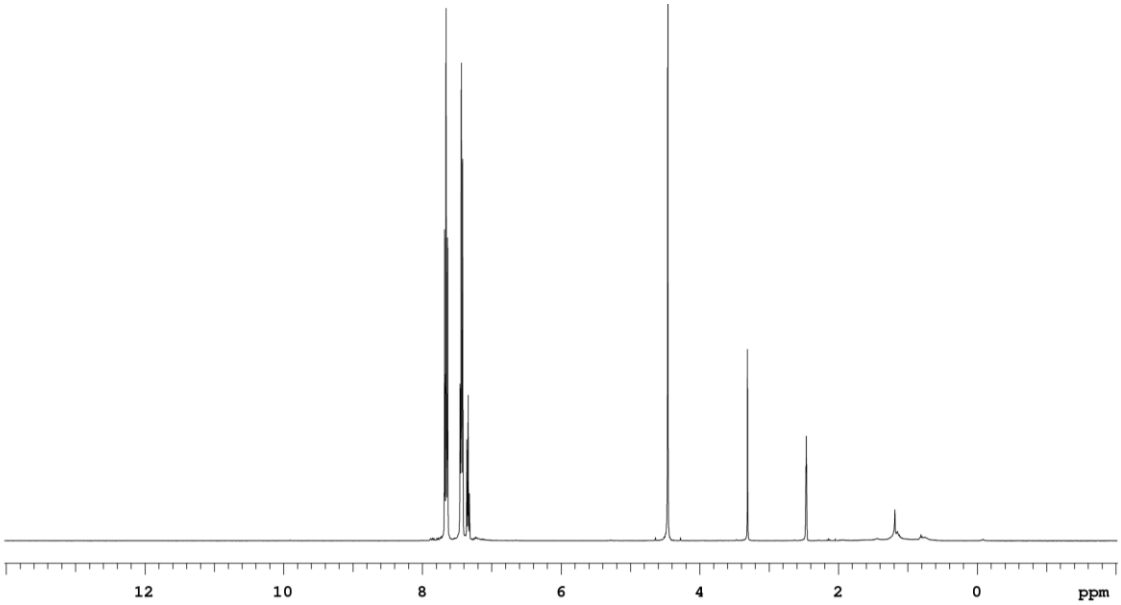

5.S-5 ^{13}C:

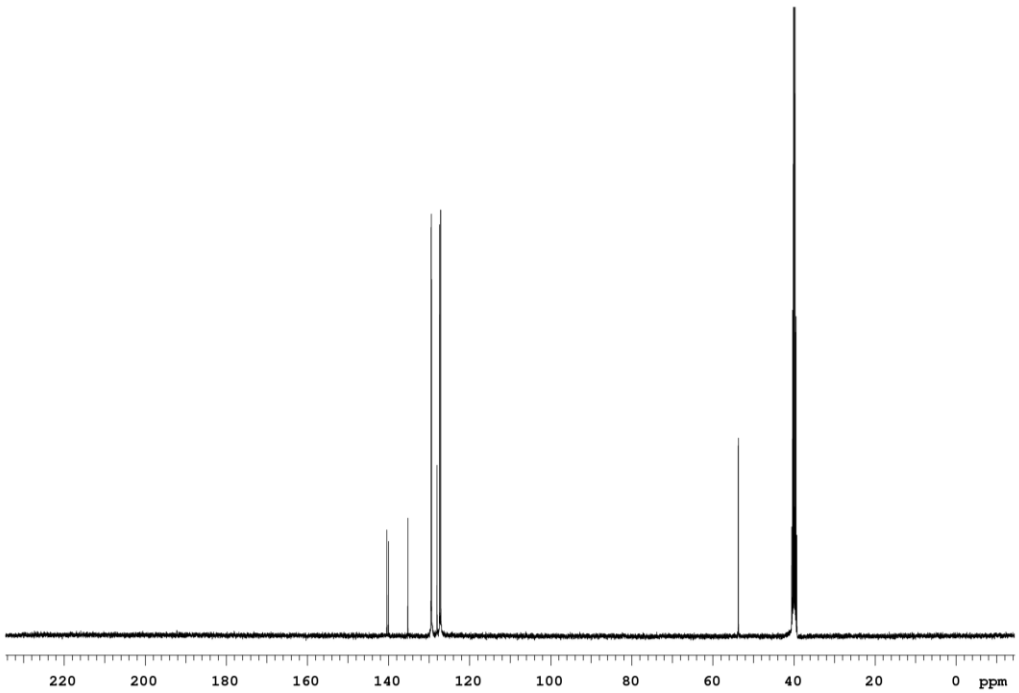

5.S-6:

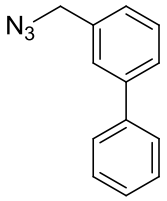

5.S-6 ^{1}H:

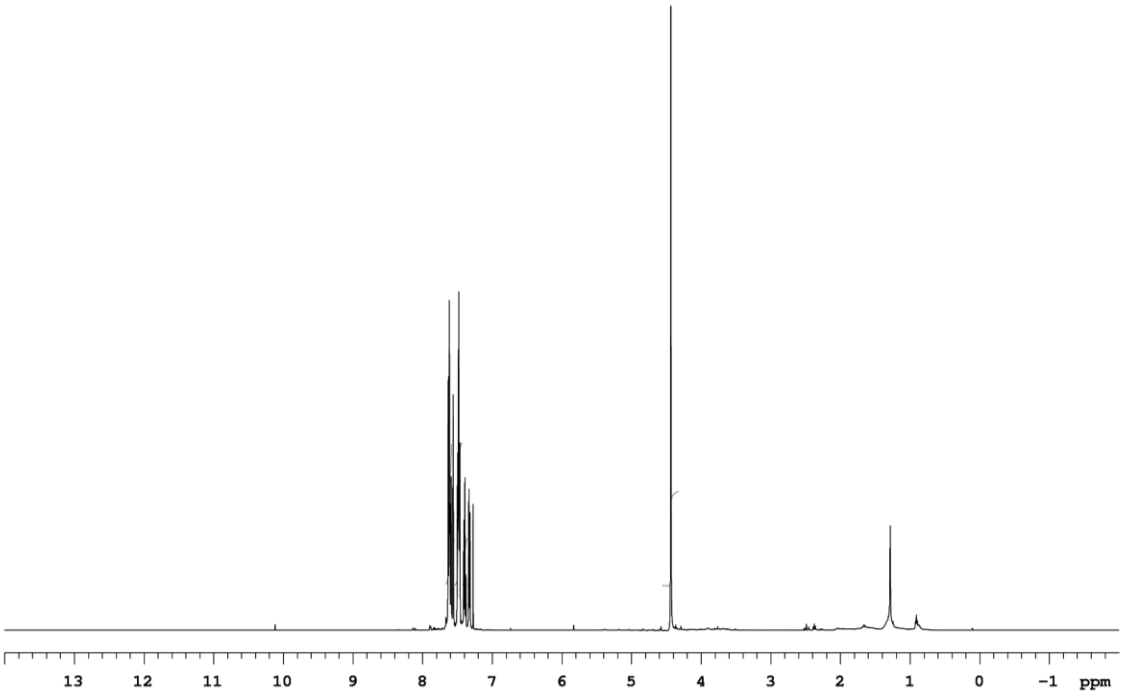

5.S-6 ^{13}C:

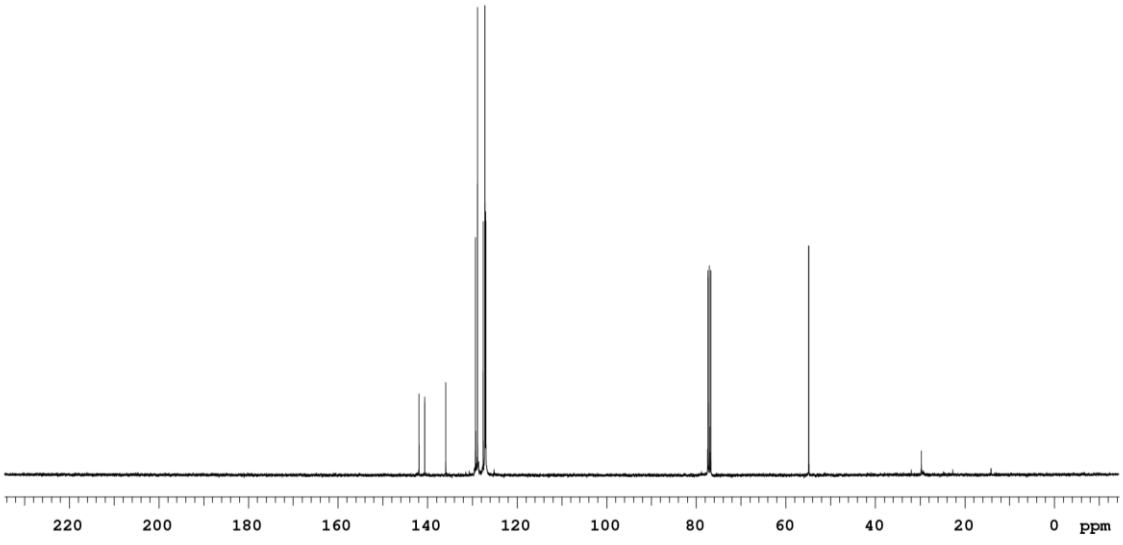

5.S-7:

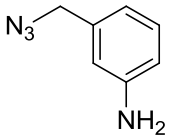

5.S-7 ^{1}H:

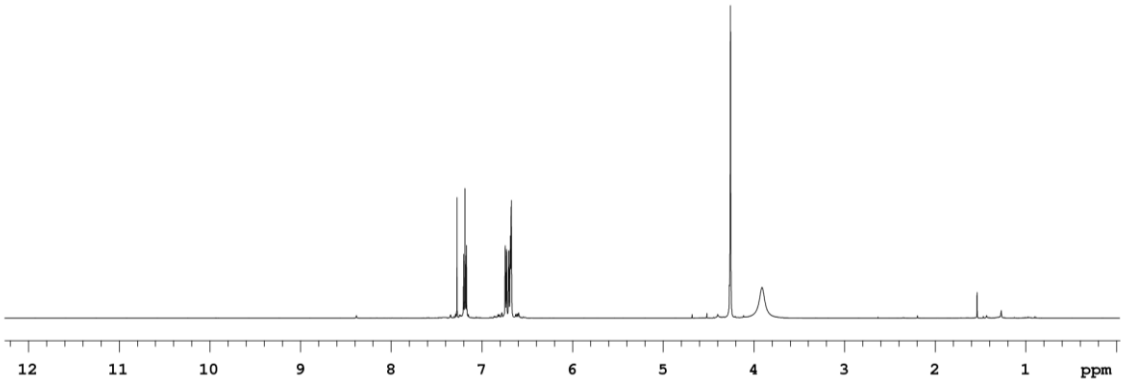

5.S-7 ^{13}C:

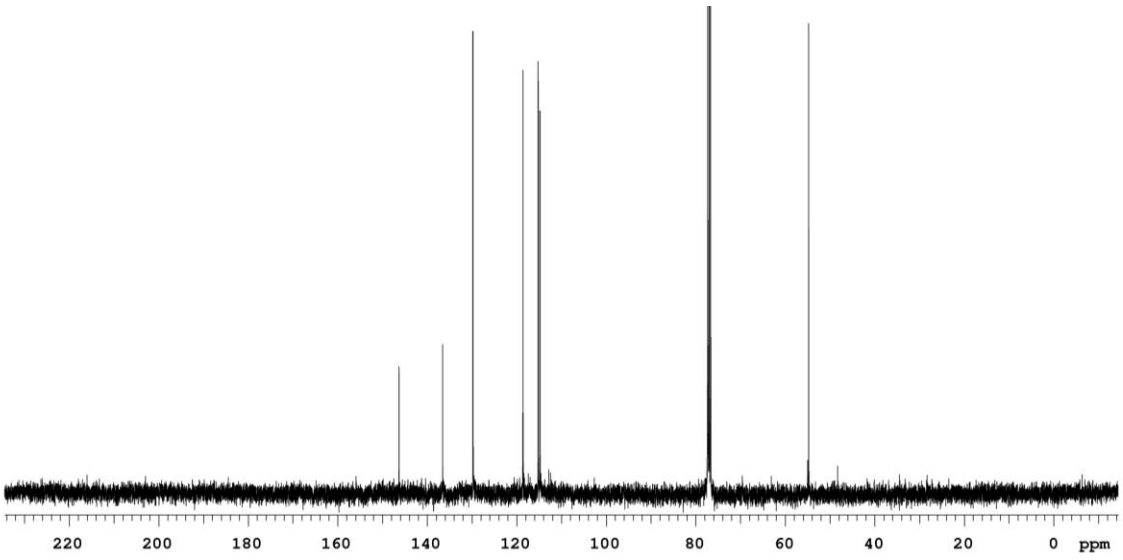

5.S-8:

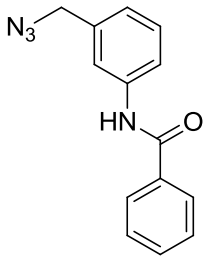

5.S-8 ^{1}H:

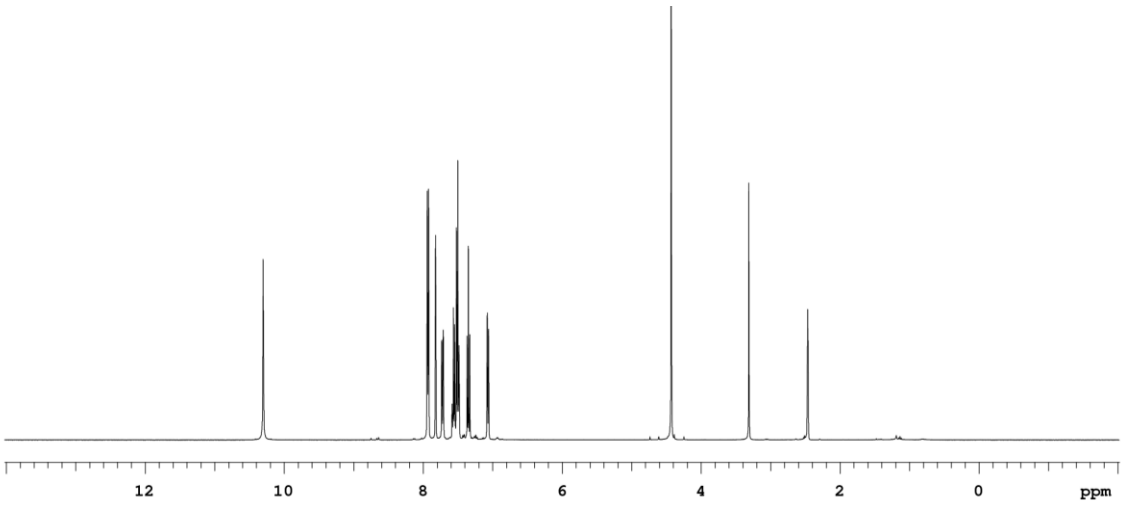

5.S-8 ^{13}C:

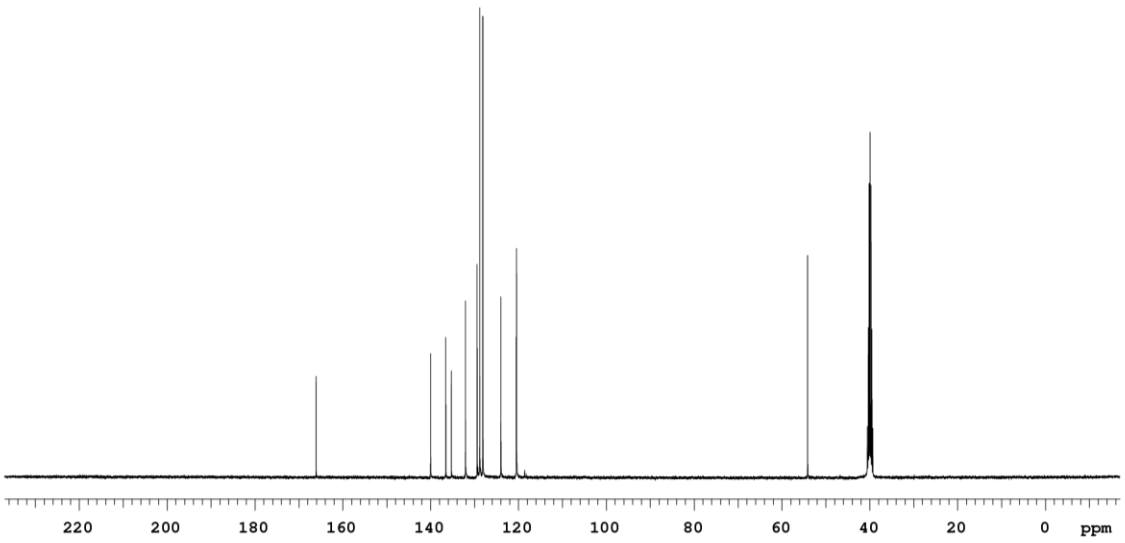

5.S-9:

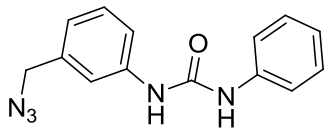

5.S-9 ^{1}H:

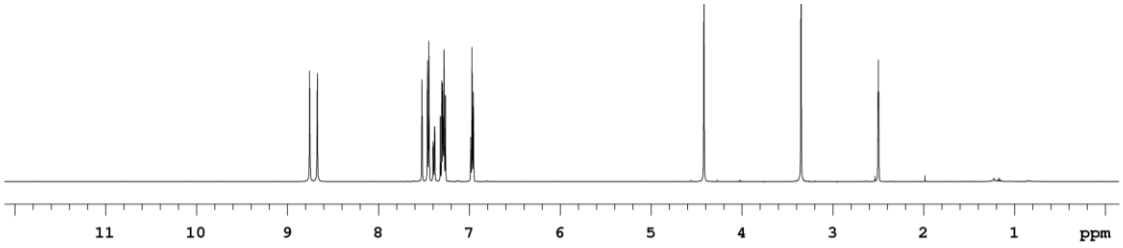

5.S-9 ^{13}C:

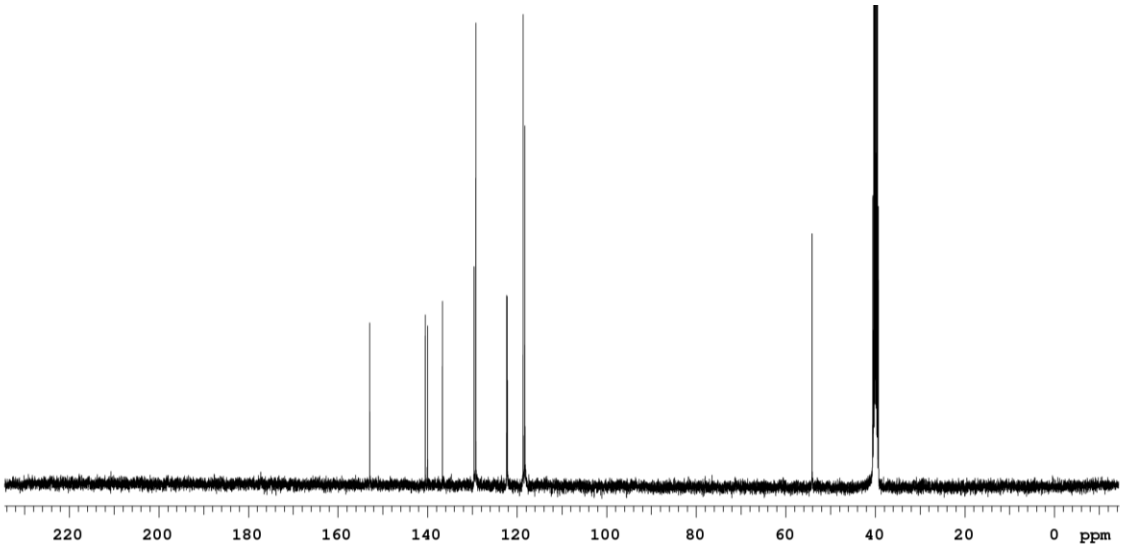

5.2:

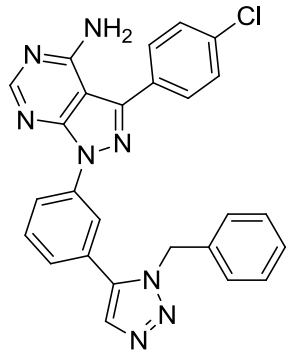

5.2 ^{1}H:

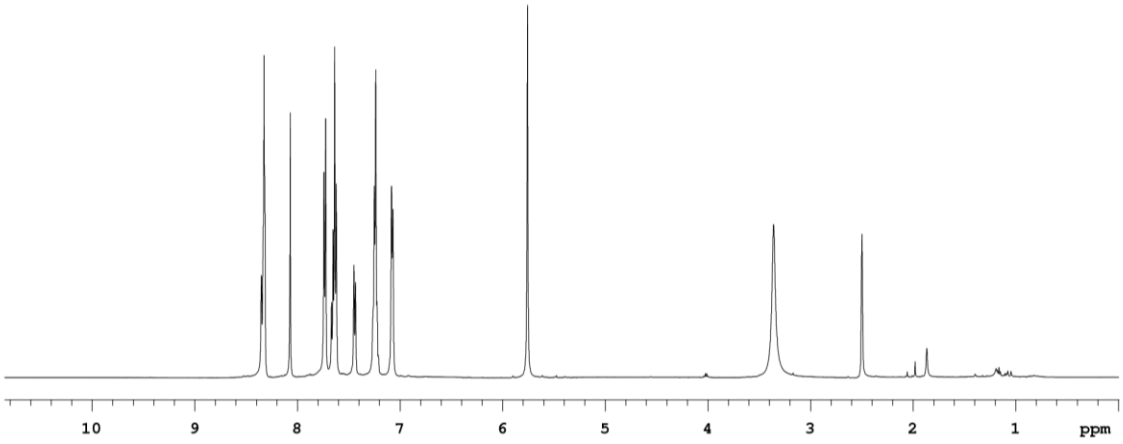

5.2 ^{13}C:

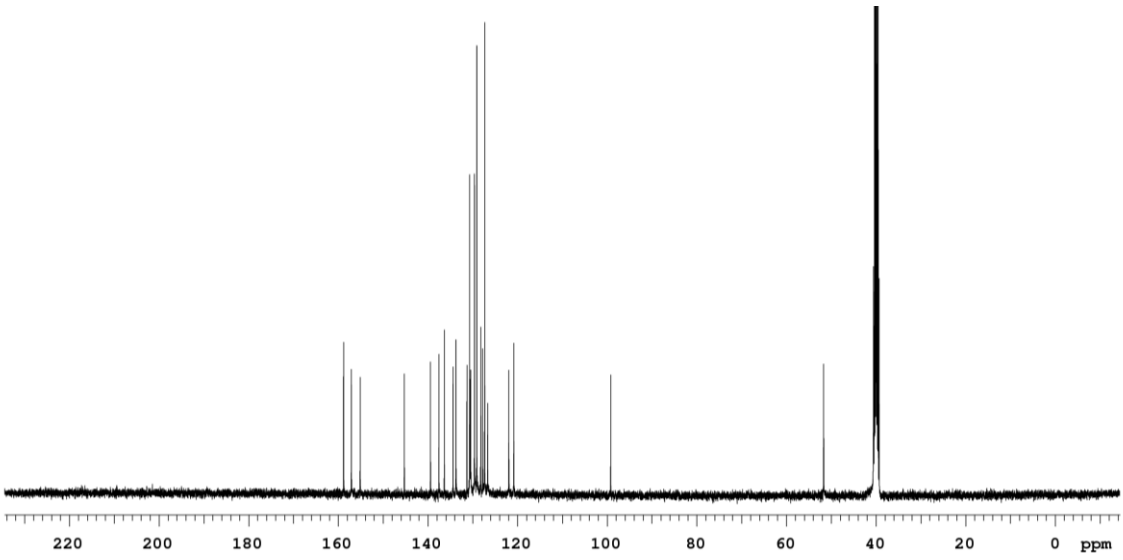

3:

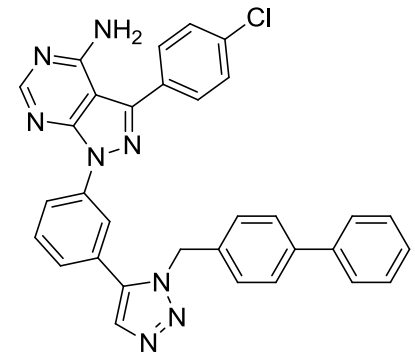
NH2
Cl
N
N
N
N
N
N
N

5.3 ^{1}H:

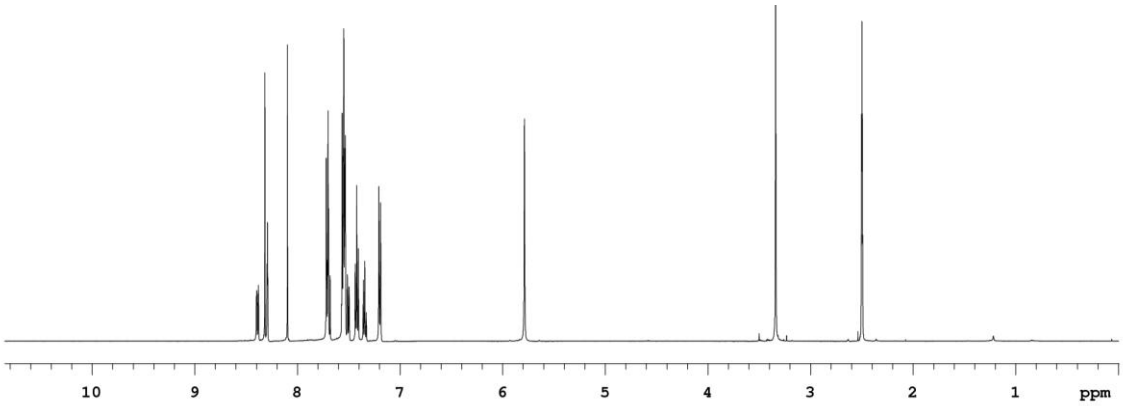
10
9
8
7
6
5
4
3
2
1
ppm

5.3 ^{13}C:

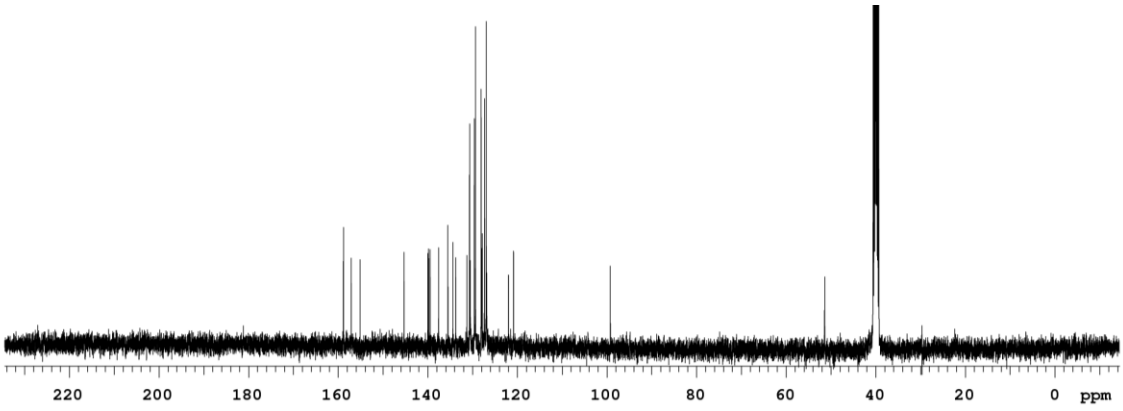
220
200
180
160
140
120
100
80
60
40
20
0
ppm

5.4:

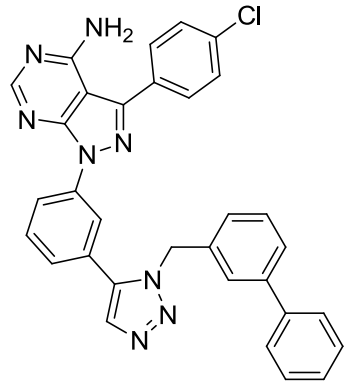

5.4 ^{1}H:

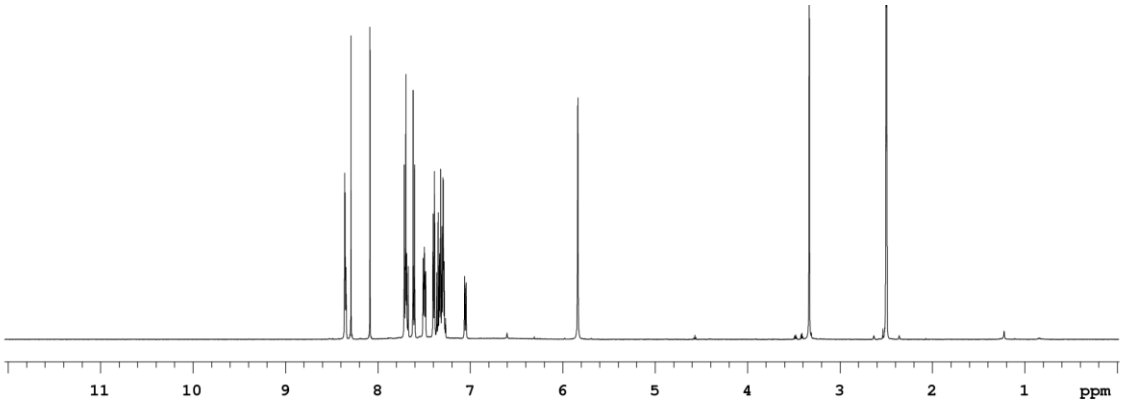

5.4 ^{13}C:

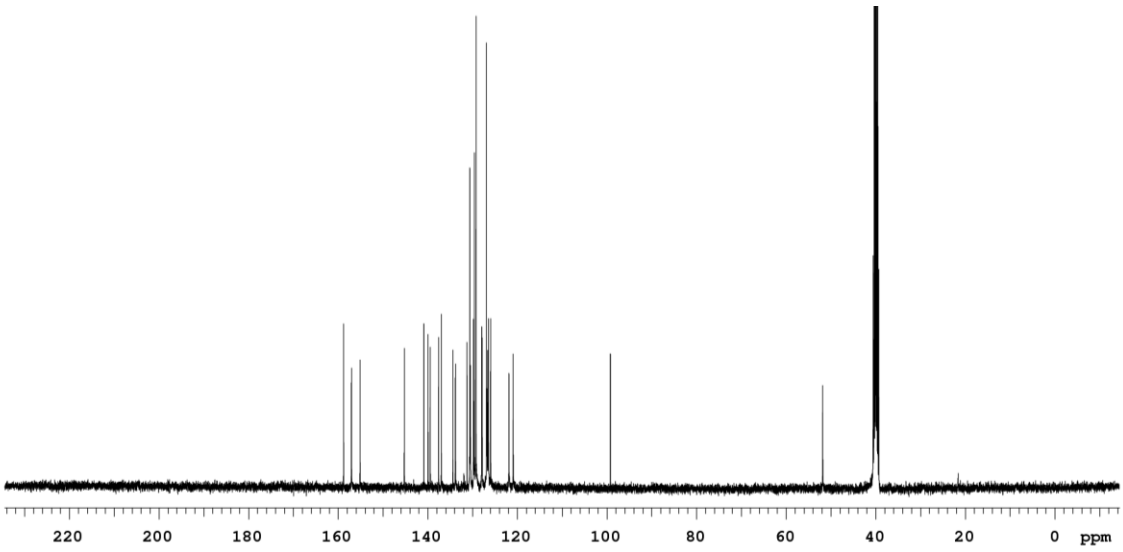

5.5:

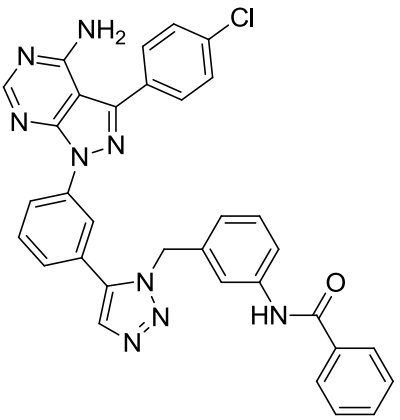

5.5 ^{1}H:

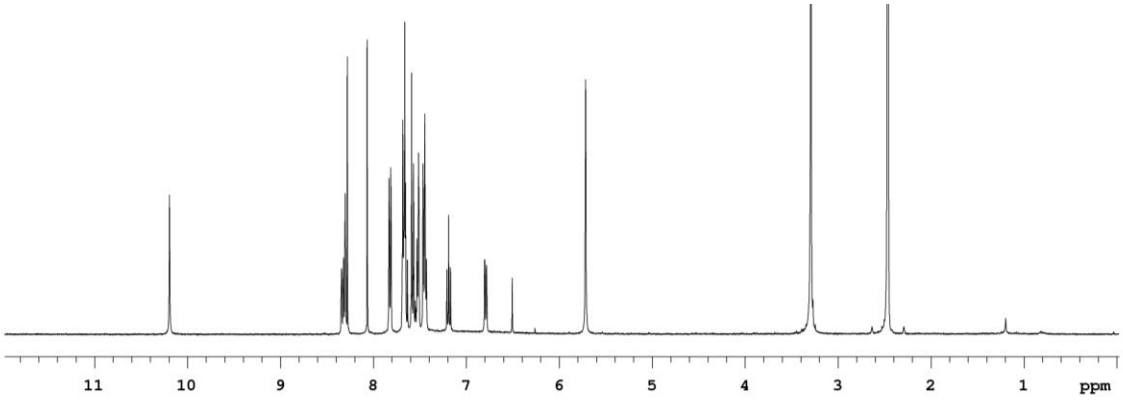

5.5 ^{13}C:

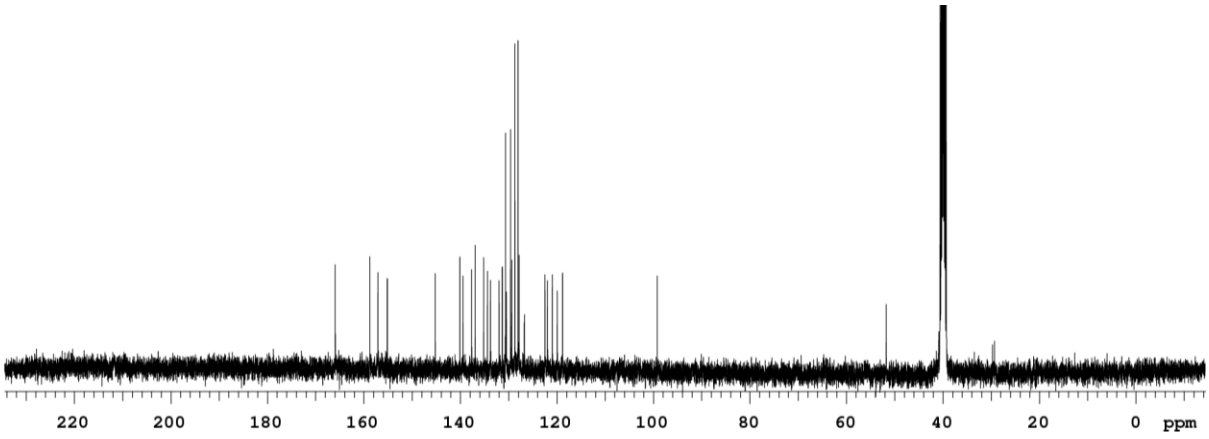

5.6:

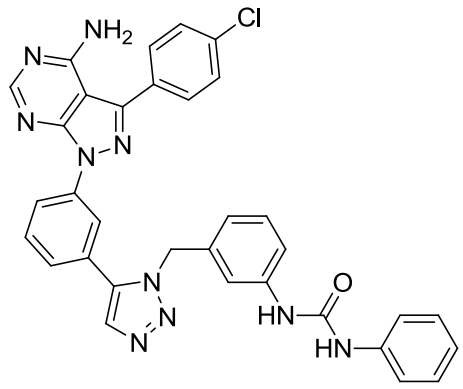

5.6 ^{1}H:

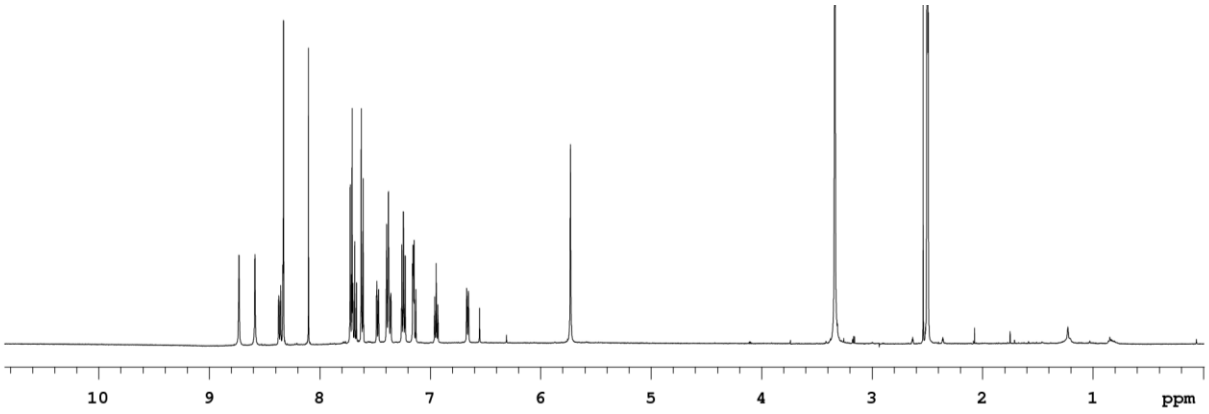

5.6 ^{13}C:

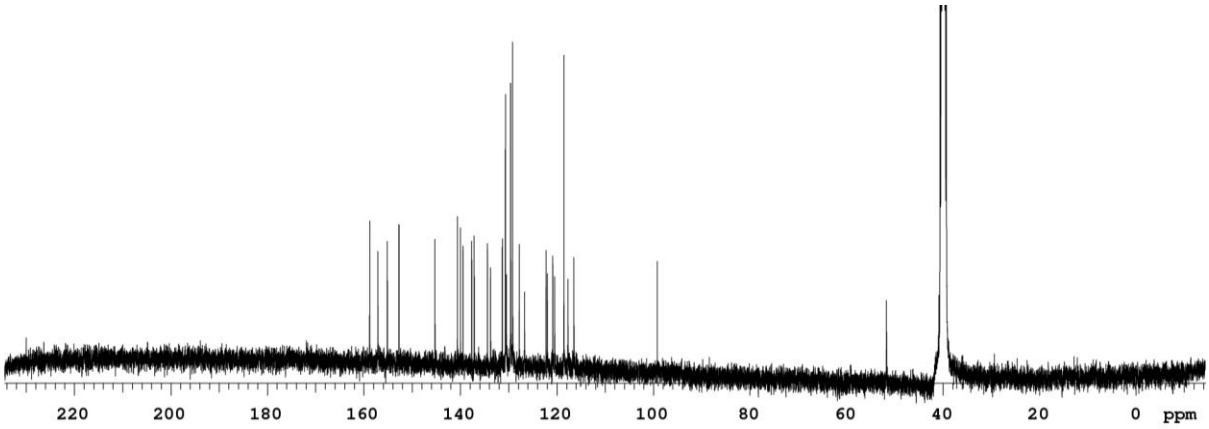

5.S-10:

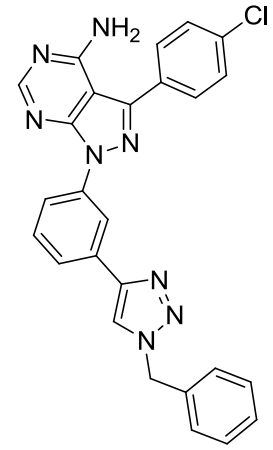

5.S-10 ^{1}H:

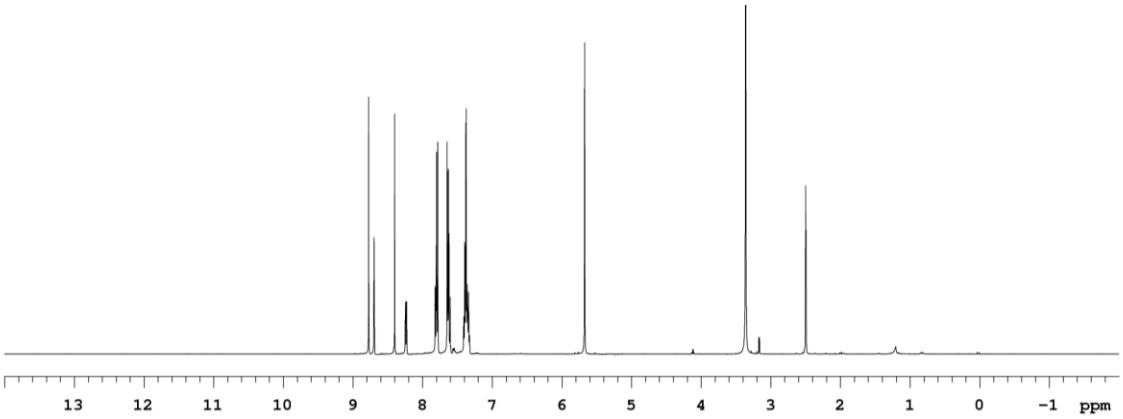

5.S-10 ^{13}C:

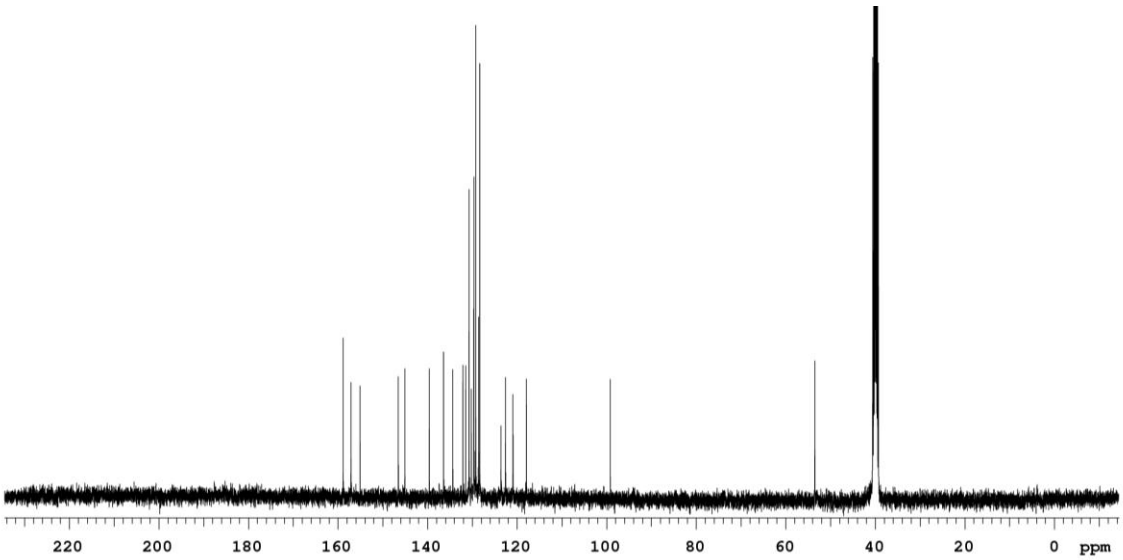

V. BIOCHEMICAL CHARACTERIZATION

General procedure for determination of inhibitor K_i. A continuous fluorescence assay[30] was used to determine K_i. Reaction volumes of 100 µL were used in 96-well plates. 85 µL of enzyme in buffer was added to each well. 2.5 µL of the appropriate inhibitor dilution (typically 5000, 1666, 555, 185, 61, 20, 6.8, 2.2, 0.76, 0 µM in DMSO) was then added. 2.5 µL of a substrate peptide ("compound 3" as described in Wang et al)[31] solution (1.8 mM in DMSO) was added. The reaction was initiated with 10 µL of ATP (1 mM in water), and reaction progress was immediately monitored at 405 nm (ex. 340 nm) for 10 minutes. Reactions had final concentrations of 30 nM enzyme, 45 µM peptide substrate, 100 µM ATP, 100 µM Na_3VO_4, 100 mM Tris buffer (pH 8), 10 mM $MgCl_2$, 0.01% Triton X-100.The initial rate data collected was used for determination of K_i values. For K_i determination, the kinetic values were obtained directly from nonlinear regression of substrate-velocity curves in the presence of various concentrations of the inhibitor. The equation Y = Bottom + (Top – Bottom)/(1 + 10^X – LogEC50), X = log(concentration) and Y = binding; was used in the nonlinear regression.

Analytical data for c-Src K_i determination. Each inhibitor K_i value was determined using at least three independent experiments, a representative inhibition curve is shown.

5.1:

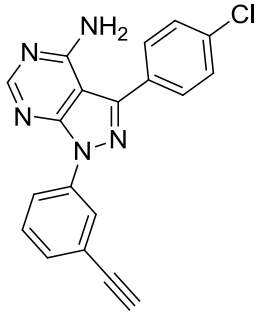

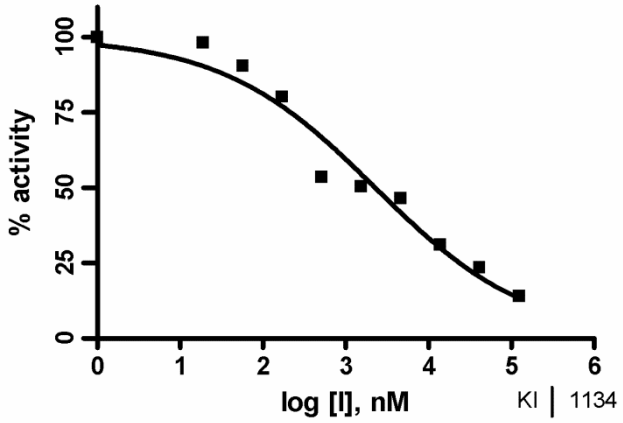

Avg K_i = 1,452 ± 562 nM

5.2:

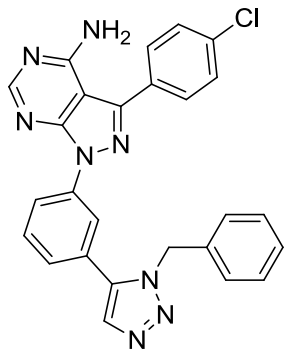

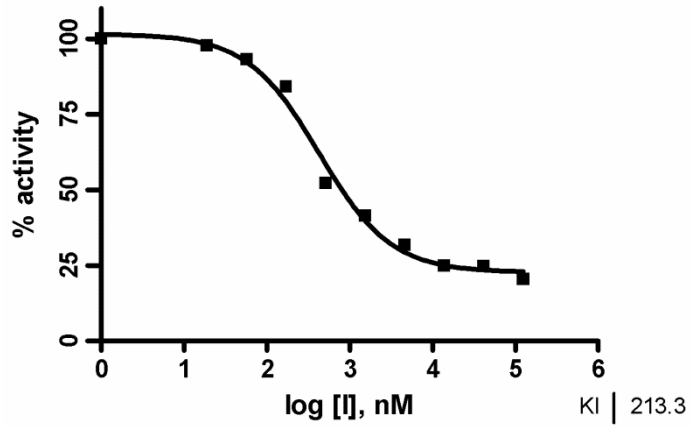

Avg K_i = 207 ± 13 nM

5.3:

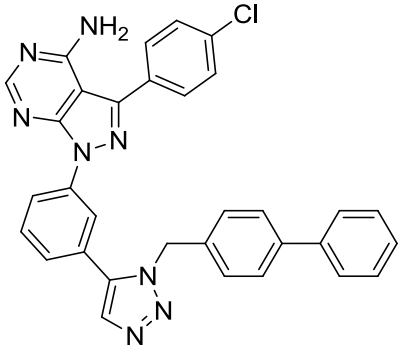

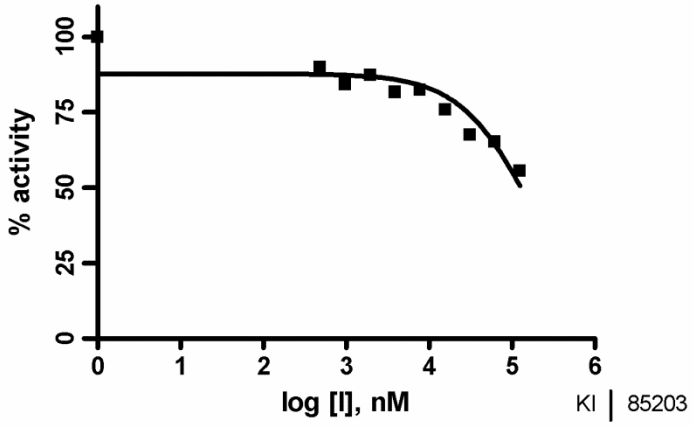

Avg K_i ≥ 60 µM

5.4:

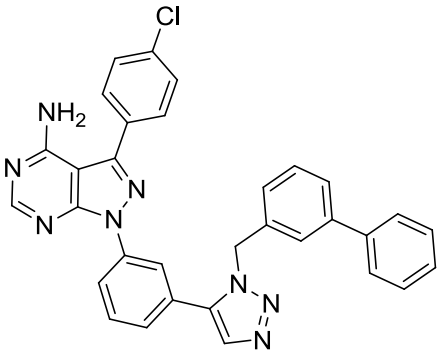

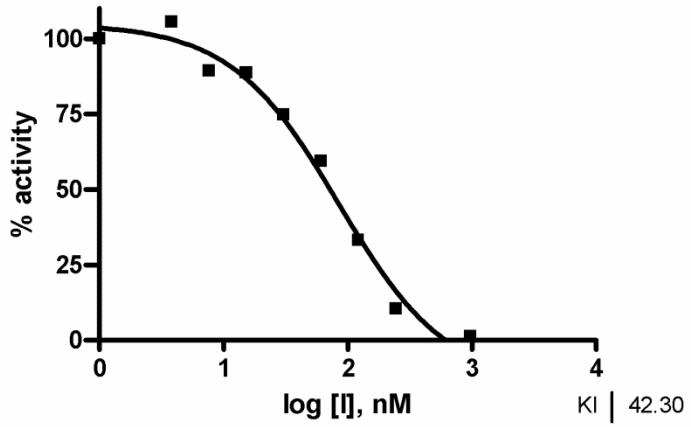

Avg K_i = 44 ± 11 nM

5.5:

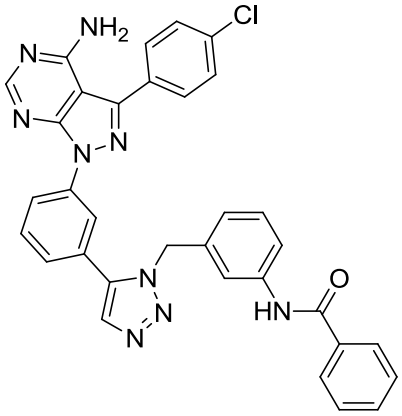

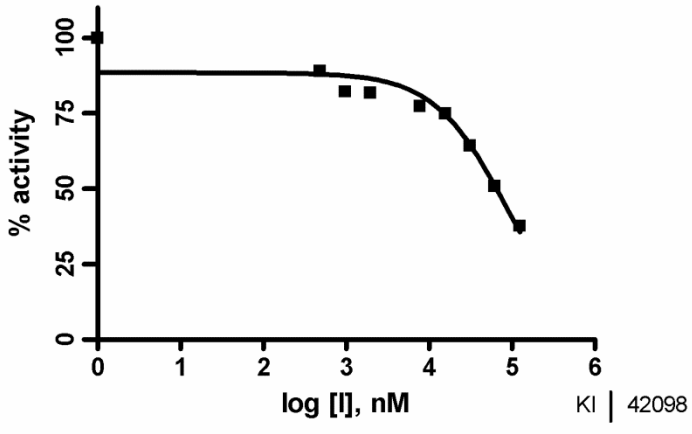

Avg K_i = 37 ± 21 µM

5.6:

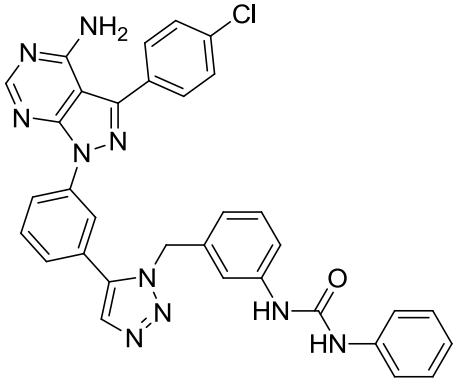

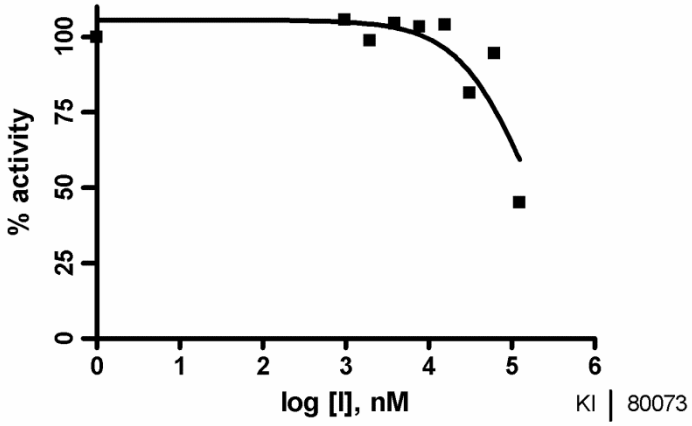

Avg K_i ≥ 60 µM

5.S10:

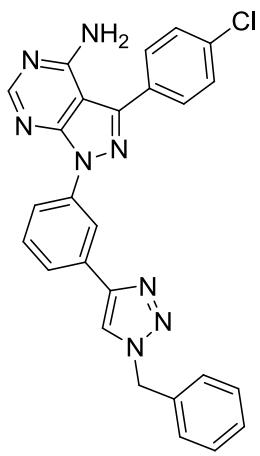

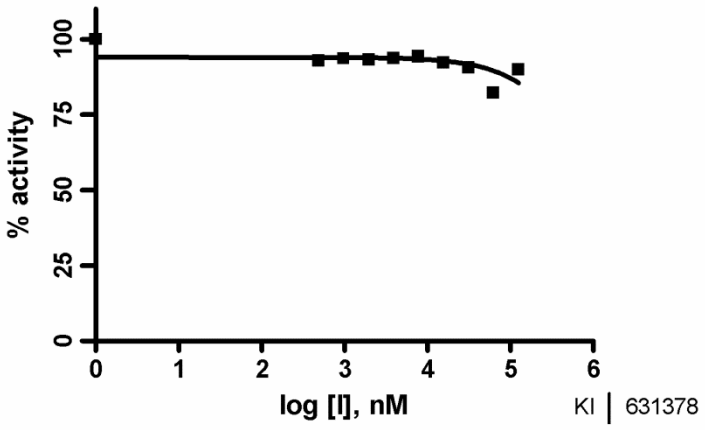

Avg K_i ≥ 60 µM

PP2:

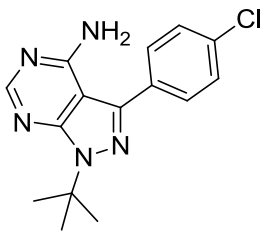

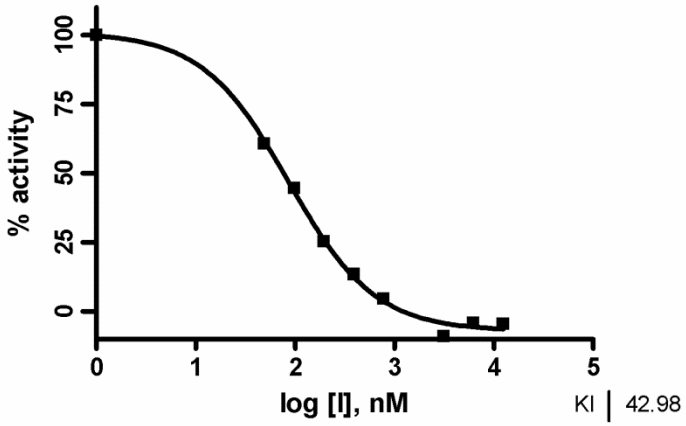

Avg K_i = 33 ± 7 nM

Analytical data for c-Abl K_i determination. Each inhibitor K_i value was determined using three independent experiments, a representative inhibition curve is shown.

5.1:

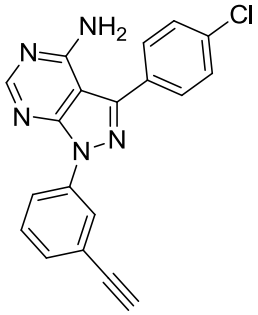

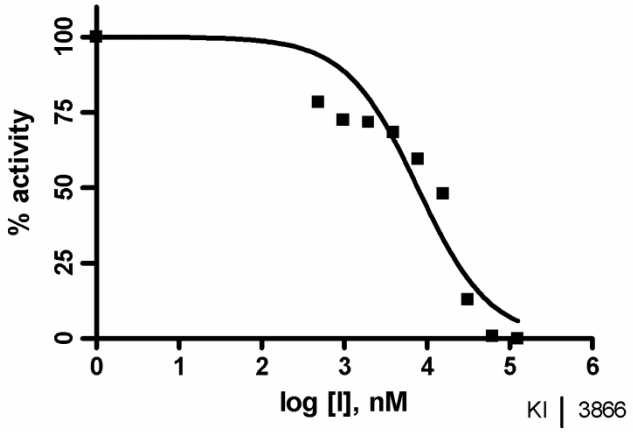

Avg K_i = 7,150 ± 3,390 µM

5.2:

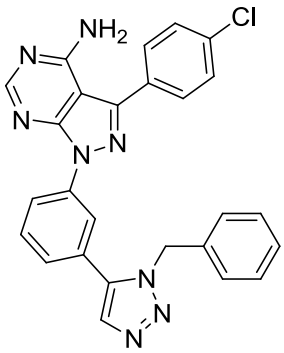

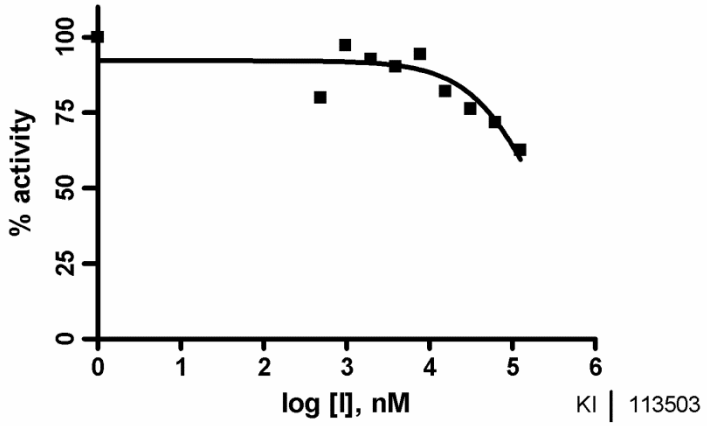

Avg K_i ≥ 60 µM

5.4:

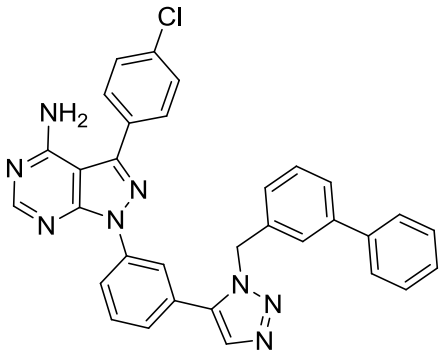

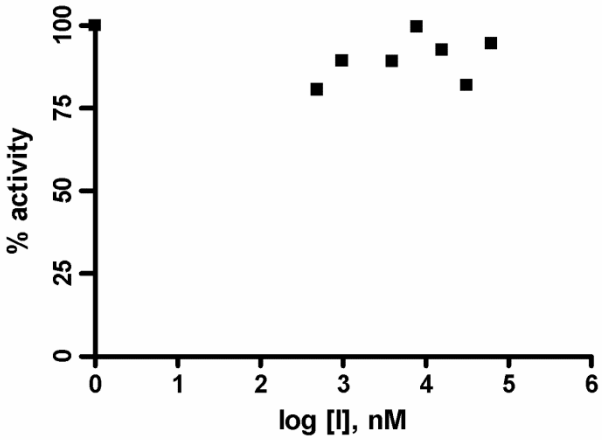

Avg K_i > 125 µM

PP2:

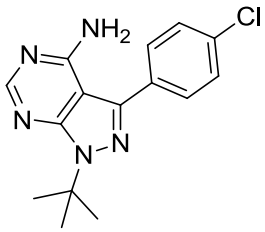

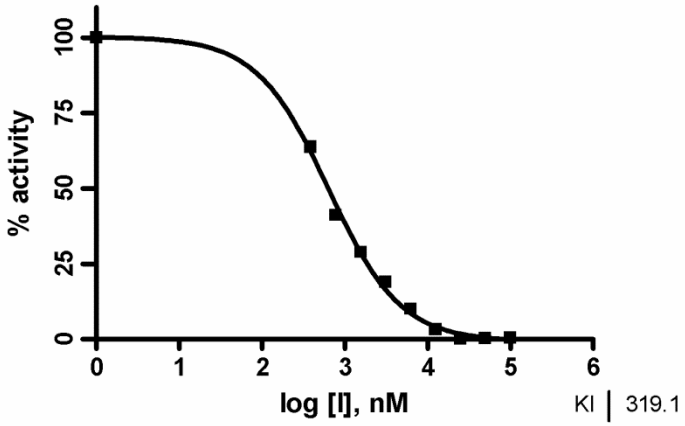

Avg K_i = 325 ± 8 nM

Analytical data for c-Src-TM (Q275G, C277Q, F278Y) K_i determination. Each inhibitor K_i value was determined using three independent experiments, a representative inhibition curve is shown.

5.4:

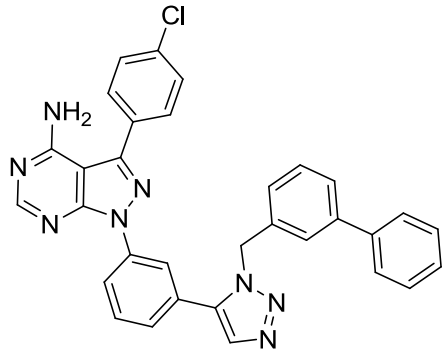

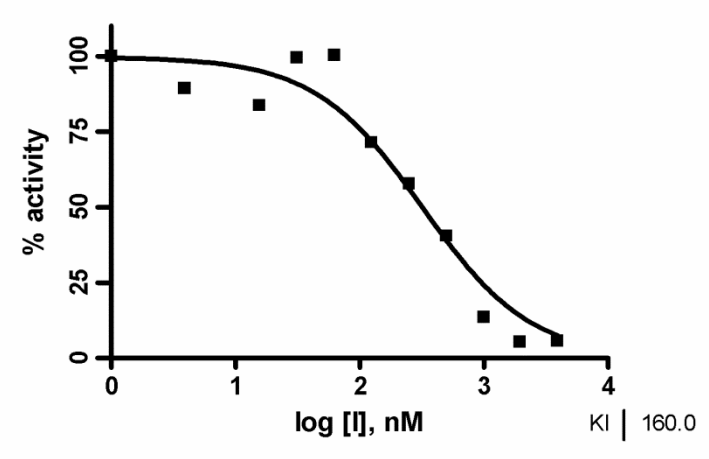

Avg K_i = 175 ± 21 nM

Analytical data for phosphorylated c-Src K_i determination. Each inhibitor K_i value was determined using three independent experiments, a representative inhibition curve is shown.

5.4:

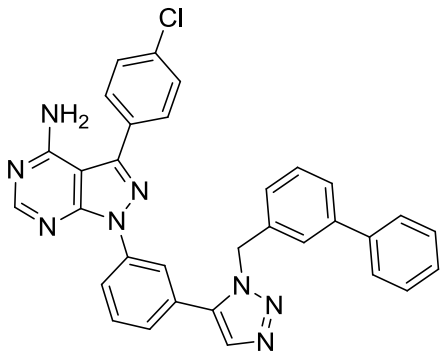

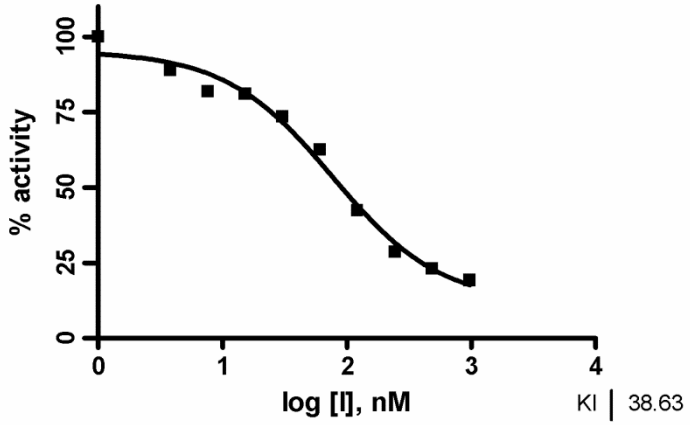

Avg K_i = 49 ± 11 nM

Analytical data for three-domain c-Src K_i determination. Each inhibitor K_i value was determined using three independent experiments, a representative inhibition curve is shown.

5.4:

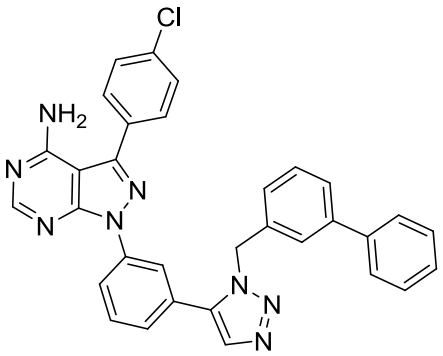

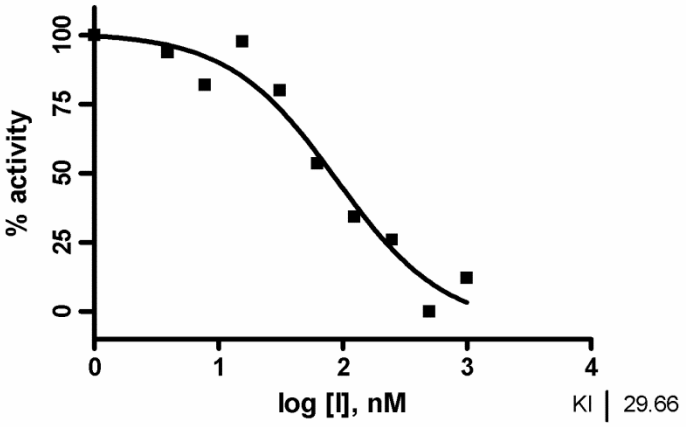

Avg K_i = 46 ± 22 nM

VI. MOLECULAR MODELS

Molecular visualization of c-Src and c-Abl structures was performed using PyMol v.1.4 (Schrodinger). The starting structure for c-Src was 3DQW and the starting structure for c-Abl was 2G21.

A. PP2 bound to c-Src.
P-loop (residues 273–281) is denoted in red:

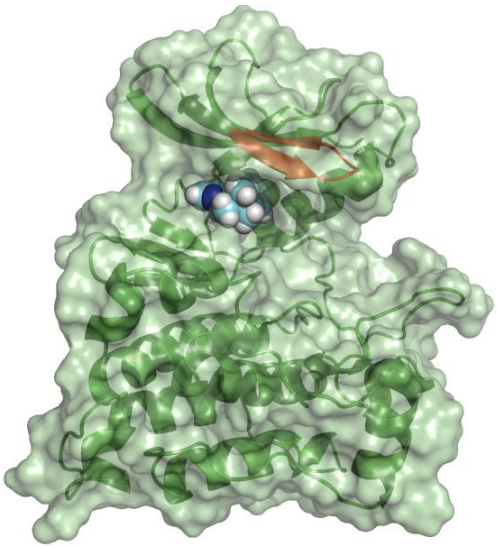

B. PP2 bound to c-Abl.
P-loop (residues 248–256) is denoted in red:

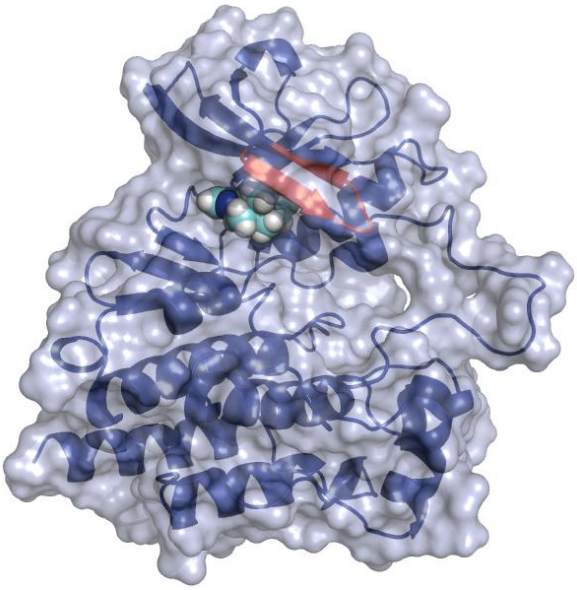

C. Overlay of c-Src and c-Abl structures with PP2 bound.

c-Src P-loop is denoted in yellow and c-Abl P-loop is denoted in red:

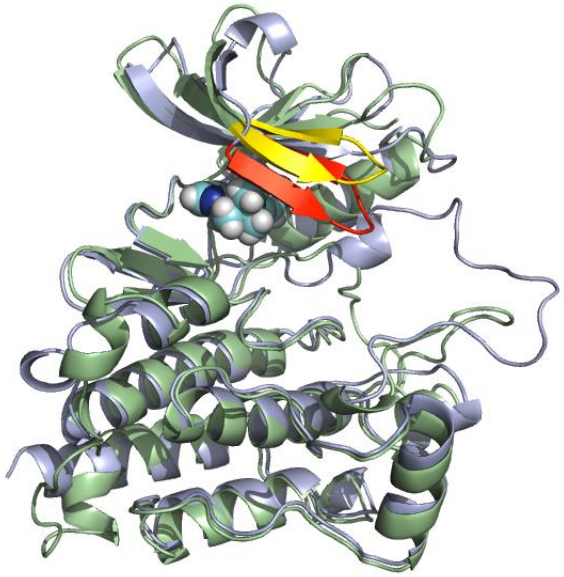

D. Molecular modeling of inhibitors bound to c-Src

Molecular modeling was performed using MOE 2011.05 (Chemical Computing Group). The starting structure for c-Src was 3DQW and the starting structure for c-Abl was 2G2I. Structures of PP2 bound to Src-family kinases were used to obtain a model of PP2 bound to both c-Src and c-Abl (main text Figure 2).

E. Model image of PP2~alkyne (5.1) bound to c-Src:

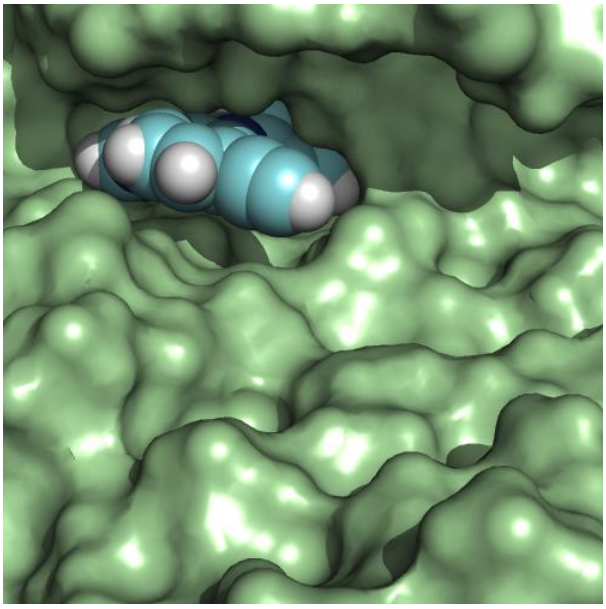

F. Model image of compound 5.2 bound to c-Src:

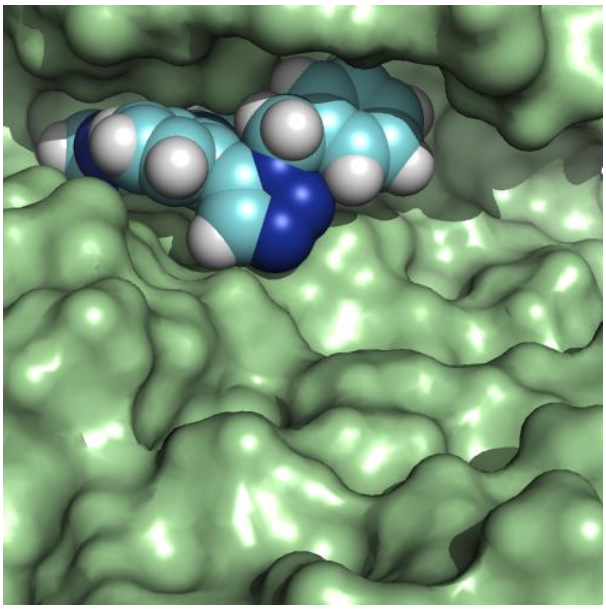

G. Model image of compound 5.4 bound to c-Src:

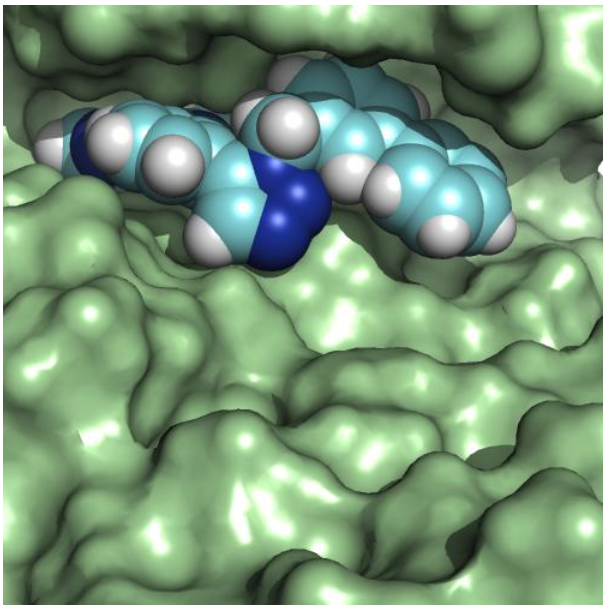

H. Molecular modeling of inhibitors bound to homologous kinases.

Molecular modeling was performed using MOE 2011.05 (Chemical Computing Group). The starting structure for c-Src was 3DQW, the starting structure for c-Abl was 2G2I, the starting structure for Hck was 2HK5, and the starting structure for Lck was 1QPE. Compound **5.4** was docked into c-Src structure and protein alignment performed by PyMol v.1.4 (Schrodinger). K_d values were obtained from KINOMEscan (DiscoveRx) as reported on page S49 of Supporting Information.

A.

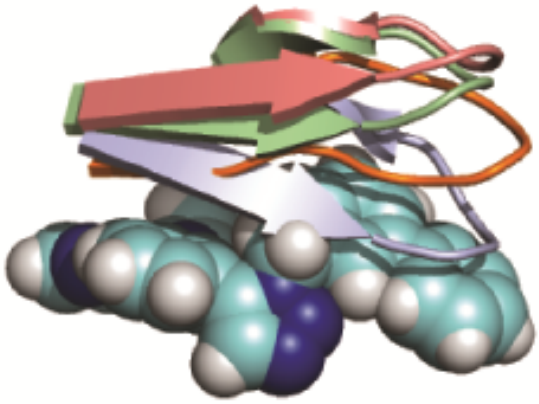

B.

kinase	K_d
c-Src	86 nM
Lck	160 nM
Fgr	240 nM
Yes	720 nM
Lyn	3200 nM
Hck	4400 nM
Fyn	>40000 nM
c-Abl	>40000 nM

X. KINOME PROFILING OF PP2 AND COMPOUND 5.4.

Kinome profiling for PP2 and compound **5.4** was performed by KINOMEScan (DiscoveRx, Fremont, CA). Both compounds were profiled at a concentration of 10 μM.

A. PP2 TREEspot analysis:

1% of control: **10% of control:** **35% of control:**

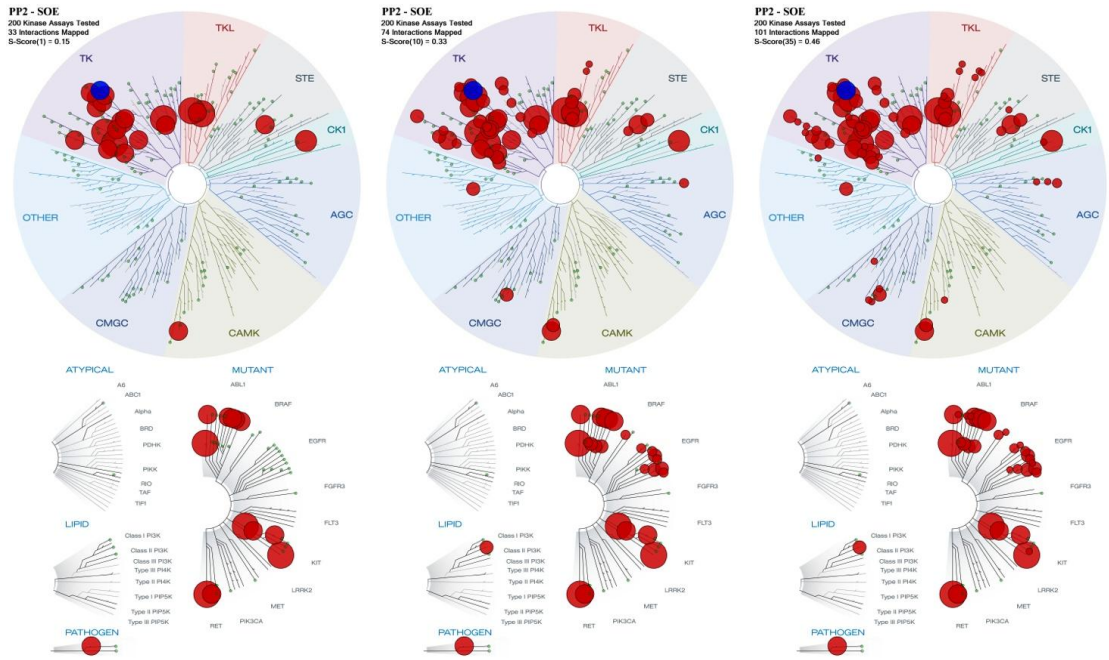

B. S-Scores for PP2:

S(1) = 0.147

S(10) = 0.313

S(35) = 0.448

C. Tabulated data for PP2:

Kinase	% of control	Kinase	% of control
ABL1(E255K)-phosphorylated	0.8	JNK1	66
ABL1(F317I)-nonphosphorylated	6.6	JNK2	20
ABL1(F317I)-phosphorylated	23	JNK3	12
ABL1(F317L)-nonphosphorylated	3.4	KIT	0
ABL1(F317L)-phosphorylated	18	KIT(A829P)	97
ABL1(H396P)-nonphosphorylated	0.05	KIT(D816H)	52
ABL1(H396P)-phosphorylated	0.35	KIT(D816V)	0.45
ABL1(M351T)-phosphorylated	32	KIT(L576P)	0.9
ABL1(Q252H)-nonphosphorylated	2.6	KIT(V559D)	0
ABL1(Q252H)-phosphorylated	0.9	KIT(V559D,T670I)	84
ABL1(T315I)-nonphosphorylated	92	KIT(V559D,V654A)	30
ABL1(T315I)-phosphorylated	84	KIT-autoinhibited	73
ABL1(Y253F)-phosphorylated	0.5	LCK	0.4
ABL1-nonphosphorylated	2.6	LIMK1	52
ABL1-phosphorylated	0.55	LIMK2	100
ABL2	6.8	LKB1	86
ACVR1	0	LOK	44
ACVR1B	10	LYN	9.2
ACVR2A	2.8	MAP3K4	100
ACVR2B	2.4	MAP4K2	84
ACVRL1	4.4	MAP4K3	72
ADCK3	84	MAP4K4	70
AKT1	100	MAP4K5	79
AKT2	97	MAPKAPK2	100
ALK	100	MARK3	53
AURKA	71	MEK1	0.65
AURKB	99	MEK2	1.2

AXL	60	MEK3	70
BLK	0.75	MEK4	70
BMPR2	20	MEK5	6.8
BMX	21	MET	87
BRAF	14	MKNK1	100
BRAF(V600E)	9	MKNK2	62
BRK	0.1	MLK1	81
BTK	3.4	MRCKA	8
CDK11	29	MRCKB	13
CDK2	79	MST4	74
CDK3	100	NLK	1.4
CDK7	80	p38-alpha	57
CDK9	95	p38-beta	13
CHEK1	100	PAK1	98
CSF1R	13	PAK2	75
CSK	0.95	PAK4	87
CSNK1D	24	PCTK1	94
CSNK1E	0.1	PDGFRA	28
CSNK1G2	79	PDGFRB	0.15
DCAMKL1	96	PDPK1	100
DDR1	0.25	PFCDPK1(P.falciparum)	0.25
DDR2	0	PFPK5(P.falciparum)	96
DMPK	84	PIK3C2B	100
DMPK2	28	PIK3CA	79
DYRK1B	76	PIK3CG	4.7
EGFR	6.2	PIM1	100
EGFR(E746-A750del)	7.4	PIM2	74
EGFR(G719C)	3.4	PIM3	100
EGFR(G719S)	2.9	PKAC-alpha	49
EGFR(L747-E749del, A750P)	14	PKMYT1	77

EGFR(L747-S752del, P753S)	12	PKNB(M.tuberculosis)	81
EGFR(L747-T751del,Sins)	6.3	PLK1	100
EGFR(L858R)	18	PLK3	97
EGFR(L858R,T790M)	57	PLK4	32
EGFR(L861Q)	5	PRKCE	55
EGFR(S752-I759del)	7.8	RAF1	25
EGFR(T790M)	2	RET	0
EPHA1	2.8	RET(M918T)	0.55
EPHA2	8.2	RET(V804L)	75
EPHA3	14	RET(V804M)	76
EPHA4	11	RIOK2	67
EPHA5	3.2	RIPK2	0
EPHA6	9.1	ROCK1	76
EPHA7	90	ROCK2	44
EPHA8	0.9	RSK2(Kin.Dom.1-N-terminal)	44
EPHB1	3.6	SIK	0.35
EPHB2	29	SIK2	1.4
EPHB3	0.85	SLK	77
EPHB4	5.4	SNARK	80
EPHB6	4.6	SRC	0.15
ERBB2	3	SRMS	42
ERBB3	8.2	SRPK3	100
ERBB4	9.3	STK36	41
ERK1	95	SYK	85
FAK	78	TEC	45
FGFR1	58	TESK1	36
FGFR2	58	TGFBR1	10
FGFR3	88	TGFBR2	0.5
FGFR4	43	TIE2	63

FGR	1.2	TNIK	34
FLT1	72	TNK2	8
FRK	0.3	TNNI3K	23
FYN	0.4	TRKA	59
GAK	3.8	TSSK1B	29
GCN2(Kin.Dom.2,S808G)	93	TXK	0.2
GSK3B	100	TYK2(JH1domain-catalytic)	91
HCK	0.45	ULK2	98
IGF1R	100	VEGFR2	71
IKK-alpha	100	WEE1	100
IKK-beta	100	YANK3	59
INSR	72	YES	1.5
JAK2(JH1domain-catalytic)	73	ZAK	68
JAK3(JH1domain-catalytic)	100	ZAP70	100

D. Compound 5.4 TREEspot analysis:

1% of control: **10% of control:** **35% of control:**

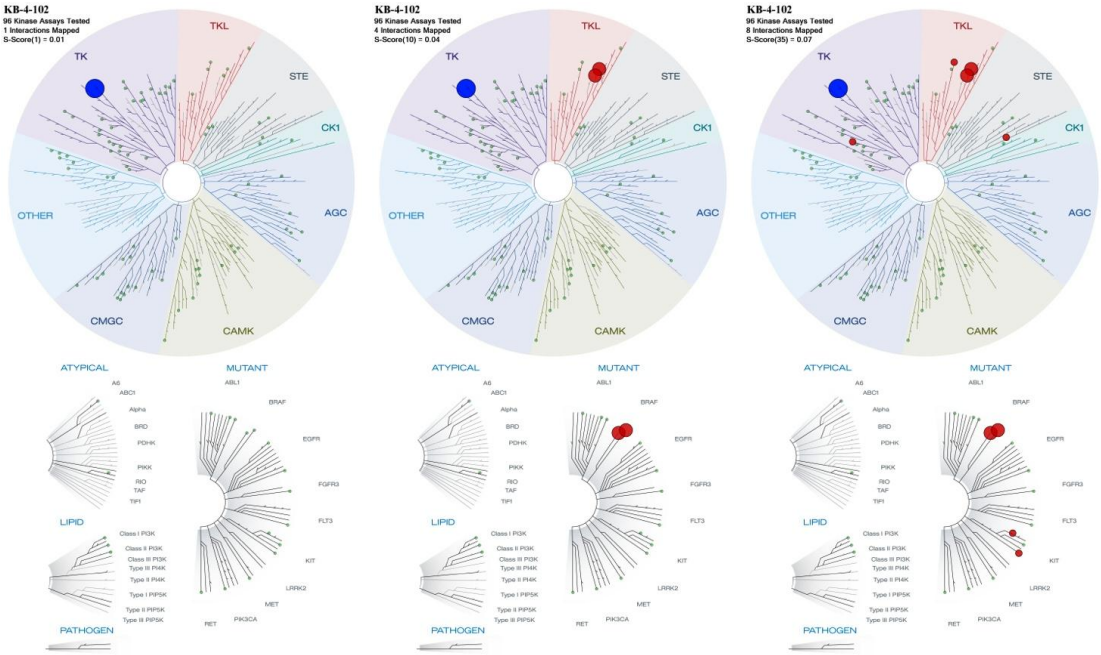

E. S-Scores for Compound 5.4:

S(1) = 0.011

S(10) = 0.033

S(35) = 0.067

F. Tabulated data for Compound 5.4:

KINOMEscan Gene Symbol	Percent Control	KINOMEscan Gene Symbol	Percent Control
ABL1(E255K)-phosphorylated	100	LKB1	100
ABL1(T315I)-phosphorylated	84	MAP3K4	32
ABL1-phosphorylated	100	MAPKAPK2	99
ACVR1B	55	MARK3	93
ADCK3	37	MEK1	80
AKT1	100	MEK2	100
AKT2	100	MET	100
ALK	100	MKNK1	78
AURKA	100	MKNK2	90
AURKB	96	MLK1	100
AXL	100	p38-alpha	100
BMPR2	100	p38-beta	56
BRAF	4.2	PAK1	100
BRAF(V600E)	1.7	PAK2	95
BTK	92	PAK4	100
CDK11	100	PCTK1	85
CDK2	83	PDGFRA	76
CDK3	100	PDGFRB	36
CDK7	92	PDPK1	100
CDK9	100	PIK3C2B	95
CHEK1	83	PIK3CA	100
CSF1R	99	PIK3CG	58
CSNK1D	99	PIM1	100
CSNK1G2	100	PIM2	100
DCAMKL1	100	PIM3	100
DYRK1B	100	PKAC-alpha	100
EGFR	65	PLK1	87

EGFR(L858R)	71	PLK3	74
EPHA2	94	PLK4	78
ERBB2	43	PRKCE	100
ERBB4	99	RAF1	3.2
ERK1	100	RET	100
FAK	100	RIOK2	74
FGFR2	60	ROCK2	100
FGFR3	62	RSK2(Kin.Dom.1-N-terminal)	92
FLT3	100	SNARK	91
GSK3B	90	SRC	0.55
IGF1R	100	SRPK3	100
IKK-alpha	79	TGFBR1	33
IKK-beta	82	TIE2	47
INSR	85	TRKA	100
JAK2(JH1domain-catalytic)	84	TSSK1B	83
JAK3(JH1domain-catalytic)	79	TYK2(JH1domain-catalytic)	84
JNK1	87	ULK2	99
JNK2	100	VEGFR2	73
JNK3	100	YANK3	98
KIT	28	ZAP70	100
KIT(D816V)	20		
KIT(V559D,T670I)	90		

G. TREEspot comparison using scanEDGE (96 kinase) diverse panel (35% of control):

PP2: **Compound 5.4:**

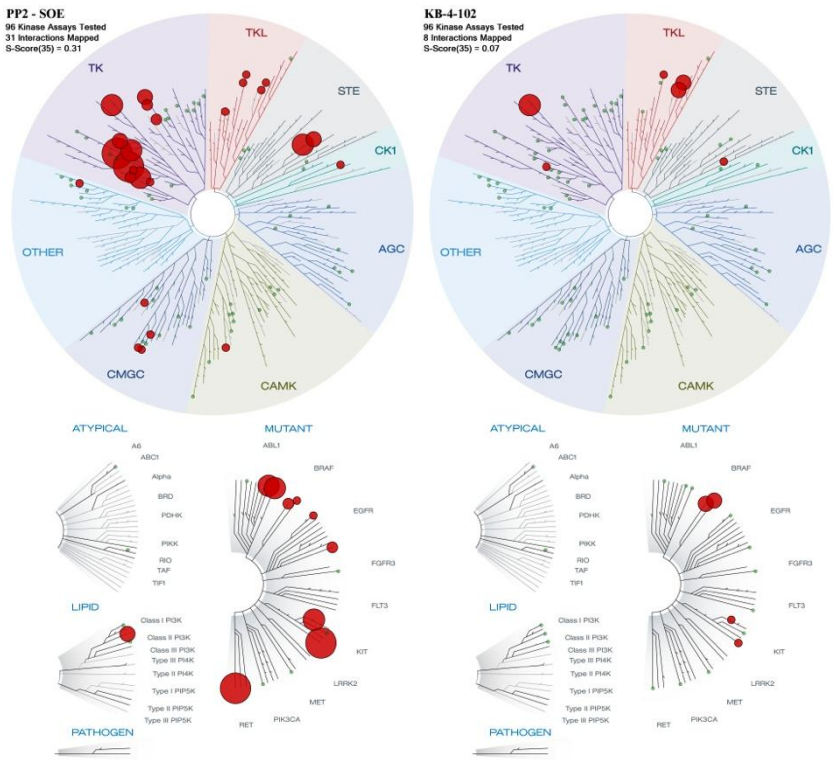

H. S-Score comparison using scanEDGE panel (96 diverse kinases):

PP2	Compound 5.4
S(1) = 0.07	S(1) = 0.01
S(10) = 0.16	S(10) = 0.04
S(35) = 0.31	S(35) = 0.07

VIII. K_D DETERMINATION FOR COMPOUND 5.4.

K_d measurements were performed using KINOMEscan technology (DiscoveRx, Fremont, CA). An 11-point 3-fold serial dilution of compound **5.4** was prepared in 100% DMSO at 100x final test concentration and subsequently diluted to 1x in the assay (final DMSO concentration = 2.5%). K_d was determined using a compound top concentration = 30,000 nM. A K_d value reported as 40,000 nM indicates that the K_d was determined to be >30,000 nM.

Compound Name	KINOMEscan Gene Symbol	Kd (nM)
KB-4-102	FGR	240
KB-4-102	FYN	40000
KB-4-102	HCK	4400
KB-4-102	LCK	160
KB-4-102	LYN	3200
KB-4-102	SRC	86
KB-4-102	YES	720

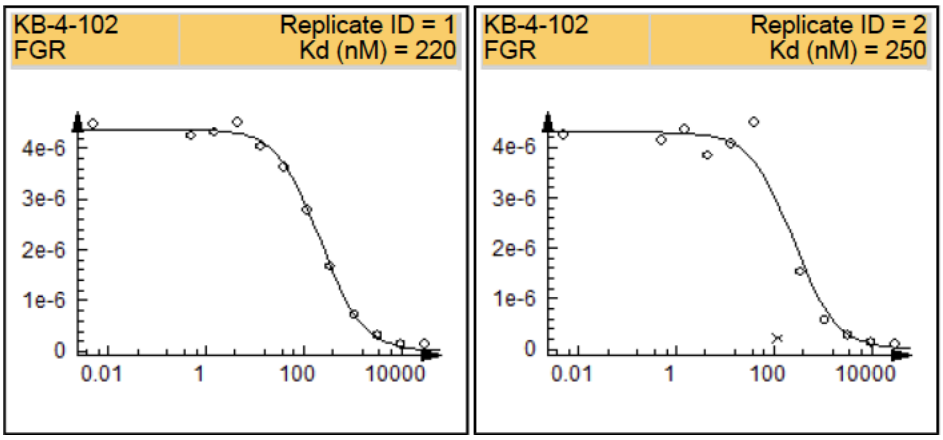

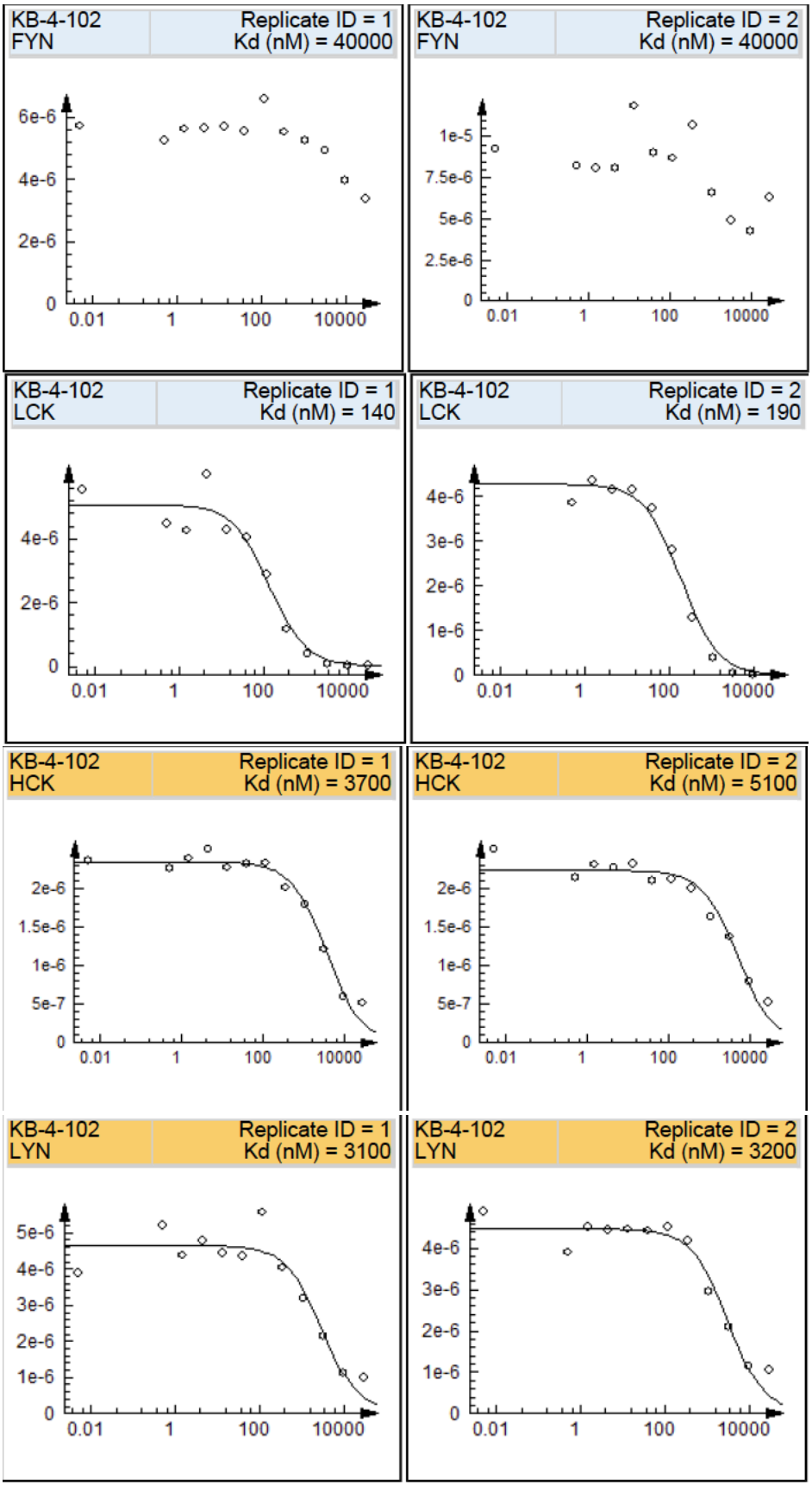
KB-4-102
FYN
Replicate ID = 1
Kd (nM) = 40000
6e-6
4e-6
2e-6
0
0.01
1
100
10000
KB-4-102
FYN
Replicate ID = 2
Kd (nM) = 40000
1e-5
7.5e-6
5e-6
2.5e-6
0
0.01
1
100
10000
KB-4-102
LCK
Replicate ID = 1
Kd (nM) = 140
4e-6
2e-6
0
0.01
1
100
10000
KB-4-102
LCK
Replicate ID = 2
Kd (nM) = 190
4e-6
3e-6
2e-6
1e-6
0
0.01
1
100
10000
KB-4-102
HCK
Replicate ID = 1
Kd (nM) = 3700
2e-6
1.5e-6
1e-6
5e-7
0
0.01
1
100
10000
KB-4-102
HCK
Replicate ID = 2
Kd (nM) = 5100
2e-6
1.5e-6
1e-6
5e-7
0
0.01
1
100
10000
KB-4-102
LYN
Replicate ID = 1
Kd (nM) = 3100
5e-6
4e-6
3e-6
2e-6
1e-6
0
0.01
1
100
10000
KB-4-102
LYN
Replicate ID = 2
Kd (nM) = 3200
4e-6
3e-6
2e-6
1e-6
0
0.01
1
100
10000

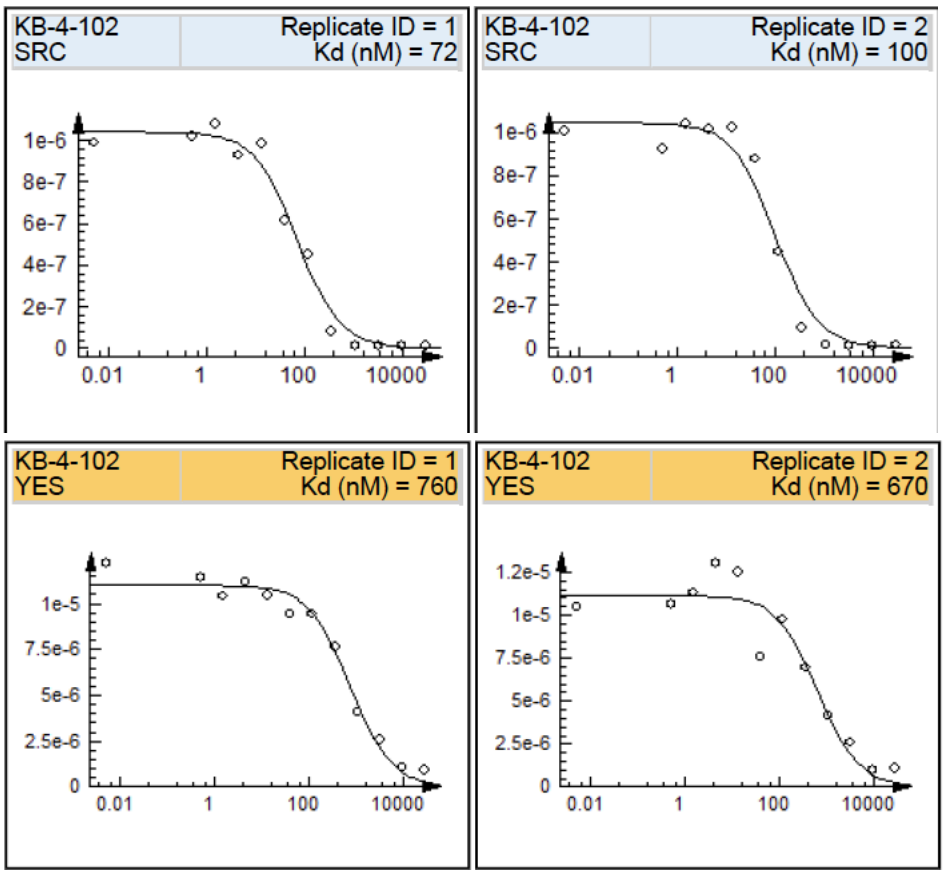
KB-4-102
SRC
Replicate ID = 1
Kd (nM) = 72
1e-6
8e-7
6e-7
4e-7
2e-7
0
0.01
1
100
10000
KB-4-102
SRC
Replicate ID = 2
Kd (nM) = 100
1e-6
8e-7
6e-7
4e-7
2e-7
0
0.01
1
100
10000
KB-4-102
YES
Replicate ID = 1
Kd (nM) = 760
1e-5
7.5e-6
5e-6
2.5e-6
0
0.01
1
100
10000
KB-4-102
YES
Replicate ID = 2
Kd (nM) = 670
1.2e-5
1e-5
7.5e-6
5e-6
2.5e-6
0
0.01
1
100
10000

IX. CELLULAR CHARACTERIZATION.

A. c-Src Autophosphorylation. This assay was performed by ProQinase GmbH (Freiburg, Germany). Murine embryonal fibroblast (MEF) cells were used that express a high level of exogenously introduced full-length Src. The high Src expression level results in a constitutive tyrosine autophosphorylation of Src at Tyr418. MEF-SRC cells were plated in DMEM supplemented with 10% FCS in multiwell cell culture plates. Compound incubation was done in serum-free medium. Quantification of Src phosphorylation was assessed in 96-well plates via ELISA using a phospho-Src specific antibody and a secondary detection antibody. Raw data were converted into percent phosphorylation and the IC_{50} value was determined using GraphPad Prism software. Each concentration has n = 2 data points and the graph below represents the average at each concentration.

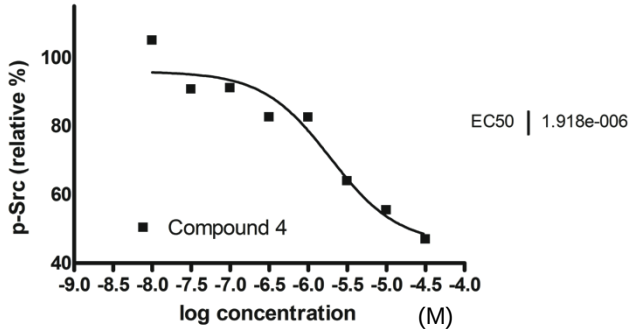

B. p-Erk AlphaScreen. SKBR3 cells (ATCC) were plated in 96-well plates at a density of 1.0–2.0 x 10^4 cells per well. The cells were grown to 80-90% confluency prior to overnight serum-starvation in DMEM, 0.1% BSA. The serum-free media was then removed and replaced with DMEM containing 100 μM compound **5.4** (or PP2) in 1% DMSO. The cells were incubated for 60 min prior to addition of EGF (Sigma Aldrich). After incubation, the media was removed and 50 μL AlphaScreen lysis buffer (PerkinElmer) was added to each well. The lysates were analyzed using the AlphaScreen SureFire Erk1/2 (p-Thr202/Tyr204) assay kit (PerkinElmer) according to the manufacturer's protocol. For each compound, n = 4.

C.

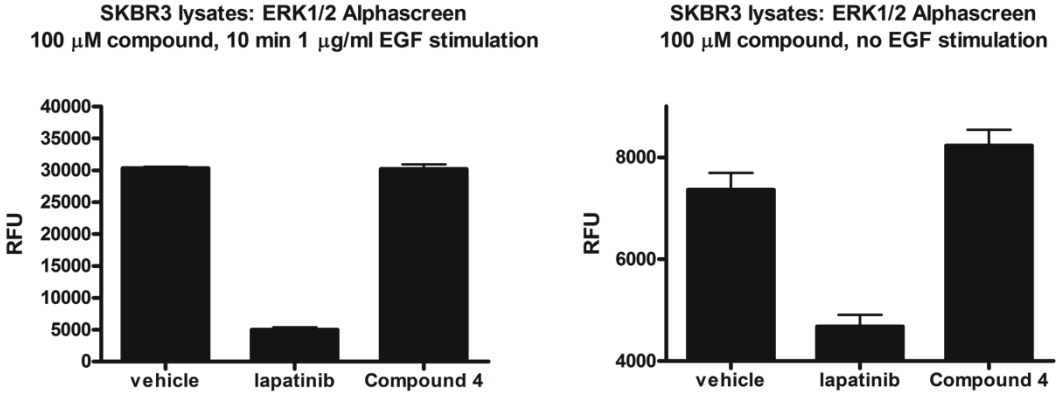

Treatment of SKBR3 cells with 100 μM compound **5.4** showed no change in p-Erk levels. As a positive control, treatment with 100 μM lapatinib (a selective dual-ErbB2/EGFR inhibitor) shows a large decrease in p-Erk levels. These data are consistent with compound **5.4** not inhibiting B-Raf or c-Raf in SKBR3 cells. Lapatinib reduces p-Erk levels by reducing p-ErbB2 and p-EGFR levels.

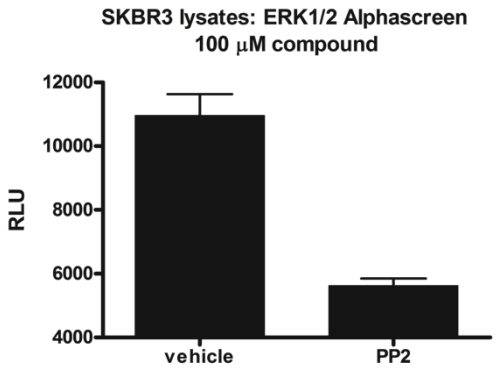

In contrast to compound **5.4**, PP2 shows a decrease in p-Erk levels upon treatment of 100 μM PP2 to SKBR3 cells. PP2 inhibits ErbB2 and EGFR (see kinome profiling section) and cellular inhibition of these kinases will lead to decreased p-Erk levels.

C. Cancer cell growth inhibition assays.

General procedure:

1. **Cell culture and seeding**: Cells are dispersed from flasks and collected by centrifugation (125xg for 5 minutes at room temperature). An aliquot of the resuspended cells is mixed with trypan blue solution and the cell number is quantified using a hemacytometer. In general, depending on the growth rate of the untreated cells, the cells will be plated at 5.0 – 7.5 x 10^3 cells per well. 100 μL of the cell mixture will be added to each well so the concentration should be 10X the cells per well in cells per mL. The cells are plated into sterile, clear bottom 96 well plates and cultured under normal growth conditions overnight prior to dosing with compound.
2. **Dosing**: The 100% DMSO compound stocks need to be prepared to 100X the final concentration that is desired in the assay. 3 μL of the DMSO stock solution is then added to 297 μL of the cell growth media to give a DMSO concentration of 1%. The cell media is removed by aspiration for adherent cells and replaced with 100 μL per well of the cell growth media containing the compound. In

general each compound concentration is dosed in triplicate wells. The plates are returned to normal culture conditions for 24 – 72 hours.

3. **Assay**: After the required incubation period the plates are removed from the incubator and 10 µL per well of WST-1 reagent is added. The plates are returned to the incubator and the color change is visually monitored for 0.5 – 2 hours. When sufficient color change has occurred the plates are shaken on a plate shaker for 60 seconds and read in the appropriate plate reader.
4. **Data Analysis**: The reference absorbance reading is subtracted from the formazan absorbance and the data is plotted as a percentage of the vehicle (1% DMSO alone). Data analysis and curve fitting was performed using Graphpad Prism. For each cell line, there were n = 3 data points for each concentration. Each dose response curve was performed at least twice, providing n ≥ 6 for each data point.

C1. HT-29:

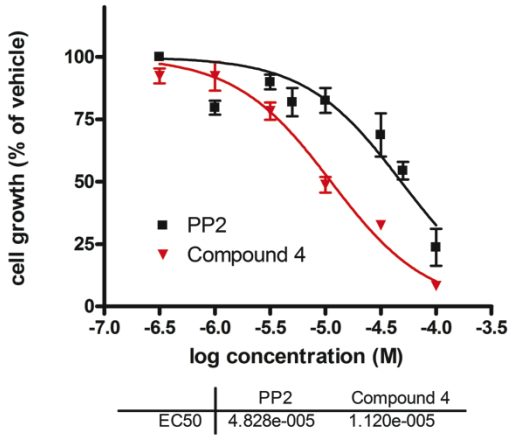

C2. SK-BR-3:

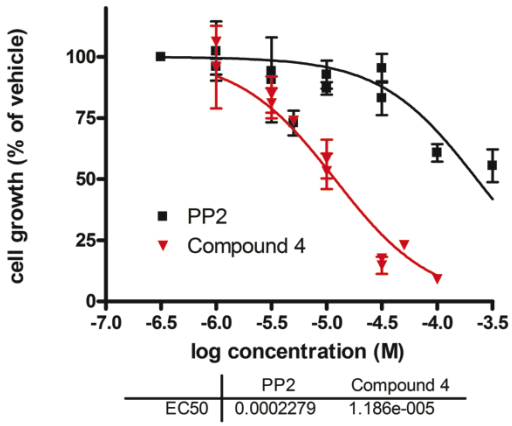

C3. MCF7:

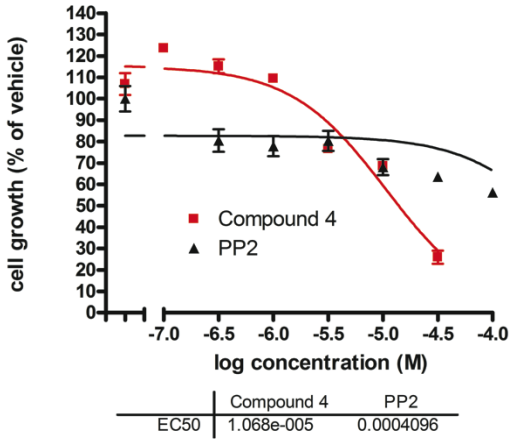

C4. MDA-MB-453:

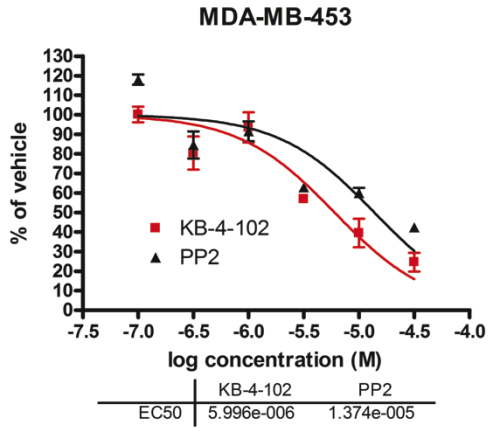

C5. NIH-3T3:

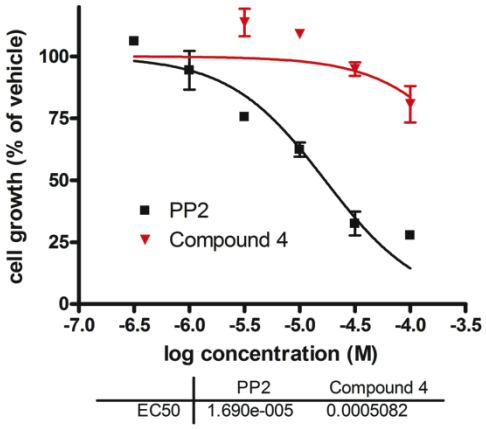

D. NCI-60 cancer cell profiling:

One-dose (10 μM) cell profiling of compound **5.4** was performed by the NCI Developmental Therapeutics Program. The assigned NSC number for compound **5.4** is 761450.

Developmental Therapeutics Program

One Dose Mean Graph

NSC: D-761450 / 1	Conc: 1.00E-5 Molar	Test Date: Sep 06, 2011
Experiment ID: 1109OS20		Report Date: Sep 22, 2011

Panel/Cell Line	Growth Percent
Leukemia	
CCRF-CEM	81.39
HL-60(TB)	85.74
MOLT-4	76.19
RPMI-8226	70.40
SR	40.34
Non-Small Cell Lung Cancer	
A549/ATCC	59.02
EKVX	82.30
HOP-62	70.25
HOP-92	49.12
NCI-H226	79.95
NCI-H23	80.40
NCI-H322M	89.36
NCI-H460	76.69
NCI-H522	38.15
Colon Cancer	
COLO 205	82.14
HCC-2998	79.99
HCT-116	77.91
HCT-15	87.51
HT29	65.65
KM12	82.92
SW-620	86.45
CNS Cancer	
SF-268	81.64
SF-295	66.77
SF-539	57.81
SNB-19	76.21
SNB-75	20.46
U251	71.00
Melanoma	
LOX IMVI	82.10
MALME-3M	72.49
M14	92.01
MDA-MB-435	80.09
SK-MEL-2	80.51
SK-MEL-28	60.19
SK-MEL-5	67.88
UACC-257	53.33
UACC-62	76.24
Ovarian Cancer	
IGROV1	84.96
OVCAR-3	112.00
OVCAR-4	27.26
OVCAR-5	72.55
OVCAR-8	67.77
NCI/ADR-RES	69.46
SK-OV-3	64.54
Renal Cancer	
786-0	63.40
ACHN	46.68
CAKI-1	68.93
RXF 393	52.53
SN12C	67.24
TK-10	85.22
UO-31	67.77
Prostate Cancer	
DU-145	70.59
Breast Cancer	
MCF7	65.75
MDA-MB-231/ATCC	60.81
HS 578T	68.54
BT-549	86.68
T-47D	81.56
MDA-MB-468	87.93
Mean	71.10
Delta	50.64
Range	91.54

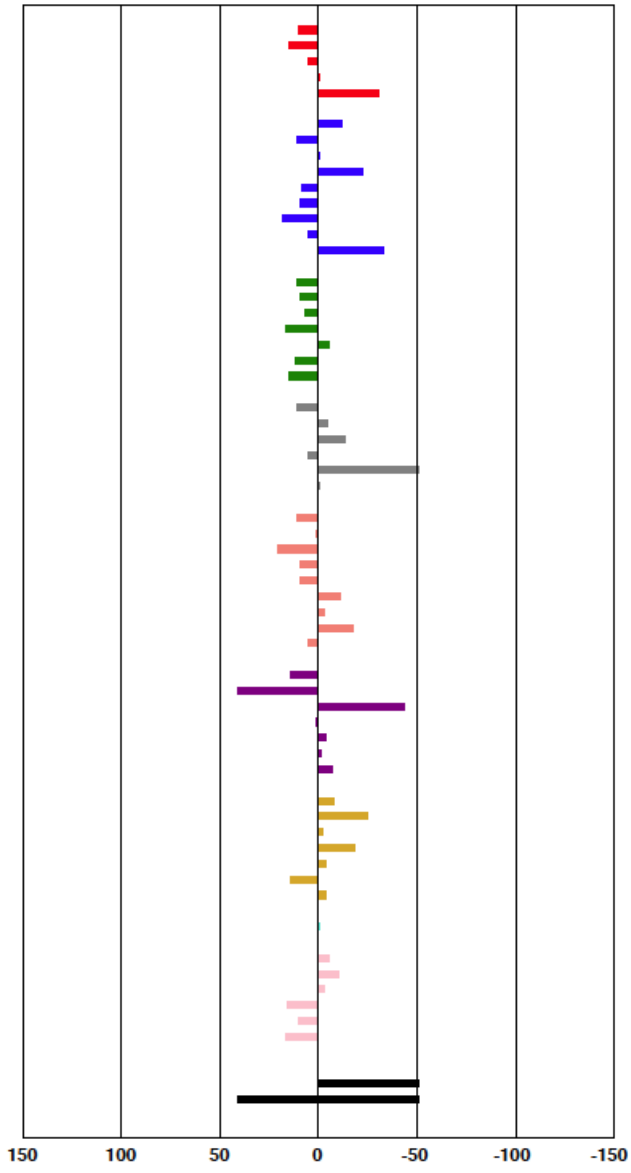

5.5 References

(1) Thomas, S. M.; Brugge, J. S. *Annual Review of Cell and Developmental Biology* **1997**, *13*, 513-609.

(2) Martin, G. S. *Nature Reviews Molecular Cell Biology* **2001**, *2*, 467-475.

(3) Zhang, S.; Huang, W.-C.; Li, P.; Guo, H.; Poh, S.-B.; Brady, S. W.; Xiong, Y.; Tseng, L.-M.; Li, S.-H.; Ding, Z.; Sahin, A. A.; Esteva, F. J.; Hortobagyi, G. N.; Yu, D. *Nature Medicine* **2011**, *17*, 461-U101.

(4) Metz, J. T.; Johnson, E. F.; Soni, N. B.; Merta, P. J.; Kifle, L.; Hajduk, P. J. *Nature Chemical Biology* **2011**, *7*, 200-202.

(5) Bishop, A. C.; Ubersax, J. A.; Petsch, D. T.; Matheos, D. P.; Gray, N. S.; Blethrow, J.; Shimizu, E.; Tsien, J. Z.; Schultz, P. G.; Rose, M. D.; Wood, J. L.; Morgan, D. O.; Shokat, K. M. *Nature* **2000**, *407*, 395-401.

(6) To be considered highly selective the probe should be profiled against a panel of diverse kinases and shown to inhibit < 5% of kinases in the panel at 10 uM.

(7) Murphy, S. T.; Alton, G.; Bailey, S.; Baxi, S. M.; Burke, B. J.; Chappie, T. A.; Ermolieff, J.; Ferre, R.; Greasley, S.; Hickey, M.; Humphrey, J.; Kablaoui, N.; Kath, J.; Kazmirski, S.; Kraus, M.; Kupchinsky, S.; Li, J.; Lingardo, L.; Marx, M. A.; Richter, D.; Tanis, S. P.; Tran, K.; Vernier, W.; Xie, Z.; Yin, M.-J.; Yu, X.-H. *Journal of Medicinal Chemistry* **2011**, *54*, 8490-8500.

(8) Hanke, J. H.; Gardner, J. P.; Dow, R. L.; Changelian, P. S.; Brissette, W. H.; Weringer, E. J.; Pollok, K.; Connelly, P. A. *Journal of Biological Chemistry* **1996**, *271*, 695-701.

(9) Bain, J.; Plater, L.; Elliott, M.; Shpiro, N.; Hastie, C. J.; McLauchlan, H.; Klevernic, I.; Arthur, J. S. C.; Alessi, D. R.; Cohen, P. *Biochemical Journal* **2007**, *408*, 297-315.

(10) Fabian, M. A.; Biggs, W. H.; Treiber, D. K.; Atteridge, C. E.; Azimioara, M. D.; Benedetti, M. G.; Carter, T. A.; Ciceri, P.; Edeen, P. T.; Floyd, M.; Ford, J. M.; Galvin, M.; Gerlach, J. L.; Grotzfeld, R. M.; Herrgard, S.; Insko, D. E.; Insko, M. A.; Lai, A. G.; Lelias, J.-M.; Mehta, S. A.; Milanov, Z. V.; Velasco, A. M.; Wodicka, L. M.; Patel, H. K.; Zarrinkar, P. P.; Lockhart, D. J. *Nat Biotech* **2005**, *23*, 329-336.

(11) Davis, M. I.; Hunt, J. P.; Herrgard, S.; Ciceri, P.; Wodicka, L. M.; Pallares, G.; Hocker, M.; Treiber, D. K.; Zarrinkar, P. P. *Nat Biotech* **2011**, *29*, 1046-1051.

(12) Ishizawar, R. C.; Miyake, T.; Parsons, S. J. *Oncogene* **2007**, *26*, 3503-3510.

(13) Muratore, K. E.; Seeliger, M. A.; Wang, Z.; Fomina, D.; Neiswinger, J.; Havranek, J. J.; Baker, D.; Kuriyan, J.; Cole, P. A. *Biochemistry* **2009**, *48*, 3378-3386.

(14) Zhu, X.; Kim, J. L.; Newcomb, J. R.; Rose, P. E.; Stover, D. R.; Toledo, L. M.; Zhao, H.; Morgenstern, K. A. *Structure* **1999**, *7*, 651-661.

(15) Kolb, H. C.; Finn, M. G.; Sharpless, K. B. *Angewandte Chemie-International Edition* **2001**, *40*, 2004-+.

(16) Georghiou, G.; Kleiner, R. E.; Pulkoski-Gross, M.; Liu, D. R.; Seeliger, M. A. *Nature Chemical Biology* **2012**, *8*, 366-374.

(17) Maly, D. J.; Choong, I. C.; Ellman, J. A. *Proceedings of the National Academy of Sciences* **2000**, *97*, 2419-2424.
(18) Patel, R. Y.; Doerksen, R. J. *Journal of Proteome Research* **2010**, *9*, 4433-4442.
(19) Seeliger, M. A.; Nagar, B.; Frank, F.; Cao, X.; Henderson, M. N.; Kuriyan, J. *Structure* **2007**, *15*, 299-311.
(20) Shah, N. P.; Nicoll, J. M.; Nagar, B.; Gorre, M. E.; Paquette, R. L.; Kuriyan, J.; Sawyers, C. L. *Cancer Cell* **2002**, *2*, 117-125.
(21) This assay was performed by ProQinase GmbH (Freiburg, Germany).
(22) O'Hare, T.; Druker, B. J. *Nat Biotech* **2005**, *23*, 1209-1210.
(23) Morphy, R. *Journal of Medicinal Chemistry* **2010**, *53*, 1413-1437.
(24) The four cells lines tested for growth inhibition were: HT-29 (colon cancer), SK-BR-3 (breast cancer), MCF7 (breast cancer), MDA-MB-453 (breast cancer).
(25) Zheng, X.; Resnick, R. J.; Shalloway, D. *International Journal of Cancer* **2008**, *122*, 1999-2007.
(26) Allington, T. M.; Schiemann, W. P. *Cells Tissues Organs* **2011**, *193*, 98-113.
(27) Allington, T. M.; Galliher-Beckley, A. J.; Schiemann, W. P. *Faseb Journal* **2009**, *23*, 4231-4243.
(28) Adrian, F. J.; Ding, Q.; Sim, T.; Velentza, A.; Sloan, C.; Liu, Y.; Zhang, G.; Hur, W.; Ding, S.; Manley, P.; Mestan, J.; Fabbro, D.; Gray, N. S. *Nat Chem Biol* **2006**, *2*, 95-102.
(29) Shoemaker, R. H. *Nature Reviews Cancer* **2006**, *6*, 813-823.
(30) Wang, Q.; Cahill, S. M.; Blumenstein, M.; Lawrence, D. S. *Journal of the American Chemical Society* **2006**, *128*, 1808-1809.
(31) Castanedo, G.; Clark, K.; Wang, S.; Tsui, V.; Wong, M.; Nicholas, J.; Wickramasinghe, D.; Marsters Jr, J. C.; Sutherlin, D. *Bioorganic & Medicinal Chemistry Letters* **2006**, *16*, 1716-1720.